KfK 4508
Februar 1989

Annual Report on Nuclear Physics Activities

July 1, 1987 - June 30, 1988

Editors:
P. Doll, G. Meisel
Institut für Kernphysik

Kernforschungszentrum Karlsruhe

KERNFORSCHUNGSZENTRUM KARLSRUHE

Institut für Kernphysik

KfK 4508

ANNUAL REPORT

on

NUCLEAR PHYSICS ACTIVITIES

July 1, 1987 - June 30, 1988

Editors:

P. Doll, G. Meisel

Kernforschungszentrum Karlsruhe GmbH, Karlsruhe

Kernforschungszentrum Karlsruhe GmbH
Postfach 3640, 7500 Karlsruhe 1

ISSN 0303-4003

ABSTRACT

This report surveys the activities in basic research from July 1, 1987 to June 30, 1988 at the Institute for Nuclear Physics (IK) of the Kernforschungszentrum Karlsruhe. The research program of this institute comprises nuclear astrophysics, laser spectroscopy, nuclear reactions with light ions, neutron physics, neutrino physics and high energy physics, as well as detector technology.

ZUSAMMENFASSUNG

Der vorliegende Bericht gibt einen Überblick über die Arbeiten am Institut für Kernphysik (IK) des Kernforschungszentrums Karlsruhe im Zeitraum vom 1. Juli 1987 bis zum 30. Juni 1988. Das Forschungsprogramm umfaßt die Gebiete nukleare Astrophysik, Laserspektroskopie, Kernreaktionen mit leichten Ionen, Neutronenphysik, Neutrinophysik und Hochenergiephysik sowie Detektor-Technologie.

P R E F A C E

This annual report on nuclear physics activities at the Kernforschungszentrum Karlsruhe describes experiments carried out in sections I and III of the Institut für Kernphysik (IK). Work in the field of intermediate energy physics performed during the years 1987 and 1988 in the earlier Institute für Kernphysik II is also included. In the meantime these activities have been transferred to the Karlsruhe University.

The groups in Section IK I are working in experimental nuclear and particle physics:

- Fast Neutron Physics: The polarized neutron beam of the facility POLKA at the Karlsruhe Cyclotron has been used for a new measurement of the n-p spin correlation parameter A_{yy}. In a series of experiments we studied the capture reactions of fast polarized neutrons on light nuclei. Analyzing power distributions for neutron induced reactions on ^{3}He and ^{12}C were determined. Neutron spin-spin cross sections on ^{27}Al and on ^{93}Nb are analyzed in the framework of the Optical Model. The investigation of cryogenic detectors for low energy particles has started. Prototype detectors have been succesfully tested in a ^{3}He cryostat using laser pulses and α-particles. Material research and Monte Carlo simulations are carried out for the design of an detector array for the study of extensive air showers.

- Neutrino Physics: The group is performing neutrino physics experiments making use of beam dump neutrinos in the energy range of about 10 to 50 MeV from the neutron spallation facility ISIS of the Rutherford Appleton Laboratory (RAL) in England. The program involves experimental studies of fundamental questions in the fields of particle physics, nuclear physics and astrophysics. A collaboration of KfK, University of Erlangen, University of Karlsruhe, University of Oxford and Queen Mary College of London is using the 60 t scintillator detector system KARMEN 1 (Karlsruhe-Rutherford-Medium-Energy-Neutrinoexperiment), which has been installed in a massive blockhouse of steel set up by KfK at ISIS. A first engineering and data taking run has confirmed the design figures of the experiment. This project carried out in cooperation with Karlsruhe University, was partly supported by BMFT through the "Verbund Kern- und Mittelenergyphysik".

- High Energy Physics: The group was mainly working on the data analysis for the experiments performed with an international collaboration using the CELLO detector at the PETRA accelerator (DESY). Emphasis is laid on the analysis of hadronic final states in e^+e^- annihilation for QCD tests and for the determination of the coupling constant α_S. In the study of electroweak interactions the analysis of inclusive leptons in multihadronic events yields information on the heavy c- and b-quarks. A search for new particles in e^+e^- -annihilations was performed.

- Detector Development: The work is concentrating on liquid ionization chambers using room temperature liquids as active media. The investigations are continued to enable the use of this type of detectors in large scale calorimeters for particle physics and astrophysics experiments. For an air shower calorimeter hermetically sealed that chambers are under investigation. The conditions and premises for mass production are studied. First prototype chambers were successfully tested in a 6 GeV particle beam of pions, myons and electrons.

Section IK III is mainly working in the following fields:

- Nuclear Astrophysics: Capture cross sections of fast neutrons in the keV to MeV range are measured in order to understand in detail the synthesis of heavy elements in stars. In this work, a considerable increase in accuracy is expected from a novel 4π-BaF2 scintillation detector which has come into operation. For the interpretation of these data, additional nuclear structure information is required. This has initiated a series of experiments at the high flux reactor of the Institut Laue Langevin, Grenoble. These data are being evaluated.

- Nuclear Reactions: Work in this field makes use of the 26 MeV/nucleon 6Li beam from the Karlsruhe Isochronous Cyclotron and of the magnetic spectrometer for investigating continuous spectra in break-up reactions. Theoretical studies had shown that Coulomb break-up should allow the determination of radiative capture cross sections between light nuclei at very low relative velocities. Such cross sections are of great importance in astrophysics. The experiments have demonstrated the feasibility of the method, and detailed evaluation of the results is under way.

- Laser Spectroscopy: This technique is applied so sub-ng amounts of radioactive atoms in order to determine hyperfine structure and isotopic shifts of atomic transitions. The results yield information on nuclear moments and on the change of nuclear charge radii due to varying neutron number. Work at present concentrates on elements beyond lead using different experimental techniques such as spectroscopy on collimated atomic beams and on ions stored in an rf trap.

- Applied Gamma-Ray Spectroscopy: Here instruments are developed to determine concentration and isotopic composition on fissile materials. The instruments make use either of the intrinsic radioactivity or of X-ray absorption and fluorescence. Their main applications are in the safeguards of nuclear fuel and in process control during fabrication and reprocessing.

- Section IK III is also responsible for operating the three accelerators of our institute. The Karlsruhe Isochronous Cyclotron which is mainly used for fast neutron physics and nuclear reaction experiments; the 3.75 MeV Van de Graaff accelerator which serves mainly as a source of keV neutrons for the nuclear astrophysics studies; and a compact cyclotron which is basically a commercial installation to produce radioactive isotopes for nuclear medicine and mechanical engineering.

(B. Zeitnitz) (G. Schatz)

CONTENTS

1. NUCLEAR PHYSICS

1.1 NUCLEAR ASTROPHYSICS

1.1.1 THE $^{7}Li(n,\gamma)$ CROSS SECTION AND ITS IMPORTANCE FOR BIG BANG NUCLEOSYNTHESIS

M. Wiescher*, F. Käppeler, R. Steininger

The suggestion, that the phase transition from the quark-gluon plasma to the era of hadrons may have caused strong density fluctuation in the early universe (1), has stimulated discussions on big bang nucleosynthesis (2, 3). The new aspects concern the possible occurence of extremely neutron rich regions. In such regions, neutron induced reactions may become important, which were completely negligible in standard big bang nucleosynthesis. One can even think of a sequence of reactions bridging the gap to carbon and the heavier elements in kind of a big bang r-process.

The possibility of such a "leak" to heavier elements is mainly based on the cross section for $^{7}Li(n,\gamma)^{8}Li$. As the only measurement of this cross section dates back to 1959 (4), and as the reported value of $\sim$ 50 µb at 30 keV neutron enery implies serious background problems, a reinvestigation seemed adequate in order to provide more firm grounds for the above speculations.

The measurement was carried out via the activation technique. Neutrons were produced via the $^{7}Li(p,n)^{7}Be$ reaction by bombarding metallic lithium targets at the Karlsruhe 3.75 MV Van de Graaff accelerator. After the sample was irradiated for 4 sec by the neutrons, the proton beam was switched off, and the decay $^{8}Li \xrightarrow{\beta^-} {}^{8}Be \xrightarrow{\alpha} {}^{4}He$ was observed by detecting the alpha particles of the ^{8}Be decay. Two types of detectors were used, which differed by their characteristic uncertainties: (i) a lithium glass scintillator of 1 mm thickness, loaded with 8.1% natural lithium and viewed by a fast photomultiplier, and (ii) an ionization chamber with a thin layer of LiF as a sample. The measurements covered the neutron energy range from 25 to 420 keV. Data analysis is still in progress, but first results indicate a significantly smaller cross section than reported in 1959.

(1) E. Witten, Phys. Rev. D30 (1984) 272

(2) G.M. Fuller, G.J. Mathews, C.R. Alcock, "Origin and Distribution of the Elements", ed. G.J. Mathews, (World Scientific: Singapore) (1988) p. 36

(3) R.A. Melaney, W.A. Fowler, "Origin and Distribution of the Elements", ed. G.J. Mathews, (World Scientific: Singapore) (1988) p. 76

(4) W.L. Imhof, R.G. Johnson, F.J. Vaughn, M. Walt, Phys. Rev. 114 (1959) 1037

* University of Notre Dame, Notre Dame, Indiana 46556, U.S.A.

1.1.2 THE CROSS SECTION OF $^{14}N(n,p)^{14}C$ AT STELLAR ENERGIES AND ITS ROLE AS A NEUTRON POISON FOR s-PROCESS NUCLEOSYNTHESIS*

K. Brehm**, H.W. Becker**, C. Rolfs**, H.P. Trautvetter**,

F. Käppeler, W. Ratynski*** (1)

The absolute average cross section $\langle\sigma\rangle$ of the $^{14}N(n,p)^{14}C$ reaction has been measured using neutron spectra that closely resemble Maxwell-Boltzmann distributions with thermal energies of kT = 25.0 and 52.4 keV: $\langle\sigma\rangle$=0.81±0.05 and 0.52±0.06 mb, respectively. The resulting reaction rates are nearly the same at T_9=0.29 and 0.61, and their average, $N_A\langle\sigma v\rangle=(1.3\pm0.1)\times10^5$ cm^3 s^{-1} mol^{-1}, is about a factor of three smaller than the previously adopted values obtained by extrapolation between thermal and higher-energy data. Thus the $^{14}N(n,p)^{14}C$ reaction plays a correspondingly smaller role as a neutron poison for s-process nucleosynthesis.

PACS: 95.30.C; 97.10.C; 25.70

(1) Z. Phys. A - Atomic Nuclei 330 (1988) 167

* Supported in part by the Deutsche Forschungsgemeinschaft (Ro 429/15-2)

** Institut für Kernphysik, Universität Münster, Münster, FRG

*** On leave from the Institute of Nuclear Studies, Swierk, Poland

1.1.3 A NEW EXPERIMENTAL SETUP TO MEASURE STELLAR (n,p) AND (n,α) CROSS SECTIONS AND THE EXAMPLE ^{33}S.

R. Steininger, F. Käppeler

The explanation of the isotopic abundances produced in neutron capture nucleosynthesis requires in some cases to consider (n,p) and (n,α) reactions in addition to the dominant (n,γ) channel. One such example is ^{33}S : starting from the abundant seed nucleus ^{32}S the production of the rare isotope ^{36}S by successive (n,γ) reactions is almost blocked by the competing (n,α) reaction at ^{33}S. Previous results for the respective cross section at kT = 30 keV are highly discrepant: $\langle\sigma v\rangle/v_T$ = 690 ± 170 mb (1) in contrast to 234 ± 20 mb (2).

In order to resolve this discrepancy an experimental setup was built and tested, which allows to measure (n,p) and (n,α) rates even from small samples. This is equally important for the investigation of expensive, isotopically enriched samples as well as for unstable isotopes, where the readioactivity should be minimized.

The 3.75 MV Van de Graaff accelerator was used for neutron production via the $^{7}Li(p,n)^{7}Be$ reaction. With a proton energy of E_p = 1912 keV the neutron spectrum resembles a Maxwell-Boltzmann distribution for kT = 25 keV, so that the effective stellar cross section can be measured directly in this spectrum. Alpha particles from the $^{33}S(n,\alpha)$ reaction were detected in a gridded ionisation chamber with internal target. The axial geometry with the sample fixed on the cathode allows for a 2Π solid angle. CF_4 is used as a counter gas to avoid energetic hydrogen recoils which could give rise to background by pulse pile-up. The chamber is operated at 200 V/cm and with 200 mb gas pressure.

With alpha sources an energy resolution of 2% was obtained, but in the neutron field this value was reduced to 3%. Under neutron irradiation two background components were observed: a rather intense low energy part corresponding to E_α < 1.8 MeV caused by neutron interactions and a relatively weak, high energy part of 0.2 counts per min and μA proton current due to the 17 MeV gamma radiation from the $^{7}Li(p,\gamma)^{8}Be$ reaction. Alpha particles from the $^{33}S(n,\alpha)^{30}Si$ reaction with energies of 3.1 MeV are well separated from the low energy background.

In order to study absorption effects, two techniques were used for the preparation of stable sulphur samples, starting from 54 mg of K_2SO_4 enriched in ^{33}S to 90.8 %. One sample with $1.6\cdot10^{16}$ ^{33}S atoms/cm^2 was produced by ion implantation into a carbon backing. The remaining K_2SO_4 was dissolved in water and dropped in a regular pattern onto freshly made layers of aluminium oxide. The thickness of the 4 samples produced in this way were between 8.1 and $15\cdot10^{16}$ ^{33}S atoms/cm^2. Of course, the effective sample thickness was considerably higher because both techniques imply strong dilution of ^{33}S in the respective host materials.

The experiment was carried out in several runs, each lasting for some hours with typical neutron fluxes of $2\cdot10^{8}$ n/sec, resulting in a total event rate of 4000 up to 20000. The cross section was measured relative to the well known $^{197}Au(n,\gamma)^{198}Au$ cross section (3). The pulse height spectrum obtained with the ionisation chamber shows a clearly resolved peak from the $^{33}S(n,\alpha)^{30}Si$ reaction (Fig. 1), but with significant tailing to lower energies due to self absorption effects in the sample.

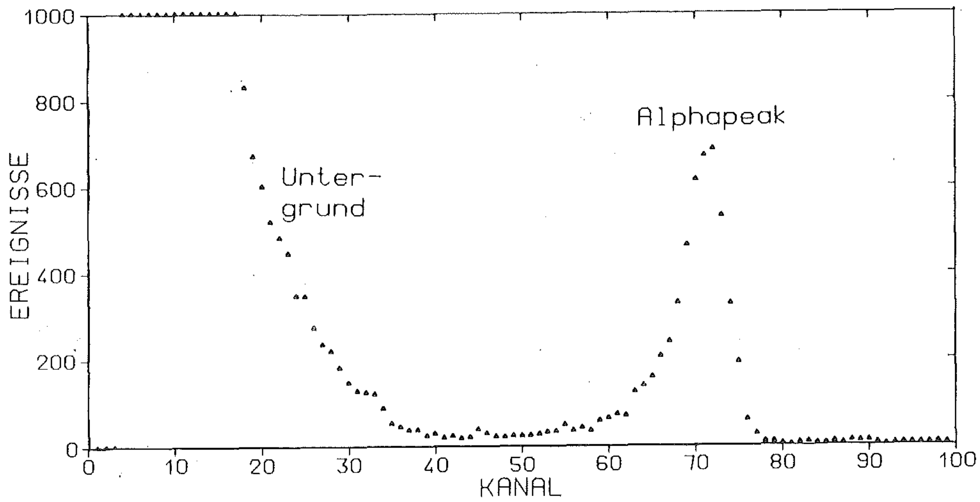

Fig. 1 Pulse height spectrum from the $^{33}S(n,p)^{30}Si$ reaction measured with the implanted sample

The efficiency was determined by extrapolating the spectrum to low pulse heights via Monte Carlo calculations. Depending on sample thickness, absorption corrections between 4 and 30% were obtained. Correspondingly, the major experimental uncertainties are due to sample effects.

For kT = 30 keV the final cross section $\langle\sigma v\rangle/v_T$ = 181 $\pm$ 10 mb is slightly smaller than the result of Wagemans et al. (2) but still in agreement within uncertainties.

A calculation with the classical s-process model shows that the observed ^{36}S abundance can be well explained as being due to the weak s-process component. This result supports the idea that ^{36}S was produced in the helium and carbon shells during hydrostatic burning in massive stars (4) under conditions similar to those required by the weak component, whereas production of ^{36}S in explosive carbon burning would imply much higher temperatures and neutron densities (5).

(1) G.F. Auchampaugh, J. Halperin, R.L. Macklin, W.M. Howard, Phys. Rev. C12 (1975) 1126

(2) C. Wagemans, H. Weigmann, R. Barthelemy, Nucl. Phys. A469 (1987) 497
(3) W. Ratynski, F. Käppeler, Phys. Rev. C37 (1988) 585
(4) F.-K. Thielemann, W.D. Arnett, Ap. J. 295 (1985) 604
(5) W.M. Howard, W.D. Arnett, D.D. Clayton, S.E. Woosley, Ap. J. 175 (1972) 201

1.1.4 β-DECAY RATE OF ^{79m}Se AND ITS CONSEQUENCES FOR THE s-PROCESS TEMPERATURE

N. Klay, F. Käppeler (1)

The branching ratio between internal electromagnetic transitions and β^- decays of the isomer ^{79m}Se was determined experimentally. Extremely clean samples of ^{78}Se were activated with thermal neutrons at a high-flux reactor. A mini-orange-Si(Li) detection system was used to measure β^- particles and conversion electrons immediately after neutron irradiation. For the β^-decay we obtain

$$\log ft = 4.70 \begin{smallmatrix} +\ 0.10 \\ -\ 0.09 \end{smallmatrix} \quad .$$

Our present result was used to recalculate the temperature dependence of the effective β^- half-life of ^{79}Se in the stellar interior. In combination with the half-life deduced from a quantitative branching analysis we obtain a possible temperature range between 182 and 295 million degrees for the weak component of the s-process.

(1) Phys. Rev. C38 (1988) 295

1.1.5 MEASUREMENT OF THE ^{85,87}Rb CAPTURE CROSS SECTIONS FOR s-PROCESS STUDIES

H. Beer, R.L. Macklin*

The present investigation provides newly measured capture cross sections of the two stable Rb isotopes. These data and other improved capture cross sections served to study the solar s-process abundances and especially the concept of a two component s-process for nuclei with mass numbers below A=90 (1, 2). From the ^{85}Kr branching, conditions about plausible pulse durations ($\Delta t \sim 3$ yr - 25 yr) of a pulsed s-process were derived.

After this phenomenological analysis the ^{85}Kr branching was used to perform calculations in the frame of the stellar AGB-models introduced by Iben (3), Iben and Truran (4), and Cosner et al. (5). These models have been discussed and questioned ever since new nuclear physics or stellar observational data became available (6-10). The present studies allowed us to give constraints for these models on the basis of more refined neutron capture cross sections.

AGB-model calculations were carried out for stars with C+O cores M_c=1.16$M_\odot$, 1.04$M_\odot$, 0.96$M_\odot$, and 0.65$M_\odot$. The time variation of the neutron bursts was given in analytic form by Cosner et al. (5), and the definition of the various parameters can be found in Iben and Truran (4). Maximum strength and duration of the pulses is essentially a function of the carbon oxygen core M_c of the red giant star, and the neutron source delivering the neutrons is the ^{22}Ne(α,n) reaction. Fig. 1 displays neutron profiles for different values of M_c.

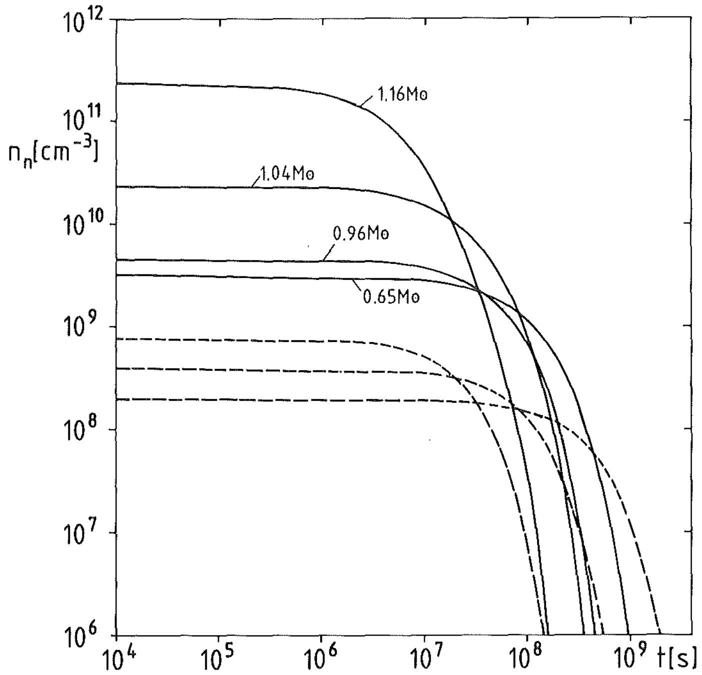

Fig. 1 The neutron density as a function of time for various AGB-models. The curves (solid lines) are labelled by M_c, the C+O core of the corresponding AGB-star. The dashed curves are artificial neutron density profiles which allowed for a reproduction of empirical data dependent on the ^{85}Kr - ^{86}Rb branchings (solar abundances and abundances in Ba stars).

Some results of our calculations are shown in Fig. 2. The AGB-models are not able to describe the solar Rb as well as Rb in Ba stars. In order to reproduce the solar s-process abundances and the abundances in Ba stars at the ^{85}Kr - ^{86}Rb branchings we can ask reversely what characteristics of the neutron pulses are required. We have carried out calculations using neutron pulses with exponential decay of the

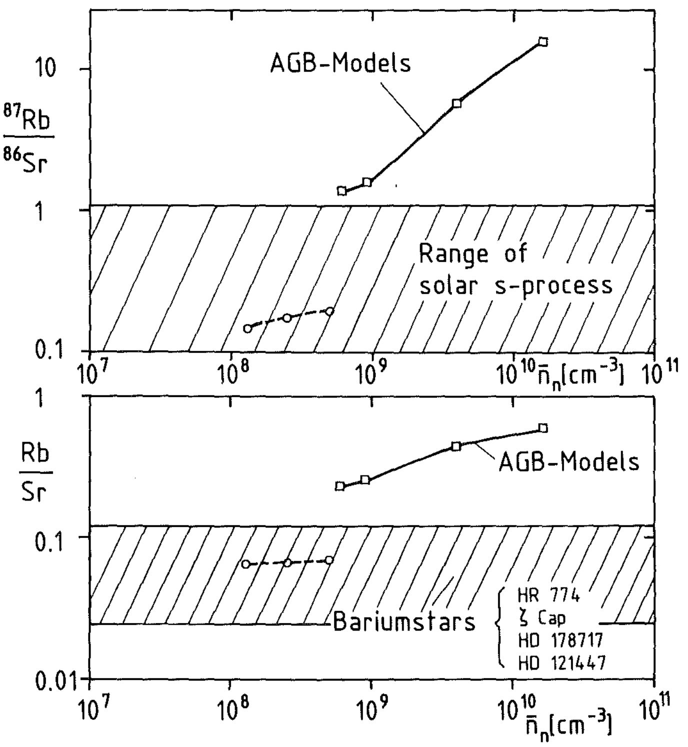

Fig. 2 Model calculations to reproduce the ratios Rb/Sr in Ba stars (below) and $^{87}Rb/^{86}Sr$ from solar abundances (above) indicated as shaded areas. The values for the various AGB-models (squares) as a function of the average neutron density of pulses is plotted. The open circles represent values, where the pulse shape was chosen so that the empirical data for Ba stars and the solar abundances are reproduced.

neutron density from an assumed maximum value. This shape of the pulse is similar to the pulse profile of the AGB-models. The curves are plotted in Fig. 1 as dashed lines. Pulses with average neutron densities and life times of $5\cdot10^8$, $2.5\cdot10^8$, $1.3\cdot10^8$ cm^{-3} and 0.69, 2.85, 11.7 yr, respectively, lead to a good agreement with the empirical data under consideration. But the constraints for the pulse conditions found from the ^{151}Sm branching (11) would allow for pulse widths not smaller than 3 yr and consequently not much greater than about $2.5\cdot10^8$cm^{-3}. Pulses with an average neutron density of $1.3\cdot10^8$ cm^{-3} and a life time of 11.7 yr would closely resemble our earlier treatment of the s-process with rectangular pulses.

(1) F. Käppeler, H. Beer, K. Wisshak, D.D. Clayton, R.L. Macklin, R.A. Ward, Ap. J. 257 (1982) 821

(2) H. Beer, 5th Moriond Astrophysics Meeting, Nucleosynthesis and its Implications on Nuclear and Particle Physics, Les Arcs, Savoie,

March 17-23, 1985, ed. J. Audouze, N. Mathieu (D. Reidel Pub. Company 1986) p. 263
(3) I. Iben, jr., Ap. J. 217 (1977) 788
(4) I. Iben, jr., J.W. Truran, Ap. J. 220 (1978) 980
(5) K. Cosner, I. Iben, jr., J.W. Truran, Ap. J. 238 (1980) L96
(6) W.M. Howard, G.J. Mathews, K. Takahashi, R.A. Ward, Ap. J. 309 (1986) 633
(7) R.A. Malaney, Ap. J. 321 (1987) 832
(8) R.A. Malaney, A.I. Boothroyd, Ap. J. 320 (1987) 866
(9) R.A. Malaney, D.L. Lambert, M.N.R.A.S 1988 (in press)
(10) I.Iben, jr., in: Astronomy in the Southern Hemisphere, ed. V.M. Blanco, M. Phillips (P.A.S.P. Press) (to be published)
(11) H. Beer, R.L. Macklin, Ap. J. 331 (1988) 1047

* Oak Ridge National Laboratory, P.O.B. X, Oak Ridge, TN 37831, USA

1.1.6 NEUTRON CAPTURE CROSS SECTIONS FOR N=50 NUCLEI

W. Zhao*, F. Käppeler, U. Ratzel

The neutron magic nuclei with N=50 are important for s-process nucleosynthesis as they act as bottle necks in the neutron capture chain due to their small (n,γ) cross sections. Therefore, these isotopes build up to large s-process abundances, which dominate the observed abundance distribution in this mass range. This means, that their cross sections are requested with good precision in order to reliably determine their s-process abundances for an unambiguous separation of s- and r-process contributions. An additional interest in this mass region comes from the fact that s-process nucleosynthesis exhibits two components, of which the so-called weak component terminates just around A = 90. The physical conditions typical for the weak component can be estimated by analysis of the s-process branchings at ^{79}Se and ^{85}Kr. The latter branching closes at A = 88, but the abundances of the weak component are strongly affected by the small cross sections at N=50 (1). Therefore, an accurate analysis can only be made, if precise cross section data are available in this mass range to separate the relative contributions from the two s-process components. Previous results led to recommended cross sections at kT = 30 keV of 6.2 ± 0.5 mb for ^{88}Sr and 21 ± 3 mb for ^{89}Y (2). The aim of this work was to remeasure these cross sections with significantly improved accuracy.

The experiments were carried out at the Karlsruhe 3.75 MV Van de Graaff accelerator via the activation technique with the ^{7}Li(p,n)^{7}Be reaction as the neutron source. In this way, the samples could be irradiated in a quasi-stellar neutron spectrum for kT = 25 keV. The neutron flux determination was based on the gold standard cross section. As both

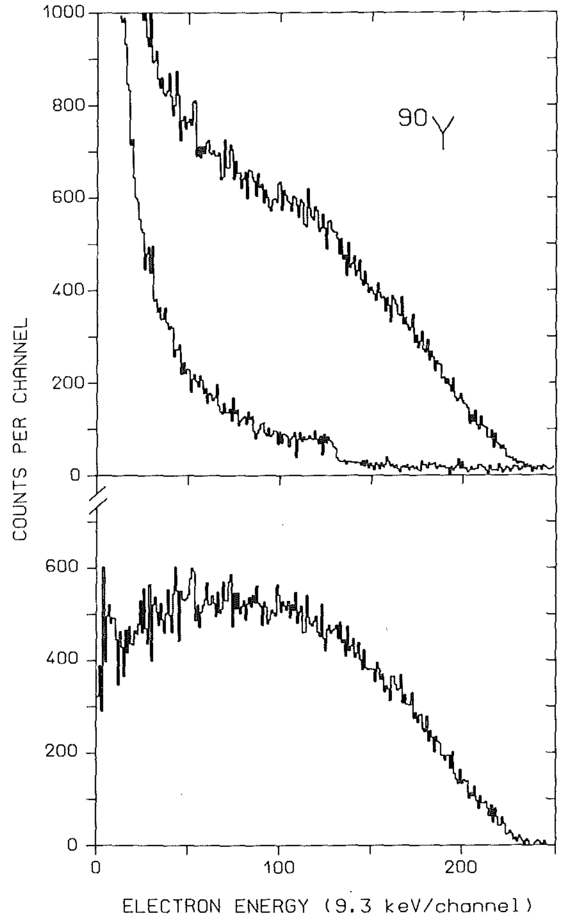

Fig. 1 The electron spectrum measured in the 4π Si(Li) spectrometer after activating a 1 mg/cm^2 thick Y_2O_3 sample for ~ 70 h.

product nuclei, ^{89}Sr and ^{90}Y beta decay to the ground states of their daughters, the induced activity could only be measured by detecting the emitted electrons. This was achieved by two Si(Li) detectors in close geometry, which covered 95% of 4π thus minimizing spectrum distortions due to electron backscattering. Fig. 1 gives an example for the signal/background ratio obtained for an activation of ^{89}Y. Corrections and systematic uncertainties were studied by repeated activations under modified experimental conditions. It will therefore be possible, to give the new cross sections with a precision of ±3%, which may finally help to decide between possible alternatives for the description of the weak s-process component (3).

(1) F. Käppeler, H. Beer, K. Wisshak, D.D. Clayton, R.L. Macklin, R.A. Word, Ap. J. 257 (1982) 821

(2) Z.Y. Bao, F. Käppeler, Atomic Data and Nuclear Data Tables 36 (1987), 411

(3) H. Beer, G. Walter, F. Käppeler, Report KfK 4508, contr. 1.1.14

* On leave from the Institute of Atomic Energy, Beijing, China

1.1.7 s-PROCESS STUDIES ON TIN

H. Beer, G. Walter*, F. Käppeler

The determination of s- and r-process contributions in the mass region of tin with the existing capture cross sections (1) and solar abundances (2) shows systematic deviations outside the quoted uncertainties. The empirical $\sigma N(^{116}Sn)$ value lies significantly above the theoretical $\sigma N(A)$ curve adjusted by means of the other s-only isotopes (Fig. 1). The r-process abundances of $^{117,119}Sn$ and $^{118,120}Sn$, respectively, are definitely higher than the neighbouring odd and even isotopic r-process abundances (Fig. 2). The question arises whether these deviations from the smooth s- and r-process distributions are simply due to systematically too high solar tin abundances or whether they represent a genuine discrepancy from the current concept of nucleosynthesis.

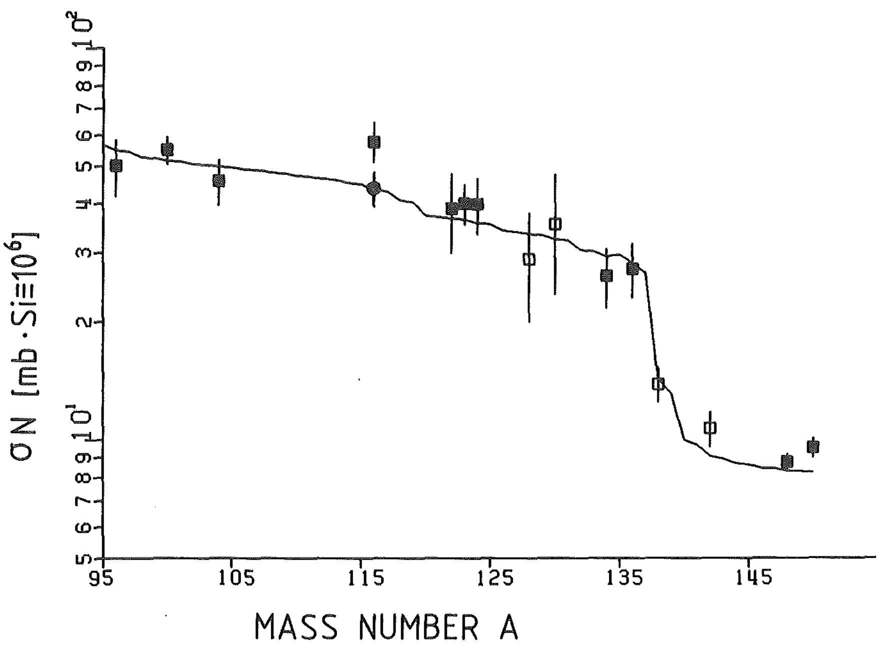

Fig. 1 The product of cross section times s-process abundance as a function of mass number in the range A = 92 to 150. The solid line is a least squares fit to the empirical data (full black quadrangles). For ^{116}Sn the value normalized to the curve is given as a full black circle.

In order to investigate this problem we have remeasured the neutron capture cross section of ^{116}Sn to exclude a possible error in this important parameter. The measurement confirmed essentially the previous capture result of (1) with improved accuracy. This could mean

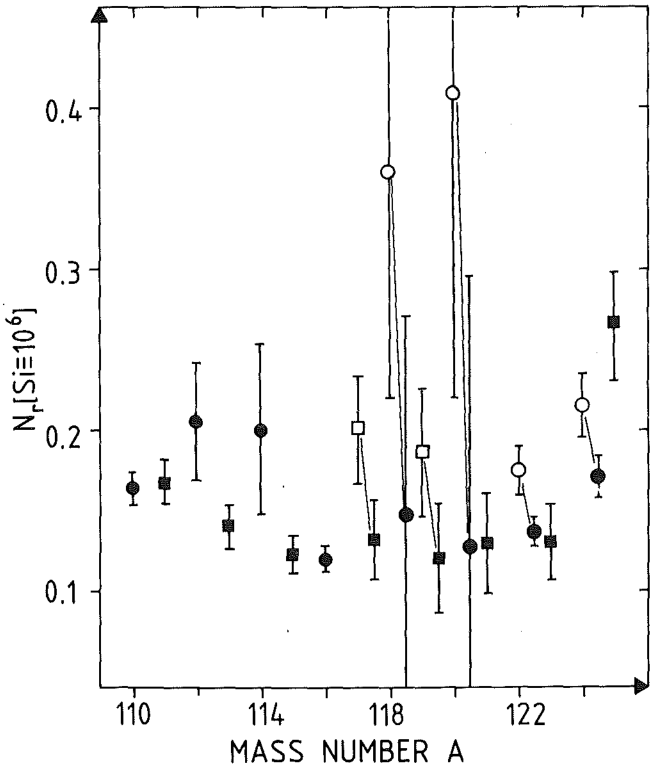

Fig. 2 r-process residuals as a function of mass number A. The even isotopes are indicated by circles, the odd isotopes by squares. The tin isotopes are represented by two data sets, one calculated with the solar tin abundance from Anders and Grevesse (open symbols), the other calculated with the tin abundance normalized to the σN systematics black symbols).

that possibly the solar abundance of tin quoted by Anders and Grevesse (2) is too high. Normalizing tin via ^{116}Sn to the σN curve by a reduction of Anders and Grevesse's value by 23% (Fig. 1) also removes the deviations in the r-process distribution (Fig. 2). This fact was taken as strong evidence that the solar tin abundance determined from meteorites has to be lowered by 23%. Further evidence that such a reduction might be correct is the lower but highly doubtful abundance value measured from the spectrum of the sun.

(1) R.L. Macklin, J.H. Gibbons, Ap .J. 149 (1967) 577

(2) E. Anders, N. Grevesse, Geochim. et Cosmochim. Acta (in press)

* Firma Bosch, Reutlingen

1.1.8 THE ^{151}Sm BRANCHING, A PROBE FOR THE IRRADIATION TIME SCALE OF THE s-PROCESS

H. Beer, R.L. Macklin* (1)

The excitation functions for the reactions $^{152,154,155,157}Gd(n,\gamma)$ have been measured over the neutron energy range of 3 keV to 500 keV. Maxwellian averaged capture cross sections for thermal energies kT=5-100 keV have been calculated. At kT=30 keV we have found: $\sigma(^{152}Gd)=1003\pm30$ mb, $\sigma(^{154}Gd)=878\pm27$ mb, $\sigma(^{155}Gd)=2721\pm90$ mb, $\sigma(^{157}Gd)=1355\pm39$ mb. The data, in conjunction with other cross sections and solar abundances, were used to carry out an s-process analysis of the branchings in the Sm to Gd mass range. The s-process is treated in the classical as well as in the pulsed model. The solution of the classical model is contained in the pulsed model as the asymptotic solution for large pulse widths. It is shown that this solution is the only one which can reproduce the abundance pattern of the different branchings. Pulse durations are limited to values larger than about 3 yr.

(1) Astrophysical Journal (in press)

* Oak Ridge National Laboratory, P.O.B. X, Oak Ridge, TN 37831, USA

1.1.9 THE PARTIAL CROSS SECTION $^{175}Lu(n,\gamma)^{176m}Lu$

W. Zhao*, F. Käppeler, U. Ratzel

In connection with the many efforts to understand the s-process production of ^{176}Lu and its potential interpretation as a cosmic clock or as a stellar thermometer (1 - 5) it seemed worth to remeasure the partial cross section for $^{175}Lu(n,\gamma)^{176m}Lu$. This reaction populates the short-lived isomeric state ^{176m}Lu which decays with 3.7 h half-life to ^{176}Hf. Hence, in first approximation (5) this fraction would be lost for the surviving, long-lived fraction of ^{176g}Lu that is still observed today and that has been used to estimate an age for the s-process elements.

Previous measurements have reported discrepant results for this cross section at kT = 25 keV, ranging from 962 ± 54 (1) to 1071 ± 52 (6) and 1244 ± 55 mb (7). All these experiments made use of the activation technique with gold as a cross section standard, and detecting the associated gamma-ray activities. For the decay of ^{176m}Lu, the only suitable gamma line stems from the 88.35 keV transition in ^{176}Hf. In order to avoid the sizeable self-absorption correction in the detection of this low-energy line and to approach the problem in an independent way, the new measurement was based on the detection of the electrons emitted in beta decay. With the 4π beta spectrometer mentioned in (8), the induced ^{176m}Lu activity could be determined practically background-free. In total, 5 activations were carried out with the relevant experimental parameters modified to study the respective systematic uncertainties.

In addition, a sixth activation was performed as in the previous measurements, using relatively thick samples and detecting the 88.35 keV gamma-rays. Good agreement was found between the two methods, yielding a partial cross section of 1135 ± 30 mb. This value represents about 88% of the total capture cross section of ^{175}Lu, in contrast to thermal energies, where an isomeric ratio of σ_p/σ_{tot} = 0.70 is reported, but in agreement with the (n,γ)-studies of Klay et al. (4, 5), who showed that at most 15% of the observed gamma transitions feed the ground state of ^{176}Lu.

The rather large isomeric ratio of 0.88 implies, however, that thermally induced transitions in the stellar plasma must have occurred in ^{176}Lu on a time scale shorter than the 3.68 h half-life of the isomer. On average, these transitions must have fed the ground state in order to explain the ^{176}Lu abundance observed today. Whether these processes can be understood quantitatively depends on the details of the level scheme of ^{176}Lu and the respective transition probabilities, as is discussed in the following contribution (5).

(1) H. Beer, F. Käppeler, Phys. Rev. C21, (1980) 534
(2) H. Beer, F. Käppeler, K. Wisshak, R.A. Word, Ap. J. Suppl. 46 (1981) 295
(3) H. Beer, G. Walter, R.L. Macklin, P.J. Patchett, Phys. Rev. C30 (1984) 464
(4) N. Klay, H. Beer, H. Börner, F. Hoyler, F. Käppeler, B. Krusche, S. Robinson, G. Schatz, K. Schreckenbach, Report KfK 4405 (1988) 7
(5) N. Klay, H. Börner, F. Käppeler, H.Beer, G. Schatz, B. Krusche, S. Robinson, F, Hoyler, K. Schreckenbach, U. Mayerhofer, T. v. Egidy, G. Hlawatsch, Report KfK 4508, contr. 1.1.10
(6) B.J. Allen, G.C. Lowenthal, J.R. de Laeter, J. Phys. G 7 (1981) 1271
(7) B.J. Allen, G.C. Lowenthal, J.W. Boldeman, "Neutron Capture Gamma-Ray Spectroscopy and Related Topics 1981", Inst. Phys. Conf. Ser. No. 62 (1982) 573
(8) W. Zhao, F. Käppeler, U. Ratzel, Report KfK 4508, contr. 1.1.6

* On leave from the Institute of Atomic Energy, Beijing, China

1.1.10 AN IMPROVED LEVEL SCHEME OF ^{176}Lu

N. Klay, H. Börner*, F. Käppeler, H. Beer, G. Schatz, B. Krusche*, S. Robinson*, F. Hoyler*, K. Schreckenbach*, U. Mayerhofer**, T. v. Egidy**, G. Hlawatsch**

Nuclear spectroscopy of ^{176}Lu is facing two difficulties: 1. The high level density and large number of corresponding γ-transitions require high resolution measurements. 2. The first excited state is an isomer with $I^{\pi} = 1^{-}$ and the deexciting E6 γ-transition to the $I^{\pi} = 7^{-}$ ground state is not observed, but only the β decay to ^{176}Hf. The excitation energy of the isomer can therefore only be deduced from β-endpoint energies and Q-values via charged particle transfer reactions. On the other hand, precise knowledge of this energy is a key for the establishment of a complete level scheme. The first reliable determination of this quantity was carried out by Minor et al. (1) who found E = 126.5 keV. This value was used in their level scheme and also in the more comprehensive work of Balodis et al. (2), who investigated the level scheme by means of high resolution (n,γ) and (n,e) measurements. However, Balodis et al. (2) assigned only γ-transitions to levels, which decay into the isomer. Energy levels, which decay into the ground state have only been observed by Coulomb-excitation studies (3, 4) and in a (t,α)-measurement (5), which led to an extension of the level scheme. Nevertheless, the assignment of neutron capture γ-rays to levels related to the ground state was still ambiguous and no level was known, which decayed both into the ground state and the isomer.

Such intermediate levels will presumably have K-quantum numbers between the extreme values K=7 for the ground state and K=0 for the isomer. From the earlier measurements (1-6) and from model considerations (6), these levels are expected at excitation energies above ~ 600 keV. We therefore performed (n,γ) and (n,e) studies for γ-ray energies up to more than 1 MeV (7, 8) using the crystal spectrometers GAMS1/2/3 and the magnetic spectrometer BILL at the ILL Grenoble. We identified 450 definite γ-transitions in ^{176}Lu and ~100 weak or questionable transitions. Multipolarities could be derived for 250 of the transitions.

An additional study of the (d,p) transfer reaction was performed at the TU München. With the high resolution of this facility, the measured (d,p)-spectrum could be used for a good determination of the excitation energy of the isomer. From the peak distance between the isomer and the

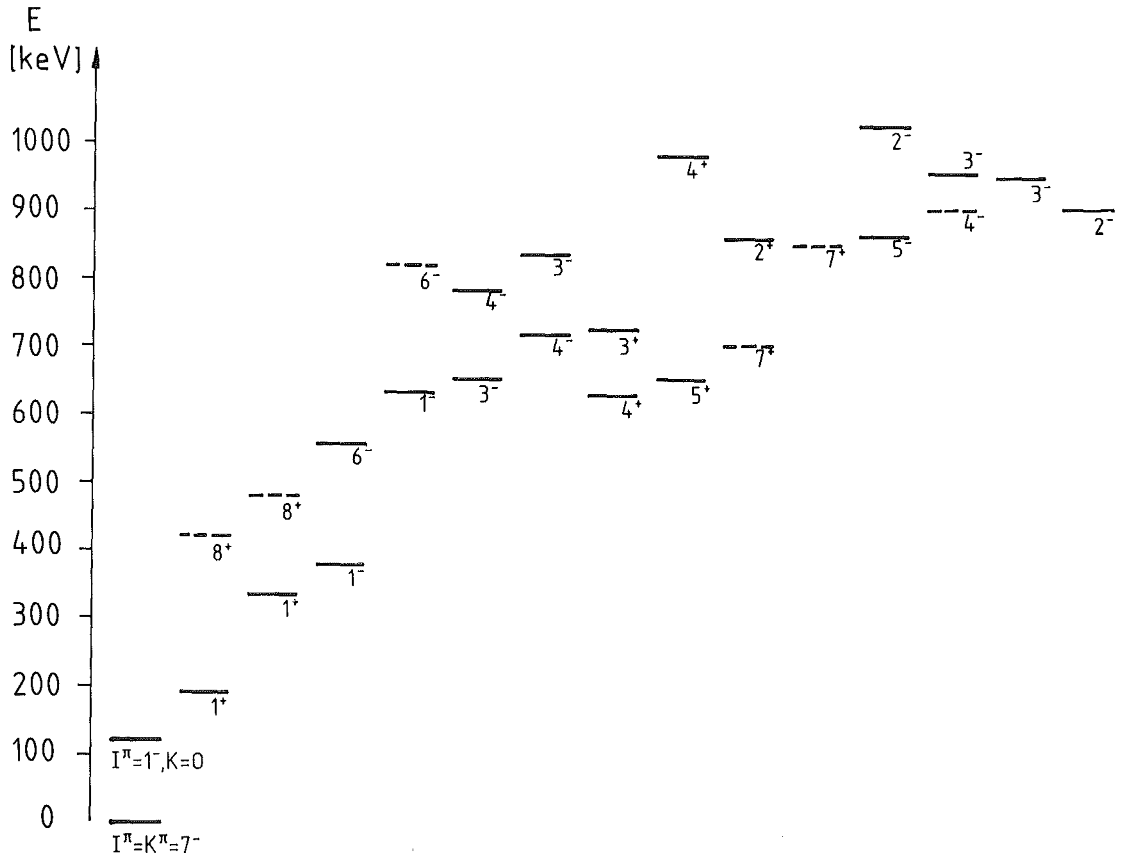

Fig. 1 Energies of rotational bandheads in ^{176}Lu. Parity and K-quantum number are designated for each level. For the $K^{\pi}=0^{-}$ band the $I^{\pi}=1^{-}$ isomeric state is drawn instead of the $I^{\pi}=0^{-}$ bandhead. Less well established levels are given by dashed lines.

8^{-} level of the ground state band, for which the energy is well known (4), we derived the value E=(122.9±0.4) keV.

Another advantage of the (d,p) reaction is, that two rotational bands with K=3^{-} and K=4^{-} are strongly populated. A comparison with the (n,γ) and (n,e) results shows that both band heads decay into the isomer. For the $I^{\pi}=5^{-}$ state of the $K^{\pi}=4^{-}$ band, however, only two very weak γ-transitions corresponding to the level system based on the isomer are found. A reasonable intensity for the depopulation of this state is only obtained by the assignment of additional transitions to the ground state. With this assignment, the energy relationship between ground state and isomer is fixed and the energy of the 1^{-} isomeric state can be determined to E= (122.843±0.017) keV. This result is in perfect agreement with the energy, which is obtained in a completely different way from the (d,p) spectrum as mentioned above. As a result of the fixed energy relationship, several additional weak γ-transitions can be assigned as links between the two level systems based on ground state and isomer, respectively.

The level scheme of ^{176}Lu obtained in the present study contains more than 80 levels. In Fig. 1 all experimentally determined rotational bandheads are shown. Comparision with a semiempirical theoretical model (6) shows that below ~ 950 keV practically all predicted bandheads between K=1 and K=8 could be established or at least be proposed. The average deviation in the bandhead energies is about 60 keV.

It is planned to complete this study with a measurement of γ-γ-coincidences which should provide additional confidence for large parts of the level scheme.

(1) M.M. Minor, R.K. Sheline, E.B. Shera, E.T. Jurney, Phys. Rev. 187 (1969) 1516

(2) M.K. Balodis, J.J. Tambergs, K.J. Alksnis, P.T. Prokofjev, W.G. Vonach, H.K. Vonach, H.R. Koch, U. Gruber, B.P.K. Maier, O.W.B. Schult, Nucl. Phys. A 194 (1972) 305

(3) Th. Elze, priv. communication

(4) M. Déléze, A. Bruder, S. Drissi, J. Kern, G.L. Struble, Phys. Rev. C36 (1987) 1826

(5) R.A. Dewberry, R.K. Sheline, R.G. Lanier, L.G. Mann, G.L. Struble, Phys. Rev. C24 (1981) 1628

(6) R.W. Hoff, R.F. Casten, M. Bergoffen, D.D. Warner, Nucl. Phys. A437 (1985) 285

(7) N. Klay, H. Beer, H. Börner, F. Hoyler, F. Käppeler, G. Schatz, K. Schreckenbach, Report KfK 4159, Kernforschungszentrum Karlsruhe (1986) p. 7

(8) N. Klay, H. Beer, H. Börner, F. Hoyler, F. Käppeler, B. Krusche, S. Robinson, G. Schatz, K. Schreckenbach, Report KfK 4405, Kernforschungszentrum Karlsruhe (1987) p. 7

* Institut Laue - Langevin, Grenoble, France

** TU München

1.1.11 NEUTRON CAPTURE CROSS SECTION OF ^{197}Au: A STANDARD FOR STELLAR NUCLEOSYNTHESIS

W. Ratynski*, F. Käppeler (1)

We have measured the neutron capture cross section of gold using the ^{7}Li(p,n)^{7}Be reaction for neutron production. This reaction not only provides the integrated neutron flux via the ^{7}Be activity of the target, but also allows for the simulation of a Maxwellian neutron energy spectrum at kT=25 keV. As this spectrum is emitted in a forward cone of 120° opening angle, the cross section can be measured in good geometry and independent of any other standard. Systematic uncertainties were studied experimentally in a series of activations. The final stellar cross section at kT=25 keV was found to be 648 ± 10 mb, and extrapolation to the common s-process temperature kT=30 keV yields 582 ± 9 mb. This result is used for renormalization of a number of cross sections which had been measured relative to gold.

(1) Phys. Rev. C37 (1988) 595

* Institute for Nuclear Studies, Swierk, Poland

1.1.12 THE ^{208}Pb(n,γ) CROSS SECTION AND THE TERMINATION OF THE s-PROCESS

U. Ratzel, H. Beer, F. Käppeler

For a study of nucleosynthesis at the end of the s-process path the cross section for the reaction ^{208}Pb(n,γ)^{209}Pb was measured at kT=25 keV via the activation technique. As ^{209}Pb beta decays directly to the ground state of ^{209}Bi (Q_β=640 keV, $t_{1/2}$ = 3.25 h) without emission of gamma rays, it was necessary to detect the electrons from beta decay. This was achieved by a Si(Li)-spectrometer with high efficiency (~ 95%) and low background (≤ 0.5 cps in the energy range from 15 - 1000 keV), which was sufficiently sensitive for beta activities down to ≃ 0.2 - 0.5 Bq. Fig. 1 shows the beta spectrum of ^{209}Pb measured after activation of a 4.9 mg/cm^2 thick ^{208}Pb sample.

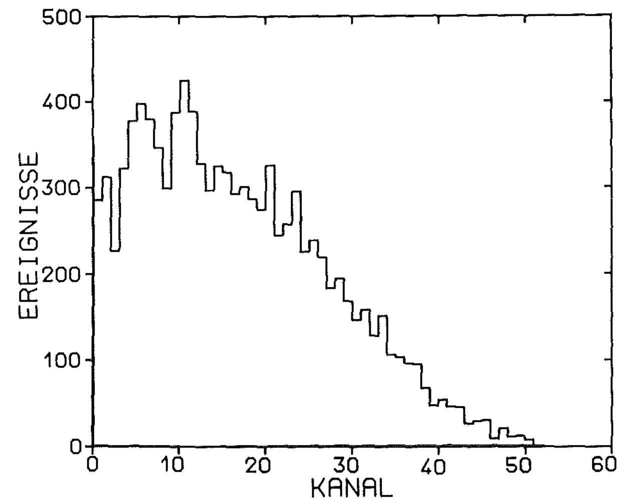

Fig. 1 Beta spectrum of ^{209}Pb (average activity 0.46 Bq) after background subtraction.

The correction for electron self-absorption was studied by variation of the sample thickness between 1 and 5 mg/cm^2. The resulting cross section for kT=30 keV of 0.36 ± 0.03 mb is significantly smaller than the value reported by Allen et al. (1973) and by Macklin et al. (1977) who quoted 0.75 and 0.6 mb, respectively. Compared with the previous results it was possible to improve the accuracy from ~25 to ± 6%.

For describing the observed abundance of the lead isotopes and of bismuth, it seemed necessary to introduce a so-called strong component in addition to the main s-process component that accounts for the abundances in the mass range between A=90 and ≈204. This strong component is characterized by a large time-integrated neutron exposure and a small seed abundance. It, therefore, contributes only in the mass region $A \geq 204$ (Beer and Macklin 1984).

As the parameter for the strong component depends sensitively on the ^{208}Pb cross section, our new value allowed for a reanalysis with improved reliability. However, there remain two concerns which both result essentially from the adopted lead abundance:

(i) Based on the s-process contribution to the observed abundances of the lead isotopes and with an appropriate correction for the r-process abundances it is possible to determine the radiogenic component of ^{207}Pb. This component being the decay product of ^{235}U can be interpreted as a clock for the age of the r-process. In terms of current chronologic models (Clayton 1987) the above result leads to unrealistically high ages.

(ii) It turns out, that the strong s-process component yields a significant contribution only for the abundance of ^{208}Pb.

These results hold, if the lead abundance is derived from σN systematics via the s-only isotope ^{204}Pb or from meteoritic analyses. A quite different situation occurs, however, if a new and much smaller lead abundance is considered, which was obtained from the solar photosphere (Grevesse and Meyer 1985). The discrepancy between this result and the σN-systematics can be removed if it is assumed that the s-process path branches at ^{205}Tl, i.e. that the half-life of ^{204}Tl is not reduced under stellar conditions. Though the difference to the meteoritic abundance remains unexplained, the lower lead abundance would help to solve the problems mentioned above: The ^{207}Pb - ^{235}U pair yields an age for the r-process of 10 ± 10 Gy (at least not in contradiction to the largest galactic ages obtained with astronomical methods), and the contribution of the strong component to the ^{208}Pb abundance is reduced from 40 ± 15 to 20 ± 16%.

Further studies are required before the abundances in the mass region 200<A<209 can be finally understood. Most important from the nuclear physics side is the question of the stellar beta half-life of ^{204}Tl. In this context it would be most useful to determine the yet uncertain spin and parity assignment for the first excited states in ^{204}Tl (Schmorak 1987).

(1) B.J. Allen, R.L. Macklin, R.R. Winters, C.Y Fu, Phys. Rev. C8, (1973)

(2) H. Beer, R.L. Macklin, Phys. Rev. C 32 (1984) 738

(3) D.D. Clayton, subm. to Monthly Not. of the Royal A. Soc.

(4) N. Grevesse, J.P. Meyer, 19th Int. Cosmic Ray Conf., La Jolla, 1985

(5) R.L. Macklin, J. Halpenin, R.R. Winters, Ap.J. 217 (1977) 222

(6) M.R. Schmorak, Nucl. Data Sheets 50 (1987) 719

1.1.13 CHRONOMETERS *

H. Beer

The existence of long lived radioactive isotopes suggests that the chemical elements have been made at some finite time. For the heavy elements this production is assumed to take place in stars. Therefore, the abundances of the long lived radionuclides are related to the history of the stars in our Galaxy. These isotopes represent potential cosmic clocks to estimate the age of the Galaxy.

The investigation of these cosmochronometers requires information about their nuclear properties and their fate during the chemical evolution of the Galaxy. In the most simple chemical evolution model (Fowler's exponential model) a two parameter adjustment (the age and an initial galactric enrichment in heavy elements) requires at least two reliable cosmic clocks (1). Necessary condition for the reliability is a well-known formation process (s- or r-process nucleosynthesis) which allows for a calculation of the abundance the chronometric isotope would have if it were stable.

The reliability of the isotopes ^{87}Rb, ^{186}Lu, ^{187}Re, ^{235}U, ^{238}U and ^{232}Th as cosmic clocks was discussed. It turned out that already the nuclear properties of these nuclides limit their application as cosmochronometers.

Crucial effects in this sense are the temperature sensitivity of the beta half-life [^{176}Lu, ^{187}Re] (2,3,4), excited state capture [^{187}Re] (5) and beta delayed fission [$^{235,238}U$, ^{232}Th] (6). Additionally the uncertainties in the involved capture cross sections and solar abundances are essential [^{87}Rb, ^{235}U, ^{187}Re] (7, 8, 9).

The use of more elaborate chronological models than Fowler's exponential model leads to an increase in the determined age (10, 11).

(1) W.A. Fowler, Q. Il. R. Astron. Soc. 28 (1987) 87
(2) H. Beer, G. Walter, R.L. Macklin, P.J. Patchett, Phys. Rev. C30 (1984) 464
(3) N. Klay, H. Beer, H. Börner, F. Käppeler, G. Schatz, B. Krusche, Spring Meeting Groningen 1987 (Verhandlungen PPG) D-3.5
(4) K. Yokoi, K. Takahashi, M. Arnould, Astron. & Astrophys. 117 (1983) 65
(5) R.L. Herschberger, R.L. Macklin, M. Balakrishnan, N.W. Hill, M.T. McEllistrom, Phys. Rev. C28 (1983) 2249
(6) F.K. Thielemann, J. Metzinger, H.V. Klapdor, Z. Phys. 309 (1983) 301
(7) D.D. Clayton, Ap. J. 139 (1964) 637
(8) H. Beer, R.L. Macklin, Phys. Rev. C32 (1985) 738
(9) R.R. Winters, R.L. Macklin, Phys. Rev. C25 (1982) 208
(10) J.J. Cowan, F.K. Thiedemann, J.W. Truran, Ap. J. 323 (1987) 543
(11) D.D. Clayton, Montly Notices R. Astron. Soc. (in press)

* Talk given at the Int. Workshop on Quests in Nucl. Astrophysics and Experimental Approaches, Crete, June 1988

1.1.14 s-PROCESS STUDIES; THE WEAK COMPONENT

H.Beer, G. Walter, F. Käppeler

The s-process analysis of the elements on the iron slope (56 < A < 90) requires a superposition of two nucleosynthetic components (1). An extra weak s-process component is added to the component which describes the elements A=90-200 alone. In this work the reproduction of the abundances of isotopes A=56-90 is tested with two different models for this weak s-process; an s-process with an exponential exposure distribution, and an s-process with a single exposure. The former s-process is supposed to occur in the shell of intermediate mass asymptotic giant branch (AGB) stars (2), the latter is associated with core He burning of massive stars (3).

For the adjustment of the astrophysical parameters (seed abundance, exposure) the capture cross sections of the two s-only isotopes ^{70}Ge and ^{76}Se are of crucial importance. The capture cross section of ^{76}Se has been measured presently; that of ^{70}Ge was determined previously (4).

The analysis shows that a consistent fit of solar abundances from A=56 to 90 is only possible with the assumption of a single exposure s-process for the weak component. The other model leads to strong overproduction of individual isotopes.

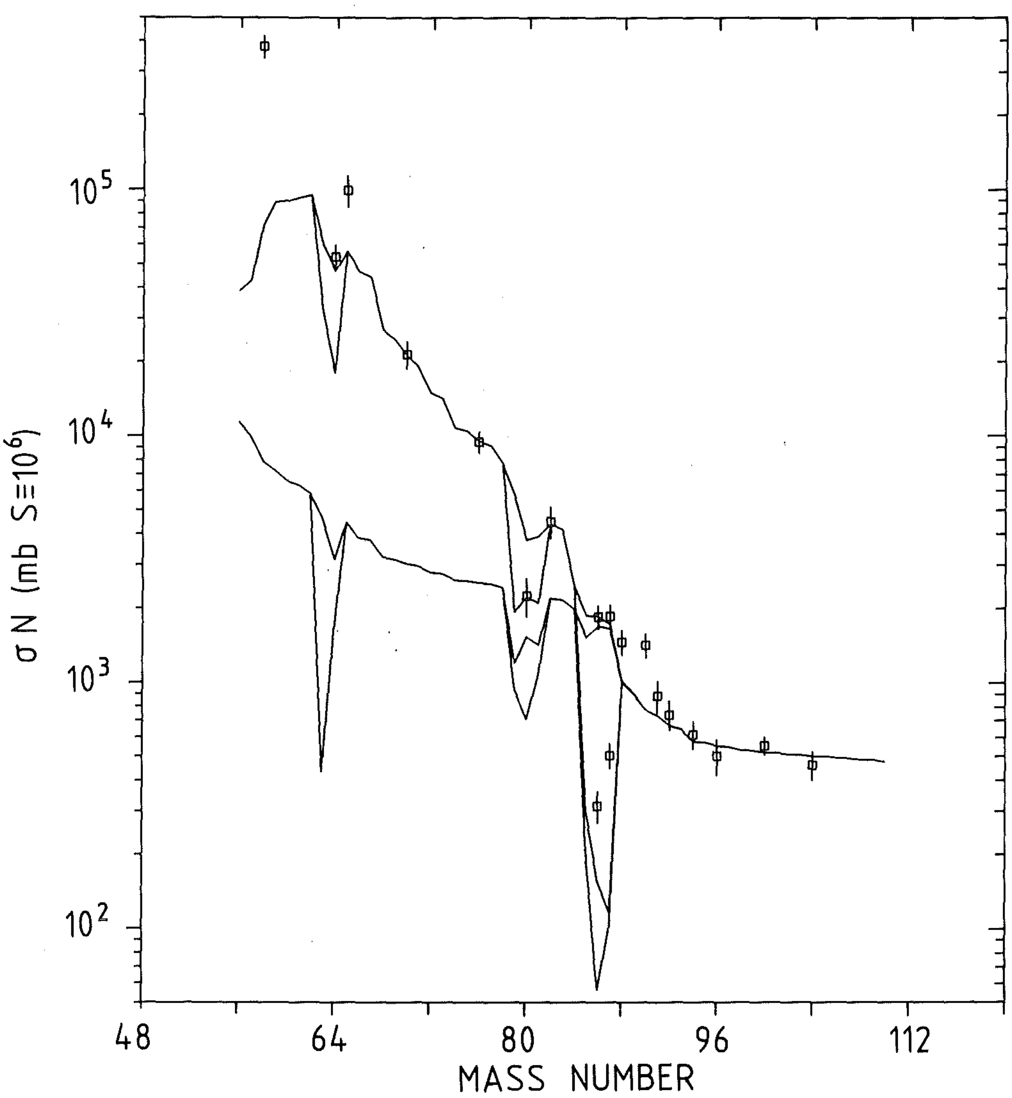

Fig. 1 The product capture cross section and abundance as a function of mass number. The empirical data (squares) are described by a superposition of two s-process components (weak component + main component). The composite curve is adjusted to the data points at ^{70}Ge and ^{76}Se. The contribution of the main component is represented by the lower curve.

Fig. 1 shows a fit of the nuclei from ^{56}Fe to ^{94}Zr assuming a superposition of the single exposure weak component and the main component which reproduces the bulk of the isotopes from A=94 to 200 alone. The contribution of this main component below A=94 is indicated in addition to the composite curve. For the description of the abundance pattern in the ^{85}Kr branching, the main component has to be a pulsed s-process.

The adjustment of the single exposure s-process to the empirical data points of ^{70}Ge and ^{76}Se requires an exposure

$$\tau = (0.23 \pm 0.03)\sqrt{\frac{kT}{30}}\ \text{mb}^{-1}$$

and an iron seed $N(^{56}Fe)$ / $N_\odot(^{56}Fe) = 0.0026 \pm 0.0014$. In addition the solar Kr abundance would be determined via s-only ^{82}Kr to be $N_\odot(Kr) = (45\pm6)/10^6$ Si.

(1) F. Käppeler, H. Beer, K. Wisshak, D.D. Clayton, R.A. Ward, Ap. J. 257 (1982) 821
(2) I. Iben, jr., Ap. J. 217 (1977) 788
(3) N. Prantzos, M. Arnould, J.P. Arwragi, Ap. J. 315 (1987) 209
(4) G. Walter, H. Beer, Astron. & Astrophys. 142 (1985) 268

1.1.15 s-PROCESS AND SOLAR ABUNDANCES

H. Beer (1)

The origin and distribution of the heavy elements (A>56) are attributed to a large extent to s-process nucleosynthesis. Structures from the s-process are clearly visible in the distribution of solar abundances. It is shown that the s-process abundances are a superposition of different s-process components which are distinguished both by the character and strength of the neutron exposure. An exponential exposure distribution with pulsed irradiations and single flux exposures for the beginning and termination of the s-process path yielded the best reproduction of the s-only isotopes. An important prerequisite for the analysis in these terms is a reliable input data basis, especially of the neutron capture rates of all nuclei on the synthesis path. Special cases are discussed in connection with their interrelation with the calculations. Solar abundances of heavy elements are classified and decomposed into its s- and r-process contributions. s-process branchings are examined because of their crucial role in elucidating the nature of the irradiations.

(1) "ORIGIN AND DISTRIBUTIONS OF THE ELEMENTS" ACS Nuclear Chemistry and Technology Division, 31. August - 4. September 1987 New Orleans, La., USA, ed. G.J. Mathews. World Scientific, Singapore, New Jersey, Hong Kong

1.1.16 NUCLEAR EXCITATION AND STELLAR TEMPERATURE

F. Käppeler (1)

The chemical elements in nature are the products of stellar burning processes. If the underlying nuclear physics is sufficiently known, it may be possible to decipher the respective nucleosynthesis mechanisms, e.g. the production of the heavy elements by slow neutron capture (s-process).

The observed abundance patterns can be strongly affected by temperature because beta decay rates and capture cross sections may become temperature dependent via significant population of excited nuclear states in the hot stellar photon bath; in turn, this allows to derive estimates for the temperature. The status of such analyses is presented with particular emphasis on the example of ^{79}Se. The results of the (empirical) classical model constitute important constraints for stellar models of helium burning zones in Red Giant stars.

The long-lived radioisotope ^{176}Lu represents a potential cosmic clock for the age of the s-process elements. For some time it is suspected that the decay of ^{176}Lu was temporarily enhanced and that this clock is therefore misadjusted. In spite of several attempts, this enhancement is not yet understood quantitatively.

(1) Inst. Phys. Conf. Ser. No. 88 / J. Phys. G: Nucl. Phys. 14 Suppl., (1988) S 297

1.1.17 EXPERIMENTAL STUDIES OF THERMAL EFFECTS DURING s-PROCESS NUCLEOSYNTHESIS

F. Käppeler (1)

Two recent experimental studies are reported which contribute to our understanding of the temperature during the s-process as well as to possible thermal effects on beta decay life-times.

(i) The determination of the temperature characteristic for the weak s-process component depends critically on the beta decay half-life of the isomeric state in ^{79}Se. A first measurement of this half-life is presented and the implications for the s-process are discussed.

(ii) In a second experiment we investigate the mechanism by which the ground state and the isomeric state in ^{176}Lu might be thermally equilibrated. This problem is the key to a possible interpretation of ^{176}Lu as a cosmic clock. As direct transitions between the long-lived ground state ($t_{1/2}$=3.6·10^{10}y) and the 3.7h isomer are strongly forbidden, equilibration may occur through thermally populated states at higher excitation. Branchings in the decay of these excited states to the ground state and to the isomer as well are searched for by high resolution gamma-ray spectroscopy at the ILL high flux reactor in Grenoble.

(1) Lecture Notes in Physics: Nuclear Astrophysics, eds. W. Hillebrand, R. Kuhfuß, E. Müller, J.W. Truran (Springer: Berlin 1987) p. 79

1.1.18 FIRST TEST MEASUREMENTS WITH THE KARLSRUHE 4Π BaF_2 DETECTOR

K. Wisshak, K. Guber, F. Käppeler, G. Rupp, H. Müller, F. Voß

The Karlsruhe 4Π BaF_2 detector has been completed by the end of 1987. Extensive test measurements have been carried out to study the energy and time resolution as well as the efficiency for gamma-rays using gamma-ray sources. During the first runs at the neutron beam, the individual background components were studied, and the neutron collimator was optimized. First cross section measurements have been performed on the monotopic elements niobium, tantalum and rhodium relative to gold as a standard.

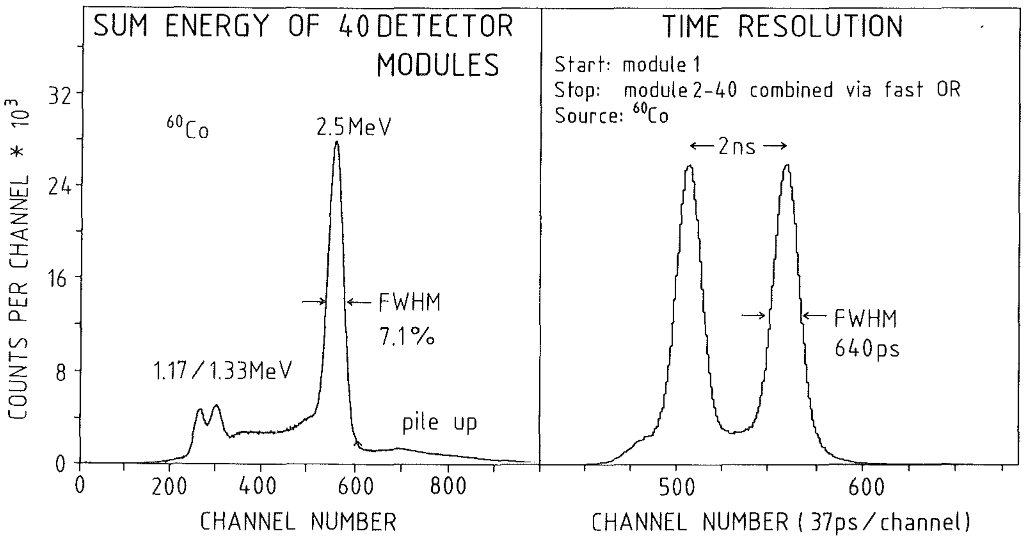

Fig. 1 Gamma-ray energy and time resolution of the total detector (with 40 out of 42 modules, ^{60}Co source).

Examples for the efficiency as well as gamma-ray and time resolution of the 4Π detector are given in Fig. 1. All measurements were made with a ^{60}Co source and with 40 instead of 42 detector modules.

Correspondingly, only a solid angle of 95% of 4Π was covered by active crystals, leading to a 5% intensity of the individual lines compared to 90% in the sum peak. The observed energy resolution of 7.1% is slightly worse than expected from the average resolution of the individual modules. This difference is mainly due to the limited resolution of the gain stabilization as the high voltage supply for the photomultipliers can only be changed in steps of 1 V. A time resolution of 640 ps was measured for one reference module versus the rest of the detector, indicating a time resolution of 500 ps for the total detector. This value impressively illustrates the outstanding timing properties of BaF_2 crystals.

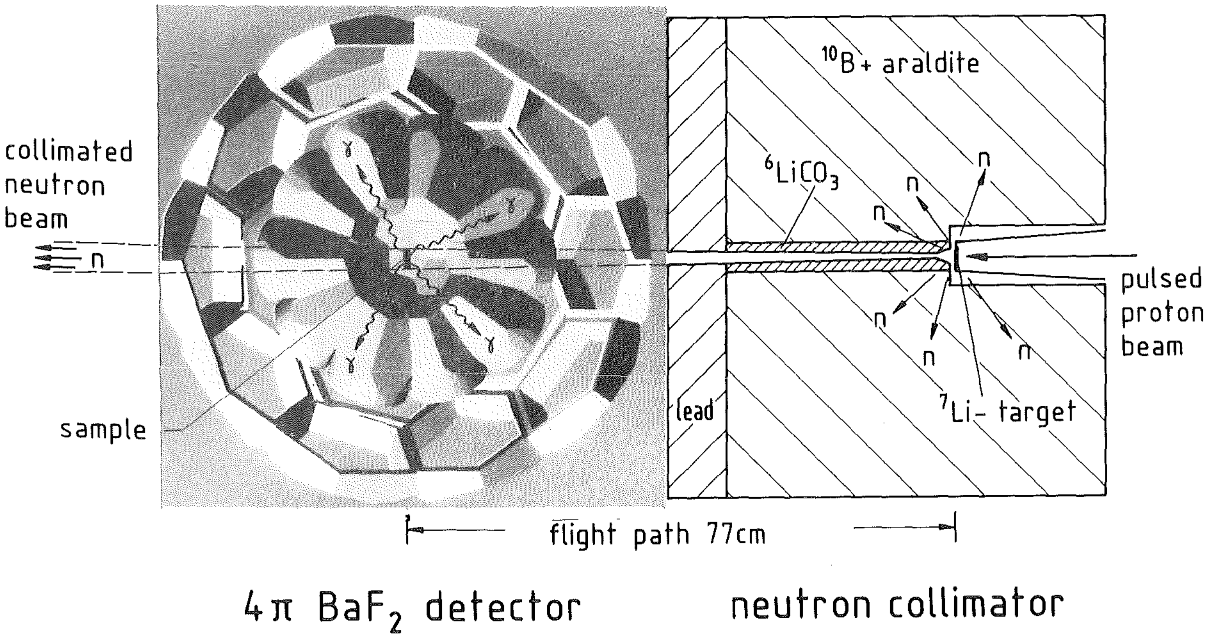

Fig. 2 Schematic setup for the determination of neutron capture cross sections in the energy range from 3 to 200 keV.

The experimental setup for the measurement of neutron capture cross sections is sketched in Fig. 2. The pulsed proton beam of the Van de Graaff accelerator (E_p = 1.97 MeV; rep. rate = 250 kHz; I_p = 2μA) falls on a metallic lithium target, producing a continuous neutron spectrum in the energy range from 3 to 200 keV via the $^7Li(p,n)^7Be$ reaction. A collimated neutron beam is produced by a carefully designed shield consisting mainly from boron, ^{6}Li-carbonate, and araldite. The neutron beam crosses the detector through holes in opposite crystals and is 25 mm in diameter at its centre. (However, the present tests had to be made without those special modules). The neutron flight path was 77 cm.

During the measurements, two-dimensional spectra containing the sum energy of the gamma-ray cascade versus the time of flight were stored on-line. In addition, the same data were also recorded in list mode together with a 42 bit word per event indicating the particular modules that have contributed. The upper part of Fig. 3 shows such a two-

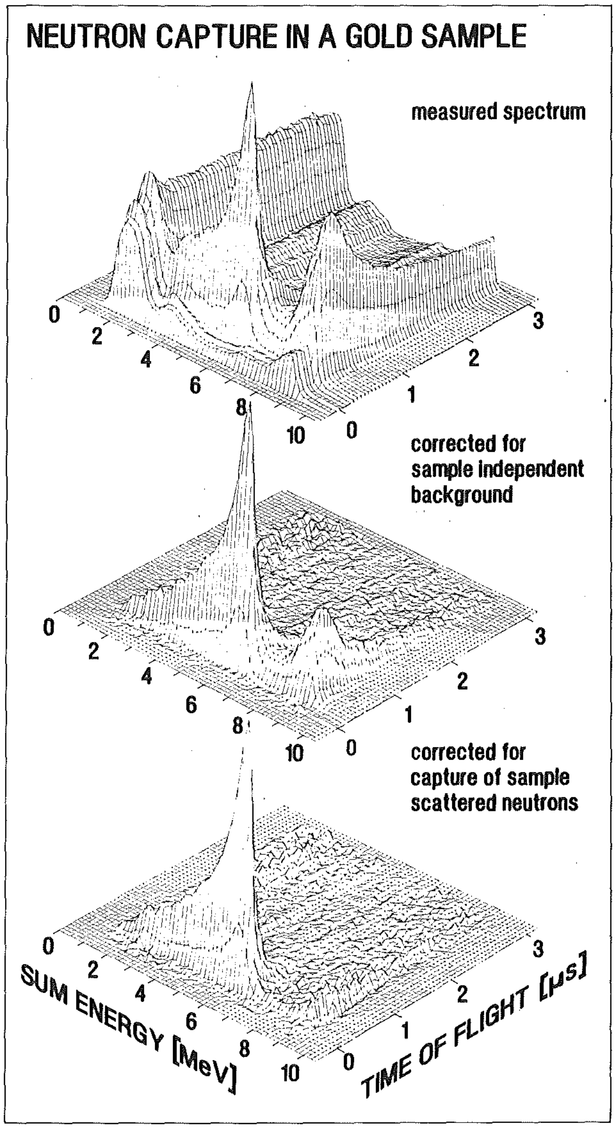

Fig. 3 Two-dimensional spectra of sum energy versus time of flight, measured with a 1 mm thick gold sample.

dimensional spectrum. The peak at a sum energy of 6.5 MeV corresponds to capture in gold and is clearly visible above the background. The time-independent background at low energies is mainly due to the radium impurities in the BaF_2 crystals, while the high energy component originates from scattered neutrons, which are captured in barium. About 60% of that latter component is due to ^{135}Ba, for which the neutron binding energy is 9.1 MeV.

The spectrum in the mid part of Fig. 3 was obtained by subtracting the sample-independent background which was measured after the sample was removed from the neutron beam. The only remaining events are therefore those from neutron capture in gold and residual background from sample scattered neutrons, which are captured predominantly in the barium isotopes of the scintillator. The following features that are essential for our new setup can be illustrated by means of this part of the figure:

(i) Most of the background due to sample scattered neutrons is located at a sum energy of ~9 MeV, well separated from primary capture events. The majority of isotopes that are important for nuclear astrophysics having binding energies of 6 to 7 MeV, this separation facilitates many future experiments.

(ii) The background due to sample scattered neutrons is spread over a time interval of ~3 µs. Therefore, only a smaller part falls into the time window of about 400 ns occupied by primary capture events. The larger spread for scattered neutrons is caused by the fact that these neutrons are captured only after having been scattered for about 20 times on average.

(iii) The integral number of background events is compatible with the number of primary capture events. As the cross section for neutron scattering in gold is about ten times larger than that for capture, this shows that ~90% of the scattered neutrons escape from the BaF_2 crystals, in good agreement with previous Monte Carlo calculations.

In the lower part of Fig. 3 the remaining background due to sample scattered neutrons has been eliminated by subtraction of a spectrum measured with a graphite sample. As a result, one obtains a clear signature for the capture events in gold. The projected pulse height spectrum shows that about 50% of all events appear in the full energy peak at the binding energy, while more than 90% are above 3 MeV. The corresponding tail will be further reduced, when all 42 detector modules are available. As only 95% of 4Π are covered by BaF_2 at present, there is a rather high probability that one of the gamma-rays of a cascade escapes detection, because the average multiplicity for gold is ~4.

Fig. 4 shows the preliminary results for the multiplicity. The experimental points represent the number of modules that have fired in a particular event, and are not yet corrected for detector-detector scattering, the limited solid angle of 95% of 4Π, and the threshold energy of ~60 keV for the individual modules. In view of all these effects, there is remarkably good agreement with a calculation by Reffo et al. (1).

In the cross section measurements on niobium, tantalum and rhodium sample masses were in the range 1.6 and 0.5 g. The main background observed in these experiments is due to neutron scattering in air and to the radioactivity of the crystals. The first component will be reduced by one order of magnitude by introducing a helium atmosphere for the neutron beam. The second component is reduced by a factor of two by replacing the seven crystals with the highest radium contamination. Therefore, in future experiments the sample mass can be reduced by at least a factor of two,

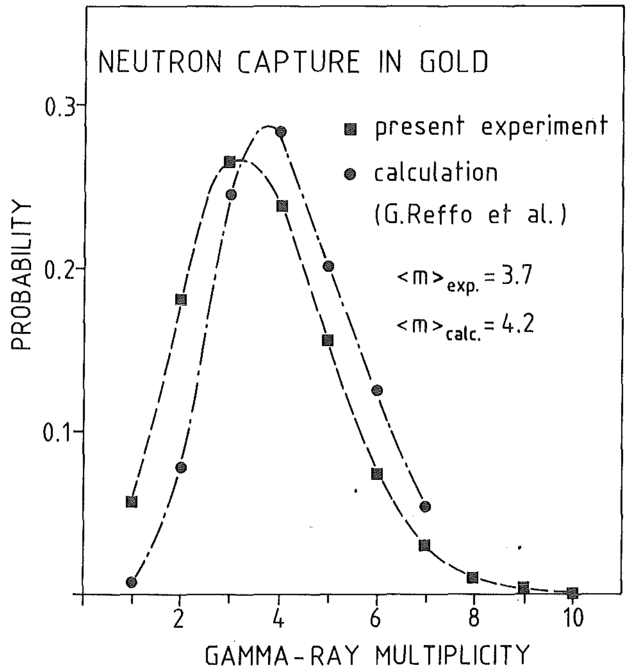

Fig. 4 Experimental distribution of cascade multiplicities following neutron capture in gold compared to a previous calculation

which is important as they will be carried out with isotopically enriched samples.

(1) G. Reffo, F. Fabbri, K. Wisshak, F. Käppeler, Nucl. Sci. Eng. 80 (1982) 630

1.1.19 EQUATION OF STATE FROM NUCLEAR AND ASTROPHYSICAL EVIDENCE

P. Doll

The equation of state of nuclear matter (1) impinges on a number of areas of physics, such as the monopole resonance, nuclear quasiparticle properties (2), high energy nuclear collisions, supernovae and neutron stars. The equation describes e.g. the energy as a function of density and depends on the precise nature of hadronic matter and the conditions under which it exsists or is probed. Nuclei are bound by the effective nucleon-nucleon force which is approximately isospin symmetric, however the extrapolation to nuclear matter is not straightforward as surface, Coulomb and asymmetry effects significantly modify the compression modulus K. High energy heavy ion collisions are assumed to probe hot matter at high compression, however the interaction time scale is much shorter than milliseconds in a supernova collapse and millions of years in neutron stars. In the latter beta equilibrium is achieved. In nuclear matter $Z \simeq 1/2\ A$, which evolves into the intermediate stage of a supernova collapse $Z \approx 1/3\ A$, because of electron capture. Neutron stars can no longer simply be characterized by Z/A like nuclear matter but are approximately considered as a big nucleus. It is therefore important to analyze the various contributions which come from the finite mass of nuclei and which

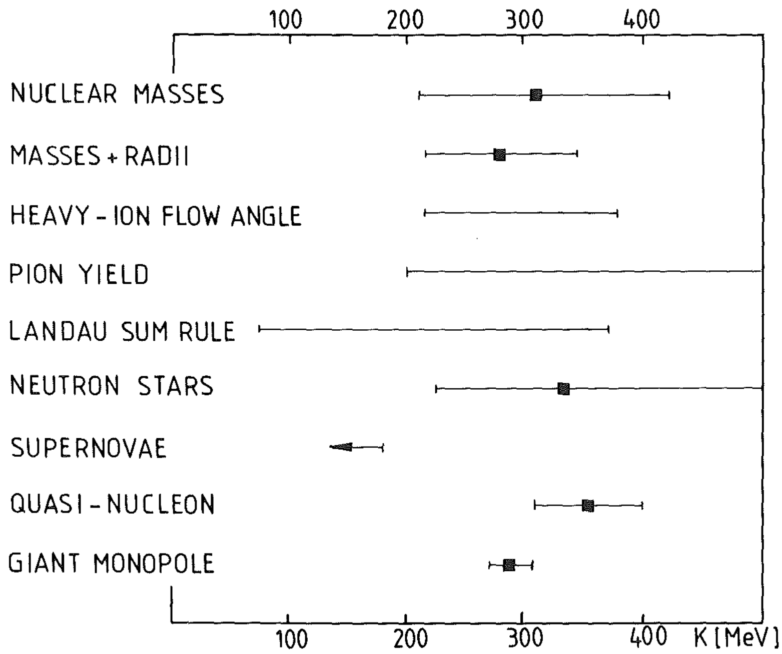

Fig.1: Summary of results for the compression modulus K (1)

contribute to the compression modulus K or the effective mass of quasi nucleons, to isolate those which are applicable to the nuclear phase of supernova and neutron star systems. We have investigated quasi particle properties in nuclei (3) especially under the aspect of isolating their coupling to phonon degrees of freedom, so far not considered explicitly for infinite nuclear matter. A summary of results for the compression modulus K from a broad range of evidence is presented in Figure 1. The prompt-bounce supernova requires a soft, the masses of neutron stars a stiff equation of state. Agreements and disagreements are not fully understood.

(1) N.K. Glendenning, Phys.Rev. 37C (1988) 2733
(2) P. Doll, LBL Preprint, 7790 (1978)
(3) P. Doll, Nucl.Phys. A292 (1977) 165

1.2 NEUTRON INDUCED INTERACTIONS

1.2.1 NEW RESULTS FOR THE n-p SPIN CORRELATION PARAMETER A_{yy}

P.Doll, V.Eberhard, G.Fink, R.W.Finlay*, T.D.Ford+, W.Heeringa, H.O.Klages, H.Krupp**, Chr.Wölfl++

The n-p spin correlation parameter A_{yy} has been measured at five angles (60° c.m. - 120° c.m.) using the polarized target facility KRYPTA (1) and the continuous energy polarized neutron beam at the Karlsruhe cyclotron. The experimental set-up and the techniques used in the measurement have been described in some detail in the last years annual report.

Briefly, the polarized neutron beam from POLKA (2) was collimated to 20 mm ⌀ and scattered from a TiH_2 sample. The target was polarized using the "brute force" method by a magnetic field of 9 Tesla at a temperature of about 10 mK. The scattered neutrons were detected with liquid scintillation detectors. Background from n-Ti interactions in the target was determined during the experiment using a Ti sampleas scattering target. The exchange of the samples was carried out at low temperature and full magnetic field about once a day.

In the offline analysis the data have been divided into 9 energy bins centered at 19 to 50 MeV with widths of 2 to 4 MeV. Extensive Monte Carlo calculations have been performed to correct for multiple scattering, finite geometry effects spin-spin dependent fluxes etc..

In this analysis 45 new results for A_{yy} have been determined. This number has to be compared to a total of 8 previous data points in the energy range from 19 to 50 MeV.

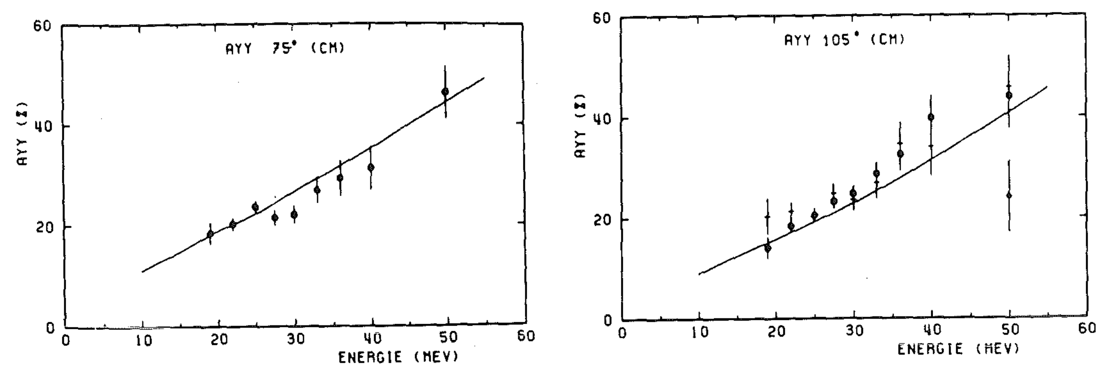

Fig.1: Results for the n-p spin correlation parameter A_{yy}. Solid line: PARIS potential prediction

Fig.1 shows our results at the angles 75° and 105° c.m. together with the predictions of the PARIS potential (3) and previous results from our group (+) as well as one data point from the work of P.Brady et al. at U.C. Davis ( ) at 50 MeV.

In a series of n-p phase-shift analyses the new results have been included together with all other available data in this energy range. Some parameters, especially the phase shift $^1P_1$ and the mixing parameter ε_1, are better constrained than before. However, the error bars on ε_1 are still too large to discriminate between predictions from different potential models. In addition, in the analyses, the $^3F_{2,3}$ parameters show a trend towards more positive values than given by the theoretical predictions. In Fig.2 our results for $^1P_1$, $^3P_1$ and ε_1 are shown together with some model predictions. There seems to be a systematic deviation of the $3P_1$ phase shifts which could be due to charge-symmetry breaking effects from up-down quark mass differences. Similar effects have been found in a recent analysis of the Nijmegen group (5).

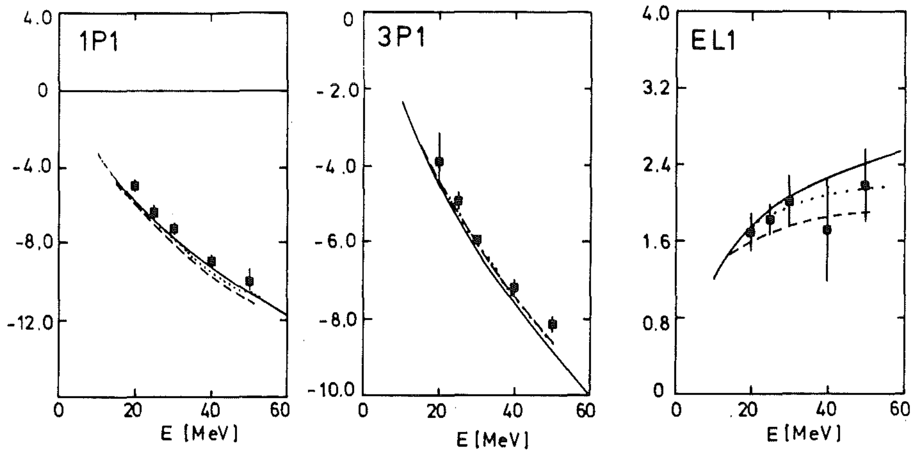

Fig.2: New results for the $^{1,3}P_1$ phase shift and for the 1=1 mixing parameter ε_1. Dashed lines: PARIS potential,solid lines: "old "BONN potential, dottes lines: new BONN potential

(1) R.Aures et al., Nucl.Instr.Meth. 224 (1984) 347
(2) H.O.Klages et al., Nucl.Instr.Meth. 219 (1984) 269
(3) M.Lacombe et al., Phys.Rev.C21 (1980) 861
(4) R.Machleidt et al., Phys.Rep. 149 (1987) 1
(5) V.G.J.Stoks et al., Phys.Rev.Lett. 61 (1988) 1702

* OHIO University, Athens, Ohio, USA
+ now at FIZ, Karlsruhe, Germany
** SIEMENS, München, Germany
++ now at DORNIER, Friedrichshafen, Germany

1.2.2 PRELIMINARY RESULTS ON THE $H(\vec{n},\gamma)^2H$ CAPTURE EXPERIMENT

P.Doll, H.Schieler, G.Fink, S.Hauber, M.Haupenthal, H.O.Klages, F.Smend*, G.Wicke*

Studies of γ-ray emission have proved to be fertile ground for the experimental and theoretical testing of basic mechanisms in nuclear collisions. Unhindered by reabsorption effects due to the strong interaction, γ-rays provide a clean, albeit experimentally challenging, signature of the collision dynamics. Recent studies of the $^2H(\gamma,n)H$ reaction (1,2) and the inverse process have indicated that besides meson exchange current (MEC) corrections even the basic reaction mechanism is not fully understood already at low photon energies. The long wavelength electromagnetic probe interacts with the magnetic moments of point nucleons (E1, M1). While the photo disintegration cross section is dominated by E1 transitions ($^3S_1 + {}^3D_1 \rightarrow {}^3P_{0,1,2} + {}^3F_2$), M1 transition ($^3S_1 + {}^3D_1 \rightarrow {}^1S_0 + {}^1D_2$) have contributions from MEC. Maximum E1, M1 interference is observed for the analyzing power at 90° because of the $b_1P_1^1$ (cos 90°) = b_1 sin 90° term.

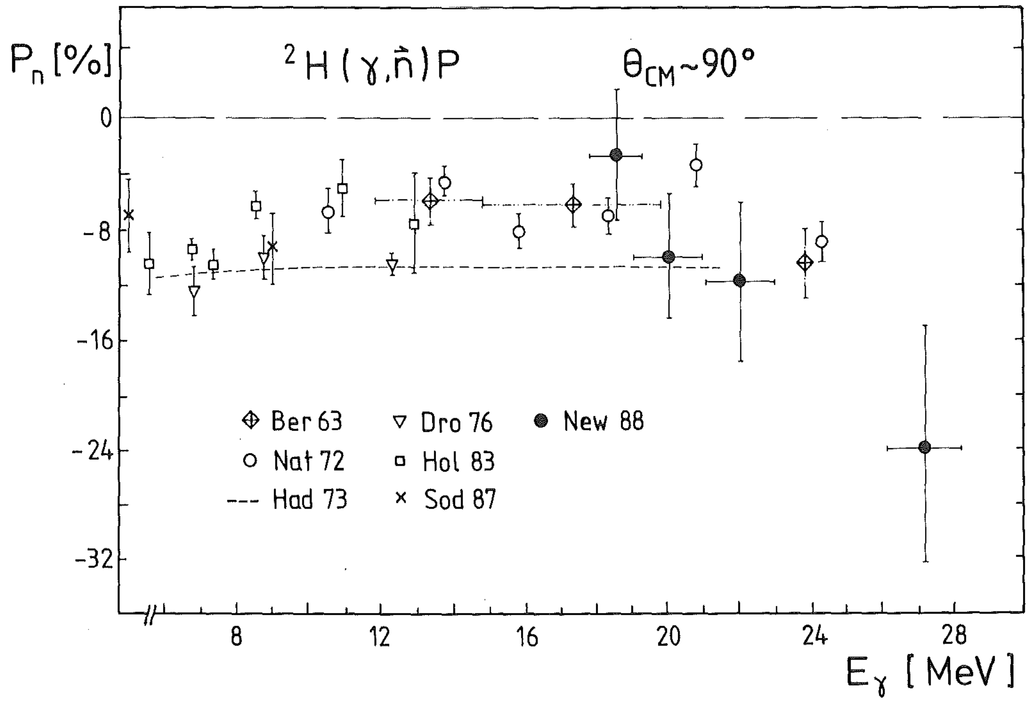

Fig.1: Analyzing power at 90°. Previous data as quoted in ref.1

We report on preliminary results of our capture experiment using polarized neutrons between 18 and 50 MeV. Our set-up is described in the previous annual report (3). We use a scintillating target (NE213) allowing simultaneous measurement of neutron-proton and neutron carbon capture (see 1.3.5). However, due to a limited pulse height resolution in the target for the first experiments, the evaluation of the photon yields is based on the NaI spectra exclusively, supported by pulse-shape discrimination techniques in the NaI crystal and the flight time measurement between the capture target and the NaI-detector. Fig.1 shows our preliminary analyzing power results converted to neutron polarization results for the inverse reaction. The figure includes recent results at lower photon energies and also rather old data (4) overlapping the energy region of the present data. Our data were analyzed on top of the background of carbon capture events included in the error analysis of the new data points. Low energy data are also included like in ref.1 as well as a theorectical prediction (5). We hope to improve our data through our recent run and to extend the angular range to 55° and 125°.

(1) J.P.Soderstrum and L.D.Knutson, Phys.Rev. 35C (1987) 1246
(2) R.J.Holt, K.Stephenson, and J.R.Specht, Phys.Rev.Lett. 50 (1983) 5
(3) M.Haupenthal, P.Doll, G.Fink, S.Hauber, H.O.Klages, H.Schieler, F.Smend, G.Wicke, KfK-Report 4405 (1987) 27
(4) W.Bertozzi, P.T.Demos, S.Kowalski, C.P.Sargent, W.Turchinetz, R.Fullwood, J.Russel, Phys.Rev.Lett. 10 (1963) 106
(5) E.Hadjimichael, Phys.Lett. 46B (1973) 14777

*University of Göttingen, Germany

1.2.3 STUDIES OF γ-RAY EMISSION IN THE $^3He(\vec{n},\gamma)^4He$ REACTION

S.Hauber, P.Doll, G.Fink, M.Haupenthal, W.Heeringa, H.O.Klages, H.Schieler, F.Smend*, G.Wicke*

Since γ-rays provide a clean signature of the collision dynamics, we started to use our neutron capture facility (1) to investigate polarized neutron capture on ^3He leading to the strongly bound nucleus ^4He. We used our liquid ^3He target (2) to achieve a reasonable density of nuclei for the low rate $^3He(n,\gamma)$ reaction in the neutron energy range from 19 to 50 MeV. At these high neutron energies we will not be able to clarify the long standing discrepancy between the photoproton and photoneutron cross section for ^4He (3), however, the experiment should provide valuable information on high multipoles in ^4He. These are characterized by (n,γ) analyzing powers and the fore-aft asymmetries (4) of the differential cross sections at various neutron energies.

With our experimental set-up of 3 large NaI-detectors at the Karlsruhe cyclotron we measured polarized neutron capture on ^3He at neutron energies from 19 to 50 MeV using an active liquid ^3He-target. In this experiment the background of scattered neutrons is about four orders of magnitude higher then the capture gamma rate produced in the target. However, for energies above 15 MeV it is possible to separate clearly neutrons from gammas using the pulse-shape information in the NaI-detector and the time-of-flight between the active target and the NaI-detector. The "white" neutron beam has been divided into 3 MeV wide energy bins.

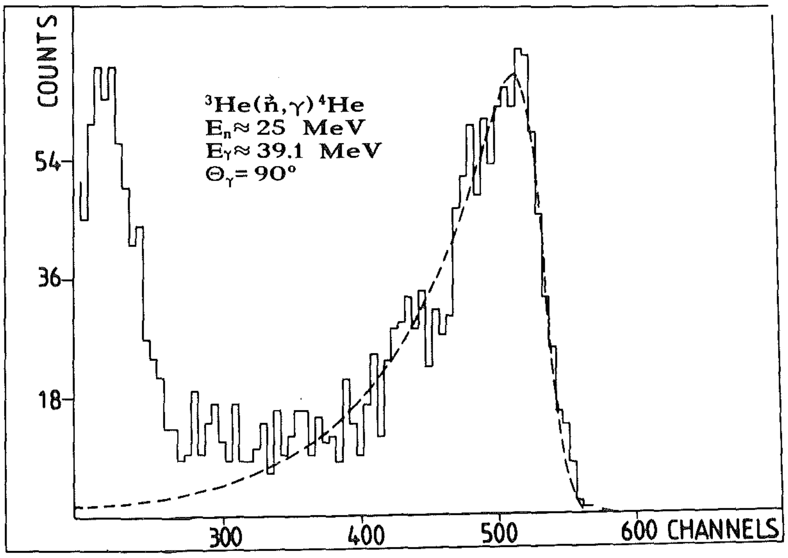

Fig. 1a: γ-ray spectrum for the $^3He(n,\gamma)$ reaction at 25 MeV. The dashed curve is a fit to the data

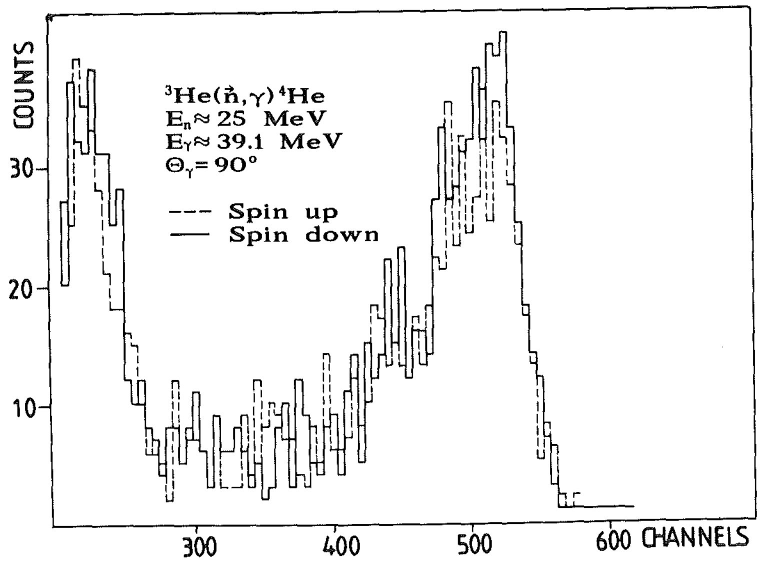

Fig. 1b: γ-ray spectrum for the $^3He(n,\gamma)$ reaction at 25 MeV for different neutron spin orientations

With a cut on the pulse-height of the recoils in the target the capture gammas are identified without background in the NaI. The line shapes can be fitted by a Gaussian folded to an exponential tail. Fig.1a shows an energy spectrum with fit curve. The same parameters are used to fit the spectra for spin up and spin down to extract count rates and thus analyzing powers from the data. Fig.1b shows pulse height spectra for spin up and down at the same energy.

(1) M.Haupenthal, P.Doll, G.Fink, S.Hauber, H.O.Klages, H.Schieler, F.Smend, G.Wicke, KfK-Report 4405 (1987) 27
(2) R.van Staa, J.Reher, B.Zeitnitz, NIM 136 (1976) 241
(3) B.Wachter, T.Mertelmeier, H.M.Hofmann, Phys.Rev. 38C (1988) 1139
(4) L.Ward, D.R.Tilley, D.M.Skopik, N.R.Roberson and H.R.Weller, Phys. Rev. 24C (1981) 317

*University of Göttingen, Germany

1.2.4 RADIATIVE CAPTURE OF POLARIZED NEUTRONS BY ^{12}C IN THE ENERGY RANGE FROM 20 TO 50 MEV

F.Smend*, G.Wicke*, P.Doll, G.Fink, S.Hauber, M.Haupenthal, H.O.Klages, H.Schieler

Radiative capture of nucleons, i.e., the inverse reaction to the nuclear photo-effect, is an important tool for the investigation of giant multipole resonances in nuclei. In the Direct-Semidirect (DSD) Model of capture, the reaction is a superposition of direct capture of the nucleon into its final bound state, and capture into that state via excitation of a collective vibration of the nucleus. In contrast to the proton, the neutron has only a small effective charge for direct capture. Therefore, neutron capture reactions are very useful for the investigation of giant resonances of the final nucleus. Use of polarized neutrons is an indispensable prerequisite for obtaining maximal information about the amplitudes and relative phases of the partial reaction amplitudes.

The polarized continuous neutron beam at the Karlsruhe cyclotron is used to study the reaction $^{12}C(n,\gamma)^{13}C$ at neutron energies between 20 and 50 MeV. Previous experiments which used monoenergetic neutrons produced at tandem accelerators were limited to energies up to 23 MeV. The capture target is a NE-213 liquid scintillator allowing the determination of neutron energies by measuring the time-of-flight between the source and the target (TOF 1). Radiative capture of high-energy neutrons is a rare event as compared to neutron scattering. Therefore, gamma rays registered by the NaI detectors have to be discriminated against signals due to neutron-induced reactions in the NaI crystals. For this purpose, a combined analysis of the time-of-flight of the reaction products between the target and the NaI detectors (TOF 2) and the pulse shape (PS) of the detector signals is employed (1).

The off-line analysis of the data is in progress. Figure 1 shows a typical gamma spectrum measured at 90° and at a neutron energy of 25 MeV. Gamma rays from neutron capture by ^{12}C produce the high-energy continuum up to about 30 MeV. A threshold has been set at 10 MeV. The peak at 15.1 MeV is due to inelastic neutron scattering by ^{12}C. The arrows mark the gamma energies expected for radiative capture of neutrons having the full incident energy of 26 MeV.

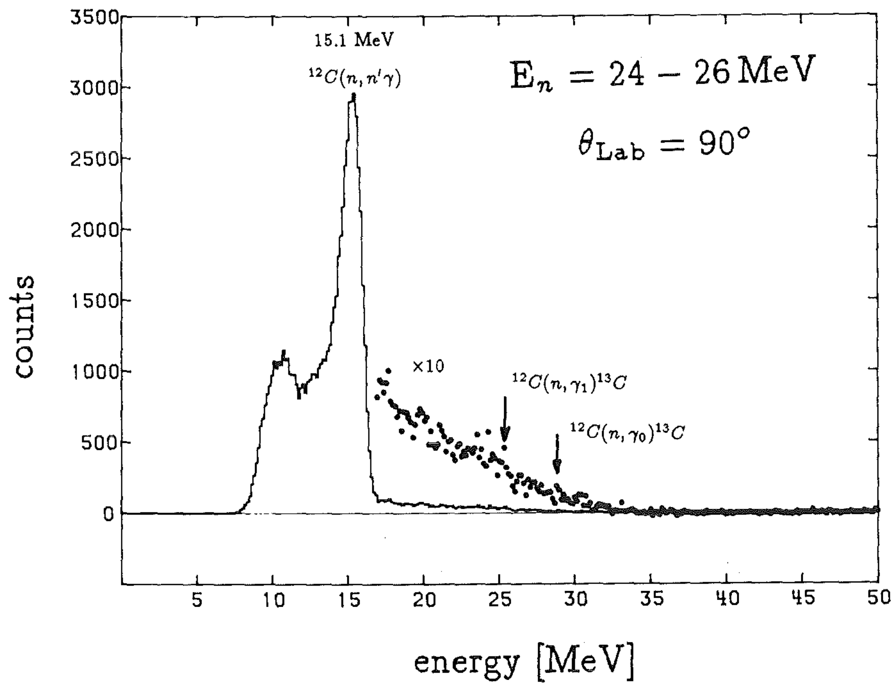

Fig.1: Gamma spectrum measured at 90° and at a neutron energy of 24 MeV to 26 MeV (lab).

In order to determine cross sections and analyzing powers from the spectra, the distribution of neutron energies and directions referring to the instant of capture have to be folded out.

(1) M.Haupenthal et al. Annual Report 1986/87

*University of Göttingen, FRG

1.2.5 FAST NEUTRON INTERACTIONS WITH A LARGE NaI CRYSTAL

P.Doll, M.Haupenthal, R.W.Finlay*, G.Fink, S.Hauber, H.O.Klages, H.Schieler, F.Smend**, G.Wicke**

Using large NaI crystals for detecting high energy photons in fast neutron capture experiments, knowledge of neutron induced reactions in NaI is mandatory. While the cross sections for photons from the capture target are of the order of 10^{-30} cm^2 , elastically or inelastically scattered neutron yields are 4 to 5 orders of magnitude larger. Therefore, techniques had to be developed to discriminate electromagnetic and hadronic interactions in NaI by means of the time-of-flight between the scintillating NE213 target and the NaI detector and through pulse-shape information (PS) (1) in the crystal. However, because of the comparatively long light decay times in NaI compared to the very short light decay times in the scintillating NE213 target, care has to be taken about the constant-fraction-timing (CFD) for a large NaI-detector. Small pulse height

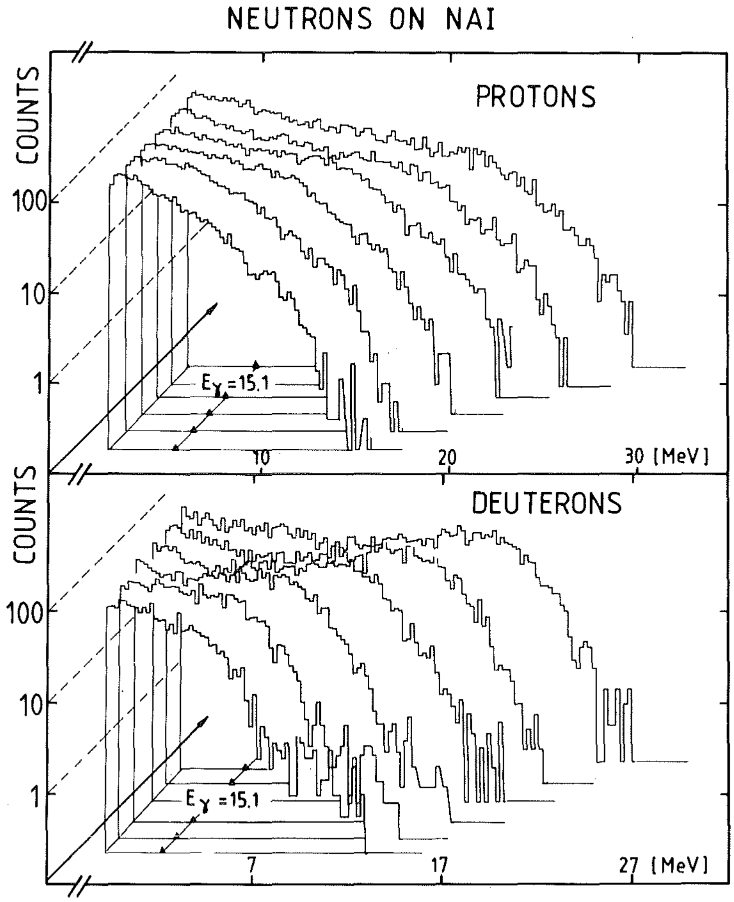

Fig.1: Charged particle spectra created by neutrons in NaI

fractions and long delay cables for the CFD can lead due to some integration in the NaI photo tube bases, to a misinterpretation (2) of the relative time information between the target and the NaI. Figure 1 shows charged particle spectra created for various neutron energies in the NaI crystal. For the corresponding proton and deuteron spectra the incident neutron energy is identical. The pulse height for 15.1 MeV photons is indicated by arrows on the bottom of each spectrum indicating the large light output for the charged particles. One interesting feature is the comparatively larger light output for deuterons than for protons, a finding independently observed at even larger proton and deuteron energies (3). The figure demonstrates the absolute need for discriminating the neutron induced charged particles from the 30 to 60 MeV photons from capture reactions.

(1) D.M.Whittal and C.U.Bartle, NIM A247 (1986) 390
(2) P.Doll, M.Haupenthal, R.W.Finlay, G.Fink, S.Hauber, H.Schieler, H.O.Klages, F.Smend, G.Wicke, KfK-preprint 140103 P11A (1988) and to be published
(3) G.A.Needham, J.L.Romero, F.P.Brady, C.M.Castaneda, T.D.Ford, to be published

* Ohio University, Athens, USA
**University Göttingen, W.-Germany

1.2.6 ANALYZING POWER OF THE $\vec{n}$-^{3}He REACTION CHANNELS

A.Vollmer, P.Doll, G.Fink, R.W.Finlay*, T.D.Ford**, W.Heeringa, H.O.Klages

In the last few years unexpected differences have been observed in the mass A = 4 system not only in the reactions ^{3}H(p,p)^{3}H, ^{1}H(t,t)^{1}H (1) and the mirror reactions ^{2}H(d,p)^{3}H, ^{2}H(d,n)^{3}He (2) but also in the radiative capture reactions ^{3}H(p,γ)^{4}He and ^{3}He(n,γ)^{4}He (3) to investigate the existence of charge symmetry violation of the nuclear force in A = 4.

Our recent experiment investigating the n-^{3}He system provides new important data. The measurement of the analyzing power of the reactions ^{3}He(n,p)^{3}H and ^{3}He(n,p)^{2}H in the energy range from 18 to 50 MeV was carried out at the polarized continuous energy beam POLKA (4) of the Karlsruhe cyclotron. A ^{3}He gas target and 8 ΔE-E telescopes (5) were employed in an evacuated scattering chamber to detect the charged reaction products in an angular range from 12.5° to 77.5° in the laboratory system. At forward angles, also tritons were detected to overcome the problem of detecting low energy protons at far backward angles. Therefore, the gas target foils and the ΔE detectors had to be rather thin. We used a cold (18K) gas target at a pressure of 2-3 bar specially developed for the feasibility of this experiment (6).

The observables are compared with very recent theoretical predictions calculated in the framework of the resonating group method which takes into account Coulomb effects (7). In figure 1 the new A_y data for the reactions $^3He(n,p)^3H$ and $^3He(n,t)^1H$ at 30 MeV are shown together with the theoretical results.

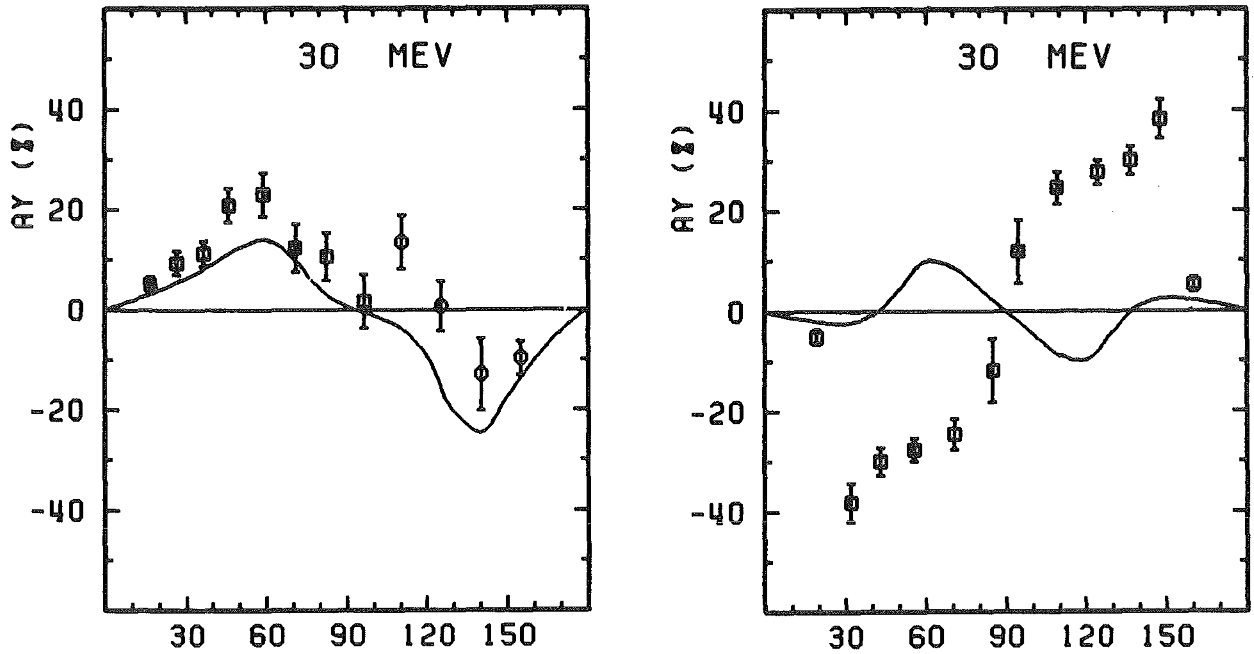

Fig.1: Comparison of calculated (solid lines) and experimental (squares) analyzing powers for the reactions $^3He(n,p)^3H$ (a) and $^3He(n,d)^2H$ (b).

There is a fair agreement between the experimental and theoretical data in the p,t-exit channel due to the inclusion of D-waves in the performed calculations. The d,d-exit channel data do not agree with the predictions. A possible explanation can be that $^5D_0$-waves are not yet taken into account in the theoretical calculations. This is a very interesting aspect in connection with the current discussion of the D-state probability in ^4He investigated in d+d capture (8).

(1) V.König, W.Grübler, R.A.Hardekopf; B.Jenny, R.Risler, H.R.Bürgi, P.A.Schmelzbach, and R.E.White, Nucl.Phys. A331, (1979) 1
(2) H.M.Hofmann, W.Zahn, and H.Stöwe, Nucl.Phys. A357, (1981) 139
(3) B.Wachter, T.Mertelmeier, and H.M.Hofmann, Phys.Rev. C38, (1988) 1139
(4) H.O.Klages et al., Nucl.Instr.Meth. 219 (1984) 269
(5) P.Doll et al., Nucl.Instr.Meth. A250 (1986) 526
(6) A.Vollmer et al., KfK report 4159 (1986) 187
(7) H.M.Hofmann, priv. Communication (1987)
(8) H.R.Weller, to be published in Ann.Rev. of Nucl. Science (1988)

*Ohio University, Athens, Ohio, USA; **now at FIZ, Karlsruhe, FRG

1.2.7 THE CHARGE EXCHANGE REACTION $^{12}C(\vec{n},p)^{12}B$

S.Scheib, P.Doll, G.Fink, H.O.Klages

As reported in the 1987 annual report (1) an improved large solid angle detector system (Θ_{lab} = 7°-29°) had been set up at the polarized neutron facility POLKA (2) to investigate neutron induced reactions (E_n = 20-50 MeV) on light nuclei leading to charged particles in the exit channel. These experiments are important because these reaction cross sections at neutron energies of a few tens of MeV are widely unknown. Especially the $^{12}C(n,p)^{12}B$ reaction is of interest to understand competing reactions in organic scintillating detectors. From the spectroscopic point of view the (n,p) reaction leads to spin and isospin excitations in the residual nucleus presenting a challenge (3) to investigate in a wide energy range.

The charged reaction products pass through the multiwire proportional chambers (4) which measure their trajectories. By calculating the proton trajectories back onto the target plane, contributions from the window of the vacuum chamber and the air outside the chamber could be discriminated and the reaction angles are determined. The data were analyzed in 2 degree wide angle bins for protons identified by ΔE-E-techniques. Because of strong variation of the light output over the area of the E-detectors a correction was necessary to improve the overall energy resolution.

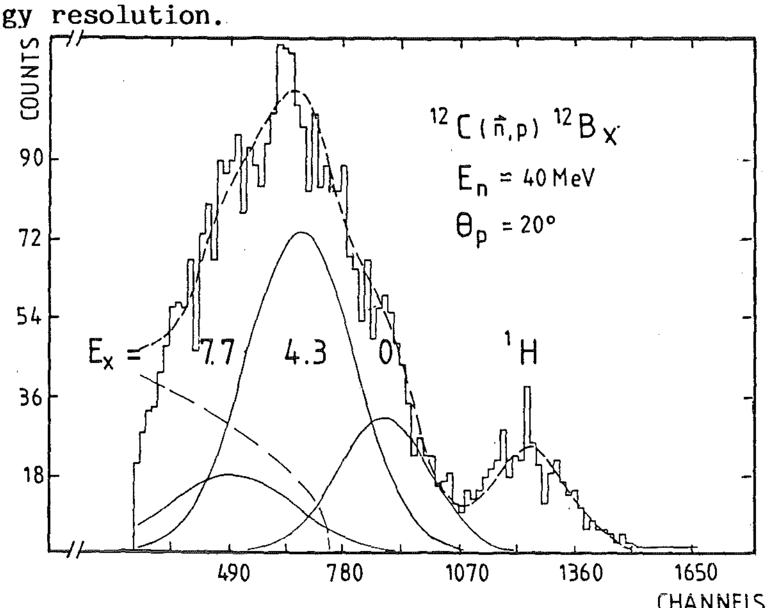

Fig.1: Energy spectrum of the $^{12}C(n,p)^{12}B$ reaction for 40 MeV neutron energy. Curves show fits to three dominating groups in ^{12}B

Due to the short flight path of the neutrons and charged particles a separation between different excited states in the residual ^{12}B nucleus is difficult. Therefore a kinematical simulation was performed to define various neutron energy cuts which lie inside a curved two dimensional window in a TOF/E matrix. Fig.1 shows a proton energy spectrum for 40 MeV neutron energy at 20° ± 1° in the laboratory system. Included are the fits for the well known ground-state transitition, the 4.3 MeV and the 7.7 MeV resonances in ^{12}B. Using the neutron-proton scattering events from a polyethylene $(CH_2)_n$ target and the neutron-proton cross sections the cross sections for the (n,p) transitions to ^{12}B will be derived based on the known hydrogen/carbon ratio in the polyethylene target because both processes are measured with the same setup. Due to the polarization of the incident neutrons the analyzing power A_y of different excitation groups in ^{12}B will be also determined.

(1) S.Scheib, P.Doll, G.Fink, H.O.Klages, KfK report 4405 (1987) p.117
(2) H.O.Klages, H.Dobiasch, P.Doll, H.Krupp, M.Oexner, P.Plischke, B.Zeitnitz, F.P.Brady, J.C.Hiebert, NIM 219 (1984) 269
(3) F.P.Brady, S.Afr.J. Phys. 10 No2 (1987)
(4) P.Doll, F.P.Brady, T.D.Ford, R.Garrett, H.Krupp, H.O.Klages, NIM A270 (1988) 4371)

1.2.8 OPTICAL MODEL SPIN-SPIN POTENTIALS FOR ^{27}Al AND ^{93}Nb

W.Heeringa, H.O.Klages, Chr.Wölfl

In the previous annual report we reported on spin-spin cross sections measured for the nuclides ^{27}Al and ^{93}Nb. They appeared to agree quite well with existing predictions based on microscopic calculations. In the present contribution we compare the data with results of optical model calculations introducing various kinds of spin-spin potentials. The calculations were carried out with a version of the code SPINSOR (1). Two kinds of potentials were investigated, a spherical one

$$U_{ss}(r) = -V_{ss} f_{ss}(r)\, \sigma\cdot I/I$$

and a tensor type

$$U_{st}(r) = -V_{st} f_{st}(r)\, \frac{\{3(\sigma\cdot r)(I\cdot r) - \sigma\cdot I\}}{2I}$$

with V the strength and f(r) the radial shape of the potential. For the spherical potential nice fits can be obtained with radial shapes, that peak at about 70% of the nuclear radius. The tensor potential gives good fits for a surface peaking radial shape. The results are shown in figure 1, the deduced parameters of the spin-spin potentials are shown in table 1. We find values for V_{ss} close to 1 MeV and for V_{st} around -2 MeV. It is interesting to note the similarity between the results for both nuclides.

Table 1: Best fit parameters of the spin-spin potentials found in this analysis, determined for spherical and tensor potentials separately. The quantity X^2/D denotes X^2 per data point, a and r are the usual optical model diffuseness and radius parameters.

	V(keV)	a_{ss}	r_{ss}	X^2/D	
^{27}Al	850 ± 350	0.65	0.89	0.45	spherical
^{93}Nb	1090 ± 230	0.40	0.85	0.55	"
^{27}Al	-2250 ± 980	1.21	1.065	0.54	tensor
^{93}Nb	-2160 ± 250	0.688	1.219	0.59	"

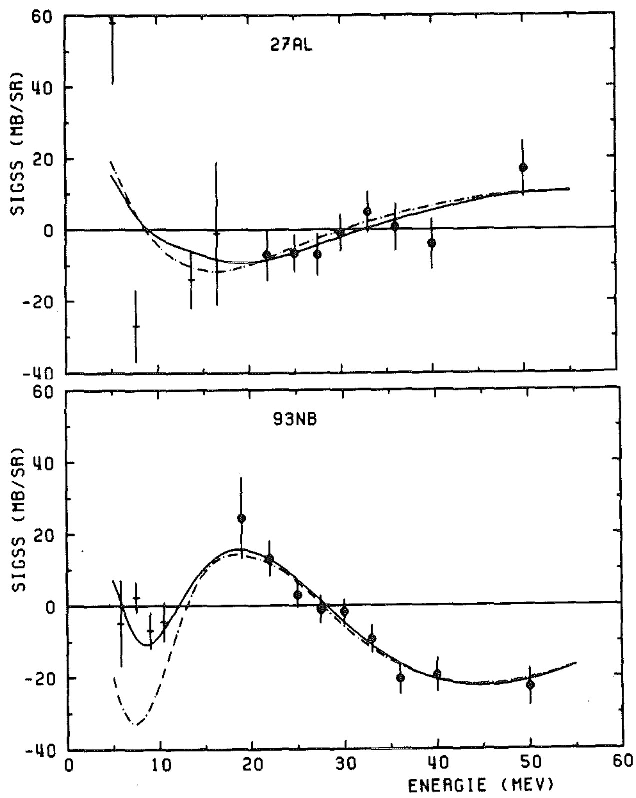

Fig.1: Optical model fits of our spin-spin cross section data (dots). Full lines are best fits with the spherical potential, dotted lines are best fits with the tensor potential. The crosses are data from Ref.2, which were not included in the fit procedure.

Our data show no indication for an imaginary spin-spin potential. Such a potential would generate a σ_{SS} with a 90° energy-shifted oscillatory behaviour (2). Our data nicely follow the energy trend given by the real spin-spin potential, hence we cannot confirm the rather large value of W_{SS} found in Ref.2 for ^{27}Al at neutron energies from 5-16 MeV.

(1) A.H.Hussein and H.S.Sherif, Phys.Rev. C8 (1973) 518
(2) C.R.Gould et al., Phys.Rev.Lett. 57 (1986) 2371.

1.2.9 HIGH-RESOLUTION RESONANCE STUDY OF THE ^{12}C+n TOTAL CROSS SECTION IN THE REGION OF ^{13}C T=3/2 STATES

F. Hinterberger[+], P. von Rossen[+], S. Cierjacks, G. Schmalz, (1)

The ^{12}C+n total neutron cross section has been studied in the region of the lowest T=3/2 states of ^{13}C. The first T=3/2 state at (15108.2±1.2) keV excitation is observed as a weak resonance anomaly. The deduced resonance parameters agreed with previous results. At higher excitation energies four sharp anomalies have been observed at (17533±3) keV, (18082±3) keV, (20057±4) keV and (21704±4) keV excitation with total widths between 12 keV and 20 keV. The results are discussed with respect to a possible T=3/2 assignment. An upper limit of the elasticity $(J=1/2)\Gamma_{no}/\Gamma$ is deduced for those T=3/2 levels which do not appear as resonance anomalies.

(1) Z. Phys. A 326 (1987) 407

+ Institut für Strahlen- und Kernphysik, Universität Bonn, Fed. Rep. of Germany

1.3 NUCLEAR REACTIONS BY CHARGED PARTICLES

1.3.1 SEQUENTIAL BREAK-UP OF 156 MeV ^{6}Li PROJECTILES

J. Kiener, H.J. Gils, H. Rebel, G. Gantenbein, G. Gsottschneider, N. Heide, H. Jelitto, J. Wentz, S. Zagromski, S.K. Basu*, G. Baur**, D.K. Srivastava*

For the break-up of ^{6}Li into an α-particle and a deuteron, a narrow resonance in the relative kinetic energy at 710 keV can be observed which corresponds to the sequential (resonant) break-up via the first excited 3^{+} state at 2.186 MeV. As the Coulomb excitation probability is well known (1), this resonant break-up is a good test for the reaction mechanism in the break-up process.

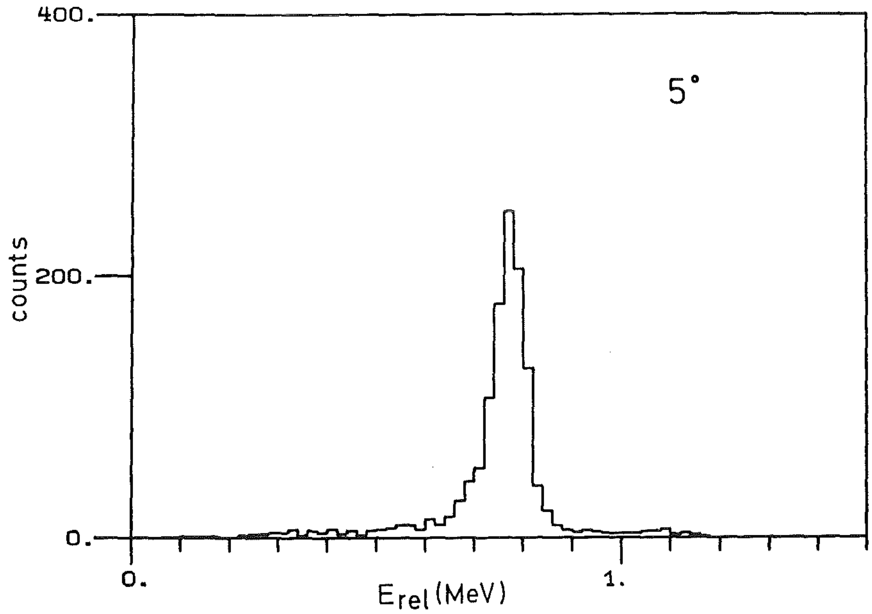

Fig. 1 Relative energy spectrum of binary break-up.

We measured the break-up of 156 MeV ^{6}Li projectiles incident on ^{208}Pb in a coincidence experiment at the Karlsruhe magnetic spectrograph "Little John". Data were taken at seven different reaction angles (2°-6°) below the grazing angle where mainly Coulomb interaction should contribute to the elastic break-up. Cross section normalization was done by the integrated beam current. Additional information for relative normalization was obtained by elastic scattering, detected in a monitor detector, and from measured inclusive spectra, which were compared with previous measurements (2). The different normalization procedures agreed within ±7.5%.

From the relative energy spectra (Fig. 1), an angular distribution for the elastic sequential break-up was extracted and compared with the prediction for pure Coulomb break-up by a simple straight line approximation and a more realistic semiclassical theory. For very small forward angles ($\theta_{cm} \leq 4°$) the experimental values and both approaches are

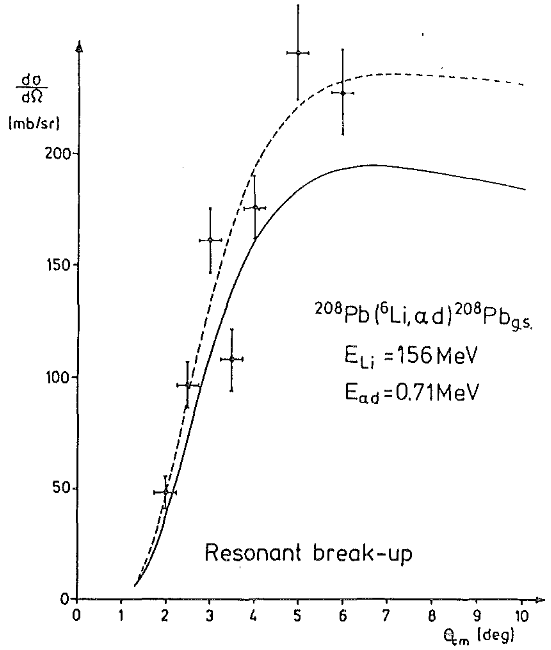

Fig. 2 Angular distribution for the reaction $^{208}Pb(^{6}Li,^{6}Li)^{208}Pb_{g.s.}$

in good agreement. There is, however, some indication for a contribution of nuclear break-up, but the reaction seems to be dominated by Coulomb interaction.

(1) F. Eigenbrod, Z. Phys. 238 (1969) 337

(2) H. Jelitto, Report KfK 4259, Kernforschungszentrum Karlsruhe (1987)

* On leave from B. A. R. C., V.E.C.C., Calcutta, India

** Institut für Kernphysik, Kernforschungsanlage Jülich

1.3.2 SEARCH FOR NONRESONANT COULOMB BREAK-UP OF ^{6}Li PROJECTILES

J. Kiener, H.J. Gils, H. Rebel, G. Gantenbein, N. Heide, H. Jelitto, J. Wentz, S. Zagromski, S.K. Basu*, I.M. Brâncuş**

The proposal of Baur, Bertulani and Rebel (1), to extract astrophysically interesting capture cross sections from measurements of projectile break-up, has focussed strong interest to the nonresonant (direct) Coulomb dissociation of nuclear projectiles. The relationship between the cross sections for direct radiative capture $b + c \rightarrow a + \gamma$ and for the direct Coulomb break-up $a + \gamma \rightarrow b + c$ is given by the detailed balance theorem:

$$\sigma(b+c \rightarrow a+\gamma) = \frac{2(2j_a+1)}{(2j_b+1)(2j_c+1)} \frac{k_\gamma^2}{k^2} \sigma(a+\gamma \rightarrow b+c) \quad .$$

Of particular interest are reactions, where the relative energies between the fragments b and c are of the same order as in stellar burning processes, i.e. the region below 100 keV.

As a feasibility study we measured the break-up of 156 MeV ^6Li projectiles into α-particle and deuteron in the Coulomb field of a heavy target nucleus (^{208}Pb) at 3° and 4° mean reaction angles. The kinematically complete coincidence experiment was done at the magnetic spectrograph "Little John" (Fig. 1). Both break-up fragments passing through the same acceptance slit and magnetic system were detected in coincidence in the divided focal plane detector. Thereby relative energies down to 20 keV could be measured. A wide angular acceptance of 1.1° x 1.4° was used to collect sufficient statistics for the direct Coulomb break-up for very low relative energies.

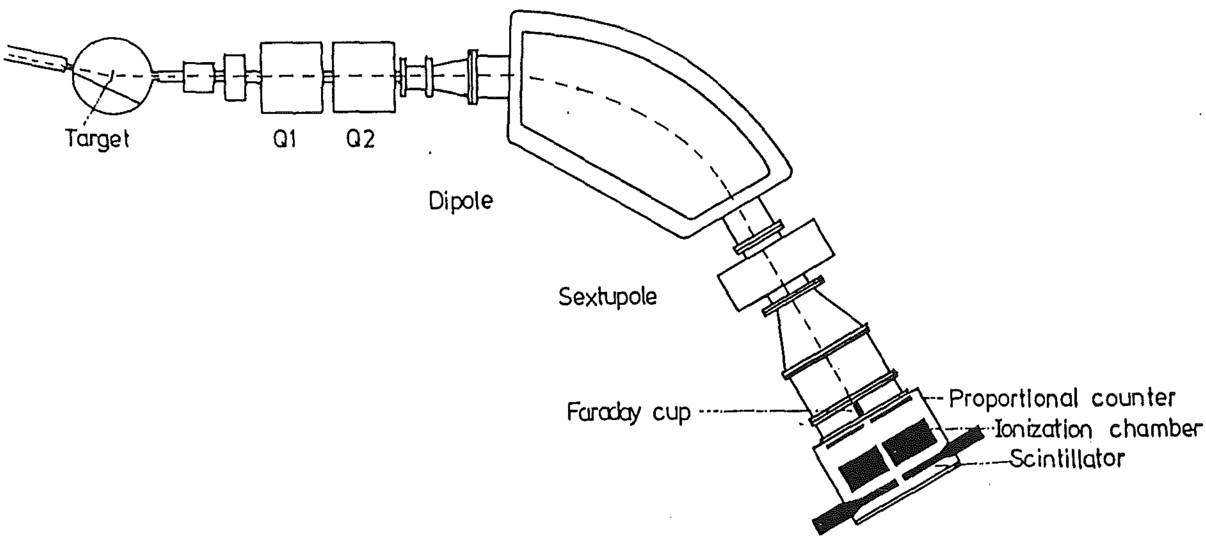

Fig. 1 Magnetic spectrograph "Little John" with focal plane detector.

In the data analysis only those events were considered, where the α particle and the deuteron reached at the same time in the scintillators and their sum energy was according to elastic break-up (154.5 ± 1 MeV), which means that the target is not excited. The dominance of Coulomb break-up at the selected reaction angles could be shown by the analysis of the sequential break-up in the same experiment, reported in another contribution (2). Fig. 2 shows preliminary relative energy spectra with clear evidence for direct break-up from 100 - 700 keV.

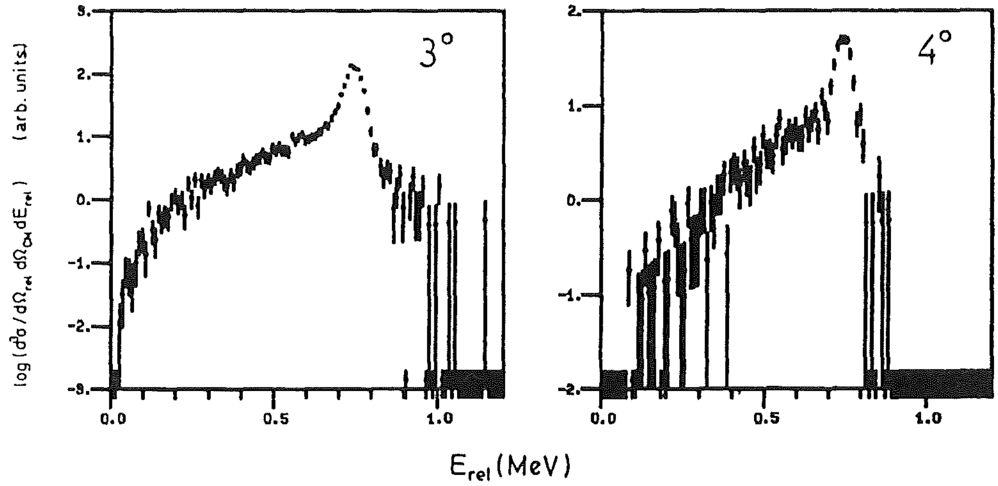

Fig. 2 Relative energy spectra of binary break-up.

(1) G. Baur, C.A. Bertulani, H. Rebel, Nucl. Phys. A458 (1986) 188
(2) J. Kiener, H.J. Gils, H. Rebel, G. Gantenbein, G. Gsottschneider, N. Heide, H. Jelitto, J. Wentz, S. Zagromski, S.K. Basu, G. Baur, D.K. Srivastava, Report KfK 4508, contr. 1.3.1

* On leave from B. A. R. C., V.E.C.C., Calcutta, India
** Central Institute of Physics, IFIN Bucharest, Romania

1.3.3 DIRECT AND SEQUENTIAL COULOMB BREAK-UP OF ^{7}Li

D.K. Srivastava*, D.N. Basu*, H. Rebel (1)

Direct and sequential break-up of ^{7}Li projectiles in the field of heavy target nuclei are studied on the basis of the Coulomb excitation approach. It is found that the experimental data observed for forward emission angles are fairly well described by Coulomb effects and that for angles more forward than 12° the direct (E1) break-up of 70 MeV ^{7}Li scattered from ^{120}Sn exceeds considerably the resonant (E2) break-up mode via the 7/2$^-$ state in ^{7}Li at E_x = 4.63 MeV.

(1) Phys. Lett. B 206 (1988) 391

* Bhabha Atomic Research Centre V. E. C. C. - Bidhan Nagar, Calcutta 700064 / India

1.3.4 INVESTIGATIONS OF DIRECT AND SEQUENTIAL COULOMB BREAK-UP OF LIGHT IONS

D.K. Srivastava*, D.N. Basu*, H. Rebel (1)

Coulomb dissociation of ^{6}Li in the field of ^{208}Pb at different energies via resonance and continuum levels is discussed in detail. Relations are given which can be used to directly relate the Coulomb break-up cross section to the astrophysical S-factor. Predictions for energy dependence and angular-distributions are given. The direct Coulomb-break-up of ^{6}Li is found to be of the same order of magnitude as the sequential break-up at higher projectile energies. The effect to elastic scattering can be accounted for by introducing a dynamic polarization potential. Predictions are given for the direct Coulomb dissociation of 26 MeV/nucleon ^{7}Li and ^{16}O incident on ^{208}Pb through dipole transitions to the continuum, and for ^{20}Ne via quadrupole transitions in similar experimental situations.

(1) KfK Report 4446, Kernforschungszentrum Karlsruhe (1988)

* Bhabha Atomic Research Centre, Variable Energy Cyclotron Centre, Calcutta, India

1.3.5 THE DYNAMIC POLARIZATION POTENTIAL FROM COULOMB DISSOCIATION OF DEUTERONS AND ^{3}He

D.K. Srivastava*, D.N. Basu*, H. Rebel (1)

We evaluate the target and the energy dependence of the Coulomb dissociation cross section for deuterons and ^{3}He nuclei in a first order Coulomb excitation theory along with a strong absorption treatment to account for the nuclear interaction. Dipole transitions are found to be dominating in both cases. For deuterons, the Coulomb dissociation is comparable to the nuclear break-up, even at high energies for heavy nuclei, whereas it is quite small for ^{3}He. We argue that this should imply a substantial long range absorptive potential to simulate the dynamic polarization potential for deuterons, which may improve the predictions of the prior-form distorted waves Born approximation theory for deuteron break-up.

(1) Nucl. Phys. A485 (1988), 221

* Variable Energy Cyclotron Centre Bhabha Atomic Research Centre 1/AF. Bidhan Nagar, Calcutta-700064, India

1.3.6 BREAK-UP OF 156 MeV ^{6}Li AT LARGE RELATIVE MOMENTA OF THE FRAGMENTS AND THE PRIOR DWBA APPROACH

N. Heide, D.K. Srivastava, D.N. Basu, H. Rebel and H.J. Gils

The triple differential cross section

$$\frac{d^3\sigma}{d\Omega_\alpha d\Omega_d dE_\alpha}$$

for the direct elastic reactions ^{208}Pb(^{6}Li,αd)^{208}Pb and ^{12}C(^{6}Li,αd)^{12}C at 156 MeV has been measured in an in-plane geometry at large relative momenta of the fragments. The data have been taken at the Karlsruhe Isochronous Cyclotron using position sensitive semiconductor E-ΔE telescopes.

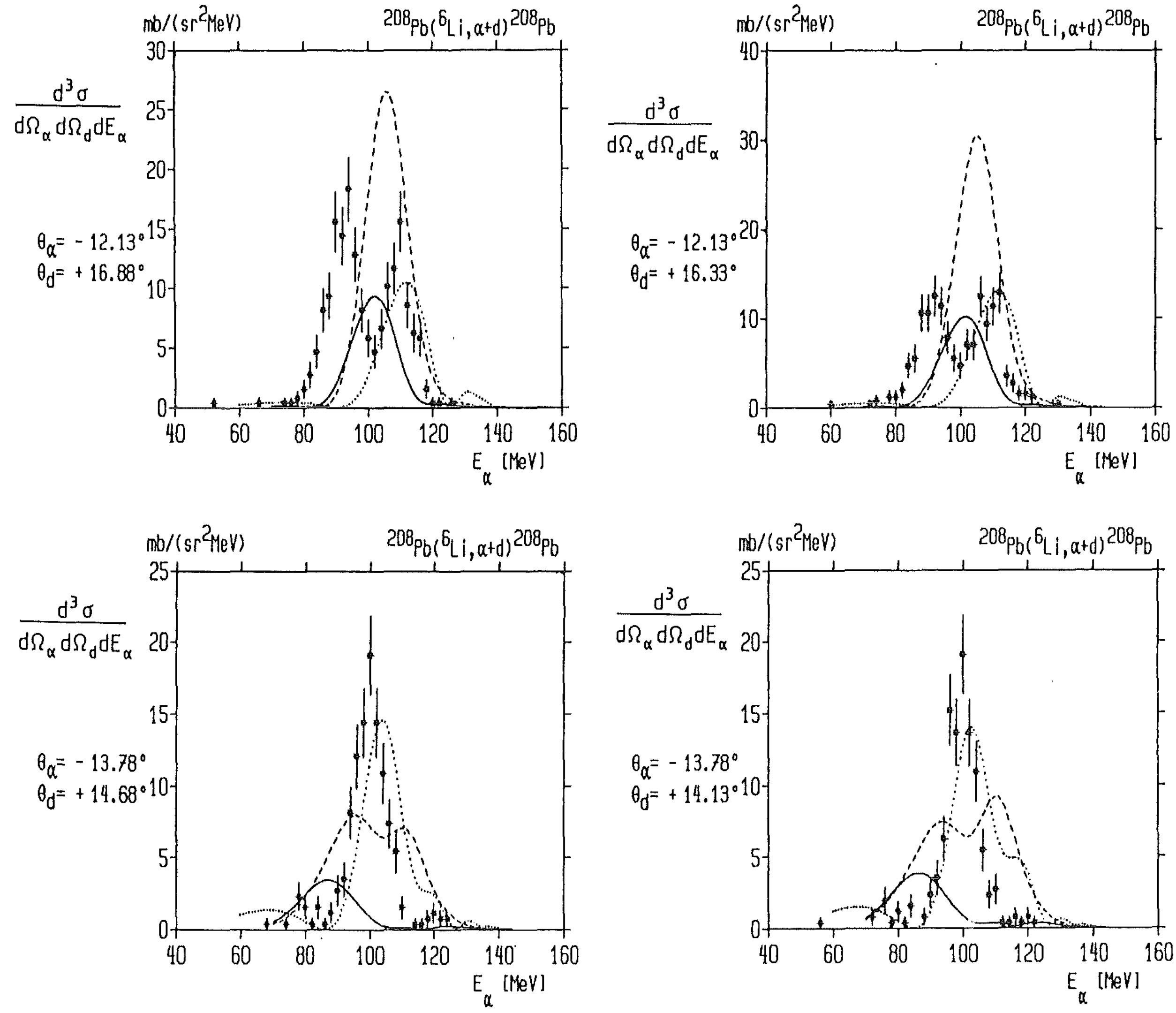

Fig. 1 Coincidence cross sections of the direct elastic reaction ^{208}Pb(^{6}Li,αd) ^{208}Pb at 156 MeV and results of prior-DWBA with complex transition potentials (solid line), real transition potentials (dotted line) and the QFBM (dashed line).

A complete listing of all the 720 measured coincidence spectra together with a detailed description of the experimental setup is given in refs. (1,2). The coincidence spectra show besides the familiar beam-velocity break-up bump at large relative momenta $k \sim 0.7\ fm^{-1}$ an up to now unobserved double structure (Fig. 1).

The data have been analysed by means of the prior-DWBA approach of Austern et.al. (3). The absolute normalisation of the prior-DWBA curves agrees fairly well with the data whereas the double structure in the theory occurs at scattering angles, where the data show only a single bump (Fig. 1). The double structure in prior-DWBA occurs due to interference between the two terms of the T-matrix containing the transition potentials U_α respectively U_d, which describe the interaction between one of the fragments and the target (2). The theory was found to be very sensitive to the transition potentials, while the influence of the αd cluster wave function for the ground state of ^{6}Li is of minor importance. The results of the Quasi-Free Break-up Model of Aarts et al. (4) are also given in Fig. 1, showing qualitatively similar features to prior-DWBA. Since the QFBM overestimates the cross section by a factor of ~ 100 the results have been renormalized, for a good perspective.

(1) N. Heide, internal Report of KfK, 1988, unpublished
(2) N. Heide, thesis, University Heidelberg, 1988
(3) M. Austern, F. Rybicki, Phys. Rev. C6 (1971) 1525
(4) E.H.L. Aarts, R.J. de Meijer, S.Y. van der Werf, Nucl. Phys. A439 (1985) 45

1.3.7 THE SENSITIVITY OF ^{6}Li BREAK-UP CROSS SECTIONS TO HALF-ON-SHELL T-MATRIX ELEMENTS OF ^{6}Li SCATTERING

N. Heide, D.K. Srivastava and H. Rebel

Very recently the triple differential cross section

$$\frac{d^3\sigma}{d\Omega_\alpha d\Omega_d dE_\alpha}$$

for the direct elastic break-up reactions $^{208}Pb(^6Li,\alpha d)^{208}Pb$ and $^{12}C(^6Li,\alpha d)^{12}C$ at 156 MeV has been measured for a variety of scattering angles at large relative momenta of the fragments (1). In the diffractional dissociation picture (2) these data are related to the half-on-shell T-matrix for ^{6}Li scattering by means of the relation

$$\left| f(Q,\varepsilon_{off}) \right|^2 = \frac{d^3\sigma}{d\Omega_\alpha d\Omega_d dE_\alpha} \cdot KF \cdot \frac{1}{\left| F\left(-\frac{m_d}{m_{^6Li}} \vec{Q}, \vec{k}_{\alpha d}\right) + F\left(\frac{m_\alpha}{m_{^6Li}} \vec{Q}, \vec{k}_{\alpha d}\right) \right|^2} \quad (1)$$

where $f(Q,\varepsilon_{off})$ is the half-on-shell scattering amplitude for ^{6}Li which depends on the total momentum transfer $\vec{Q}$ and the parameter

$$\varepsilon_{off} = \frac{\hbar^2}{2\mu} \left(k_i^2 - k_f^2\right) \quad . \quad (2)$$

KF is a kinematical factor, $\vec{k}_{\alpha d}$ is the relative momentum of α and d. Using a 1s Yukawa wave function to describe the relative motion of the clusters α and d in ^{6}Li the inelastic form factor $F(\vec{Q},\vec{k}_{\alpha d})$ can be calculated analytically (2).

Fig. 1 displays the average values of $|f(Q)|^2$ from the reaction ^{208}Pb(^{6}Li,αd)^{208}Pb which were obtained by using eq. (1) and assuming ε_{off} to be approximately constant (~12-14 MeV). The data clearly show a diffractional structure. The theoretical curves were calculated from an optical potential (3) including Coulomb effects. In the case of the reaction ^{12}C(^{6}Li,αd)^{12}C the results are qualitatively similar.

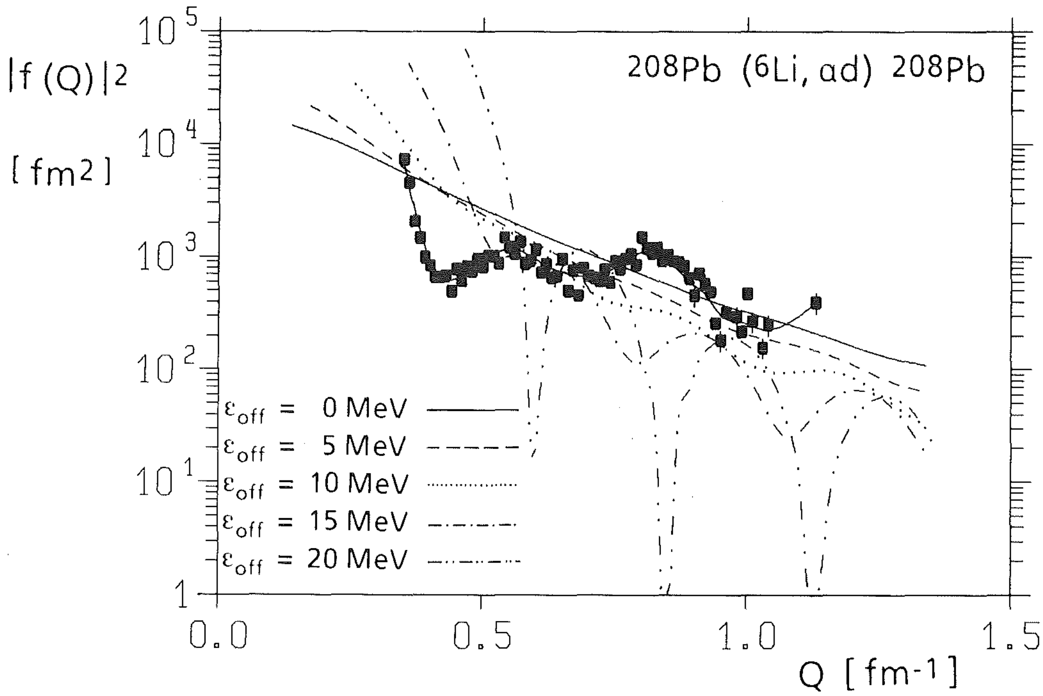

Fig.1 The average values of $|f(Q)|^2$ from the reaction ^{208}Pb(6Li,αd)^{208}Pb compared with calculations using an optical potential and including Coulomb effects for different values of ε_{off}.

A refined approach is obtained by using a realistic 2s αd relative motion wave function for the ground state of ^6Li. The inelastic form factor has to be calculated numerically in this case, causing large computational effort. This work is under progress.

(1) N. Heide, thesis, University of Heidelberg, 1988
(2) M.V. Evlanov, A.M. Sokolov, Nucl. Phys. A452 (1986) 477
(3) J. Cook, H.J. Gils, H. Rebel, Z. Majka, H. Klewe-Nebenius, Nucl.Phys. A388 (1982) 173

1.3.8 COMPOUND NUCLEUS EMISSION OF INTERMEDIATE MASS FRAGMENTS IN THE ^6Li + Ag REACTION AT 156 MeV

K. Grotowski*, J. Ilnicki*, T. Kozik*, J. Lukasik*, S. Micek*, Z. Sosin*, A. Wieloch*, N. Heide, H. Jelitto, J. Kiener, H. Rebel, S. Zagromski, A.J. Cole** (1)

It is shown that emission of intermediate mass fragments is well described by sequential binary decay of the equilibrated compound system produced in the 26 MeV/A ^6Li + Ag reaction.

(1) Phys. Lett. B in press

* Institute of Physics, Jagellonian University, Reymonta 4, Cracow, Poland
** Institut des Sciences Nucléaires, Grenoble, France

1.3.9 AN EXTENDED SUM-RULE MODEL FOR LIGHT AND INTERMEDIATE MASS FRAGMENT EMISSION IN HEAVY ION REACTIONS

I.M. Brâncuş*, H. Rebel, D.K. Srivastava**

The original sum-rule model was introduced (1) for a global description of complete and incomplete fusion processes of colliding heavy ions with energies above the Coulomb barrier. With increasing bombarding energies additional reaction modes, various types of break-up and fragmentation processes with emission of intermediate mass fragments (IMF) show up. With these phenomena following questions arise:

- Which orbital angular momentum values contribute to particular processes?
- Which reaction mechanisms lead to emission of light and intermediate mass fragments?
- Under which conditions does the system approach a partial statistical equilibrium (2) ?

We propose an extension (3) of the original sum-rule model (1) taking into account the competition of complete and incomplete fusion processes, of fragmentation reactions and IMF emission. The model basically assumes that all considered processes proceed via a partial statistical equilibrium (2). Thus, the reaction probability for each reaction channel i is taken proportional to the exponential factor (2)

$$P(i) \propto \exp\{[Q_{gg}(i) - Q_c(i)]/T\} \tag{1}$$

with Q_{gg} being the groundstate Q values, Q_c the change in the Coulomb interaction energy, and T the effective temperature. For a particular orbital angular momentum ℓ the sum-rule is written as a sum of two different contributions

$$N_\ell \{ \sum_{i=1}^{n} T_{\ell(i)} \cdot P(i) + \sum_{i=2}^{n} T'_\ell \cdot P(i) \} = 1 \tag{2}$$

represented by two different kinds of transmission coefficients T_ℓ and with N_ℓ being an overall ℓ-dependent normalisation factor. Two forms of the transmission coefficients are used, the first one

$$T_{\ell(i)} = \{1 + \exp[(\ell - \ell_{\lim(i)})/\Delta\ell]\}^{-1} \tag{3}$$

is just the transmission coefficient used in the original sum-rule model, implying a localisation in the angular momentum space of the entrance channel with $\ell_{\lim(i)}$, calculated according to the prescription of Wilczyński (4), based on the balance of nuclear, Coulomb and centrifugal forces. The expression (3) is a smooth cut-off parametrization with a "surface diffuseness" $\Delta\ell$ in the ℓ-space. The parametrization of

$$T'_\ell = \{1 + \exp[(\ell - \ell_{crit}^{dyn})/\Delta\ell]\}^{-1} \tag{4}$$

represents the emission of IMF, from a transient dinuclear system on its route to complete fusion. The transmission coefficients are identical for all exit channels and depend on the critical value $\ell_{crit}{}^{dyn}$ of angular momentum for fusion in dissipative collisions, i.e. as resulting from a dynamical consideration of the fusion process. Thus, the cross section for each channel (i=1: fusion) is given by

$$\sigma_{(i)}^{tot} = \pi\lambda^2 \sum_{\ell=0}^{\ell_{max}} (2\ell+1) \frac{(T_{\ell(i)} + T'_\ell) P(i)}{\sum_{j=1}^{n} T_{\ell(j)} \cdot P(i) + \sum_{j=2}^{n} T'_\ell \cdot P(j)} \; . \tag{5}$$

The model involves three free parameters: the effective temperature T, the relative distance R_c where the charge transfer takes place and the

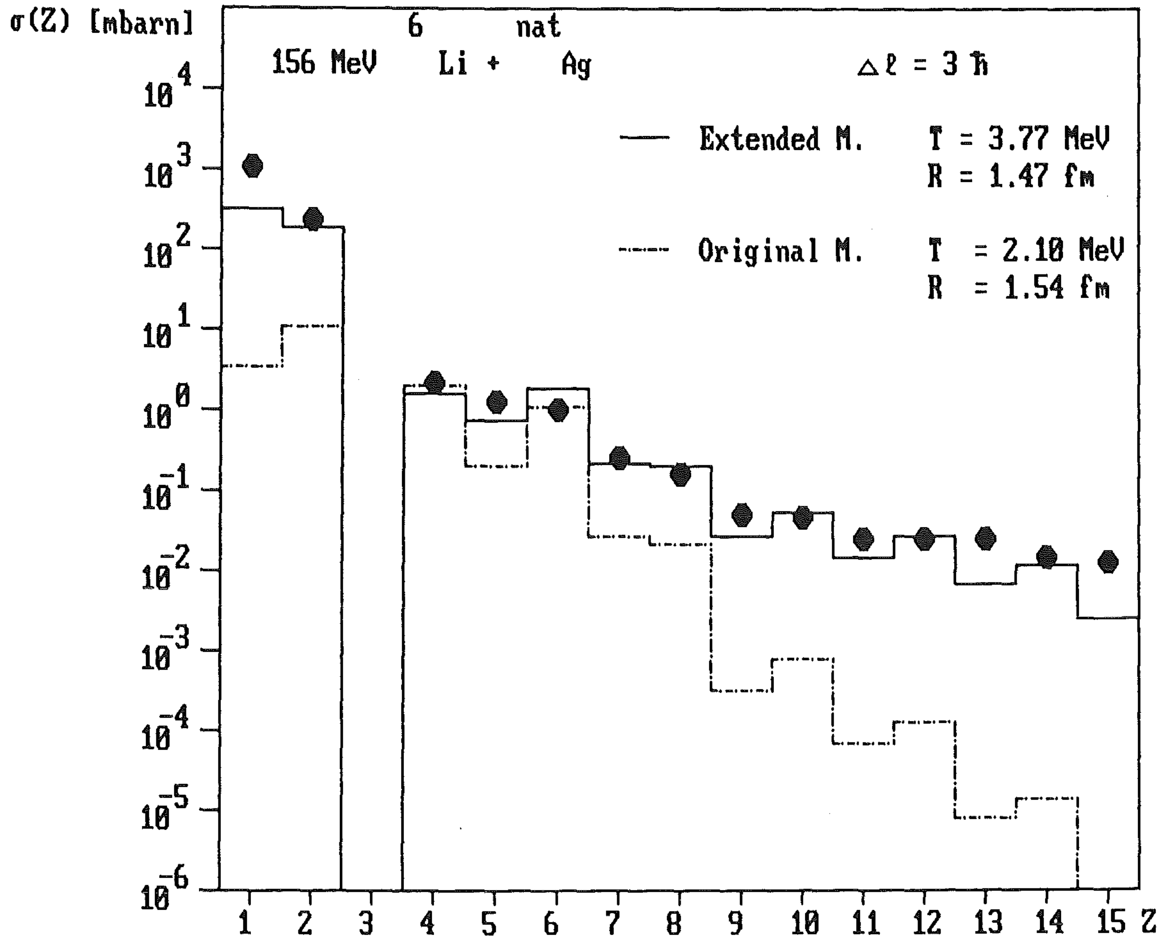

Fig. 1: Results of the sum-rule analysis of IMF emission from collisions of 156 MeV ^{6}Li ions with ^{nat}Ag.

"diffuseness" parameter $\Delta\ell$ in ℓ-space. The values of ℓ_{crit} and ℓ_{crit}^{dyn} result from independent considerations.

The extended sum-rule model has been applied to light and IMF emission in ^{6}Li induced reactions with ^{46}Ti, ^{nat}Cu and ^{nat}Ag at 156 MeV. For such very asymmetric systems and relative high incident energies the original model fails in describing the data (Fig. 1) by considerably underestimating the experimental results (5). When calculating the cross-sections, T and R_C have been adjusted to the data by a best-fit procedure while $\Delta\ell$ was fixed to $3\hbar$. Actually it has been observed that the results are rather insensitive to variations of $\Delta\ell$ around $\Delta\ell = 3\hbar$. The improvement of the description, especially for heavier targets by the extended model is remarkable. The case of ^{nat}Ag includes results for H and He products from inclusive measurements of break-up of 156 MeV ^{6}Li ions (6). The success of the extended sum-rule model suggests that all above processes are governed by the Q_{gg} systematics up to high incident energies, implying the partial statistical equilibration of the colliding systems.

(1) K. Wilczyński, K. Siwek-Wilczyńska, J. van Dreil, S. Gongrijp, D.C.J.M. Hageman, R.V.F. Janssens, J. Lukasik, R.M. Siemssen, Phys, Rev. Lett. 45 (1980) 606

(2) I.M. Brâncuş, KfK-Report 4453 (1988)

(3) J.P. Bondorf, F. Dickmann, D.H.F. Gross, P.J. Siemens, J. de Phys. 32 (1971) C 6-145

(4) J.Wilczynski, Nucl. Phys. A216 (1973) 386

(5) K. Grotowski, J. Ilnicki, T. Kozik, J. Lukasik, S. Micek, Z. Sosin. A. Wieloch, N. Heide, H. Jelitto, J. Kiener, H. Rebel, S. Zagromski, A. Cole, Phys. Lett. B (in press)

(6) J. Wentz, N. Heide, V. Corcalciuc, S. Zagromski, H. Rebel, I.M. Brâncuş (in preparation)

* Central Institute of Physics, IFIN Bucharest, Romania

** Bhabha Atomic Research Centre, V.E.C.C. Calcutta, India

1.3.10 LIGHT PARTICLE EMISSION IN THE ^{6}LI + ^{nat}AG REACTION

J. Wentz, H. Rebel, V. Corcalciuc*, H.J. Gils, N. Heide, H. Jelitto, J. Kiener

Much attention has been focussed in the past few years on the origin of the so called "intermediate mass fragments", produced in both heavy and light ion reactions. In this context the cross sections $\sigma(E,\theta,4\leq Z\leq 15)$ have been measured in the reaction ^{6}Li + ^{nat}Ag at 156 MeV incident energy (1). To complete these data, we have investigated the emission of light particles ($A\leq 4$) in the same reaction.

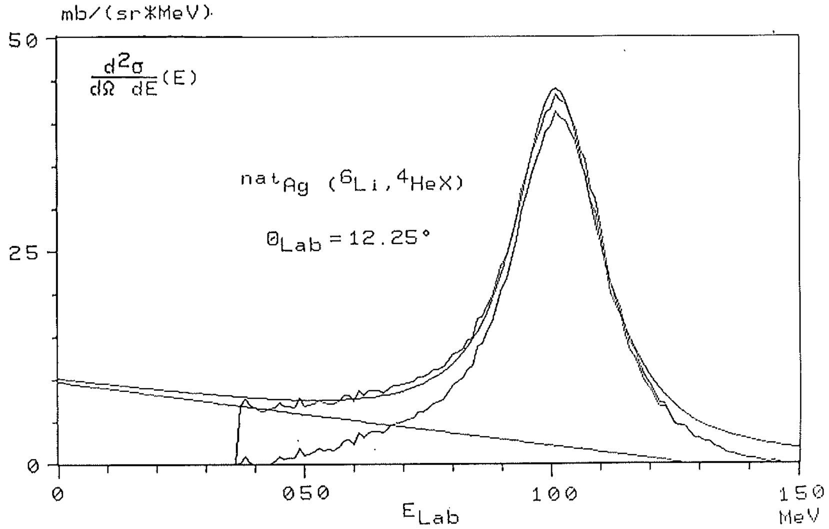

Fig. 1 Typical energy distribution with the fit for the parametrization into a Lorentz curve and a straight line (upper two curves) and the background reduced spectrum (lower curve).

The data have been taken at the Karlsruhe Isochronous Cyclotron, using a ΔE-E semiconductor telescope for the particle identification, with a position sensitive 500 µm Si ΔE-detector and a 21 mm intrinsic Ge E-detector cooled by liquid nitrogen. The target was a self-supporting silver foil of 4 mg/cm^2. The beam after passing through the target was led outside the scattering chamber and collected in a carefully shielded Faraday cup. With this experimental set-up we measured the double differential cross sections for ejectiles up to ^4He with a good separation in the single isotopes at four laboratory angles (13.5° up to 25.°). In the case of ^4He the position sensitive ΔE detector allowed the subdivision of the horizontal acceptance of 3.3° in parts of 0.5°. Fig. 1 shows a typical spectrum for ^4He at 12.25°.

All spectra are dominated by very pronounced broad bumps with maxima at energies roughly corresponding to the velocity of the incoming ^6Li particles. A physical "background" resulting from equilibrium and

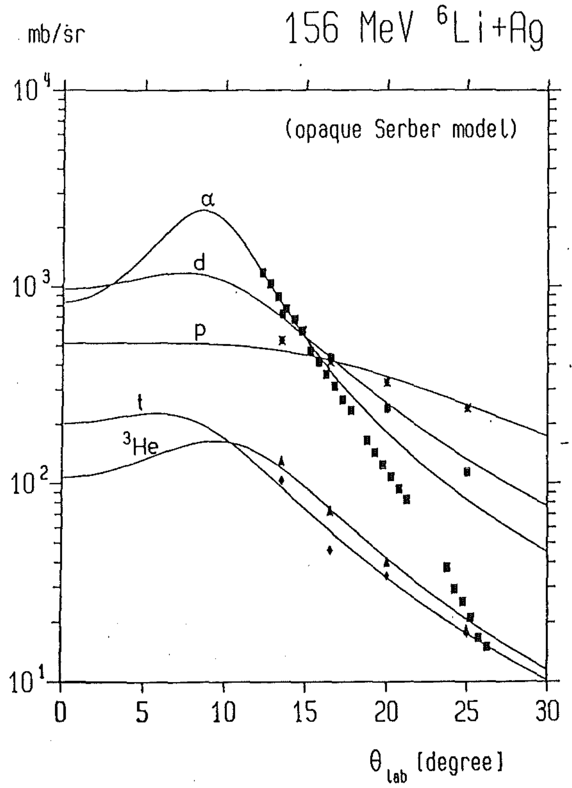

Fig. 2 Angular distributions of the different ejectiles and extrapolations to 0° based on the Serber model.

preequilibrium particle emission was approximated by a straight line added to the bumps of the fast processes, the latter are parametrized in a Lorentz form, in agreement with Serber's spectator model (2,3).

Technically this was done by fitting the shape of the double differential cross sections with the sum of a straight line and a Lorentz curve; such a fit is shown in Fig. 1. After subtracting the obtained background, we integrated the remaining bump for calculating the angular distribution (Fig. 2).

Table 1: Total cross sections for the reaction 156 MeV $^{6}Li + {}^{nat}Ag$ (preliminary results).

Ejectile	Total cross section
p	852 mb
d	451 mb
t	68 mb
^{3}He	68 mb
^{4}He	451 mb

Recently it was shown that the model of Serber is a good description of such a reaction in the region of extreme forward angles (3). Therefore we used the model of Serber to extrapolate the angular distributions (Fig. 2) over the whole solid angle. The difference between the extrapolation with this model and the simple description by an exponential function is about a factor of 2. As preliminary results we present the total cross sections for the single isotopes in Table 1. These data are used as an experimental basis of a new model for the emission of intermediate mass-fragments and ejectiles lighter than the incoming particle (4,5).

(1) K. Grotowski, J. Ilnicki, T. Kozik, J. Lukasik, S. Micek, Z. Sosin, A. Wieloch, N. Heide, H. Jelitto, J. Kiener, H. Rebel, S. Zagromski and A.J. Cole, Phys. Lett. B (in press)

(2) R. Serber, Phys. Rev. 72 (1947) 1008

(3) H. Jelitto, J. Buschmann, V. Corcalciuc, H.J. Gils, N. Heide, J. Kiener, H. Rebel, C. Samanta and S. Zagromski, Z. Phys. A (in press)

(4) I.M. Brâncuş, Report KfK 4453, Kernforschungszentrum Karlsruhe (1988)

(5) I.M. Brâncuş, H. Rebel, D.K. Srivastava, Report KfK 4508, contr. 1.3.9

* Central Institute of Physics, IFIN, Bucharest, Romania

1.3.11 INCLUSIVE MEASUREMENTS OF THE BREAK-UP OF 156 MEV ^{6}LI-IONS AT EXTREME FORWARD ANGLES AND THE QUASI FREE BREAK-UP MODEL

H. Jelitto, J. Buschmann, V. Corcalciuc*, H.J. Gils, N. Heide,

J. Kiener, H. Rebel, C. Samanta**, S. Zagromski (1)

Inclusive alpha particle and deuteron spectra from collisions of 156 MeV ^{6}Li-ions with ^{12}C and ^{208}Pb were measured at extreme forward emission angles including zero degree. The measurements were performed with the Karlsruhe magnetic spectrograph "Little John" and required an efficient reduction of the background from small-angle scattering. The observed double differential cross sections and angular distributions have been analysed on the basis of Serber's spectator break-up model. When going to angles smaller than grazing, where Coulomb effects are expected to be dominating, transitional features may appear. Corresponding effects probably associated to Coulomb break-up are observed with the ^{208}Pb-target and require a slight extension of the Serber approach. In the case of the ^{12}C-target the break-up cross sections in forward direction seem to reflect the shape of the internal momentum distribution of the alpha particle and deuteron cluster in the ^{6}Li-projectile and are in agreement with a 2S-type wave function. However, at larger angles the shape appears to be distorted possibly by final state interactions.

(1) Report KfK 4480 (1988) Kernforschungszentrum Karlsruhe

* Central Institute of Physics IFIN P.O.B. MG6, Bucharest-Magurele, Romania

** SAHA Institue of Nuclear Physics, Bidhan Nagar, Calcutta 700064, India

1.3.12 THE QQDS MAGNETIC SPECTROGRAPH "LITTLE JOHN" AT THE KARLSRUHE CYCLOTRON (I) DESIGN AND CONSTRUCTION

H.J. Gils, J. Buschmann, S. Zagromski, J. Krisch*, H. Rebel (1)

A magnetic spectrograph for charged-particle spectroscopy, named LITTLE JOHN, consisting of two quadrupoles, one dipole and one sextupole magnet was constructed and put into operation at the Karlsruhe Isochronous Cyclotron. The ion-optically rather simple system covers a particle rigidity of 2.5 T·m and was especially designed for small reaction angle experiments. A modest resolving power of $p/\Delta p$ = 5300, a momentum acceptance of $(p_{max} - p_{min})/p_{mean}$ = 20% and an acceptance solid angle of Ω = 1.5 msr were the design goals. The momentum dispersion and consequently the acceptance of the spectrograph can be varied by a factor of 2 without varying other imaging properties considerably. The design, construction and equipment of the spectrograph are described.

(1) Nucl. Instr. and Meth. (in press)

* Kernforschungszentrum Karlsruhe, Hauptabteilung Ingenieurtechnik

1.3.13 THE QQDS MAGNETIC SPECTROGRAPH "LITTLE JOHN" AT THE KARLSRUHE CYCLOTRON

(II) EXPERIMENTAL PROCEDURES AND PERFORMANCE

H.J. Gils, H. Jelitto, H. Schlösser*, S. Zagromski, J. Buschmann, W. Eyrich*, A. Hofmann*, J. Kiener, A. Lehmann*, H. Rebel (1)

The measured ion-optical properties of the Karlsruhe magnetic spectrograph "Little John" and the properties of its detector system are described. Moreover, the procedures for an efficient use of the spectrograph in particular concerning small angle and zero degree experiments are presented in detail. Characteristic experimental results from ^{6}Li-induced nuclear reactions demonstrate the performance of the whole set-up.

(1) Nucl. Instr. and Meth. (in press)

* Physikalisches Institut der Universität Erlangen-Nürnberg, D-8520 Erlangen, FRG

1.3.14 SPIN-ISOSPIN TRANSFER STRENGTH IN ^{18}O

M. Moosburger*, W. Eyrich*, H.J. Gils, A. Hofmann*, A. Lehmann*, H. Rebel, R. Rudeloff*, H. Schlösser*, H. Wirth*, and S. Zagromski

The investigation of the (^{6}Li,^{6}He) charge exchange reaction on light nuclei is an excellent method to study the mechanism of spin and isospin transfer. The selection rules $\Delta T = \Delta S = 1$ combined with measurements at extreme forward angles cause a high sensitivity for Gamow-Teller (GT) transitions with $\Delta T = 1$, $\Delta S = 1$ and $L = 0$, while $\Delta S = 0$ transitions are suppressed (1).

The experiments were performed at the ^{6}Li^{3+} beam of the Karlsruhe Isochronous Cyclotron with the Lithium source LISKA. The magnetic spectrograph "Little John" served for detecting the ^{6}He particles in an angular region 10° down to 0°.

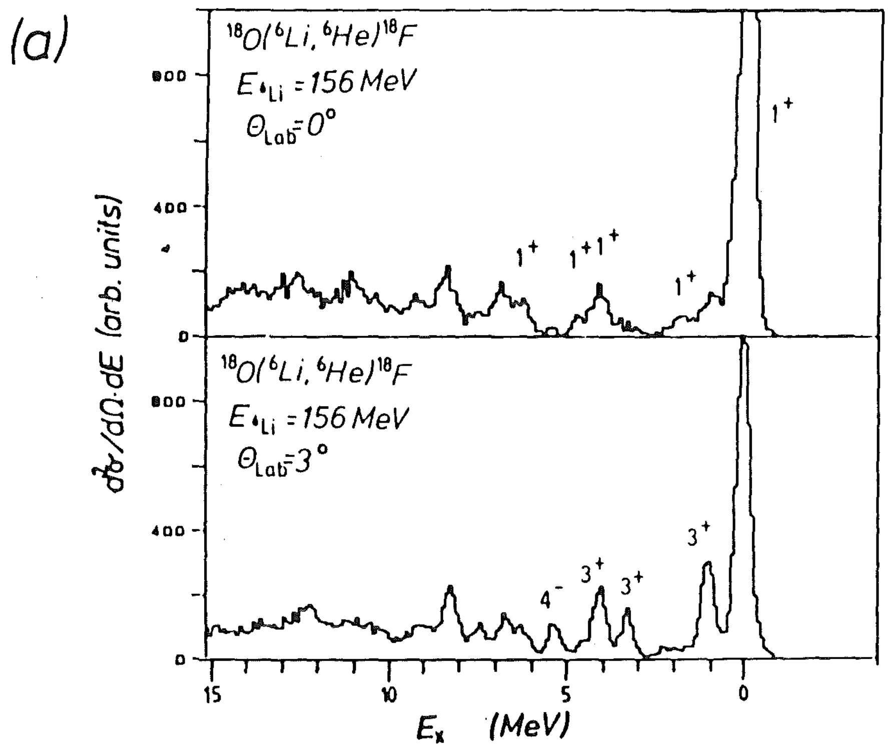

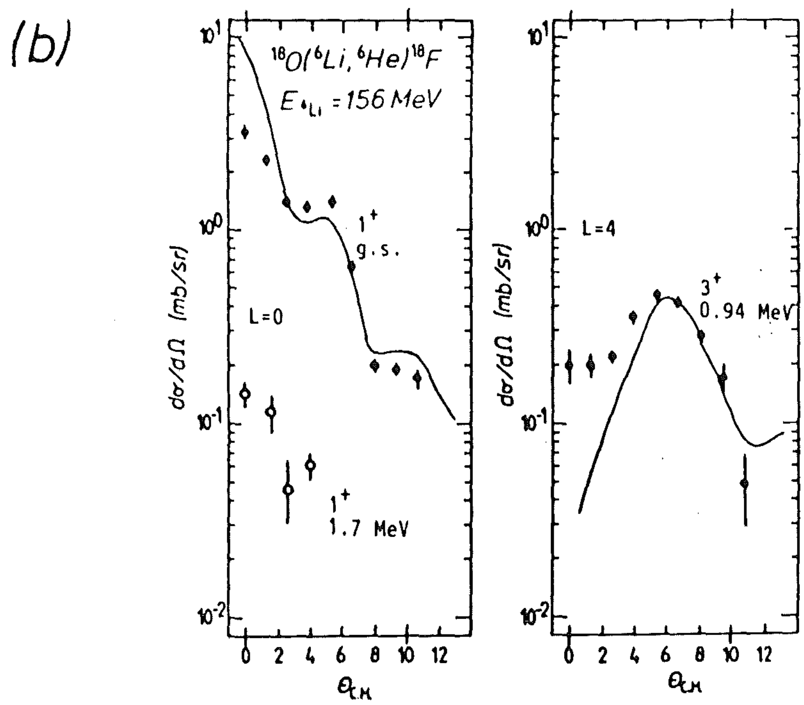

Fig. 1 a) Spectra of the reaction $^{18}O(^{6}Li,^{6}He)^{18}F$ at 0° and 3°.

b) Angular distribution of the 1^+ states at 0.0 and 1.7 MeV and of the 3^+ state at 0.94 MeV excitation energy.

Here we present some results of the measurements on oxygen 18. Fig. 1a shows the spectra of the $^{18}O(^{6}Li,^{6}He)^{18}F$ reaction at angles of 0° and 3°. Clearly identified states in the final nucleus ^{18}F are assigned with spin and parity quantum numbers, especially the 1^+ states representing most of the GT strength in this system. The angular distributions of the first two 1^+ states at excitation energies of 0.0 MeV and 1.7 MeV are shown in Figure 1b. This is a striking difference to the angular distribution of the 3^+ state at E_x = 0.94 MeV also shown in Fig. 1b.

The solid curves are DWBA calculations with a transfer of angular momentum of L = 0 an L = 4, respectively. The calculations were performed with the computer code DWUCK 4.

In Table 1 the cross sections of the two 1^+ states are compared with the values of the squared nuclear matrix elements, which were extracted from the log ft values of the β-decay of the mirror nucleus ^{18}Ne to the same final states in ^{18}F. The good proportionality between matrix elements and cross sections is remarkable. The very small upper limit for the cross section of the isobaric analogue state at 0.94 MeV shows the strong suppression of this $\Delta S = 0$ transition.

Table 1: Comparison between cross sections of the $^{18}O(^{6}Li,^{6}He)^{18}F$ reaction and squared nuclear matrix elements.

E_x in ^{18}F (MeV)	J^{π}; T	dσ/dΩ (0°) (mb/sr) $(^{6}Li,^{6}He)$	B (GT) $^{18}Ne(\beta^+)^{18}O$
0.0	1^+; 0	3.3	3.28
1.7	1^+; 0	0.13	0.16
1.04	0^+; 1	<0.08	2.0 B(F)

(1) J.S. Winfield, N. Anantaraman, Sam M. Austin, Ziping Chen, A. Galonsky, J. van der Plicht, H.-L. Wu, C.C. Chang and G. Ciangaru, Phys. Rev. C 35 (1987) 1734

* Physikalisches Institut der Universität Erlangen-Nürnberg

1.3.15 COLLECTIVE GAMOW-TELLER STRENGTH IN ^{90}Zr AND ^{48}Ca

H. Wirth*, W. Eyrich*, H.J. Gils, A. Hofmann*, A. Lehmann*, M. Moosburger*, H. Rebel, R. Rudeloff*, H. Schlösser*, and S. Zagromski

Very recently, it has been shown that the (^{6}Li,^{6}He) reaction is a valuable method to investigate spin-isopin transfer strengths, especially Gamow-Teller (GT) strengths. Two interesting nuclei to study these modes are the closed shell systems ^{48}Ca and ^{90}Zr. In addition to single GT states at low excitation energies here exist also collective ("giant") GT resonances at higher excitation energies, which exhaust most of the total GT strength. The measurements on these nuclei were performed with the 156 MeV $^{6}Li^{3+}$

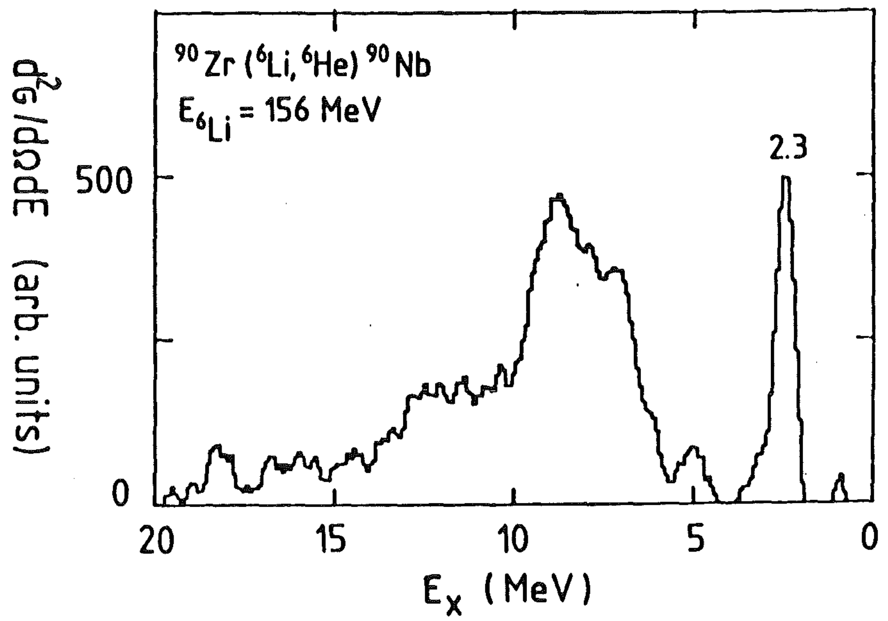

Fig. 1 Difference spectrum (θ = 0° minus θ = 2°) of the ^{90}Zr(^{6}Li,^{6}He) reaction representing the GT strength in the observed energy region $0 \leq E_x \leq 20$ MeV.

beam at the Karlsruhe Isochronous Cyclotron using the magnetic spectrograph "Little John" in an angular region $0° \leq \theta_{He,\ Lab} \leq 10°$.

In addition to the first results presented for the ^{90}Zr(^{6}Li,^{6}He)^{90}Nb reaction in our contribution to the last annual report, we meanwhile did a refined data analysis especially making use of the information from the diffraction patterns of the angular distributions. It is possible to extract L = 0 strengths with a rather high precision by simply subtracting the spectra at θ = 0° (maximum of L = 0 strength) and at an angle near the first diffraction minimum. As a result, in Fig. 1 the difference spectrum of the ^{90}Zr(^{6}Li,^{6}He)^{90}Nb reaction at θ = 0° and

$\theta = 2°$ is shown. Contributions from strengths with multipolarities L>0 have vanished almost quantitatively, as can be seen e.g. regarding the 1.0 MeV "peak". At $E_x \approx 5.1$ MeV one can see a little peak that might be identified as a remaining weak excitation of the isobaric analogue state (IAS). This illustrates the remarkably strong suppression of $\Delta S = 0$ contributions specific for the (^{6}Li,^{6}He) reaction. The extended GT strength also allows the determination of a sum rule value. The result is

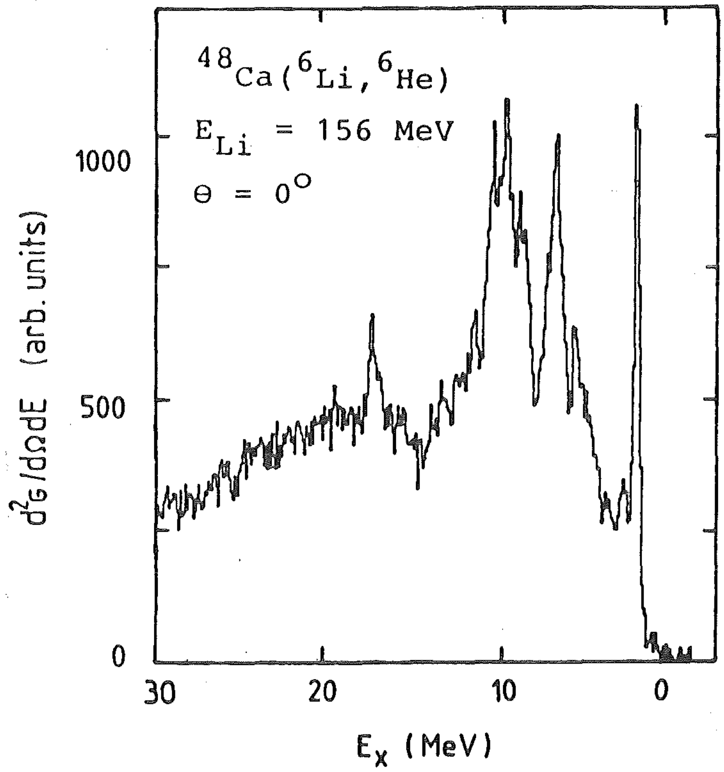

Fig. 2 Zero degree ^{6}He spectrum from the reaction ^{48}Ca(^{6}Li,^{6}He)^{48}Sc at E_{Li} = 156 MeV measured with the magnetic spectrograph "Little John"

tentatively higher (about 75%) than that obtained from the 200 MeV (p, n) data.

To get more systematic information about the excitation of spin-isospin strengths using the (^{6}Li,^{6}He) reaction we started a similar experiment on the system ^{48}Ca $\rightarrow$ ^{48}Sc. A zero degree spectrum which is dominated by GT strength is shown in Fig. 2. The distribution of the GT strength is in almost quantitative accordance with (p, n) data taken at zero degree at E_p = 134 MeV (1). One clearly recognizes the strongly excited 1^+ state at E_x = 2.52 MeV and the T = 4, 1^+ state at E_x = 16.8 MeV. As expected, at $E_x \approx 6.67$, where the IAS should appear, only a small enhancement in the cross section can be observed. In the energy region 4.5 MeV $\leq$ E_x $\leq$ 14.5 MeV an apparently structured complex of different states is composing the GT giant resonance. Work to unfold these states is still in progress as well as the analysis of the $^{48}Ca(^{6}Li,^{6}He)^{48}Sc$ data taken at the various angles > 0° to study the contributions of strengths with higher multipolarities and to extract the GT strength quantitatively.

(1) B.D. Anderson, T. Chittrakarn, A.R. Baldwin, C. Lebo, R. Madey, R.J. McCarthy, J.W. Watson, B.A. Brown and C.C. Foster Phys. Rev. C 31 (1985) 1147 and 1161

* Physikalisches Institut der Universität Erlangen-Nürnberg

1.3.16 EXCITATION AND DECAY OF ISOSCALAR GIANT RESONANCES IN ^{124}Sn

A. Lehmann*, W. Eyrich*, H.J. Gils, A. Hofmann*, M. Moosburger*, H. Rebel, R. Rudeloff*, H. Schlösser*, H. Wirth*, and S. Zagromski

Decay experiments and small angle scattering are effective methods for studying giant resonances. Combining both procedures, we investigated the excitation and the neutron decay of the isoscalar E2 and E0 giant resonances (GR) in ^{124}Sn with the 156 MeV ^{6}Li beam of the Karlsruhe Isochronous Cyclotron. This work is the continuation of earlier decay experiments at ^{208}Pb (1) and ^{90}Zr (2) of our group.

The scattered ^{6}Li particles were detected by the magnetic spectrograph "Little John" in an angular region between 1.0° and 4.5°. This angular region just covers a maximum and a minimum of the cross section of the E0 GR, whereas all other multipolarities, especially the overlapping E2 GR, remain nearly constant. Thus this region is very suitable for the investigation of the giant monopole resonance, but also the giant quadrupole resonance which is in its maximun there.

The single spectra in Fig. 1 shows the GR bump of ^{124}Sn in a minimum (2.6°, dotted line) and a maximum (4.1°, solid line) of the E0 cross section. The E0 GR can be clearly identified from the difference in both spectra at the high energy shoulder of the GR bump. Comparing both spectra, the favourable resonance-to-background ratio allows a quantitative extraction of the overlapping E0 and E2 GR's. Moreover the small contribution of the continuum in the giant resonance region is very important to get precise information from decay experiments.

To investigate the decay of the E2 and E0 giant resonance regions, we used an equipment consisting of eight large scintillation detectors at

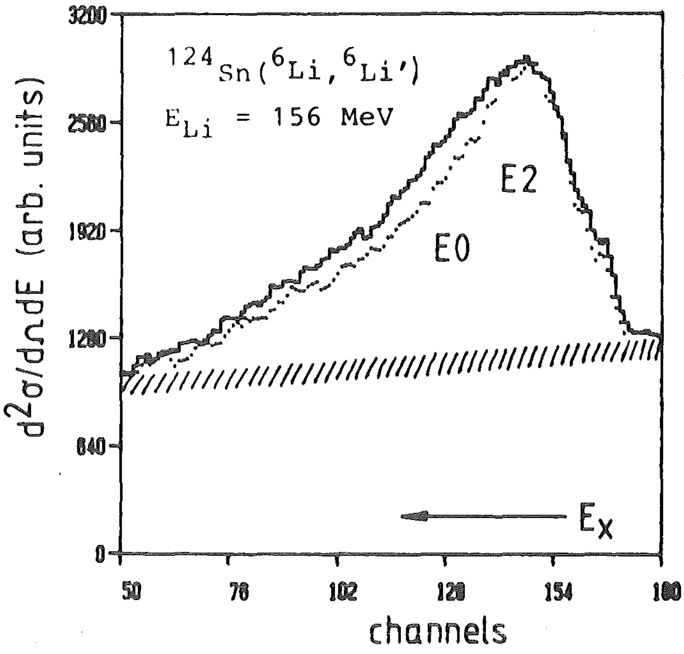

Fig. 1 $(^6Li,^6Li')$ spectra of ^{124}Sn in a maximum at 4.1° (solid line) and a minimum at 2.6° (dotted line) of the E0 GR.

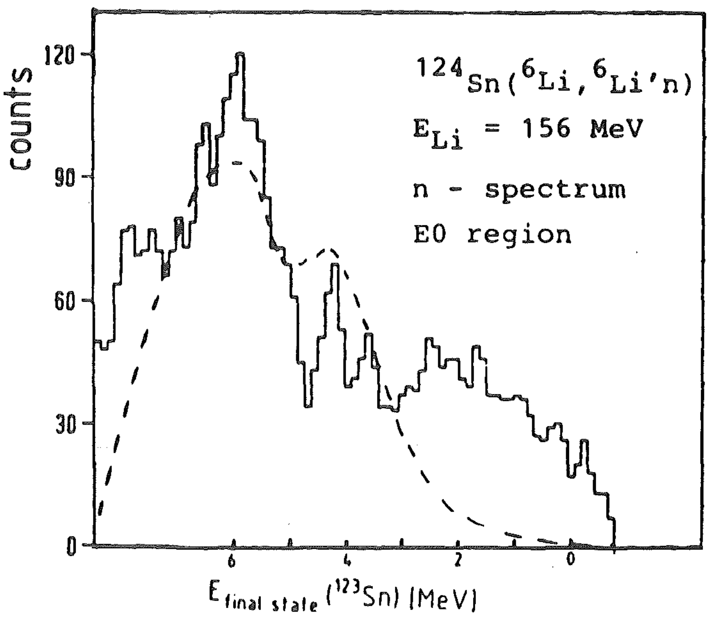

Fig. 2 n-decay spectrum of the giant monopole region in ^{124}Sn from $^{124}Sn(^6Li,^6Li'n)$ measurements.

backward decay angles. The spectroscopy of the coincident neutrons was performed using time of flight technique, similar as described in ref. 2.

While the analysis of the E2 decay is still in progress, we are able to present first results of the E0 decay. In Fig. 2 the spectrum of the decay neutrons of the giant monopole resonance region in ^{124}Sn

measured in the maximum at 4° of the resonant strength excited by ^{6}Li particles is schown. The dashed line represents an evaporation spectrum of the neutrons assuming pure statistical decay. The significant deviations at energies $E_{final} \leq 3$ MeV correspond predominantly to a direct decay of the GMR into low lying hole states of the residual nucleus ^{123}Sn. At energies $E_{final} > 1.5$ MeV additional phonon coupled states in ^{123}Sn are overlapping the hole states. Thus we assume, that also preequilibrium decay components contribute.

From the shape of the decay spectrum we roughly estimate a direct decay component of 15-20% and a preequilibrium decay component of at least about 5% for ^{124}Sn. These values are of the same magnitude as the results of our earlier experiments at ^{208}Pb (1) and ^{90}Zr (2).

(1) W. Eyrich, K. Fuchs, A. Hofmann, U. Scheib, H. Steuer, H. Rebel, Phys. Rev. C29 (1984) 418

(2) K. Fuchs, W. Eyrich, A. Hofmann, B. Mühldorfer, U. Scheib, H. Schlösser, H. Rebel, Phys. Rev. C32 (1985) 418

* Physikalisches Institut der Universität Erlangen-Nürnberg

2. LASER SPECTROSCOPY

2.1 DETERMINATION OF THE ^{242m}Am NUCLEAR MOMENTS

K. Bekk, S. Göring, W. Kälber, G. Meisel, H. Rebel, A. Ali Sameh*
(1)

The hyperfine structure of Am atoms was investigated in an atomic beam by laser spectroscopy. The observed splittings were evaluated with respect to the magnetic dipole and electric quadrupole moments of ^{242m}Am. The results are: $\mu_I(^{242m}\mathrm{Am})=+0.97(5)\,\mathrm{nm}$, $Q(^{242m}\mathrm{Am})=+6.5(2.0)$ b.

(1) Z. Phys. A - Atomic Nuclei 330 (1988) 235

* Institut für Radiochemie, Kernforschungszentrum Karlsruhe

2.2 THE 3d STATES OF ^{23}Na AND ^{7}Li : DETERMINATION OF UNRESOLVED HYPERFINE SPLITTINGS AND RADIATIVE LIFETIMES

B. Burghardt*, B. Hoffmann*, G. Meisel (1)

The electronic transitions from the ground state to the 3d states have been studied for ^{23}Na and ^{7}Li atoms by two-photon Doppler-free laser spectroscopy. The positions of the resonances are used to determine the unresolved hyperfine structure of the 3d states from which the magnetic-dipole hyperfine interaction constants A are derived. The results for the A factors are: A(3d $^2D_{3/2}$; ^{23}Na)=+527(25) kHz; A(3d $^2D_{5/2}$; ^{23}Na)= +108.5(2.4) kHz; A(3d $^2D_{3/2}$; ^{7}Li)=+843(41) kHz; A(3d $^2D_{5/2}$; ^{7}Li)= +343.6(1.0) kHz. For the fine structure intervals fs of the 3d doublets we obtain: fs(3d Na)= - 1 494 444(44) kHz and fs(3d Li)= +1 083 936(60) kHz. The linewidths of the resonances are evaluated with respect to the natural lifetimes of the 3d states. For Na the result is τ(3d Na)=19.27(23) ns.

(1) Z. Phys. D - Atoms, Molecules and Clusters 8 (1988) 109

* Institut für angewandte Physik, Universität Bonn, Bonn, FRG

2.3 A NEW METHOD TO REDUCE THE LINEWIDTH OF OPTICAL TRANSITIONS FOR STORED IONS.

W. Kälber, J. Rink, K. Bekk, G. Meisel, R.C. Thompson*

In previous experiments (1), we used optical excitation of stored thorium ions to determine isotope shifts and hyperfine splittings of several thorium isotopes. For this purpose the ions were trapped in a small volume by means of radiofrequency and static electric quadrupole fields (2, 3). Laser spectroscopy of stored ions has been shown to be highly sensitive (4) because of the long storage time of many hours that can be realized which allows for many scattering processes for each trapped ion. The method was found (1) to be well suited for the study of radioactive atomic ions.

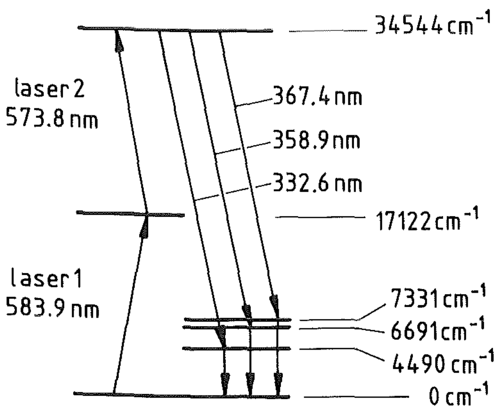

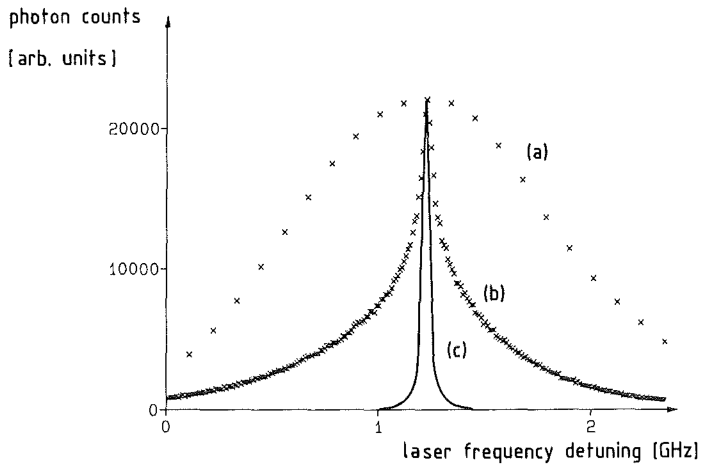

Fig. 1 Two-step excitation of stored thorium ions.
Left: Partial level diagram to indicate the laser and detection wavelengths.
Right: Lineshapes for ^{232}Th.
a) as observed with single-step excitation,
b) the narrow line as obtained for two-step excitation,
c) the approximate natural lineshape.

The resolution, however, is rather low because of the relatively wide Doppler broadening due to the fast motion of the ions in the confining field. It did not allow, e.g., to resolve the hyperfine splittings of the odd Th isotopes. In order to improve the resolution, we have investigated two-step excitation of stored ions as a new method to reduce the broadening and thus to improve the resolution.

In the two-step excitation, two parallel laser beams excite the subsequent transitions ThII $0 \rightarrow 17122$ cm^{-1} and 17122 cm$^{-1} \rightarrow 34544$ cm^{-1}, respectively (Fig.1). The excitation is monitored by detection of fluorescence light from the transitions λ = 332.6 nm, 358.9 nm, and 367.3 nm that lead into states around 6000 cm^{-1}. By a combination of spontaneous emission and collisions with buffer gas atoms the ions come back to the ground state to be reused. Spectra usually are taken with laser 1 fixed to the first step transition whereas laser 2 is tuned. In this way the ions are excited only when they happen to assume a specific velocity component along the laser beam axis resulting in a sharp velocity distribution in the 17122 cm^{-1} state for each hyperfine transition. The second laser samples the ions prepared in this way, leading to a reduced Doppler linewidth. From this simple model a lineshape corresponding to the natural one is predicted.

In the experiments, though, we observe a peculiar lineshape that is broadened as compared to a guessed natural width of about 50 MHz (Fig. 1). The broadening is due to the fact that the ions change their velocities during the short time they stay in the 17122 cm^{-1} level since they are accelerated by the applied voltages. The influence of the experimental parameters on the lineshape has been studied in more detail using ^{232}Th ions.

For the condition $v_{long} \approx 0$ it was found that the increase in resolution was about a factor of 5, allowing to resolve the hyperfine splittings in ^{229}Th as is discussed in more detail in (5). It is to be noted that there is no loss in signal strength as compared to the single-step excitation since the bottleneck that limits the signal rate is the return time to the ground state; the selection of ions according to the momentary longitudinal speed does not exclude ions from being excited because within some waiting time almost every ion assumes the speed chosen. In our two-step experiments the signal were even slightly higher than for single-step excitation mainly because the photocathode quantum efficiency is higher for the two-step detection wavelengths around 350 nm. Different schemes are considered to improve the linewidth further.

(1) K. Bekk, W. Faubel, S. Göring, W. Kälber, G. Meisel, H. Rebel, J. Rink, G. Schatz, R.C. Thompson, Report KfK 4405, Kernforschungszentrum Karlsruhe (1988) 69

(2) E. Fischer, Z. Phys. 156 (1959) 1

(3) H.G. Dehmelt, Adv. At. Mol. Phys. 5 (1969) 109

(4) W. Neuhauser, M. Hohenstatt, P.E. Toschek, H. Dehmelt, Phys. Rev. A22 (1980) 1137

(5) W. Kälber, J. Rink, K. Bekk, W. Faubel, S. Göring, G. Meisel, H. Rebel, G. Schatz, R.C. Thompson, Report KfK 4508, contr. 2.4

* Optics Section, Blackett Laboratory, Imperial College, London

2.4 STORED ION LASER SPECTROSCOPY OF THORIUM ISOTOPES WITH IMPROVED RESOLUTION

W. Kälber, J. Rink, K. Bekk, W. Faubel*, S. Göring, G. Meisel,

H. Rebel, R.C. Thompson**

Laser spectroscopy of ions stored in an rf trap has proven to be an effective method for radioactive atomic species: Its sensitivity in terms of the minimum required sample size was found to be satisfactory. This applies even to, e.g., the refractory element thorium where the transfer factor from the sample deposited onto a wire to the stored ion cloud is only about 10^{-8}; the overall sensitivity nevertheless is comparable to that of the atomic beam method which so far was found to be most effective. The resolution of the ion spectra, however, was not quite satisfactory because of the relatively broad Doppler linewidths of 1 to 1.6 GHz which is due to the electric fields required for the storage process. Therefore a spectroscopic method has been developed (1) which reduces the observed linewidths typically by a factor of 5. The method uses a two-step optical exication instead of a single photon absorption. The gain in resolution is obtained without loss in signal strength.

The new two-step method is particularly useful for odd isotopes which have a hyperfine splitting so that their optical transitions are composed of several components that overlap if the resolution is too low. Fig. 1 (left part) gives an example of an unresolved hyperfine structure

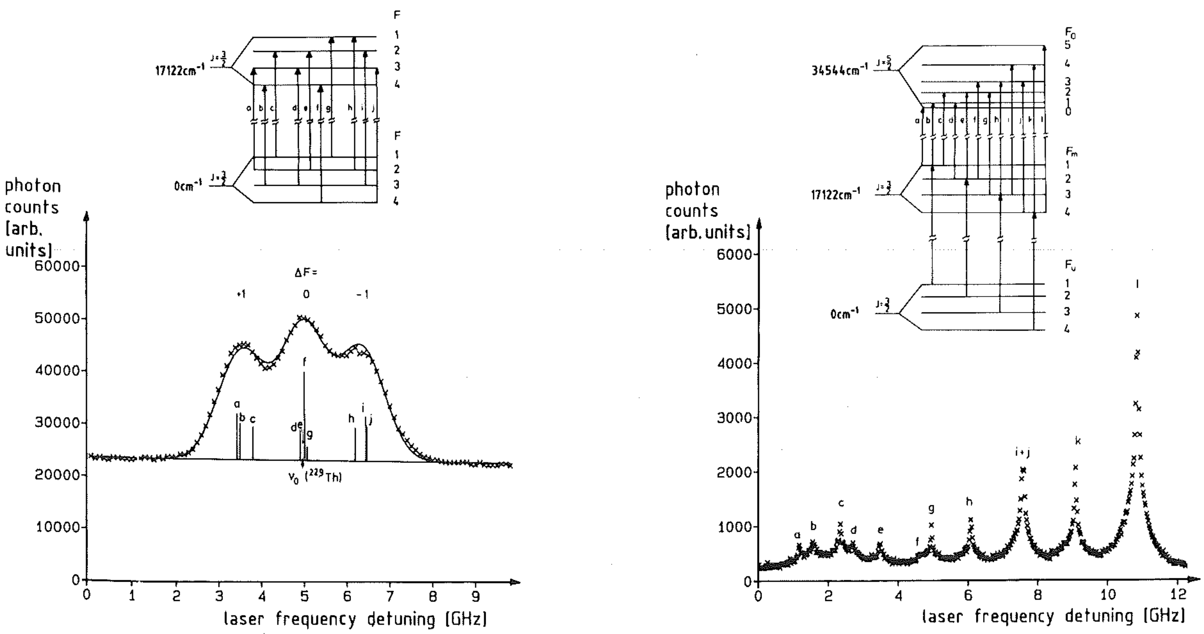

Fig. 1 Spectrum of ^{229}Th, recorded by single-step (left part) and by two-step optical excitation (right part).

in ^{229}Th. Fig. 1 (right part) shows a record as obtained with the new method. It is to be noted that the two traces are not directly comparable since they display the hyperfine splittings of different states.

Table 1: A and B factors for ^{229}Th for the levels 0,17122, and 34544 cm^{-1}.

Level $[cm^{-1}]$	A [MHz]	B [MHz]
0	-444.2 (1.9) -450(30)$^{+)}$	303(6) 420(150)$^{+)}$
17122	-442(9)	430(150)
34544	366.1(1.2)	-90(10)

$^{+)}$ values from ref. (2)

The two-step spectrum of Fig. 1 (right part) was obtained by inducing as a first step the transition shown in Fig. 1 (left part). The frequency of the laser used for the first step was fixed to the center of the line in Fig. 1 (left part) while the frequency of the laser for the second step was tuned. From the analysis of this spectrum, A and B factors of the levels 0 and 34544 cm^{-1} are determined, whereas A and B factors of the level 17122 cm^{-1} are obtained from an analysis of the Doppler broadened spectrum of ^{229}Th. The results are summarized in Table 1.

Table 2: Mean square charge radius changes for thorium isotopes, deduced from isotope shift measurements of the ThII 583.9 nm transition (3) and calculated $\delta\langle r^2\rangle$ values using spherical droplet model formulas, corrected for quadrupole deformation.

Mass-number A	Experimental ms charge radius changes $\langle r^2\rangle^A - \langle r^2\rangle^{232}$ [fm^2]	Calculated ms charge radius changes $\langle r^2\rangle^A - \langle r^2\rangle^{232}$ [fm^2]
230	-0.205(28) $^{+)}$	-0.214
229	-0.334(46)	-
228	-0.413(56)	-0.404
227	-0.508(70)	-

$^{+)}$ value from ref. (4), used as calibration factor

In previous experiments we have measured isotope shifts of the 583.9 nm transition for the isotopes ^{227}Th to ^{230}Th, with respect to ^{232}Th (3). With the calibration factor $\delta\langle r^2\rangle^{230,232} = -0.205(28)$ fm^2 (4), we have reevaluated the changes of mean square charge radii for these pairs of thorium isotopes. The results summarized in Table 2 and Fig. 2 were compared with spherical droplet model calculations (5) and corrections for changes of the mean square quadrupole deformations deduced from experimental BE2 values (6). A good agreement between experimental and calculated $\delta\langle r^2\rangle$ values is observed.

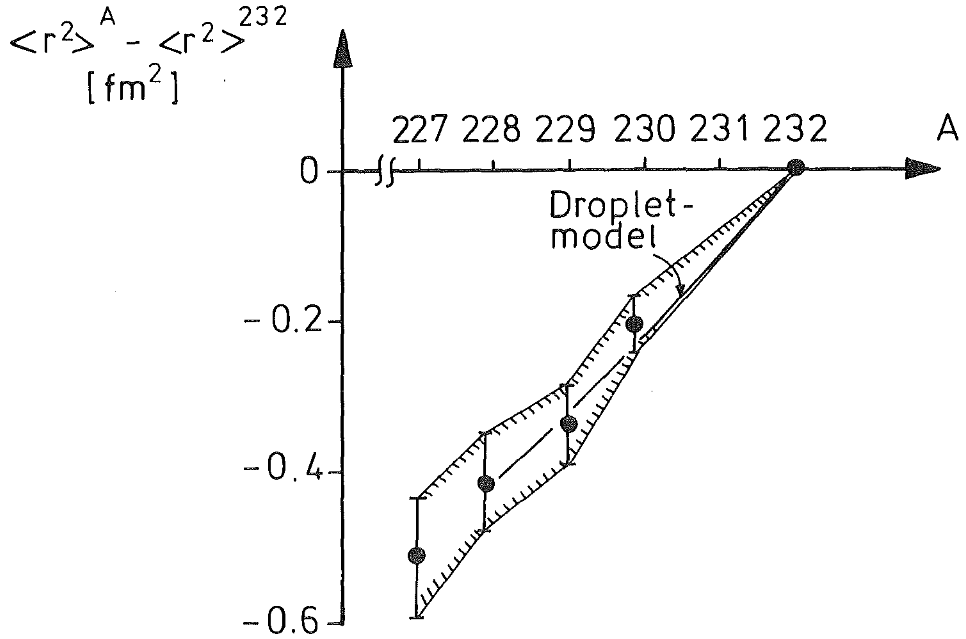

Fig. 2 Plot of mean square charge radius changes for thorium isotopes. Solid line: calculated $\delta\langle r^2\rangle$ values, using spherical droplet model and corrections for quadrupole deformations.

(1) W. Kälber, J. Rink, K. Bekk, G. Meisel, R.C. Thompson, Report KfK 4508 Contr. 2.3

(2) S. Gerstenkorn, P. Luc, J. Verges, D.W. Englekemeir. J.E. Gindler et F.S. Tomkins, Journal de Physique 35 (1974) 483

(3) K. Bekk, W. Faubel, S. Göring, W. Kälber, G. Meisel, H. Rebel, J. Rink, G. Schatz, R.C. Thompson, Report KfK 4405, Kernforschungszentrum Karlsruhe (1986) 69

(4) P. Aufmuth, K. Heilig, A. Steudel, At. Data Nucl. Data Tabl. 37 (1987) 455

(5) W.D. Myers, W.J. Swiatecki, Ann. of Phys. 55 (1969) 395

(6) S. Raman, C.H. Malarkey, W.T. Milner, C.W. Nestor, Jr., and P.H. Stelson, At. Data Nucl. Data Tabl. 36 (1987) 1

* Institut für Radiochemie, Kernforschungszentrum Karlsruhe

** Optics section, Blackett Laboratory, Imperial College, London

2.5 ATTEMPTS TO PRODUCE AND DETECT A BEAM OF RADIOACTIVE PLATINUM ATOMS

P. Pietruk, F. Feurer, H. Hanser, G. Meisel

Platinum nuclei show a shape change from predominantly prolate shape for nuclei with A $\leq$ 184 to predominantly oblate shape for A $\geq$ 188 (1). To determine the exact location of this shape transition for Pt nuclei in the ground state between A = 184 and A =186, isotope shift measurements are planned on a thermal atomic beam of the radioactive isotopes ^{186}Pt through ^{189}Pt, applying the method of laser induced fluorescence. The small amounts of Pt, produced by Os(α,xn)Pt reactions, cannot be evaporated directly from the irradiated metallic Os targets, therefore a dry and a wet chemical separation process were investigated.

In the dry process, Os was oxidized to volatile OsO_4 in an O_2 atmosphere. Only a small amount of ash remained, containing the Pt. Since it was found that the Pt cannot be evaporated at about 2000° C from this remainder within a period adequate for the measurements, this dry process was not further investigated.

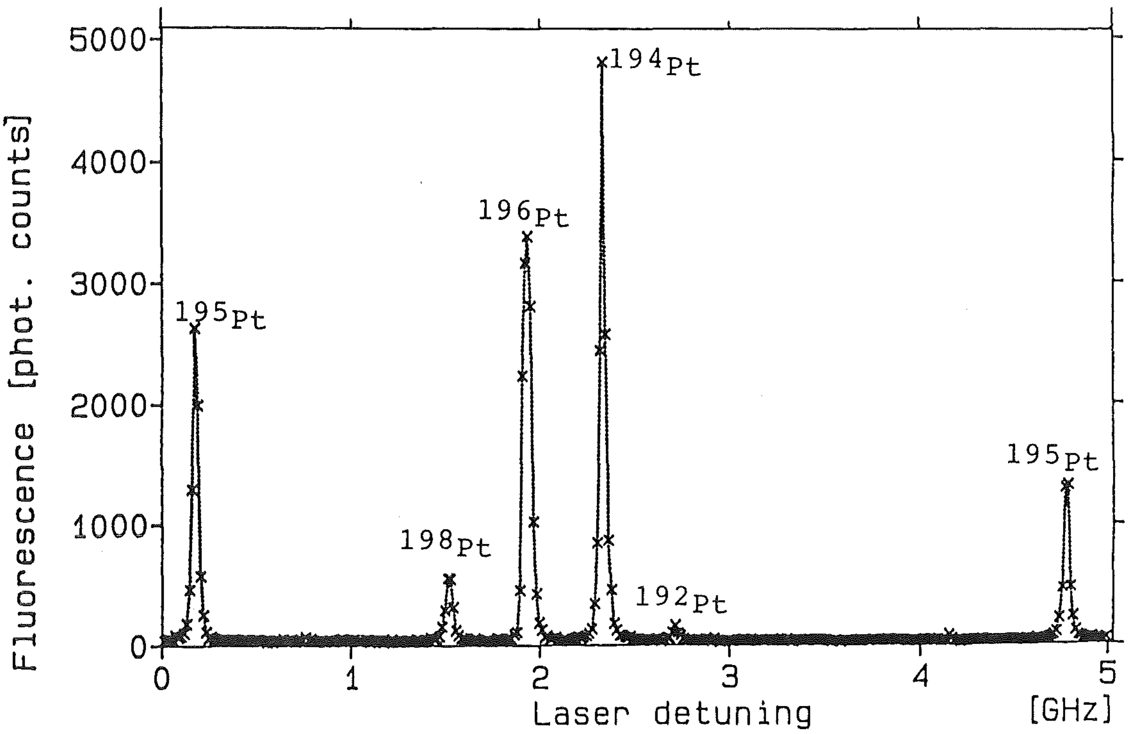

Fig. 1 Partial fluorescence spectrum of ^{nat}Pt, resonantly excited at 292.9 nm.

The wet process is based on the dissolution of Os in concentrated nitric acid under pressure at about 200° C. To keep impurities resulting from reactions with the container as low as possible, the reagents have to be sealed in an ampoule of high purity fused silica. The ampoule is placed inside a pressure vessel and heated for several minutes in a hot silicon oil bath at 200° C. Thus accidental contamination caused by leaks or by bursting can be excluded. After the Os is dissolved, it can be volatilized as OsO_4 by repeated addition and evaporation of concentrated HNO_3. The whole process takes about half an hour, which is short enough even for the separation of ^{186}Pt, having the shortest lifetime ($t_{1/2}$ = 2.0 h) among the isotopes considered. The Pt stays in the residue and has to be evaporized from it.

Since Pt is a refractory element, temperatures well above 2000° C are needed for suitable evaporation rates. Therefore a new electron bombardment oven was built and installed, with the crucible serving directly as anode. The temperatures now accessible are restricted by the crucible material only, which according to our experince must be graphite in the case of platinum. The atoms of the collimated beam are resonantly excited at 292.9 nm. A temperature tuned ADA crystal is used to produce this wavelength by frequency doubling the output of a commercial cw dye ring laser, operated at 575.8 nm. The fluorescent light is detected at 299 nm, using a cooled 9635Q EMI photomultiplier. With this setup, a beam of stable Pt isotopes was produced and detected (Fig. 1).

(1) W. Gast, G. Hebbinghaus, A. Krämer-Flecken, R.M. Lieder, W. Urban, J. Skalski, Verhandl. DPG(VI) 22 (1987) PG-98

2.6 LASERSPECTROSCOPIC INVESTIGATIONS OF ISOTOPE SHIFT AND HYPERFINE STRUCTURE OF POLONIUM ISOTOPES

D. Kowalewska, K. Bekk, S. Göring, A. Hanser, G. Meisel, H. Rebel

The present research project comprises studies of the hyperfine structure and the isotope shift for a series of polonium isotopes. The purpose is to determine their nuclear moments and changes of their mean square radii. The interest in polonium arises mainly from the question, whether light Po nuclei exhibit the prolate-oblate shape instability, as it is for example the case for light Hg nuclei. The method chosen for these investigations is laser induced fluorescence on a beam of polonium atoms.

The series of isotopes from ^{202}Po to ^{210}Po is planned to be investigated. Some of these isotopes will be produced from Bi ($^{206-207}Po$) or Pb ($^{202-205}Po$) targets at the cyclotron in the KfK, the long-lived isotopes ($^{208-210}Po$) will be purchased. A new atomic beam apparatus has been built inside a glove-box and put into preliminary operation. Tests concerning scattered laser light entering the detector have been performed; as the count rate was too high, a series of improvements has been made in order to reduce it. The present state seems satisfactory and no further improvements are expected to be necessary for the light input channel. A new high temperature oven has been thoroughly tested and it has proven to perform well. However, severe improvements are still needed to reduce the oven light reaching the photomultiplier. The new apparatus is expected to reach finally at least as good a level of performance as the old one.

The transition from the ground state $^3P_2$ of the configuration $6p^4$ to the state $^5S_2$ of the configuration $6p^3$ 7s has been chosen. It has the longest wavelength (λ = 255.8 nm) among all E1 resonance transitions in Po. Generation of this wavelength has now become possible in cw operation through frequency doubling of light with λ = 511.6 nm; the latter one lies within the operation range of Coumarin dyes. Reasonably efficient frequency doubling is possible since only recently with the use of a new nonlinear material - β-barium borate (BBO). Both extracavity and intracavity frequency doubling schemes have been considered; the estimates of the UV power to be expected in both cases indicate, that to ensure sufficient power for the experiment to be obtained, the intracavity frequency doubling scheme has to be applied.

The laser induced fluorescence from the $^5S_2$ state occurs in two ways, each of them being possible to be detected. These transitions are: to the metastable $^3P_1$ state of the $6p^4$ configuration with the wavelength λ = 449.3 nm or back to the ground state at the incident wavelength. The former one has a wavelength different from the one exciting, which makes the separation from the scattered incident light easier; the latter, on the other hand, is stronger. The choice of the more favorable transition to be detected has to be made experimentally.

The test experiments concerned with the laser system have begun in January 1988. The problems to be solved were: the choice of a proper dye to generate the wavelength λ = 511.6 nm and determination of a proper pump source - either an Ar^+ or a Kr^+ laser; an Ar^+ laser was preferred because the other experiments carried out simultaneously in the laser laboratory require this laser as a pump source. Tests have been performed in a linear laser (Spectra-Physics model 375). The dye found most efficient at the required wavelength and possible to be pumped with an Ar^+ laser is Coumarin 510. The peak efficiency for this dye has been found to be around

20%, in agreement with literature data; the power obtained at our non-peaking wavelength λ = 511.6 nm is, however, only 75% of the peak level. At λ = 511.6 nm an internal power of 30 W has been obtained for an almost empty laser resonator. In the final setup with several intracavity optical elements we expect an internal power which is lower by about one order of magnitude. Preparations of the final setup are in progress. The ring laser resonator (Coherent model CR 699-21), inside which the frequency doubling will be performed, requires improvements and rearrangement of the mechanics and adapting for intracavity frequency doubling. These steps are worked on at present and are expected to be finished soon.

2.7 cw DYE RING LASERS FOR PRECISE HETERODYNE FREQUENCY MEASUREMENTS

A. Dorn, G. Meisel

We prepare precision measurements of frequency differences in the optical region. As an alternative to conventional interferometric measurements of frequency ratios, a multistep method using heterodyning of two tunable dye-lasers is realized (1,2). Due to the precision inherent in the heterodyne method , the lasers used have to meet extremely high standards in terms of frequency stability and reproducibility. This is achieved by stabilizing the lasers to reference interferometers which in turn are locked to an iodine stabilized HeNe laser. A special technique to stabilize the lasers to the transmission peak of the reference interferometers is applied. The feedback system is designed for a cutoff frequency of about 1 MHz.

The experimental setup was completed by the second dye laser identical to the first one. Both were improved in several aspects improving their dependability and simplifying their operation while the output power was increased. For this purpose the ring geometry was modified (see Fig. 1) resulting in a decrease of the angles of incidence on the concave mirrors M5 and M6 which reduces the astigmatism inside the resonator. This change leads to an improved mode quality of the outcoupled beam which is important for the beam handling as, e.g., mode matching to the confocal Fabry Perot reference interferometers.

In order to increase the output power, the number of intracavity optical elements is minimized. Only two low loss dispersive elements for longitudinal mode selection are used, namely a Lyot filter and a 1 mm

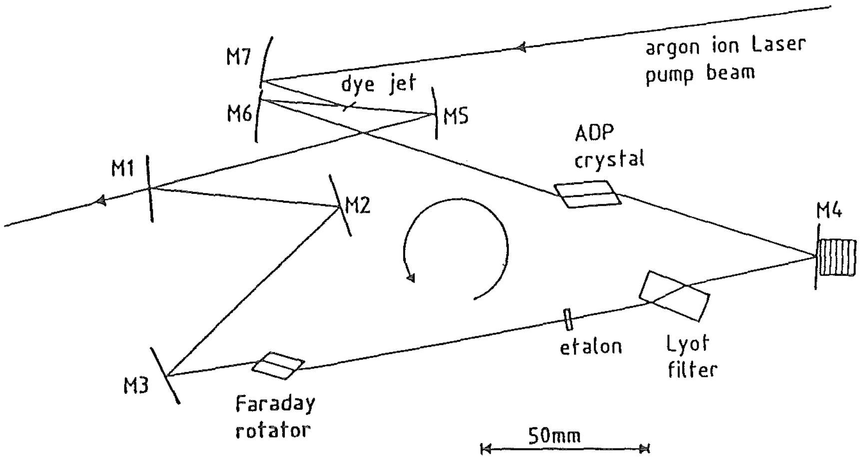

Fig. 1 To-scale diagram of the ring dye lasers. The radius of curvature of mirrors M 5, 6, 7 is R = 50 mm. All other mirrors are flat.

thick uncoated glass etalon. As a consequence of this concept, several competing longitudinal modes can start to oscillate after a perturbation occured. The number of possible modes could be restricted to only two to three by reducing the resonator circumference to about 65 cm.

The losses were further reduced by decreasing the angle of incidence on mirror M2. At the angle used before, M2 was partially transmitting. Due to the modifications the output power was increased from 320 mW to 500 mW with 3 W pump power and DCM dye. This corresponds to a single-mode efficiency of 17% which is almost twice as high as for a conventional setup.

The frequency jitter of the laser is caused by changes of the cavity circumference due to vibrations of mirrors and dye jet density and thickness fluctuations. The laser frequency is stabilized by a feedback system. The error signal is devided into two channels. Slow but wide frequency corrections are fed to the piezo driven mirror M4, fast but small corrections are fed to the electro-optic ADP crystal. The piezo transducer used so far (3) was replaced by a more advanced design (3). As a result, the lowest mechanical resonances, which determine the usuable feedback frequency bandwidth, were shifted from a few kHz to 39 kHz and 49 kHz. Thus they lie well above the slow channel cut-off frequency of 4 kHz.

In conclusion, both lasers are in a status, that dependable and easy high power operation with a frequency jitter less than 1 kHz rms is possible.

(1) B. Burghardt, H. Hoeffgen, H. Kriz, and G. Meisel, in: PTB report PTB-E-18 (1981) 171

(2) B. Burghardt, H. Hoeffgen, G. Meisel, W. Reinert, and B. Vowinkel, in: Precision Measurement and Fundamental Constants II, eds. B.N. Taylor and W.D. Phillips; Natl. Bur. Stand. (U.S.), Spec. Publ. 617 (1984) p. 49

(3) W. Jitschin, G. Meisel Appl. Phys. 19 (1979) 181

3. NEUTRINOPHYSICS

KARMEN Collaboration

Th.Czabo, G.Drexlin, V.Eberhard, H.Gemmeke, G.Giorginis, W.Grandegger, R.Gumbsheimer, H.Hucker, L.Husson, J.Kleinfeller, R.Maschuw, P.Plischke, J.Rapp, F.K.Schmidt, G.Spohrer, J.Wolf, S.Wölfle, J.Wochele, B.Zeitnitz
Kernforschungszentrum Karlsruhe and Universität Karlsruhe

B.Bodmann, F.Burtak, E.Finckh, W.Kretschmer, F.Schilling, D.Vötisch, R.Stegen, E.Zell
Universität Erlangen-Nürnberg

N.E.Booth
Oxford University

J.A.Edgington, T.Gorringe, A.Malik
Queen Mary College, London

A.Dodd, A.G.D.Payne
Rutherford Appleton Laboratory, Chilton

After several years of preparation the 50 t scintillation calorimeter KARMEN has for the first time been looking for neutrinos from ISIS:

The KArlsruhe Rutherford interMediate Energy Neutrino experiment KARMEN makes use of the pulsed "beam dump" neutrinos ν_μ, ν_e and $\bar{\nu}_\mu$ from π^+-decay at rest produced at the spallation facility ISIS of the Rutherford Appleton Laboratory, England. Its major physics aims are to look for appearance oscillations $\nu_\mu \rightarrow \nu_e$ and $\bar{\nu}_\mu \rightarrow \bar{\nu}_e$, to observe charged and neutral current excitations of ^{12}C by ν_e and ν_μ and to measure the ν_e-e elastic scattering. (The physics program has been described elsewhere (1,2)).

After the large detector vessel (3.2*3.5*6.0 m) had been equipped with 2300 phototubes and optical fibres for calibration and monitoring purposes it was filled with 56000 ltrs. of liquid scintillator carefully watching its mechanical behaviour of wall bending not to excess the design value of 1.5 mm and to make sure that no leakage occurred. Simultaneously assembly of the optical segmentation dividing the detector volume into 512 individual cells of 18.1 * 17.7 * 350.0 cm3 size went ahead. Nine submodules each comprising 4 rows of 16 standard individual scintillator cells had to be inserted. One submodule is assembled from 38 vertical and 152 horizontal acrylic doublesheets of 3.0 mm thickness to form a honeycomb structure of 3.5 * 3.2 * 0.7 m^3 size (see fig.1). Because of the flimsiness of the lucite structure assembly had to be performed with great care; in addition, to remain within the tolerances the dimensions of each module had to be recorded within a tenth of a millimeter to make sure that subsequent substructures in the detector vessel fit exactly on top of each other.

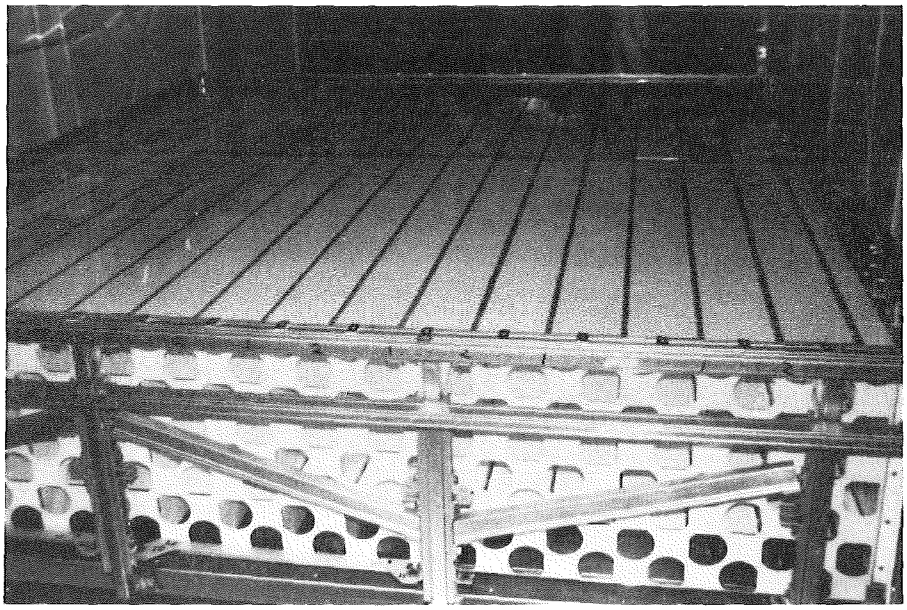

Fig.1: An optical segmentation submodule in its mounting frame just before insertion into the KARMEN detector tank

After an optical submodule had been completed it was lifted to the top of the detector vessel. The lid was then pneumatically opened but only to be sealed off again immediately by the insertion structure which slowly lowers the optical segmentation down into the liquid scintillator to find its position 6 m deep with millimeter accuracy.

Four out of nine of these submodules had been installed when it was decided to stop detector assembly and to prepare the calorimeter for first data taking still during the 1988 ISIS beam period. Thus all the cabling and testing of phototubes with the electronics had to be completed before acces to the phototubes was blocked off by the 180 mm passive steel shield. Finally 136 outer shield detectors (3 cm NE110 scintillator slabs) had to be mounted and tested. The entire detector was then moved into the shielding bunker on air cushions followed by the electronics trailer on its own air pad system (see fig.2).

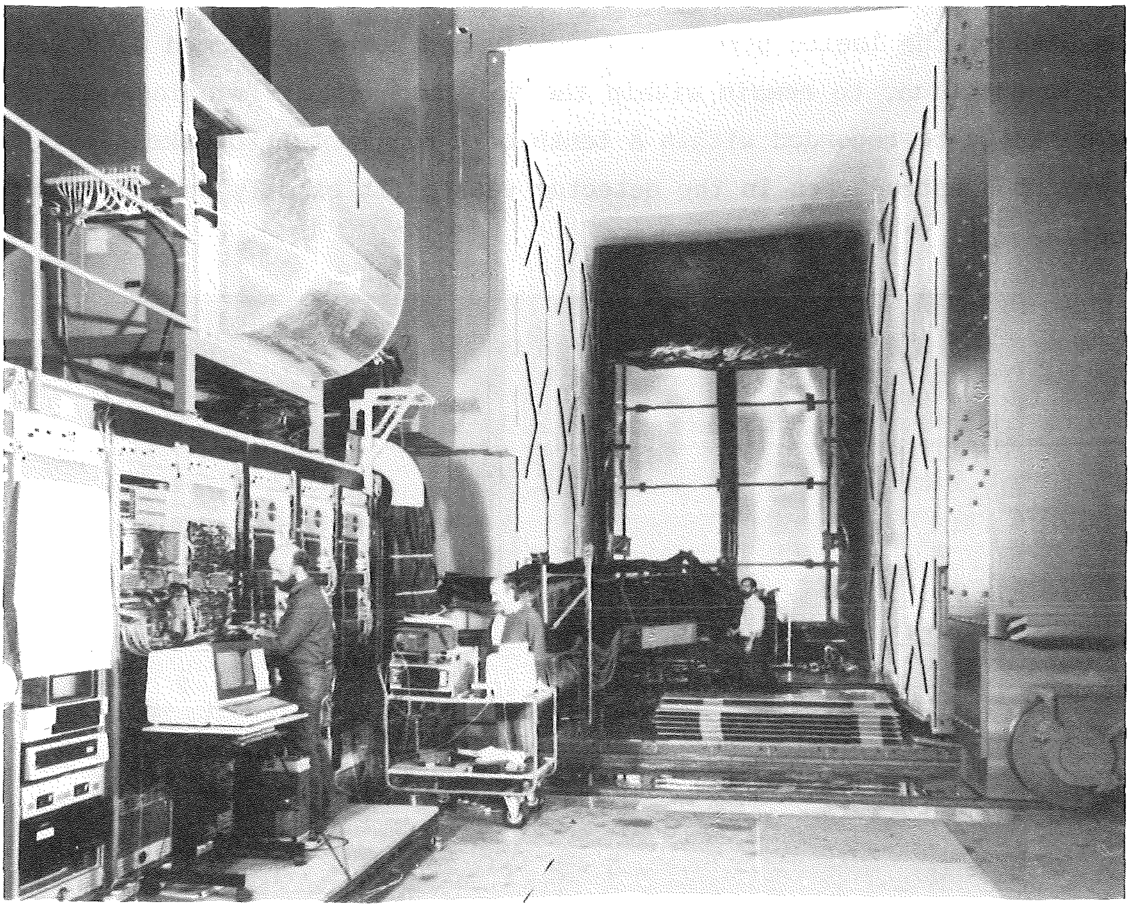

Fig.2: The KARMEN detector in the neutrino bunker linked to the electronics trailer

The electronics has extensively been tested and calibrated as soon as the first optical substructure had been inserted. Cosmic muons served as an ideal tool to calibrate all scintillator modules and data channels with respect to energy, time and position and to determine the corresponding resolution figures. Fig. 3a shows the typical Landau distribution of the energy loss of throughgoing muons in a scintillator module after position correction; this is taken from fig. 3b where the light output of 30 MeV energy deposit of minimum ionizing muons summed from either end of the scintillator module is plotted versus the position in that module given by time difference measurement. Energy resolution was deduced from those measurements as well as from pulsed UV-laser calibration to be $\sigma(E)/E = 12.4\%/\sqrt{E(MeV)}$; the time differene resolution has been measured with the laser at 8.4 MeV energy equivalent to be $\sigma(\Delta t) = 0.62$ nsec (3) which for 30 MeV energy deposit means a spatial resolution of $\Delta x = 6.2$ cm.

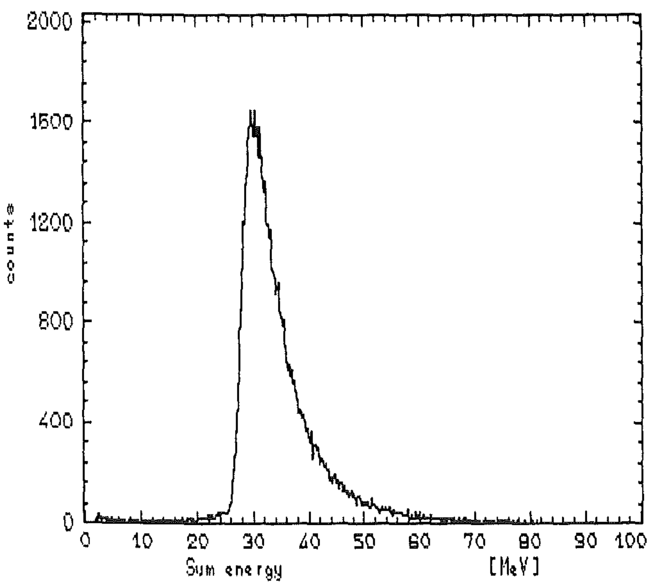

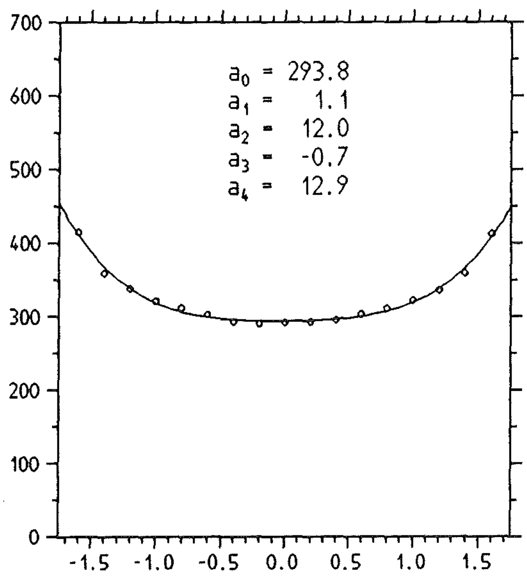

Fig.3: a) Energy loss of m.i. μ's penetrating one scintillator module.
b) Light output versus position for 30 MeV energy deposit.

The detectors capability to recognize sequential decay signatures as they occur with the neutrino reactions $^{12}C(\nu_e,e^-)^{12}N \xrightarrow{16\ msec} {}^{12}C + e^+ + \nu_e$ or $^{1}H(\bar{\nu}_e,p)n \rightarrow Gd(n,\gamma)\ \Sigma E_\gamma = 8$ MeV can best be demonstrated by stopped muons as shown in fig.4: A stopped μ in the central detector with prongs in the shield detector as well, is followed 8.8 μsec later by an electron (e^+ or e^-) releasing 35.7 MeV just at the end of the preceeding μ-track. Taking several thousand of those events the μ-lifetime was measured to be $\tau_\mu = 2.15 \pm 0.05$ μsec in fair agreement with the predicted value of 2.16 μsec when μ^--capture by ^{12}C is taken into account. The energy spectrum of the decay electrons in fig.5 nicely represents the Michel shape of the μ-decay and also demonstrates the good overall resolution of the detector.

For data taking at ISIS the detector had to be calibrated not only for energy and position measurement but also for absolute time measurement with respect to the beam spill. In addition the trigger logic had to be installed. The data acquisition basicly consists of the front-end electronics, and ADC system and the trigger logic all linked to an intelligent CAMAC bus as shown in fig.6. The decision on an event to be "valid" is made within 500 nsec by a programmable trigger processor based

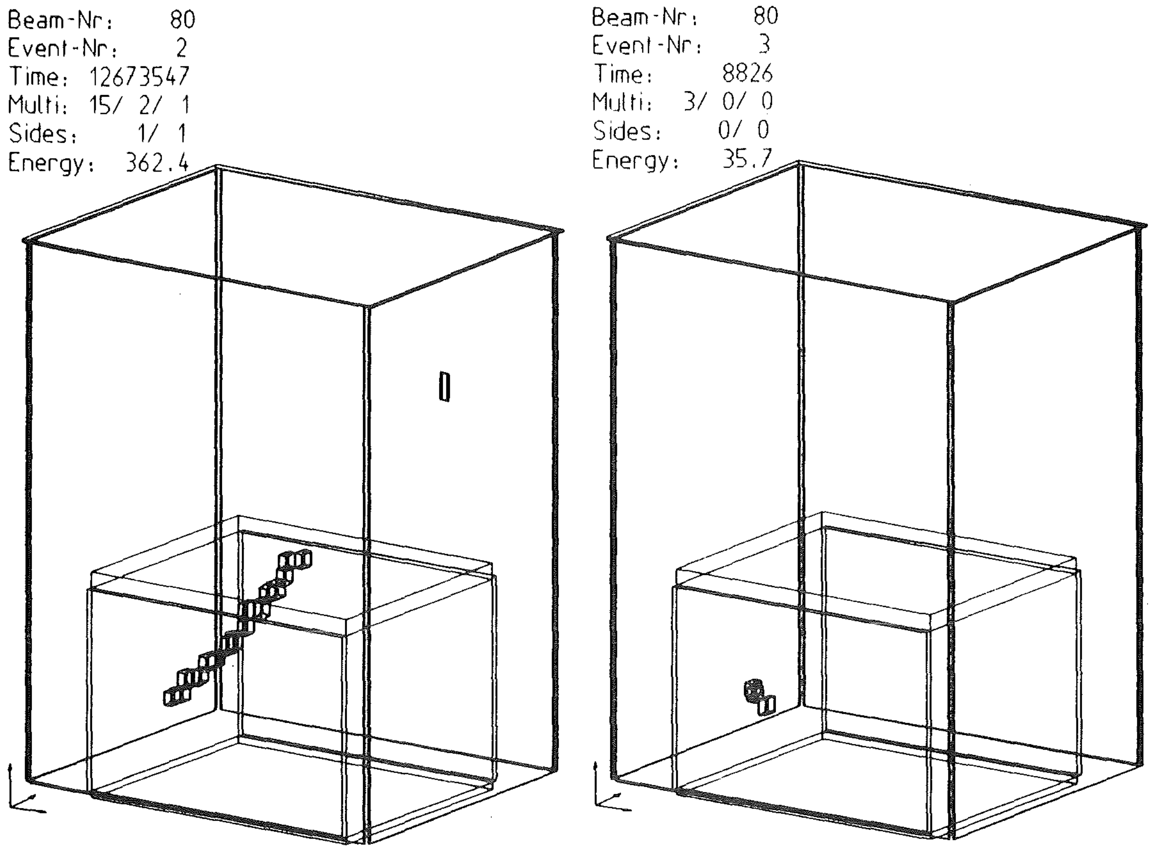

Fig.4: Track of a stopped muon and its subsequent decay 5.8 μsec later

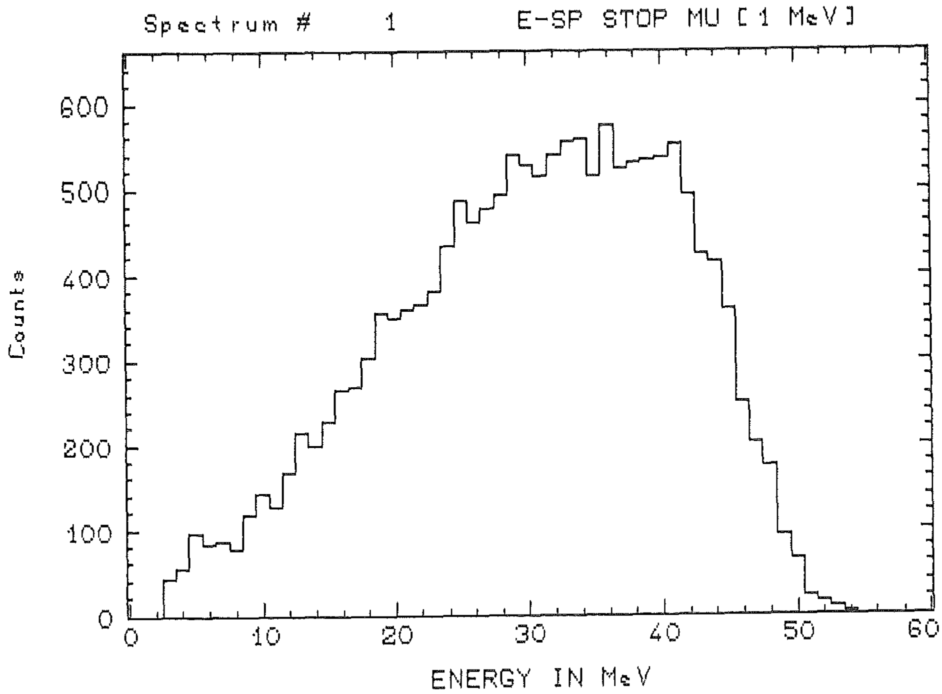

Fig.5: Energy spectrum of e(+,-) from stopped μ-decay

on the module multiplicity and the summed energy of all modules having fired during an "event time" of 70 nsec. A "Valid event" decision during the prompt ν-beam time window of 5 μsec alerts the system for the subsequent 16.6 msec of a beam period to look for any spatially correlated sequential decay pattern. For each event the analog information of the upstream amd downstream energy E_u and E_d, the time difference T_{diff} and the absolute event time T_{rel} stored in the front end electronics is digitized by the ADC's for all scintillator modules and finally recorded on tape.

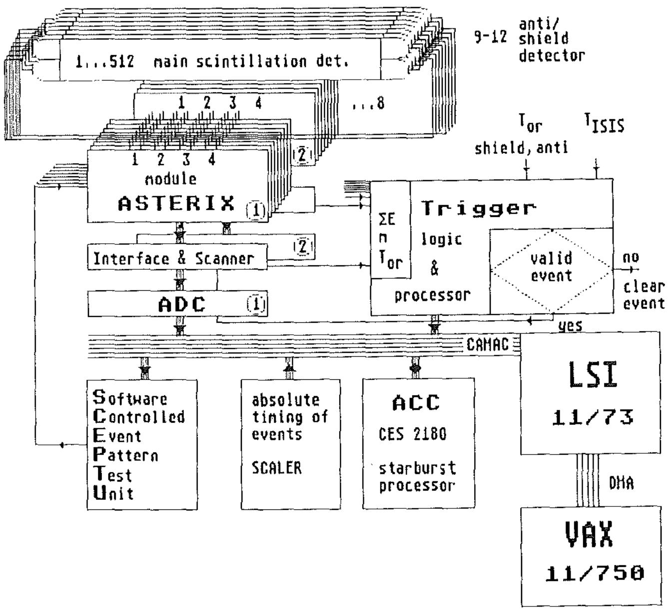

Fig.6: Block diagramm of the KARMEN electronics

Since August KARMEN has been taking data from ISIS for 1.25 * 10^{21} protons on the spallation target. Data evaluation is currently going on not only to extract the first neutrino events but also to study carefully any possible source of background before the detector after completion is commissioned for long term data taking in 1989.

(1) KARMEN collaboration, Proc. of Int. Workshop on Neutrino Physics, Heidelberg 1987, Springer Verlag, S. 147-152
(2) B.Zeitnitz, Progress in Particle and Nuclear Physics 13 (1985)
(3) H.Gemmeke, L.Husson, R.Maschuw, P.Plischke, J.Wochele, B.Zeitnitz, B.Deimling, O.Fromheim, W.Heep, G.Hellmann, W.Karbstein, to be published in IEEE Trans. of Nucl. Sci.

4. INTERMEDIATE ENERGY PHYSICS

4.1 LOW ENERGY PION SCATTERING WITH LEPS AT PSI/SIN

B.M.Barnett*, H.Clement*, W.Gyles****, J.Jaki, R.R.Johnson**, Ch.Joram, W.Kluge, S.Krell*, H.Matthäy, M.Metzler, R.Tacik, G.J.Wagner*, U.Wiedner***

In the last year the first systematic investigations with the new magnetic spectrometer LEPS (Low Energy Pion Spectrometer), commissioned in 1986, have been carried out. First results for the elastic and inelastic scattering of 50 MeV positive and negative pions on ^{12}C have been obtained. The set-up and performance of LEPS has been described in a series of reports elsewhere (1). A dispersive beam spot is used. Traceback to the target determines the initial momentum as well as the scattering angle. The traceback is extracted from the coordinates and angles of the scattered particles measured at an intermediate focus between the quadrupole triplet and the split pole by means of multi wire proportional chambers. The momentum of the scattered particles is determined by measurements of the coordinate and angle in the dispersive direction at the focal plane of LEPS by a vertical drift chamber. The muon background is drastically reduced by time-of-flight (TOF) measurements between a scintillation counter in the focal plane and the RF of the cyclotron and by checking the correlation between the angle of incidence at the entrance and the exit of the split pole.

The incident flux, the beam profiles in two dimensions perpendicular to be beam axis, and the beam composition (by TOF relative to the RF of the cyclotron) are monitored continuously by a scintillator hodoscope positioned behind the scattering chamber (downstream). It consists of two planes with areas of 120 mm by 240 mm containing 16 scintillator strips each.

The absolute normalisation of the pion-nucleus cross-sections is obtained by relating them to the electromagnetic electron (positron)-nucleus and muon-nucleus cross-sections which are well known both experimentally and theoretically. This is achieved by detecting and identifying all kinds of incident and scattered particles (electrons or positrons, muons, and pions).

The first production runs with the carbon target have revealed a strong selectivity to low spin transitions, a feature which can be qualitatively understood from the unfavourable matching condition for high angular momentum transfers at low bombarding energies. As an example consider the 12.7 MeV (T=0) transition at 55°, corresponding to a momentum transfer of about 120 MeV/c, an optimum value for M1 transitions. This transition generates the largest inelastic peak in the spectrum except for the 2_1^+ transition, which is at that angle of similar strength. This is due to the fact that at 50 MeV the angular distribution of the 1^+ spin-flip transitions just peaks in the minimum of the non spin-flip transitions which are peaked towards back angles.

At resonance energies the angular distributions, being dominated by black discattering, peak for different angular momentum transfer at neighbouring angles and do not show the particularly selective M1 window in the easily accessible angular range of 40° - 60°. This M1 window may provide a valuable tool to study M1 excitations in the future, complementing electron scattering.

In a similar manner, 0^+ transitions are strongly enhanced in low energy pion scattering at forward angles if compared to high spin transitions such as the collective 3^- excitation. Recently Jennings and de Takacsy (2) pointed out that 0^+ transitions provide the most convincing experimental evidence for the Lorentz-Lorenz-Ericson-Ericson (LLEE)-effect. The LLEE-effect produces medium modifications in the p-wave scattering term due to short range correlations and ρ-meson exchange and leads to a strong suppression of multiple scattering processes. The point is that neither the elastic nor the 2^+ scattering is uniquely sensitive to the LLEE-term in the optical potential. Sensitivity to the LLEE-term can, however, be expected from the monopole excitation which critically depends on the transition formfactor - which has a node - and to which extent the incident pion can penetrate the nuclear interior, but does not depend on the angular momentum transfer. A resonance pion strongly absorbed at the nuclear surface does not feel the node in the form factor and the resulting angular distribution is forward peaked contrary to the observation at low energies.

Our observations go beyond these findings. The angular distributions for π^+ and π^- show different shapes which, in the absence of some effect attributable to the Coulomb force, would be a very surprising: this excitation has been considered so far to be of purely isoscalar nature.

A problem not finally evaluated at present is the degree of

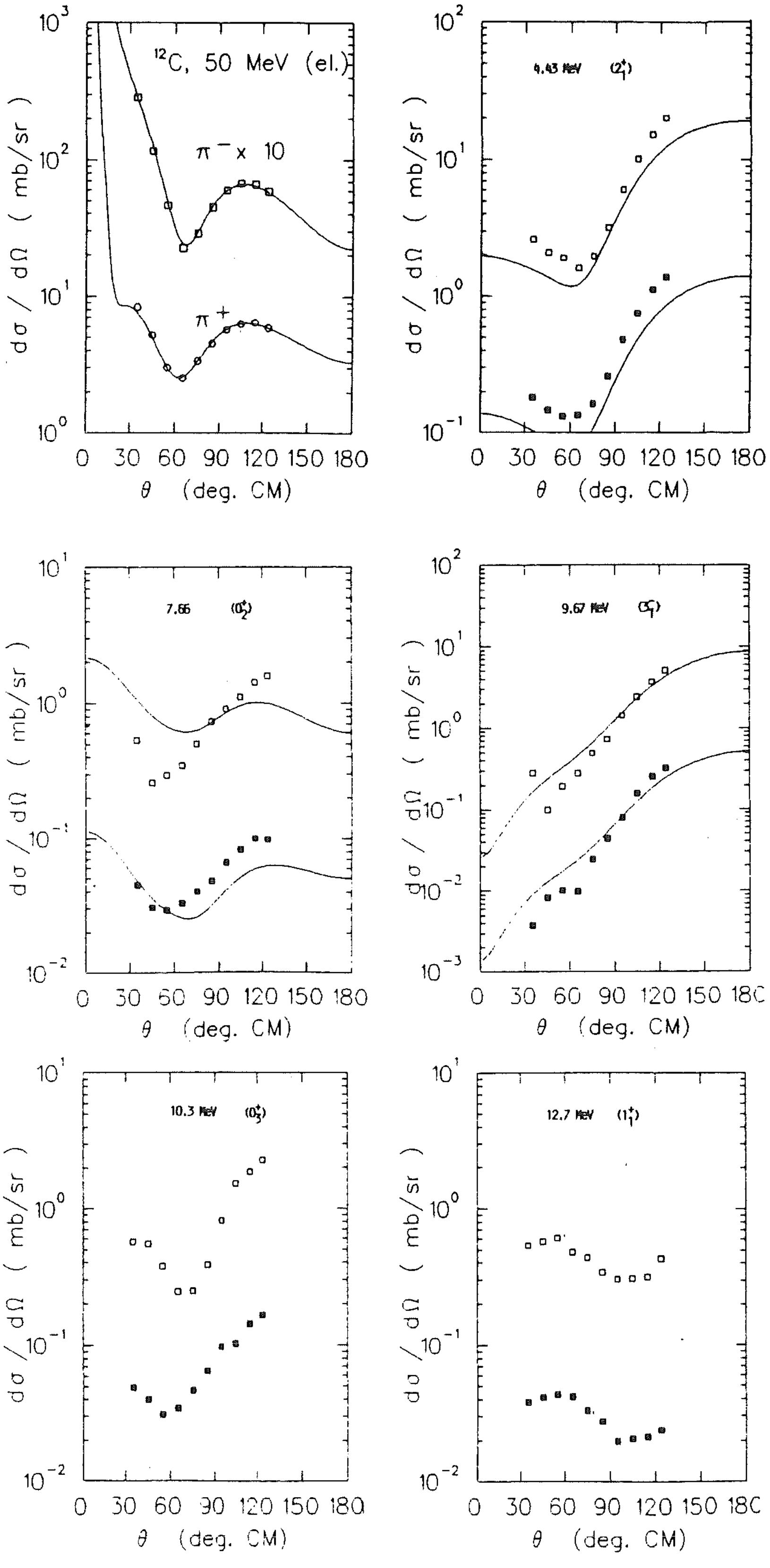

Fig. 1:

The angular distributions of the scattering of 50 MeV pions on ^{12}C for the ground state (0^+), and for the excited states at 4.44 MeV (2_1^+), 7.65 MeV (0_2^+), 9.64 (3_1^-), 10.3 MeV (0_3^+), 12.7 MeV (1_1^+).

isospin mixing between the famous pair of 1+ states at 12.7 (T=0) and 15.1 MeV (T=1).

The angular distributions for the following states are given in Fig.1: for the ground state (0_1^+), and for the excited states at 4.44 MeV (2_1^+), 7.65 MeV (0_2^+), 9.64 (3_1^-), 10.3 MeV (0_3^+), 12.7 MeV (1_1^+).

The calculations have been obtained by means of a slightly modified "standard potential" of the Michigan group (3) with the computer code DWPI (4). The angular distributions for the excitation of the collective states (2_1^+, 3_1^-), are reasonably described by the calculations, while no agreement is found for the 0_2^+ state. Obviously either the reaction mechanism of the excitation or the nuclear structure of this state (or both ?) are poorly understood at present. No attempt has been made so far to calculate the excitation of the broad 0_3^+ state at 10.3 MeV and of the 1_1^+ state at 12.7 MeV.

The results obtained so far are very encouraging from the standpoint of nuclear spectroscopy. The high optical transparancy of low energy pions combined with their extreme isospin selectivity might provide a unique tool to study neutron degrees of freedom (with negative pions) in nuclear excitations of natural parity, which will complement the studies of proton excitations in electron scattering. In spin-flip transitions we see large differences between isovector and isoscalar modes which is unique in hadron scattering and complementary to the situation found in electromagnetic scattering.

(1) Annual Report on Nuclear Physics Activities 1982/83 p.208, p.210; 1983/84 p.164; 1984/85, p.181; 1985/86, p.183
SIN Jahresberichte 1982, p. JB23; 1984, p.JB25; 1986, p.JB16
J.Jaki, Bau und Test einer vertikalen Driftkammer, Diploma thesis, Universität Karlsruhe 1983, unpublished.
M.Metzler, Untersuchung der magnetoptischen Eigenschaften des Magnetspektrometers LEPS, KfK-report 4010 B (1986)
K. Göring, Untersuchungen von Vieldrahtproportionalkammern für das Magnetspektrometer LEPS, to be published as KfK-report
H.Matthäy et al., The LEPS spectrometer at SIN, Proceedings of the Conf. of collective phenomena in nuclear and subnuclear long range interactions in nuclei, p.542, ed. by P.David, Bad Honnef 1987, World Scientific Publ. Company, Singapore
(2) B.K.Jennings, Proc. of the International Conf. and Symposion on unified concepts of many-body problems, Stony Brook, Sept.1986
B.K.Jennings and N.de Takacsy, Phys.Letters 124B (1983) 302
(3) J.A.Carr, H.McManus, K.Stricker-Bauer, Phys.Rev. C25 (1982) 952
(4) R.A.Eisenstein and G.A.Miller, Comp.Phys.Comm. 8 (1974) 130 and Comp. Phys. Comm. 11 (1976) 95

* Universität Tübingen, Physikalisches Institut, Tübingen, FRG
**TRIUMF, Vancouver, Canada; ***now at Institut für Physik, Universität Mainz, FRG; ****now at TRIUMF, Vancouver, Canada

4.2 MECHANICS FOR THE CRYSTAL BARREL DETECTOR

I. Augustin, P. Blüm, S. Cierjacks, G. Grossmann, S. Kelzenberg, H. Koch, F. Kröner, M. Kunze, J. Plotzitzka, S. Ravndal, W. Schott, H. Schuhmann[+], N. Winter

Mechanical Support for the 4π CsI Detector. The mechanical support of the CsI-crystals represented a special problem, because of the high weight (4 t) of the crystals, and of the large solid angle (95% of 4π) envisaged for the neutral detector which precluded massive walls between the crystals. Also the inner walls of the support (in direction of the target) needed to be as thin as possible, in order to avoid a substantial conversion of γ-rays before reaching the sensitive volume of the detector. The latter argument introduced also a restriction on possible materials for the inner walls to light elements, since the radiation length decreases rapidly with increasing atomic number. To enable accessibility of the JDC, located in the center of the calorimeter, the holding structure had to be designed in two self-supporting halves. Finally, material and machining costs had to be kept as low as possible.

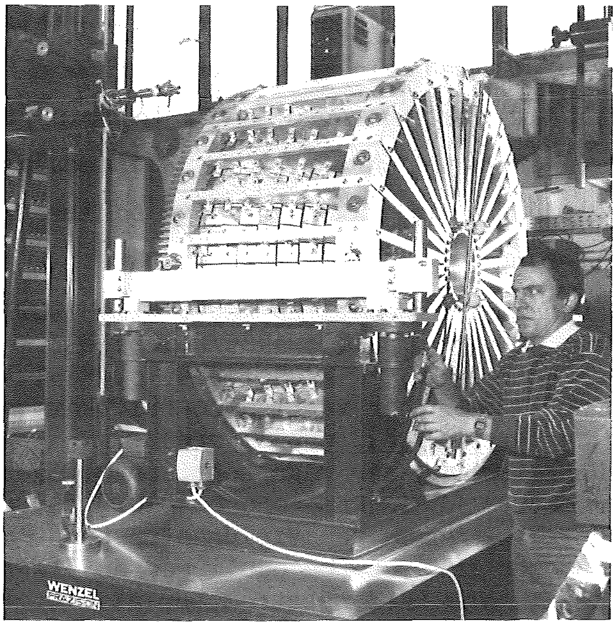

Fig. 1. Side view of the half-detector support structure loaded with metal mock-ups on the large IRE test stand at KfK.

On this basis, several preconceptional design studies have been made, considering carbon-fiber, glas-fiber, beryllium, aluminum and stainless steel as possible structural materials. For all technical concepts extensive static calculations and Monte Carlo studies were performed for predicting the resulting mechanical and physical properties of the detector. From these studies a final support concept was developed which involves special aluminum alloys for all support components. Minimum load on the inner walls of the mechanical support is achieved by a suitable suspension of the crystals on the outer support structure. For this purpose, the crystals and the electronic caps will be tightly connected by individual titanium cans of 0.1 mm thickness. The static of this support concept has been tested by loading a half-barrel prototype with metal mock-ups of Al and Zn (Fig. 1) producing an overload of 1 t (33%). The tests showed that the maximum elastic deformations under load are less than 0.5 mm for all support components. In the mean time, the mechanical supports for both detector halves have been produced in final form, assembled and tested. They have been recently delivered to the CB Collaboration at CERN.

CB Detector Handling Facilities. CB detector handling for assembly, disassembly and repairment work outside of the magnet requires special auxiliary equipment, because of the high weight of the various components (~7 t for the fully assembled detector). The major manipulations in this work refer to: i) The tensionless mounting of the CsI crystals in the half-barrel support structure which has to be performed in a dry-air housing of limited space. ii) The assembly or disassembly of the various detector components (Two half-barrels, JDC, XDC or MWPC, cooling systems, detector electronics and cables, etc.) or the replacement of individual elements (single crystals etc.) which ought to be done in an unrestricted large working area. iii) The transport of the premounted half-barrels between the mounting and the working area, and the transport of the total detector system between magnet and the working area.

Several approaches for a solution of the detector handling problem have been worked out and presented to the CB Collaboration. From these a final concept was chosen which involves three rail-based manipulators:

1. A mounting-tipping table for crystal mounting in a half-barrel support and for tipping of the premounted half barrels by 90° around their vertical axis.
2. A working table (Fig. 2) for insertion or removal of the complete CB detector system into or out of the magnet. This table allows also to take the two half barrels apart for mounting and extraction of the JDC, located in the center position. For special repairment work on the CsI detector the table enables rotation of the fully assembled counter around its rotational axis.
3. A tranfer table (Fig. 2) for transport and height adjustment between mounting and working table. This table is constructed to serve also as a half-barrel support during special calibration measurements at the three

possible irradiation facilities (SC and LEAR at CERN, and the AVF cyclotron at PSI), and is adjustable to the largely different beam heights at the three machines.

In the report period, all three manipulators have been built in collaboration with the Munich group, and their safe and easy operation was tested at KfK. After shipment to CERN, the rail-based handling facilities were installed in the LEAR area for final use.

\+ Physik Department, Universität München, Fed. Rep. of Germany

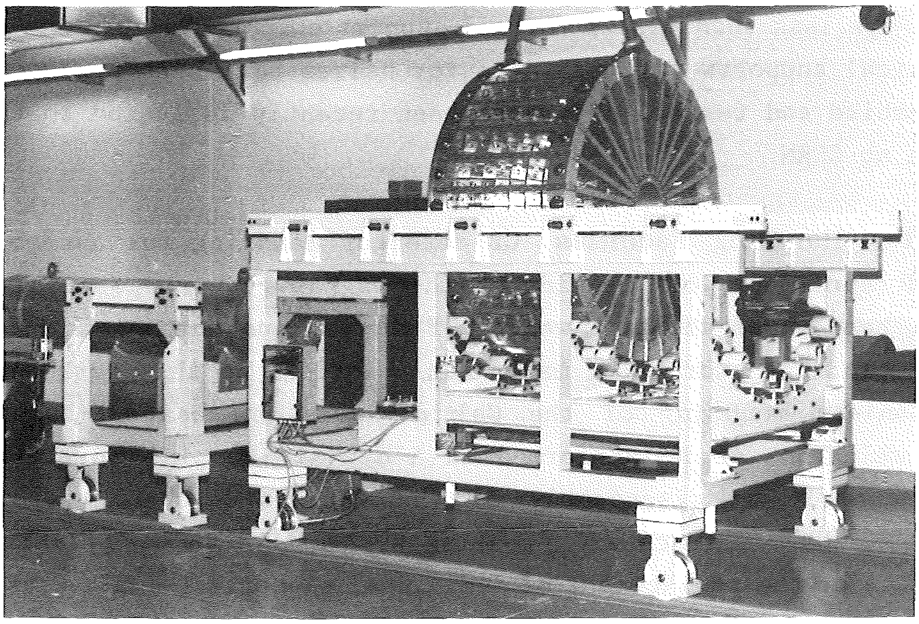

Fig. 2. The large working table carrying a loaded half-barrel and the transfer table on ground rails during final tests in the IKVT hall at KfK.

4.3 SYSTEMATICS OF ANGULAR-DEPENDENT NEUTRON PRODUCTION BY 585 MEV PROTONS ON TARGETS WITH $12 \leq A \leq 238$:

Differential Cross Section Measurements

S. Cierjacks, Y. Hino[+], F. Raupp[++], L. Buth [*], D. Filges[**], P. Cloth[**], T.W. Armstrong[**], (1)

Validation of Intranuclear Cascade-evaporation Model Calculations

D. Filges[**], P. Cloth[**], T.W. Armstrong[**], S. Cierjacks, Y. Hino[+], F. Raupp[++], L. Buth[*], (2)

Double differential cross sections $d^2\sigma/d\Omega\, dT_n$ for the production of neutrons from 585 MeV proton bombardment of C, Al, Fe, Nb, In, Ta, Pb, and U targets have been measured at emission angles of 30°, 90°, and 150° and for neutron kinetic energies between 0.9 and 585 MeV (all quantities in the laboratory system). The measured cross sections are compared with previous experimental results from other laboratories. The experimental energy-dependent cross sections all reveal a clear two-component structure with contributions from evaporation processes and intranuclear cascade reactions. For heavy and medium-weight target nuclei the data in the evaporation region are indicative of an isotropic angular distribution in the zero-linear-momentum coordinate system. Data in the cascade energy region are strongly forward peaked, and the fraction of cascade neutrons increases with decreasing emission angle. This fraction increases also with decreasing target mass number.

The intranuclear casacade-evaporation model of a high-energy nucleon-meson transport code has been used to calculate neutron production from non-elastic interactions of 585 MeV protons with C, Al, Fe, Nb, In, Ta, Pb, and U targets at emission angles of 30°, 90°, and 150°. These model predictions are compared with measurements of double differential cross sections $d^2\sigma/d\Omega\, dT_n$ of neutrons with kinetic energies between 0.9 and 585 MeV. In general, the model predicts approximately the correct neutron production in the evaporation region, whereas in the high-energy region ($E_n \geq 20$ MeV) systematic discrepancies between measurements and model predictions occur. These increase rapidly with increasing neutron energy and increasing emission angle.

(1) Phys. Rev. C 36 (1987) 1976

(2) Phys. Rev. C 36 (1987) 1988

+ Now at Electrotechnical Laboratory, Umezono, Ibaraki, Japan

++ Now at Elektronik System Gesellschaft, München, Fed. Rep. of Germany

* Institut für Neutronenphysik und Reaktortechnik, KfK

** Institut für Reaktorentwicklung, Kernforschungsanlage Jülich

4.4 THREE- AND FOUR NUCLEON PION ABSORPTION MODES OBSERVED IN TRIPLE COINCIDENCES FROM ^{4}He

G. Backenstoss[*], S. Cierjacks[+], M. Furic[++], A. Hoffart[+], M. Izycki[*], T. Petkovic[++], R. Powers[*], B. Rzehorz[+], P. Salvisberg[*], M. Steinacher[*], H. Ullrich[+], P. Weber[*], H. J. Weyer[*]

In the last few years there is increasing evidence for new pion absorption modes, which are beyond the scope of the 2N-absorption approach. It has been known for some time(1), that the 2N-processes by far do not exhaust the total absorption cross section. One part of the missing cross section certainly is located in channels with composite particle emission or in kinematical regions characterized by small nucleon-nucleon relative momenta, i.e. regions of "soft" final state interaction. Another part may be contained in sequential processes, where the 2N-absorption is combined with scattering or charge exchange before or after the genuine absorption. The states between the different steps are near the mass shell. Thus the final state will reflect in its kinematical signature the different steps involved. The most exciting part of the missing cross sections, however, is expected to show up in processes, in which the pion interacts in the genuine absorption process with more nucleons. Such a reaction type will not be confined to specific parts of the phase space, but will cover it entirely.

First evidence for a genuine 3N-absorption process which indeed covered the whole phase space with constant matrix element(2) was found in ^{3}He. In order to extend this research to other nuclei we have performed now a triple coincidence experiment on ^{4}He. Since in this case the final state is determined in a kinematically complete way we are able to identify 3N-processes as well as 4 N-processes.

The experiment was conducted at the Swiss Institute for Nuclear Research. A positive pion beam with 220 MeV/c momentum impinged upon a liquid ^{4}He-target. The triple coincidence system included a charged particle total absorption scintillator hodoscope and two time-of-flight detectors for neutrons and charged particles. The total absorption plastic scintillator was divided into twelve hodoscope components and subtended a solid angle of 0.2 sr. Two MWPC systems with a total of six planes were located in front of the scintillation blocks. The TOF detectors were large- area position-sensitive plastic scintillators designed for subnanosecond timing. They subtended solid angles of 0.075 sr and 0.09 sr with an energy resolution around 5% for 100 MeV nucleons. Thin anticoincidence-counters in front of the TOF scintillators served for identification of neutrons. Charged particle identification for all three detectors was performed off- line imposing cuts upon the pulse-height versus time-of-flight arrays. The positions of the detectors relative to the beam direction were 72°, 240° and 305° for the centers of the detectors. All three detectors were at beam height. More detailed information on the setup is available elsewhere(3,4).

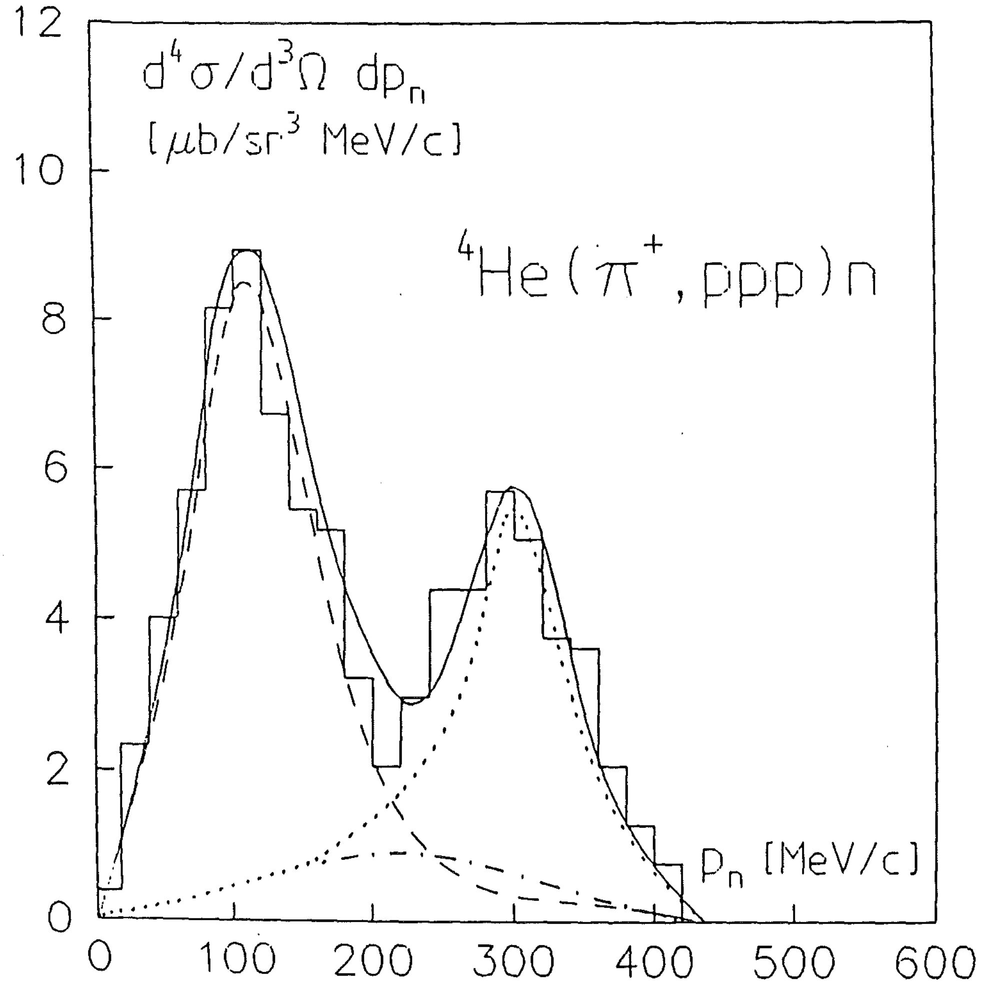

Fig. 1: Differential cross section of the reaction ^{4}He(π^+,ppp)n as function of the momentum of the undetected neutron (see text)

Coincidences of the type ppp and ppn were registrated simultaneously. Fig. 1 shows ppp coincidences as function of the momentum of the undetected nucleon (histogram). Also shown is a Monte-Carlo-simulation for a 3N-absorption process with constant matrix element (peak at low energies) weighted with the known Fermi momentum distribution in ^{4}He. In addition MC simulations for a 4N-process (flat curve) and a process with "soft" final state interaction (peak at high energies) are shown. The sum of the three simulations provide a good fit of the measured data. We find integrated cross sections of (2,1 ± 0,5) mb, (4,4 ± 1,3) mb and (0,5 ± 0,15 mb) for the processes 3 N_{ppp}, $3N_{ppn}$ and 4N, respectively.

The results clearly prove the existence of quasifree three nucleon absorption processes in ^{4}He. Also four nucleon processes have been observed, however, with relatively small integrated cross sections.

(1) D. Ashery, J.P.Schiffer, Ann.Rev.Nucl.Part.Sci.36,207(1986)

(2) G. Backenstoß et al.,Phys.Rev.Lett.55,2782(1985)

(3) S.Cierjacks et al.,Nucl.Instrum.Methods Phys.Res.,Sect.A238,354(1985)

(4) S.Ljungfelt, Diss. University of Karlsruhe 1984
KfK-report No. 3792(1985)
T. Petković, Diss. University of Zagreb, 1986 (unpublished);
P. Weber, Diss. University of Basel, 1987 (unpublished).

* Institut für Physik der Universität Basel,Klingelbergstr.82,CH-4056 Basel

\+ Kernforschungszentrum Karlsruhe, Institut für Kernphysik und Universität Karlsruhe, Institut für Experimentelle Kernphysik, Postfach 3640, D-7500 Karlsruhe 1

++ Faculty of Science and Faculty of Electrical Engineering, University of Zagreb, 4100 Zagreb, Yugoslavia.

5. HIGH ENERGY PHYSICS

CELLO Collaboration

H.-J.Behrend, J.Bürger, L.Criegee, J.B.Dainton, H.Fenner, J.H.Field, G.Franke, J.Fuster, Y.Holler, J.Meyer, V.Schröder, H.Sindt, U.Timm, G.G.Winter, W.Zimmermann

Deutsches Elektronen-Synchrotron, DESY Hamburg, Germany

P.J.Bussey, C.Buttar, A.J.Campbell, D.Hendry, G.McCurrach, J.M.Scarr, I.O.Skillicorn, K.M.Smith

University of Glasgow, United Kingdom

J.Ahme, V.Blobel, M.Feindt, J.Harjes, M.Poppe, H.Spitzer

II.Institut für Experimentalphysik, Universität Hamburg, Germany

W.-D.Apel, A.Böhrer, J.Engler, D.C.Fries, K.Gamerdinger, J.Jung, J.Knapp, H.Küster, P.Mayer, H.Müller, H.Schneider, J.Wolf

Kernforschungszentrum Karlsruhe and Universität Karlsruhe, Germany

W.de Boer, G.Buschhorn, G.Grindhammer, B.Gunderson, Ch.Kiesling, R.Kotthaus, H.Kroha, D.Lüers, H.Oberlack, B.Sack, P.Schacht, G.Shooshtari, W.Wiedenmann

Max-Planck-Institut für Physik und Astrophysik, München, Germany

A.Cordier, M.Davier, D.Fournier, M.Gaillard, J.F.Grivaz, J.Haissinski, P.Janot, V.Journé, F.Le Diberder, E.Ros, A.Spadafora, J.-J.Veillet

Laboratoire de l'Accélérateur Linéaire, Orsay, France

B.Fatah, R.George, M.Goldberg, O.Hamon, F.Kapusta, F.Kovacs, L.Poggioli, M.Rivoal

Laboratoire de Physique Nucléaire et Hautes Energies, Université de Paris, France

G.D'Agostini, F.Ferrarotto, M.Gaspero, B.Stella

University of Rome, Italy

R.Aleksan, G.Cozzika, Y.Ducros, Y.Lavagne, F.Ould Saada, J.Pamela, F.Pierre, J.Zacek

Centre d'Etudes Nucléaires, Saclay, France

G.Alexander, G.Bella, Y.Gnat, J.Grunhaus, A.Levy

Tel Aviv University, Israel

5.1 PROMPT LEPTONS FROM HEAVY QUARK PRODUCTION IN e^+e^- ANNIHILATIONS AT 35 GeV AND 43 GeV

Using the CELLO detector at the PETRA e^+e^- storage ring we have studied properties of the charm and bottom quarks by investigating events with prompt leptons in multihadronic final states.

The data were taken at a centre of mass energy of $\sqrt{s}$ = 35 GeV and in the energy range between 38.00 GeV and 46.78 GeV ($\langle\sqrt{s}\rangle$ = 43 GeV) with integrated luminosities of 87.0 pb^{-1} and 42.7 pb^{-1}, respectively. A selection of multihadronic events results in 24216 events at $\sqrt{s}$ = 35 GeV and in 8473 events at $\langle\sqrt{s}\rangle$= 43 GeV

Among these we find 814/207 events with identified electrons at low/high beam energies respectively and 637/211 events with identified muons. The predominant source of these multi hadronic events with leptons are weak decays of b- and c-quarks. The b- and c-quarks are separated using the transverse momentum of the decay lepton with respect to a suitably chosen event axis which serves as an estimator for the original quark direction. Due to the high mass of the b quark the decay lepton has, on average, a larger transverse momentum relative to the quark direction than the decay products of c quarks or the hadrons resulting from the fragmentation of light and heavy quarks.

The average semileptonic branching ratios of heavy mesons can be derived from the yield of prompt leptons at different transverse momenta. The inclusive branching fractions depend on the relative production rates of the different charm and bottom flavoured mesons and baryons in $c\bar{c}$ and $b\bar{b}$ events.

The transition from quarks to multihadronic final states is described by QCD motivated fragmentation models. Flavour-dependent phenomenological fragmentation functions are introduced to model the probability for a hadron to carry a certain fraction of the parent quark momentum. Independent of the details of the fragmentation process, kinematical arguments suggest that hadrons containing the heavy quarks obtain a larger fraction of (longitudinal) momentum than hadrons originating from light quark fragmentation.

To study fragmentation we chose the scaling variable

$$z = \frac{(E+p_{\parallel})^{hadron}}{(E+p)^{quark}}$$

and use the parametrization of the longitudinal fragmentation function of heavy quarks proposed by Peterson et.al.:

$$f(z;\varepsilon_{c,b}) \sim \frac{1}{z}\left[1-\frac{1}{z}-\frac{\varepsilon_{c,b}}{(1-z)}\right]^{-2}$$

Here only one parameter $\varepsilon_{c,b}$ determines the hardness of the fragmentation. We performed a X^2-fit to the p-pT distribution of the lepton candidates after subtraction of the background of misidentified hadrons. The fragmentation parameters ε_c and ε_b and the semileptonic branching ratios BR(c $\rightarrow$ l + X) and BR(b $\rightarrow$ l + X) were used as free parameters. The number of events in each p-p_T bin and in each of the three contributing channels q = b $\rightarrow$ l, b $\rightarrow$ c $\rightarrow$ l and c $\rightarrow$ l is predicted to be

$$n_q(p,p_T) = 2N_q BR_q \varepsilon_q(p,p_T)\cdot \frac{\int_0^1 f(z;\varepsilon_q)p_q(z;p,p_T)dz}{\int_0^1 f(z;\varepsilon_q)dz},$$

where N_q denotes the number of b or c events, ε_q the muon detection efficiency, and BR_q the branching ratio for each leptonic channel. The probabilities p_q (z;p,pT) for a heavy hadron with a given value of z to decay into a lepton with momentum p and transverse momentum p_T were determined by Monte Carlo simulation in 10 bins of z.

We obtain for the Peterson fragmentation parameter of c and b quarks

$$\varepsilon_c = 0.025^{+0.034+0.013}_{-0.020-0.009} \; and \; \varepsilon_b = 0.003^{+0.011+0.006}_{-0.003-0.002},$$

corresponding to mean values of the fragmentation variable z of

$$\langle z\rangle_c = 0.74^{+0.10+0.03}_{-0.07-0.03} \; and \; \langle z\rangle_b = 0.085^{+0.15+0.03}_{-0.07-0.04}.$$

The first errors quoted are statistical and the second ones are systematic. The semimuonic branching ratios, as determined from the simultaneous fit, are BR(c $\rightarrow$ μ + X) = (9.2 $\pm$ 1.0 $\pm$ 1.8)% and BR (b $\rightarrow$ μ + X) = (12.7 $\pm$ 2.2 $\pm$ 2.4)%.

The electroweak interference between photon and Z^0 exchange in e^+e^--annihilation as predicted by the standard model of Glashow, Salam and Weinberg (GSW) allows one to probe the neutral current properties of heavy quarks. The differential cross section for the pair production of massive fermions is given in lowest order by

$$\frac{d\sigma}{d\Omega}f\bar{f} = \frac{\alpha^2}{4s}\cdot \ [C_1^f(1+cos^2\Theta)+C_2^f cos\Theta], \tag{1}$$

$$with\, C_1^f = \frac{\beta}{2}(3-\beta^2)\cdot \left[Q_e^2Q_f^2+2Q_eQ_fv_ev_fReX(s)+(v_e^2+a_e^2)v_f^2\left|X(s)\right|^2\right]$$

$$+\beta^3\cdot \left[(v_e^2+a_e^2)a_f^2\left|X(s)\right|^2\right] \tag{2}$$

$$C_2^f = \beta^2\cdot \left[4Q_eQ_fa_ea_fReX(s)+8v_ev_fa_ea_f\left|X(s)\right|^2\right],$$

$$X(s) = \frac{1}{16\,sin^2\Theta_W cos^2\Theta_W}\cdot \frac{s}{s-M_Z^2+iM_Z\Gamma_Z},$$

where v_e, v_f, a_e and a_f denote the weak vector and axial vector coupling constants of the initial and final state fermions. Θ is the scattering angle between the produced fermion (antifermion) and the electron (positron) beam. The effect of the final state fermion masses is included through the threshold factors depending on the fermion velocity β. The electroweak charge asymmetry in the fermion pair production arises because of the different couplings of left and right handed fermions to the Z^0, i.e. $a_f \neq 0$. The forward-backward asymmetry parameter is defined as

$$A_{FB}^{f\bar{f}} = \frac{\int_0^1 (\frac{d\sigma}{d\Omega}^{f\bar{f}})d\,cos\Theta - \int_{-1}^0 (\frac{d\sigma}{d\Omega}^{f\bar{f}})d\,cos\Theta}{\int_{-1}^{+1} (\frac{d\sigma}{d\Omega}^{f\bar{f}})d\,cos\Theta} = \frac{3}{8}\cdot \frac{C_2^f}{C_1^f}. \tag{3}$$

The asymmetry depends on the centre of mass energy $\sqrt{s}$ via the Z^0 propagator $x(s)$ and on the electroweak couplings. Compared to lepton pair production, it is substantially larger for quark final states due to the fractional charges of the quarks: At $\sqrt{s}$ = 35 GeV one expects for the lowest order muon- and tau-asymmetry

$$A_{FB}^{\mu\bar{\mu},\tau\bar{\tau}} = -8.8\%$$

whereas one expects for the c quarks

$$A_{FB}^{c\bar{c}} = -13.1\%$$

and for the b quarks

$$A_{FB}^{b\bar{b}} = -25.3\%.$$

In order to measure the charge asymmetry of quark production, one has to identify the quark charge and flavour. The sign of the heavy quark charge can be determined from the charge of the leptons coming from semileptonic decays of heavy mesons: negatively charged leptons result from b or $\bar{c}$ decays whereas positively charged leptons come from $\bar{b}$ or c decays. Accordingly, using prompt leptons to tag the quark charge, the observed forward-backward asymmetry has the opposite sign for $c \to \bar{l}\nu X$ and $b \to c \to \bar{l}\nu X$ cascade decays compared to $b \to l\nu X$ decays.

The asymmetry parameter A_{FB} is determined by fitting the expected lowest order probability density function $p(x) = \{3/8\ (1+x^2) + A_{FB}\ x\}$, $x = \cos\Theta$, to the angular distribution of the thrust axis in the region $|x| \leq x_{max} = 0.865$ after background subtraction, correction for acceptance, and radiative corrections. A maximum likelihood fit with the free parameter A_{FB} was performed using the following likelihood function:

$$L = \prod_{i=1}^{N_{tot}^{data}} \left[f_s \cdot \frac{\{\frac{3}{8}(1+x_i^2) + A_{FB}x_i\} g_A(x_i) g_R(x_i)}{\int_{-x_{max}}^{+x_{max}} \{\frac{3}{8}(1+x^2) + A_{FB}x\} g_A(x) g_R(x) dx} + (1-f_s) \cdot \ g_B(x_i) \right],$$

where

$$f_s = \frac{N_s^{MC}}{N_{tot}^{data}}$$

is the MC expected fraction of the signal ($b,c \to e,\mu$). The functions $g_B(x)$, $g_A(x)$ and $g_R(x)$ denote the normalized distributions of background and for acceptance and radiative corrections, respectively, and have been determined by MC simulation.

The results of the maximum likelihood fit for the charge asymmetries of b and c quark production in the electron and muon channels at $\sqrt{s}$ = 35 GeV and 43 GeV are summarized in Table 1. They can be compared to the Born level predictions of the GSW-theory. We find a forward-backward b-asymmetry of

$$A_{FB}^{b\bar{b}} = -(46 \pm 16 \pm 7)\%$$

in the muon channel at 35 GeV. At 43 GeV, in the same channel, we observe

$$A_{FB}^{b\bar{b}} = -(21 \pm 29 \pm 4)\%.$$

Taking M_Z = 92.5 GeV/c^2 and $\sin^2\Theta_W$ = 0.23, the theoretical prediction is -25.3% at $\sqrt{s}$ = 35 GeV and -38.6% at $\sqrt{s}$ = 43 GeV.

For the channel b → μ at 35 GeV the corrected cosΘ distribution of the data is shown in Fig.1 together with the fit result.

$\sqrt{s}$	channel	lepton candidates	A_{FB}[%]	A_{GSW}[%]
43 GeV	c → e	207	+(2.5 ± 34 ± 5)	
43 GeV	c → μ	211	-(26 ± 21 ± 7)	
43 GeV	c → l	418	-(17 ± 19)	-21.3
43 GeV	b → e	76	-(12 ± 38 ± 6)	
43 GeV	b → μ	108	-(21 ± 29 ± 4)	
43 GeV	b → l	184	-(18 ± 23)	-38.6
35 GeV	c → e	814	-(2.0 ± 20 ± 6)	
35 GeV	c → μ	637	-(11 ± 13 ± 5)	
35 GeV	c → l	1451	-(8.6 ± 11)	-13.1
35 GeV	b → e	220	-(30 ± 26 ± 5)	
43 GeV	b → μ	344	-(46 ± 16 ± 7)	
35 GeV	b → l	564	-(42 ± 15)	-25.3

Table 1: Measurement of the charge asymmetries in $c\bar{c}$ and $b\bar{b}$ production compared to the Born term prediction of the standard model (with M_Z = 92.5 GeV/c^2 and $\sin^2\Theta_W$ = 0.23). The first errors quoted are statistical and the second ones are systematic.

According to the expressions (2) and (3), in the PETRA energy range the charge asymmetry is primarily sensitive to the value of the weak axial vector coupling constants a_f of the incoming and outgoing fermions.

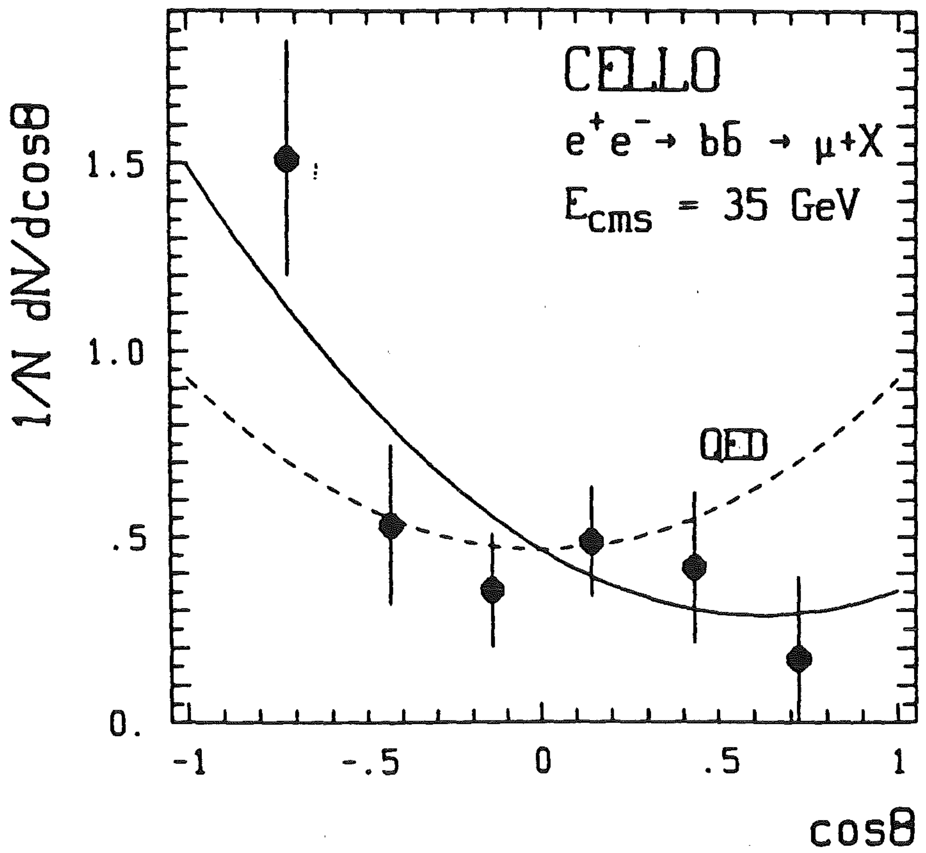

Fig.1: Corrected angular distribution for the b-enriched inclusive muoun sample at $\sqrt{s}$ = 35 GeV with the signal distribution from the maximum likelihood fit superimposed (solid curve).

The standard model predictions for the axial vector coupling constants are: $a_{e,\mu,\tau}$ = -1, $a_{u,c,t}$ = +1, $a_{d,s,b}$ = -1. The sensitivity to the vector couplings v_f is minor due to the smallness of $v_e = -1 + 4 \sin 2\, \Theta_W = -0.08$.

The $B^0\bar{B}^0$ mixing effect recently observed by the UA1 and ARGUS collaborations tends to lower the observed charge asymmetry of b quarks compared to the parton level value because quarks can turn into antiquarks and vice versa before they decay. The relation between the observable asymmetry and the GSW Born term prediction (3) is

$$(A_{FB}^{b\bar{b}})_{GSW} = \frac{1}{1-2X_l} \cdot (A_{FB}^{b\bar{b}})_{obs} \qquad (4)$$

The mixing parameter Xl is given by the expression

$$Xl = \frac{f_d BR_d X_d + f_s BR_s X_s}{f_d BR_d + f_s BR_s + f_u BR_u}, (0 \leq Xd,s,l \leq 0.5),$$

where the parameters $X_{d,s}$ are defined as

$$\frac{\Gamma(B^0_{d,s} \to (B^0_{d,s} \to l^- \nu X)}{\Gamma(B^0_{d,s} \to (B^0_{d,s} \to l^{\pm} \nu X)}$$

The factors $f_{d,s,u}$ with $f_d + f_s + f_u = 1$, denote the fractions of $B_{d,s,u}$ mesons (with quark content $\bar{b}d$, $\bar{b}s$, and $\bar{b}u$, respectively) in $b\bar{b}$ events. The semileptonic branching ratios of the $B_{d,s,u}$ mesons are denoted by $BR_{d,s,u}$. With the assumptions $B_u:B_d:B_s = 1:1:0.3$ and $BR_u = BR_d = BR_s$, and the present knowledge of the mixing parameters ($X_d = 0.17 \pm 0.05$ and $X_s = 0.25 \pm 0.25$, the correction factor in (4) is

$$\frac{1}{1-2X_l} = 1.27 \pm 0.13.$$

The results determined from the expressions (2) and (3) (in the limit $\beta \to 1$) for the axial vector coupling constants a_c and a_b of charm and bottom quarks in the inclusive lepton channels at 35 GeV and 43 GeV is:

$$a_c = +(0.70 \pm 0.63),$$

$$a_b = -(0.91 \pm 0.46) \text{ without } B^0B^0 \text{ mixing},$$

$$a_b = -(0.99 \pm 0.65) \text{ with } B^0B^0 \text{ mixing}.$$

The measurements are in good agreement with the standard model predictions of $a_c = +1$ and $a_b = -1$.

5.2 4-JET EVENTS IN e^+e^--ANNIHILATION

M.Hahn H.Müller

With a cluster- and in invariant-mass algorithm we get multi-jet events from data taken with the CELLO detector at PETRA at 35 GeV center-of-mass energy. The analysis is based on 24017 multihadronic events.

Cluster algorithm

Over a matrix of angles in space we search for maxima of a generalized energy flow. The directions of these maxima serve as initial jet axes. Jets are then established by an iterative procedure which uses only the particle momenta. Particles are merged into the nearest jet if the angle to the proposed jet axis is below a preset half cone angle, typically 45°. After merging a new jet axis is determined by the sum of the momenta of the particles in the jet and the procedure is repeated with this new axis until a stable situation is reached.

Invariant-mass algorithm

The algorithm replaces the two particles i and j with the smallest invariant mass M_{ij} by a "pseudoparticle" with the four-momentum

$$p_{pseudo} = p_i + p_j$$

if the squared invariant mass

$$M_{ij}^2 = 4 p_i p_j \sin^2 \alpha/2$$

is less than

$$M_{ij}^2 \leq y_c \cdot E_{cms}^2$$

The cut y_c in the invariant mass is varied in the analysis from 0.01 to 0.05, corresponding to M = 3 - 7 GeV.

This procedure is repeated until there are no 2 particles or pseudoparticles found which fulfil this condition. The remaining number of "pseudoparticles" is then called the jet multiplicity.

EFFECT OF THE GLUON SELF-COUPLING

One of the essential features of QCD is the gluon self-coupling. This effect should show up in 4-jets events in the opening angle distribution of the two lowest energy jets, which come with high probability from gluons. We distinguish QED-like and QCD-like 4-jet events. QED-like means that the gluons are only Bremsstrahlung-gluons or the gluon creates a quark-antiquark pair, whereas QCD-like means that a gluon splits up into two gluons. The relevant diagrams are shown in figure 1.

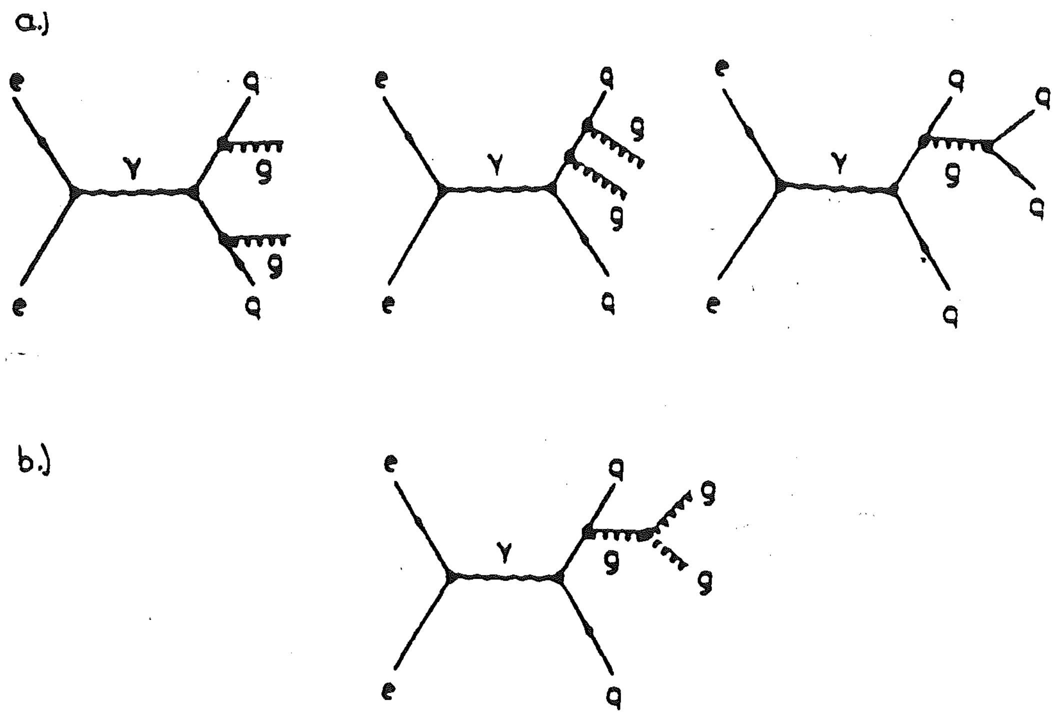

Fig.1: a.) QED- and b.) QCD-like 4-parton events

Theory predicts (1) that the angle between the gluons in the QCD-like event is peaked at small angles between the gluons, whereas in the QED-like gluon-Bremsstrahlung event only a small correlation from spin effects is present.

For the Monte-Carlo study we use the second order QCD string-model (2). A analysis is done with the cluster algorithm. We generate two Monte-Carlo samples. One, where QCD- and QED-like events are involved (standard version) and another sample without QCD-like events (without gluon self-coupling), but with the cross sections for QED-like events increased to get the same total 4-parton rate. The QED-like sample of 4-jet events is dominated by Bremsstrahlung-gluons. The opening angle distributions of the two lowest energy jets for the two 4-jet samples are shown in figure 2. The distributions are normalized in a way that the integral is equal to one. A peaking at small angles is present in the distribution based on 2nd order QCD, but absent in the QED-like model. The parton-shower model gives a similar opening angle distribution as the standard second order string-model.

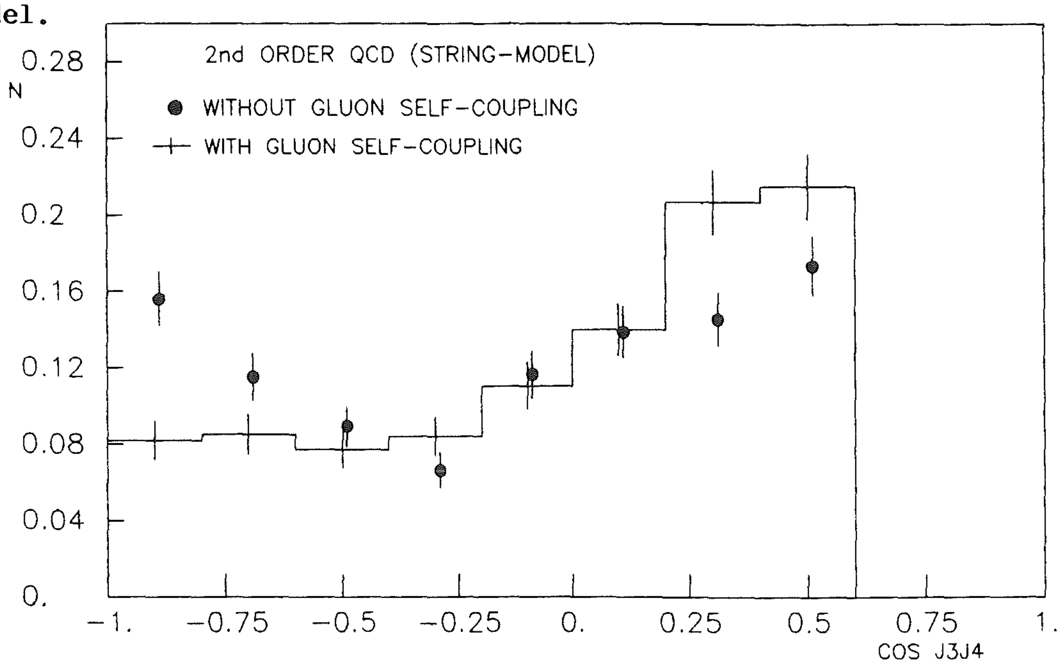

Fig.2: Angular distribution of the generator events

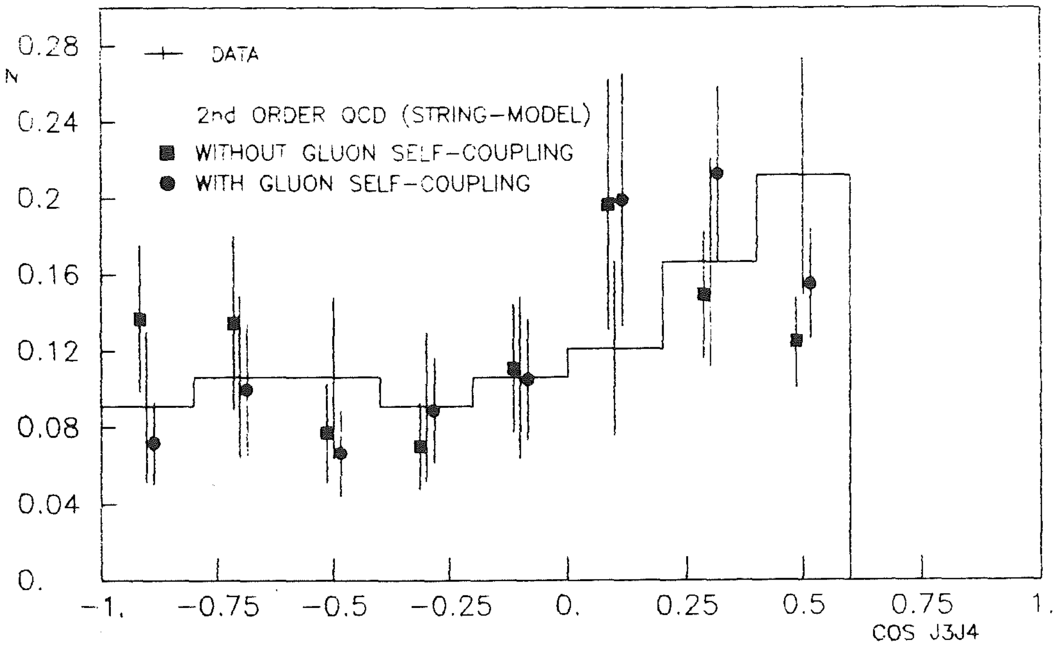

Fig.3: Comparison between data and corrected generator events with gluon self-coupling and without gluon self-coupling

In the data we find only 66 4-jet events. We correct the generator events for detector effects. The comparison between data and corrected generator events without and with gluon self-coupling is shown in figure 3. We get X^2 = 4.02 for 7 degrees of freedom in the case where no QCD-like events are involved and X^2 = 3.0 where the gluon self-coupling is included. We see no significant difference because of the low statistic of the data.

QUANTITATIVE DESCRIPTION OF THE 4-JET RATE

The annihilation $e^+e^- \rightarrow$ partons can be calculated with perturbation theory and with parton-shower models. The fragmentation of partons into hadrons can at present be described only with phenomenological models. We use for the fragmentation of the partons into hadrons the LUND string-model. The 4-jet rate is a sensitive test for the higher order contributions in these models. We compare the jet rates of the experimental data at E_{cms} = 35 GeV with that from Monte-Carlo events, which are based on second order QCD, parton-shower model and optimized second order QCD (3). For the analysis with the cluster algorithm the result are given in table 1.

TABELE 1: Jet rates for data and models(cluster algorithm)

jet rates in %	2-jet	3-jet	4-jet
data	53.7 ± .8	11.6 ± .3	.52 ± .06
2nd order QCD	56.8 ± .4	11.8 ± .2	.39 ± .03
parton-shower	55.8 ± .9	11.6 ± .3	.39 ± .04
optimized 2nd order	57.3 ± .8	11.9 ± .3	.53 ± .05

The second order QCD LUND-model does not describe the 4-jet rate well. Only 75% of the 4-jet events in the data are given in the model. The parton-shower model gives also a too low 4-jet rate. The divergences of the theory have to be removed by renormalisation. For the scale parameter μ one takes traditionally the energy Q of the virtual photon. But there is no justification for this choice. Optimizing (3) means that a value for μ can be found where the neglection of the higher orders is compensated, Figure 4 shows the variation of the 3-jet and 4-jet rates. With $\mu = 0.1 \cdot Q$ and Λ = 80 MeV best agreement with the data is obtained.

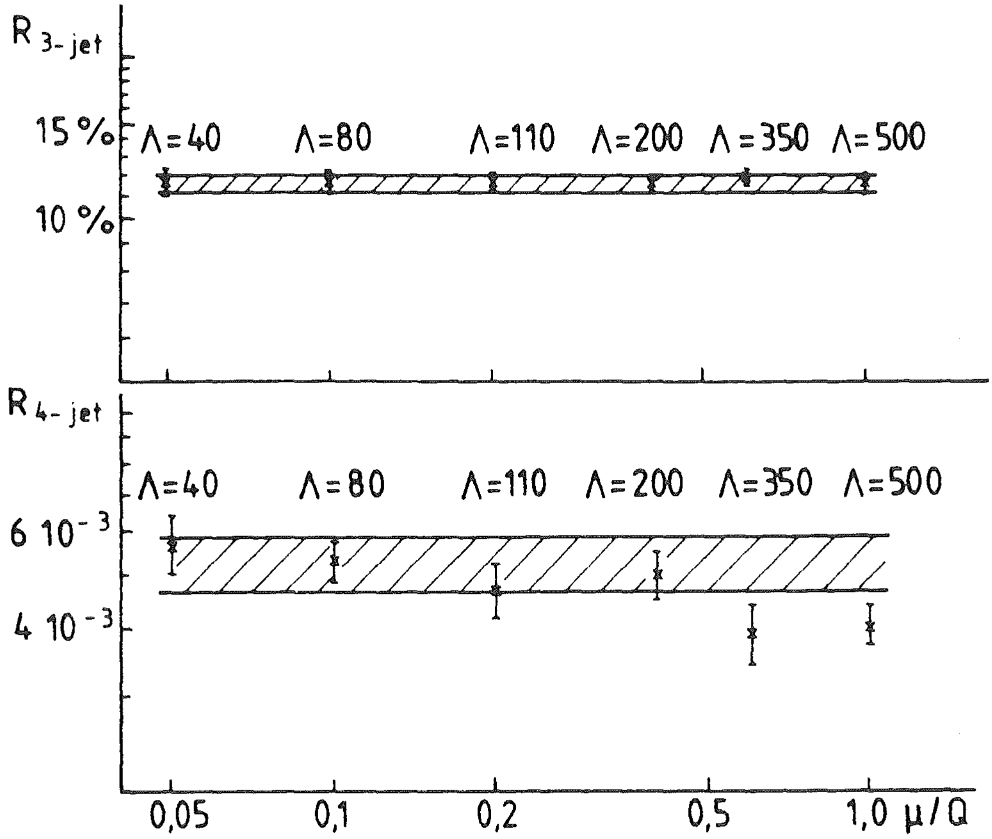

Fig.4: Rates of 3-jet and 4-jet events for data and optimized 2nd order QCD for different renormalisation scale parameter $\mu = x \cdot Q$. Symbols: model; band: data

The analysis with the invariant-mass algorithm yields the same result. The second order model cannot describe the data (Fig.5) and also in the parton-shower model (Fig.6) the 4-jet rate is too low.

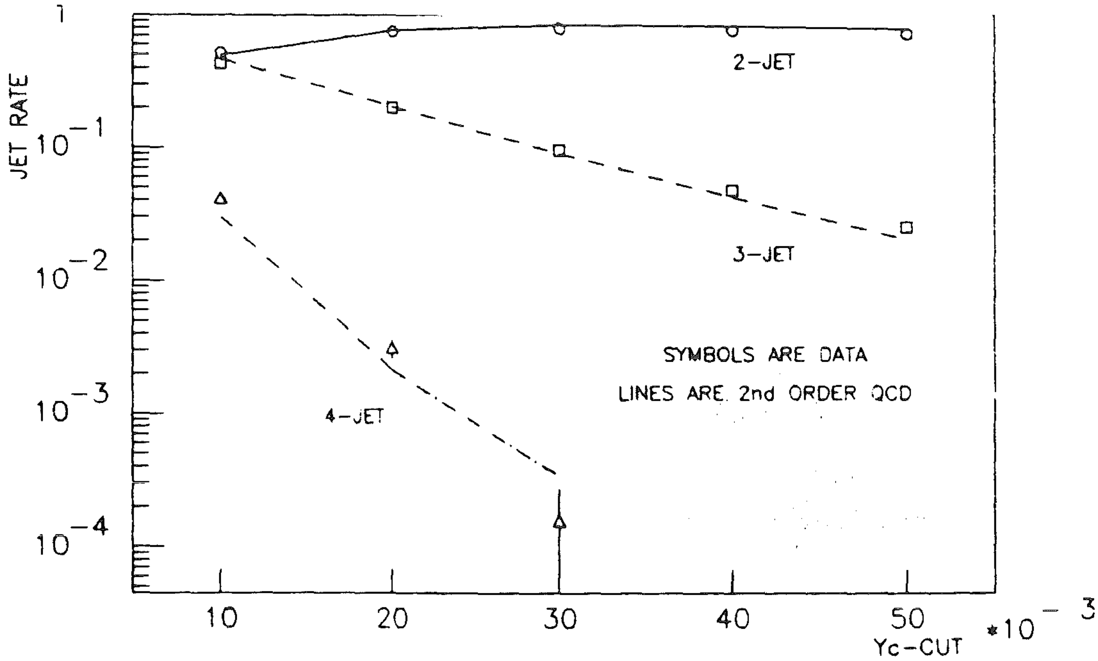

Fig.5: Jet rate of the data and 2nd order QCD LUND-model (invariant-mass algorithm)

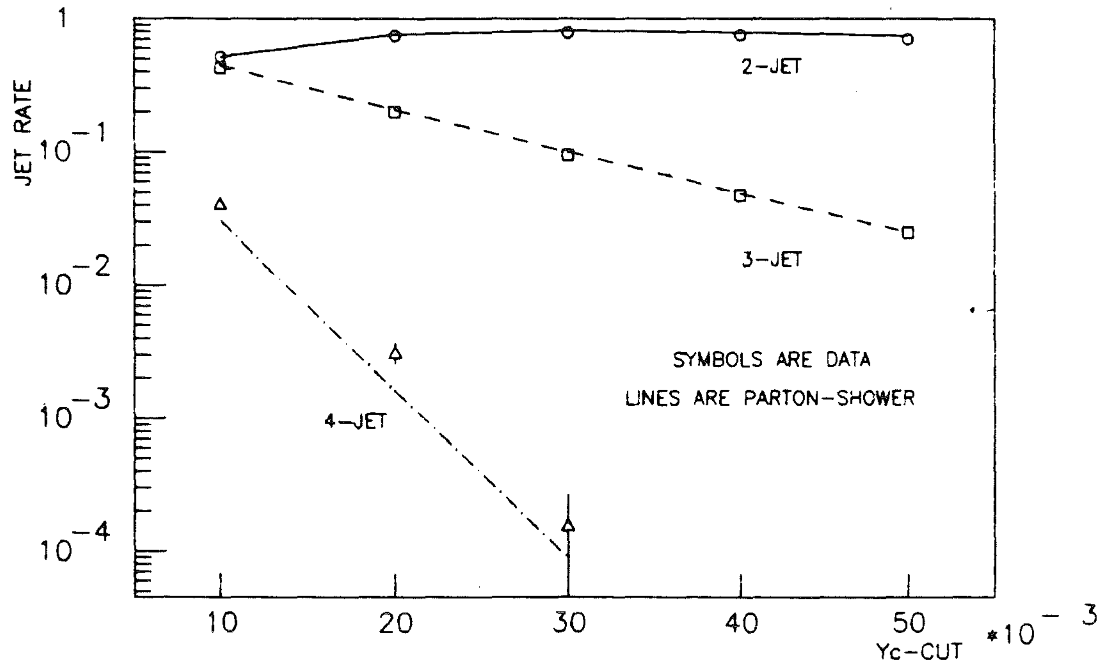

Fig.6: Jet rate of data and parton-shower (invariant-mass algorithm)

For the optimized second order QCD the 4-jet rate is in good agreement with the data for the same values of μ and Λ as in the analysis with the cluster routine (Fig.7).

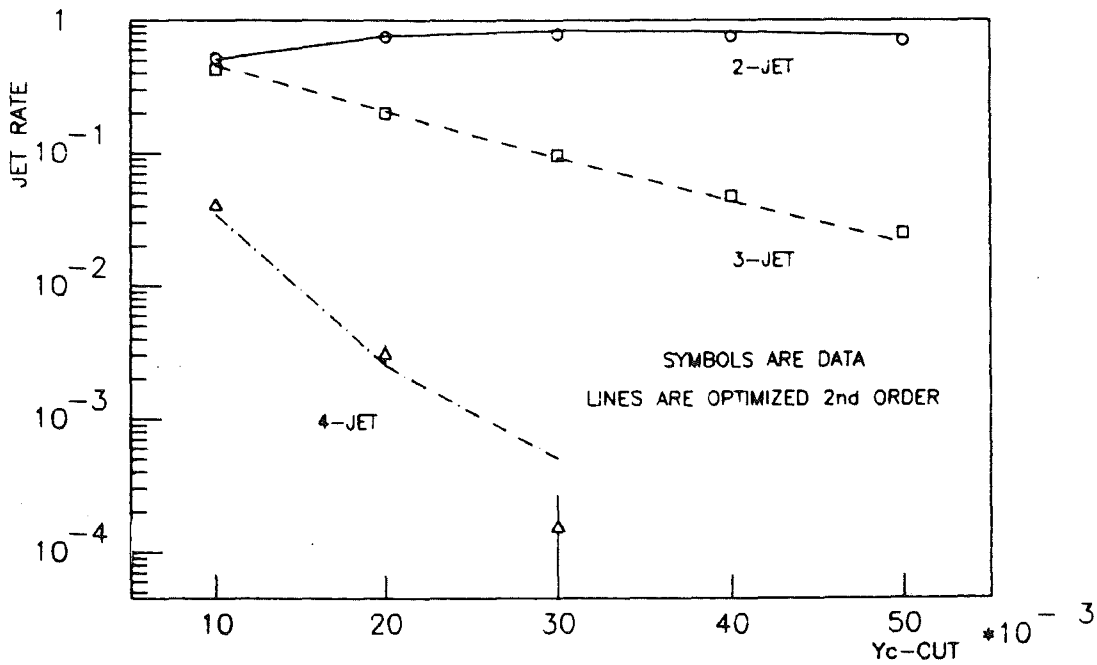

Fig.7: Jet rate of data and optimized 2nd order QCD LUND-model (invariant-mass algorithm) μ = 0.1 Q; Λ = 80 MeV

Independently of the algorithm used for the jet search the 3-jet and 4-jet rate cannot be described simultaneously in the second order QCD LUND-model nor in the parton shower model. Only the model based on optimized second order QCD gives the observed 4-jet rate.

(1) Körner, Schierholz, Willrodt, Nucl.Phys. B185 (1981) 365
(2) T.Sjöstrand, Computer Phys. Communication 39 (1986) 347-407
(3) P.M.Stevenson, Phys.Rev. D23 (1981) 2916
G.Kramer, B.Lampe, DESY 87-106

5.3 TRIGGERCOUNTERS FOR THE ELECTROMAGNETIC CALORIMETER OF THE DELPHI DETECTOR CERN/LEP)

D.C.Fries, M.Kopf, H.H.Mielke

A prompt neutral trigger for the electromagnetic Calorimeter (HPC) of the DELPHI detector (CERN/LEP) will be obtained from three scintillation counters installed in each of the 144 HPC modules. The counter signals are read out using wavelength-shifting (w.l.sh.) optical fibers.

In the "Annual Report on Nuclear Physics Activities" of the KfK (KfK 4405) we reported on the design and test of prototype counters.

During the past year some 300 counters of the type descried there have been mass-produced. They have been assembled at the University of Warsaw and installed in the HPC modules and tested at CERN under major participation of Karlsruhe physicists. The counters have been tested after being installed into the HPC module using both, Cosmic rays and a 3 to 50 GeV Pion/Electron Beam in the CERN West Hall. The Modules have been placed in a 1 Tesla magnetic field and were scanned with the incident beam. Results of the overall performance averaged over the number of modules tested so far are shown in the figure 1 below, where it was plotted:

a) the effective attenuation length of the scintillation counters along the direction of the wavelenght shifting read-out fiber (Fig.1a),

b) the response of the counters for an incident electron (after 4 rad. length) as a function of energy. The average signal output is given in ADC channels above threshold (Fig.1b).

The attenuation length obtained in these measurements over about 50 cm length of the trigger counter was 193 ± 21 cm. The energy response for electrons after 4 rad. length let us expect that a trigger level of less than 1 GeV can be reached. For the timing of the trigger counters and in order to controll the counter trigger efficiency it is essential to feed a calibration light signal to all counters simultaneously. For this purpose a UV laser is used which generates short UV lightpulses (3 nsec). By illuminating a block of scintillation material and feeding the (secondary) scintillation light pulses via 144 x3 optical fibers into the individual trigger counters we can controll the performance of the counters.

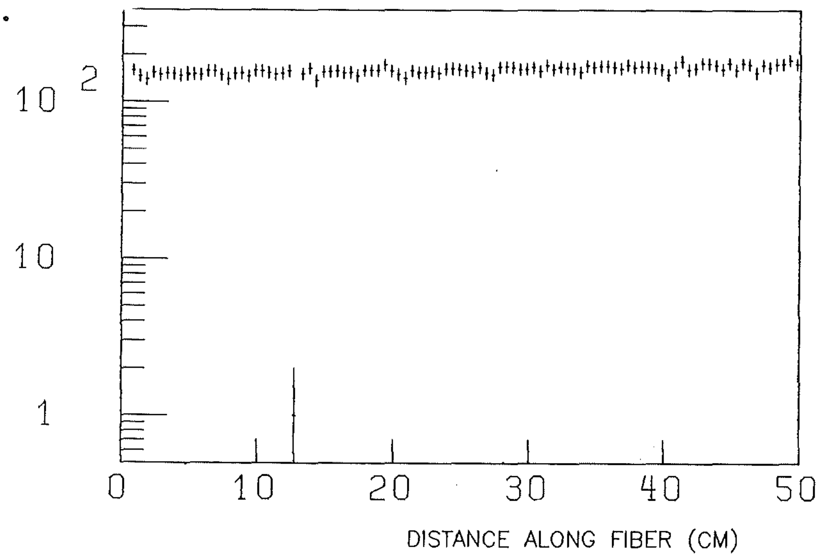

Fig. 1a: Effective attenuation length of the counters (read out with w.l.sh. fibers) in the direction of the read-out fibers

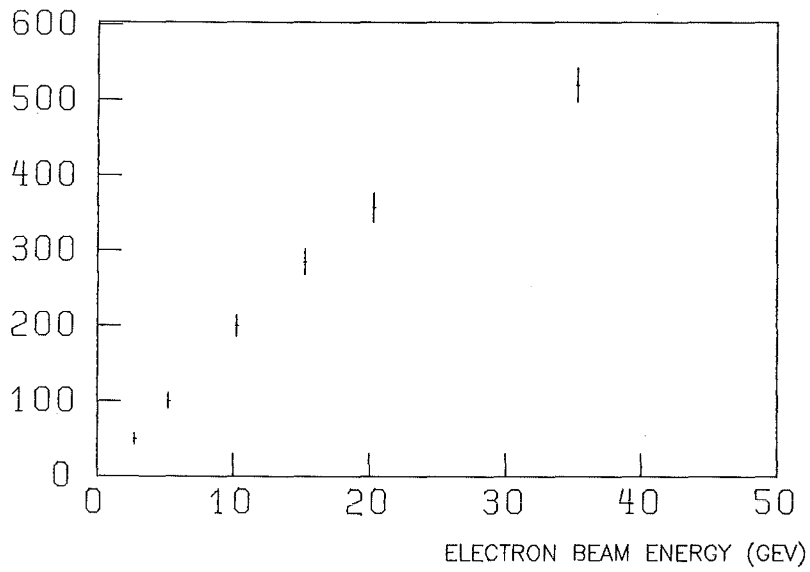

Fig. 1b: Average pulse height of the counters as a function of energy of an incident electron (installed in the HPC after 4 rad. length)

In Fig.2 we measured the homogeneity of the scintillation light signals channelled into 48 optical fibers which are tapping the UV illuminated scintillator block.

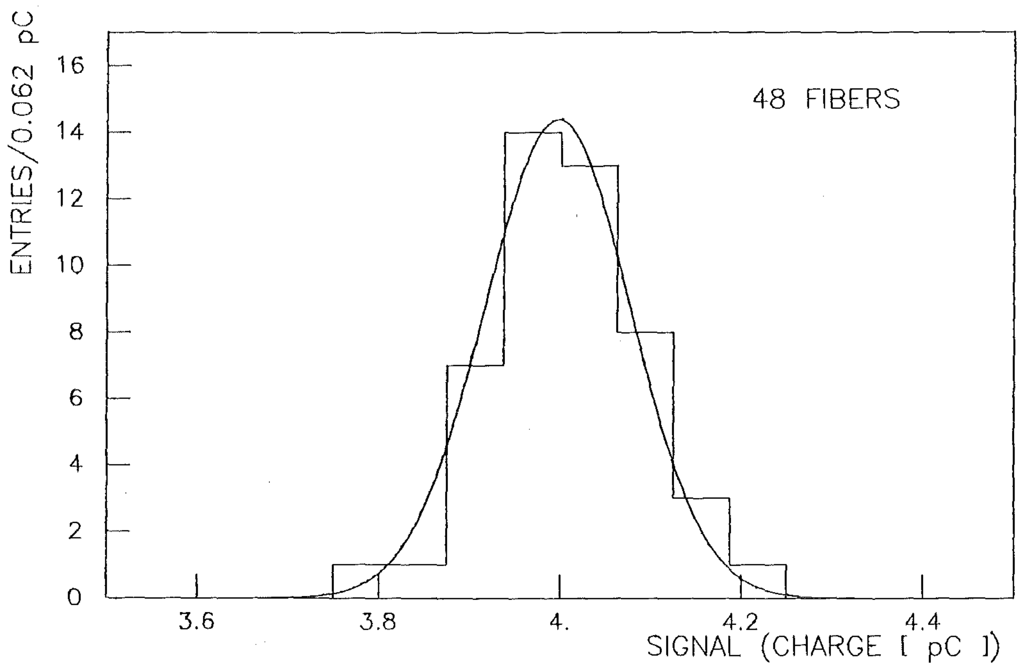

Fig.2: Homogeneity distribution of the calibration signals which are fed into 48 optical fibers tapping the UV illuminated scintillator block out-put signal of the counters in pC

6. DEVELOPMENTS AND INSTRUMENTATION

6.1 DETECTORS

6.1.2 DETECTION OF LASER PULSES AND α-PARTICLES WITH SUPERCONDUCTING TUNNEL JUNCTIONS

P.Jany, F.Finkbeiner, W.Heeringa, H.O.Klages, H.Skacel, T.Strobelt

A superconducting tunnel junction detector is a powerful tool for the detection of ionizing radiation with a potentially high energy resolution (1).This arises from the fact that the energy required to break a Cooper pair is of the order of 1 meV which is three orders of magnitude smaller than the gap of a semiconductor.

Aluminium tunnel junctions were produced in a high vacuum chamber by evaporation (see 5.1.3) and cooled down to about 300 mK in a ^3He cryostat (see 5.2.1). Measured current-voltage-characteristics are shown in figure 1. The Josephson current was suppressed by a magnetic field.

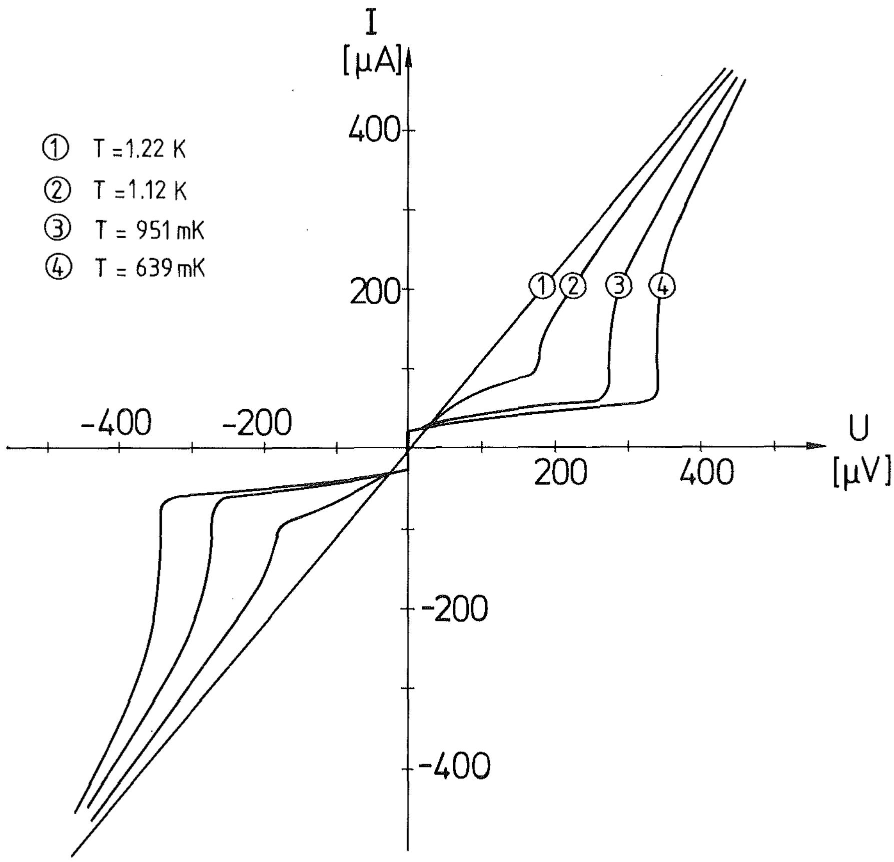

Fig.1: Measured current-voltage-characteristics of aluminium tunnel junctions (T_c = 1.19 K)

First irradiation experiments were performed with light pulses through fiber optics from luminescence diodes and a pulsed N_2-Laser. The charge tunneled through the tunnel barrier was collected by a commercial semiconductor charge preamplifier at room temperature connected to the tunnel junction by about 1.5 m long twisted pair wires.

Next the junctions were irradiated by 5.2 MeV α-particles from a ^{210}Po source. The α-particles deposit about 175 keV in the Al-layers of the junction before they are stopped in the substrate within 10 µm. Part of the phonons created in the substrate also contribute to the signal. Therefore the energy calibration of the peak in the pulse height spectrum of figure 2 is not known. We estimate it to correspond to about 2 MeV. The events with pulse heights below the peak are due to quasiparticle diffusion out of the junction, α-particles stopped in the substrate near the junction and α-particles that hit the contact leads. When the α-source is removed no background events remain in the pulse height region shown in figure 2. The noise level is below the threshold.

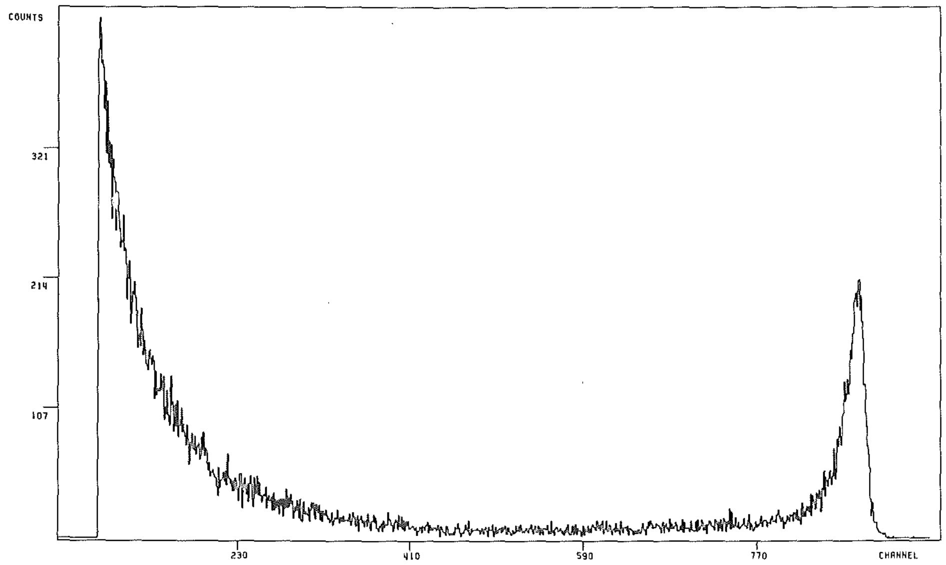

Fig.2: Pulse height spectrum of a tunnel junction irradiated with α-particles

We intend to detect X-rays and measure energy resolution in the near future. For this purpose the quality of the junctions has to be improved. The use of photolithographic processes for the production of tunnel junctions is in preparation in collaboration with the Institut für Kernverfahrenstechnik of the KfK.

(1) W.Rothmund, A.Zehnder, PSI Preprint PR-88-10 (1988)

6.1.2 PREPARATION OF ALUMINIUM TUNNEL JUNCTION BY EVAPORATION TECHNIQUES

F.Finkbeiner, W.Heeringa, P.Jany, H.O.Klages, H.Skacel, T.Strobelt

Superconducting tunnel junctions can be used as detectors with high energy resolution (5.1.2). They consist of two overlapping strips of superconducting material less than 1 µm thick separated by an insulating layer of a few tens of Angstroms thickness (figure 1).

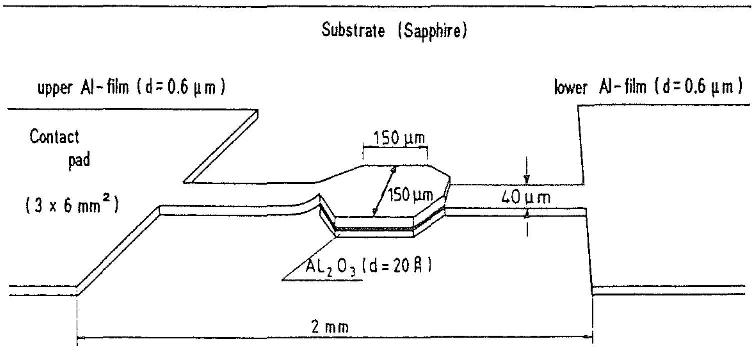

Fig.1: Junction geometry

We use aluminium for the strips and its natural oxide as insulating barrier. Aluminium has the advantage of easy formation of a stable and thin oxide layer. The substrates we use are polished sapphire and quartz single crystals (27*7*0.5 mm). They are carefully cleaned and examined for scratches and dust particles under a microscope. To improve the electrical connection gold pads are thermally evaporated onto the substrates in a small evaporation chamber. The next steps of junction production take place in a varian evaporation chamber 28" high and 18" in diameter. Four installed pumping systems (molecular-drag pump, getter-pumps, tetan sublimation pump, cryogenic pump) can provide a vacuum down to 10^{-9} mbar. The junctions are usually prepared at 10^{-6} mbar using only the molecular-drag pump. Two sources are available for the evaporation: A resistance-heated canoe and a magnetically focused 10 kW electron gun with three crucibles. Because of its stable evaporation rate and its capability of melting almost all materials (important for future applications) the electron gun is preferred.

Evaporation rate and film thickness are monitored by a crystal oscillator. The substrates are fixed in a substrate holder and pressed onto a nickel mask (27*7*0.1 mm) through which the aluminium is deposited. The substrate temperature during evaporation is important for the film characteristics. Therefore, the holder is equipped with a cooling and a heating system. Temperatures in the range from 100 K to 500 K can be achieved with an accuracy of about 3 K. As the mask is fixed in front of the substrate and contains the total structure of the junction sample evaporation through the mask would not generate the structure shown in fig.1. Therefore, a movable shutter below the mask subsequently exposes only one half of the junction and shadows the other (figure 2). The two positions of this shutter have to be adjusted accurately by micrometric screws. For that purpose a halogen projection lamp is placed below the substrate with mask and shutter and a lense system above it. The magnified picture is then projected onto a screen.

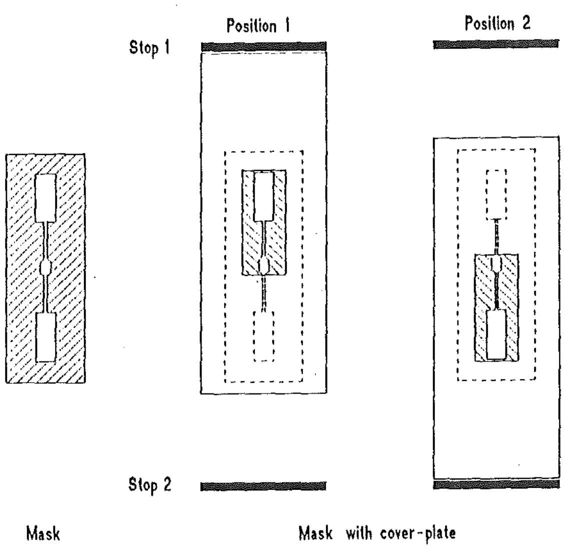

Fig.2: Mask alignment

After a pressure of 10^{-6} mbar is reached the substrate is heated up to 100°C for 1 1/2 hours for cleaning. Half an hour later the first aluminium layer of about 0.5 µm thickness is evaporated with an evaporation rate of 200 A/sec, a substrate temperature of +10°C and an oxygen pressure of $3 \cdot 10^{-5}$ mbar. The oxygen is added to improve the film quality.

After the evaporation is finished the oxygen pressure is increased to 3 mbar. The oxidation is carried out during 2 hours at a substrate temperature of +60°C. Finally the second layer is evaporated under the same conditions as the first.

Experiments performed with these junctions are described in 5.1.2.

6.1.3 IMPROVEMENTS IN THE OPERATION OF A 3HELIUM CRYOSTAT

T.Strobelt, F.Finkbeiner, W.Heeringa, P.Jany, H.Skacel

The 3Helium cryostat described in the previous annual report (1) was improved by increasing the cooling power of the 1K-stage and the 3Helium-stage. Also a very accurate temperature sensor was installed. The lowest temperature achieved was 276 mK and the normal operating temperature is about 280 mK.

The 1K-stage, a pumped 4Helium-bath, was improved by designing a new needle valve. The advantage of this allmetal valve, which consists of a stainless steel needle in a brass fitting, in comparison to the old teflon sealed valve is a better adjustable flow rate and a smaller leakage rate. In addition the pumping speed was increased by the use of a second rotary pump (now: 2x60 m^3/h) in the 4Helium pumping line.

The cooling power of the 3Helium-stage was increased by replacing the molecular-drag pump by an oil diffusion pump and by filling copper powder into the 3Helium bath on the copper bottom plate which improves its thermal coupling to the liquid 3Helium. Copper radiation shields were inserted into the 3Helium pumping line.

With these changes the 3Helium circulation rate is 5 μmol/s at 280 mK. This corresponds to a total 3Helium cooling power of 130 μW. The net cooling power of the cryostat was measured at several temperatures. It is

$$P\ (280\ \text{mK}) = 0\ \mu\text{W}$$
$$P\ (285\ \text{mK}) = 10\ \mu\text{W}$$
$$P\ (300\ \text{mK}) = 25\ \mu\text{W}$$
$$P\ (330\ \text{mK}) = 80\ \mu\text{W}$$

For the accurate measurement of the temperature a Germanium sensor was installed which is measured by a resistance bridge in four wire technique. Proper electric shieldings asure the correct determination of the temperature.

The now available temperature is approximately the physical limit for 3Helium pumping cryostats. Below this temperature the steeply decreasing vapour pressure of 3Helium limits the pumped 3Helium rate and so its total cooling power. Experiments performed with this cryostat are described in 5.1.2.

(1) Annual report Institut für Kernphysik, KfK 4405 (1988)

6.1.4 SCINTILLATOR MATERIAL TESTS FOR EXTASE

H.O.Klages, W.Kriegleder, G.Völker

For the study of ultrahigh energy cosmic rays in an EXTensive Air Shower Experiment (EXTASE) two different detector systems are under study. For the detection of the electron-photon component in an EAS a liquid (or cheap plastic) scintillator with high light output and fast decay time is needed, whereas for the muon detection plastic scintillator sheets with WLS readout or PVC limited streamer tubes could be used. Here we report on tests of various scintillator materials for both applications.

A schematic view of the set-up for the measurement of the light output and attenuation length of large scintillator sheets is shown in figure 1. Cosmic muons are selected by coincidence of two scintillation detectors (Paddle 1, Paddle 2).

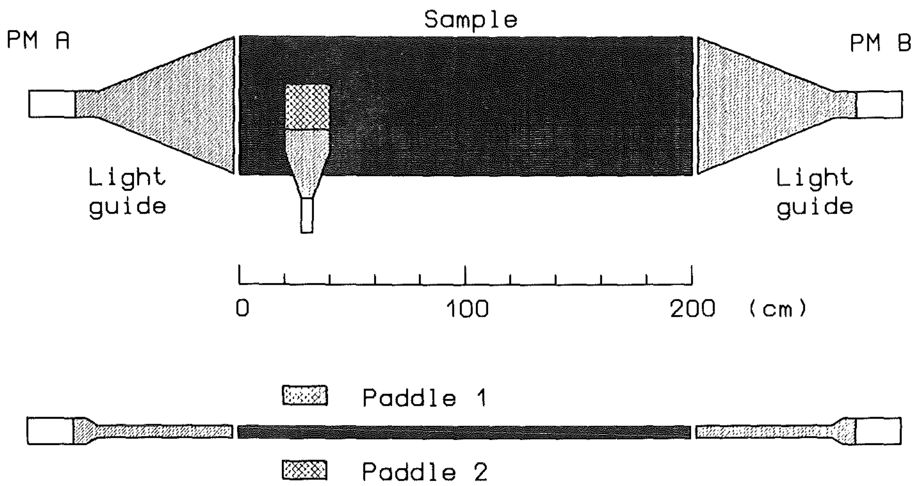

Fig.1: Schematic view of the test set-up with cosmic muons

The standard sheet size was 200*60*2 cm^3. The results for three thicker sheets were normalized appropriately. To achieve a reproducible optical coupling to the light guides an air gap of 0.8 mm was used. The use of silicon oil was found to improve the pulse heights by about 20%, nearly independent of position.

We tested eleven different materials from five factories. A sample of the results is shown in figure 2. These three scintillators will be used in more detailed studies of the detector geometry and the WLS readout efficiency.

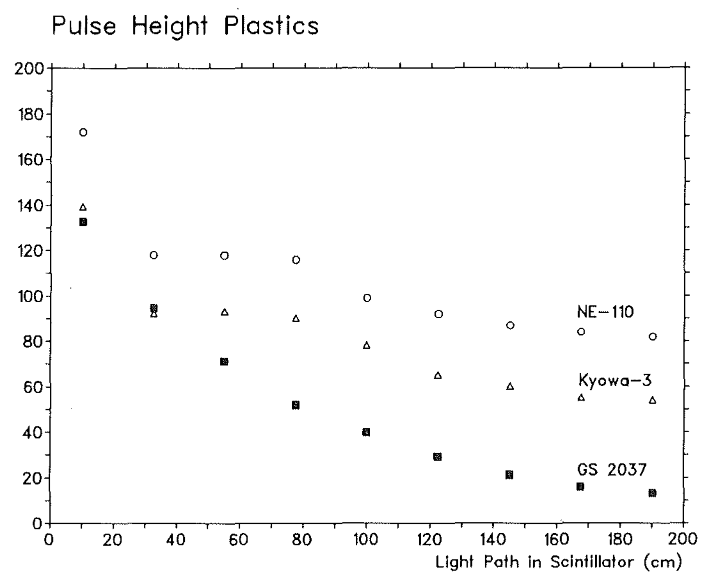

Fig.2: Light attenuation curves of three plastic scintillators

The detectors for EXTASE will be placed in field stations with only moderate temperature stability. Therefore, the scintillator material should be working properly in a wide temperature range. Three different special petroleum-based liquid scintillators have been tested together with NE213 and with the mineral oil-based scintillator of the KARMEN experiment.

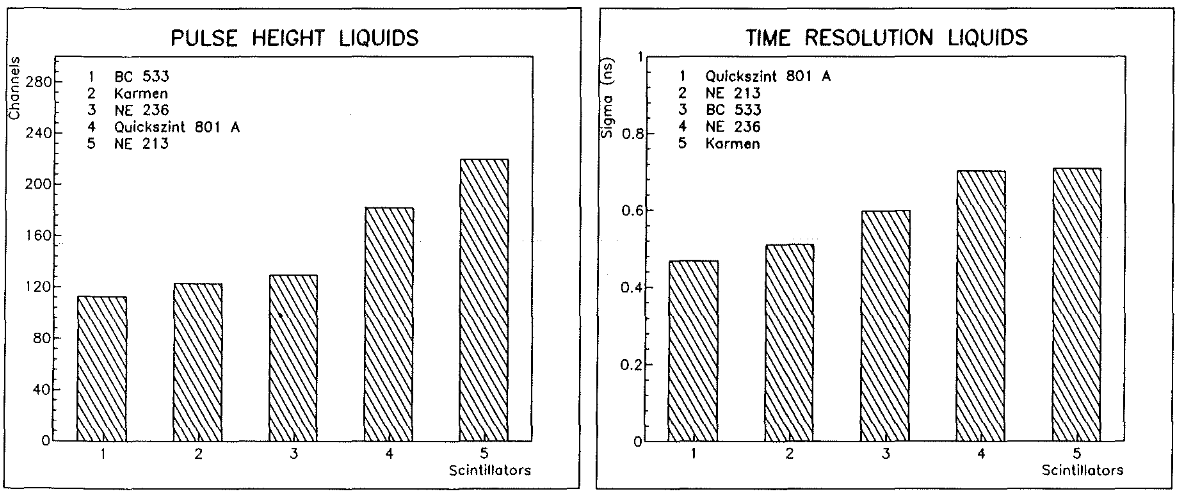

Fig.3: Relative light yield and time response of five liquid scintillator materials

Light output and time response of the liquids were measured using cosmic muons and triggered by a fast coincidence detector. The temperature response was determined by a set of measurements with a gamma ray source (Cs-137) inside a chamber with regulated T_c. The PM tube, the HV supply and the electronics were outside the chamber and were held at constant temperature. In figure 3 the results of the tests with cosmic muons are shown.

The temperature dependence of NE213 and the KARMEN material are not shown in figure 4.Both scintillators seem to be not the best choice at low temperatures. Especially the mineral oil becomes cloudy below -10°C.

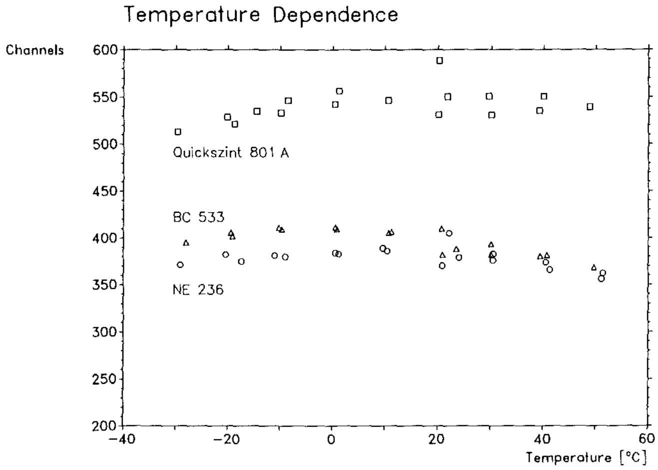

Fig.4: Temperature dependence of three liquid scintillators

The detector design study is continued using a 1 m Ø prototype with 2" of QUICKSCINT 801 liquid scintillator viewed by a 3" PMT XP3462 at a distance of about 60 cm.

6.1.5 IONIZATION CHAMBERS USING ROOMTEMPERATURE LIQUIDS

J.Engler, H.Keim, M.Gettert, A.Hoss, J.Knapp

R&D work on ionization chambers using molecular, roomtemperature liquids was persued along the following lines. Mainly tetrametylsilane (TMS) was used.

- We continued to investigate the resistivity of TMS against radiation. As a result it was observed that at low dose rates of approximately 10 krad the purity of the liquid becomes improved. This improvement, however, lasts only for periods in the order of 10 hours. In long terms a degradation is observed which amounts to an impurity of about 25 ppb/Mrad measured oxygen equivalent. The mechanism of the short term improvement is not yet understood.

- With a gridded chamber the ultimate energy resolution of liquid ionization chambers was studied. The energy spectrum of a ^{207}Bi source is shown in Fig.1.

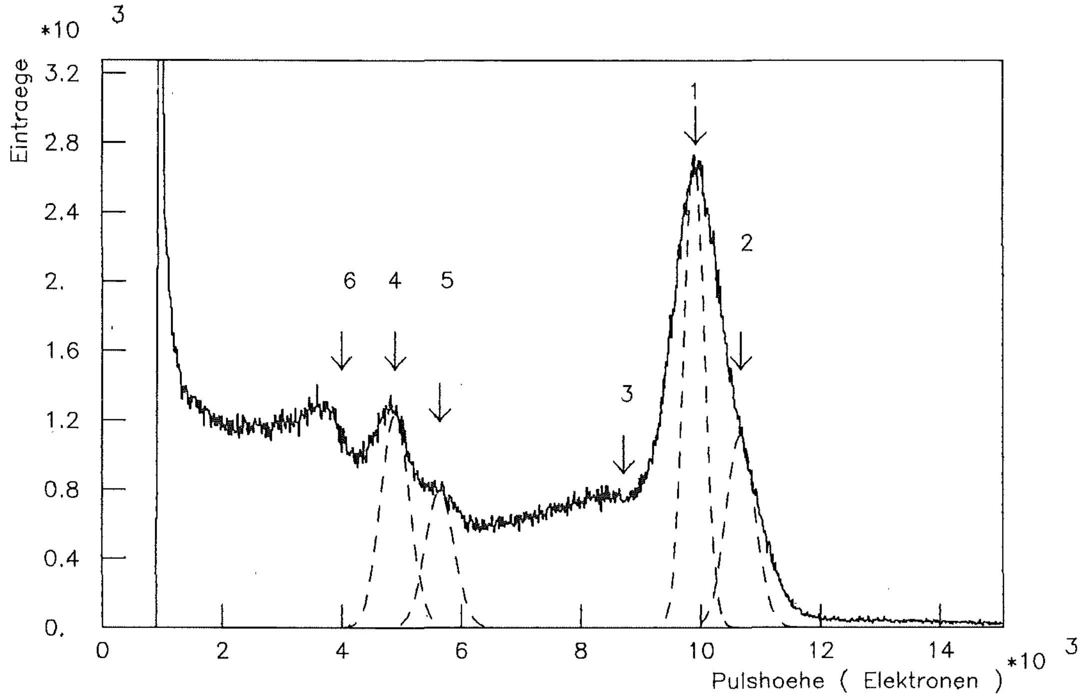

Fig.1: Pulse-height spectrum for a ^{207}Bi source in a TMS ionization chamber. The dotted lines indicate the positions of the K and L conversion electrons for the two γ-lines

The peak of the 1 MeV electrons has a rms resolution of 48 keV. This is worse than expected from Poisson statistics and Fano factor calculation. Probably the degradation can be explained by strong fluctrations in δ-ray production.

- The influence of impurities in liquids was studied under various aspects. Fig.2 shows the long term stability of a typical chamber. The

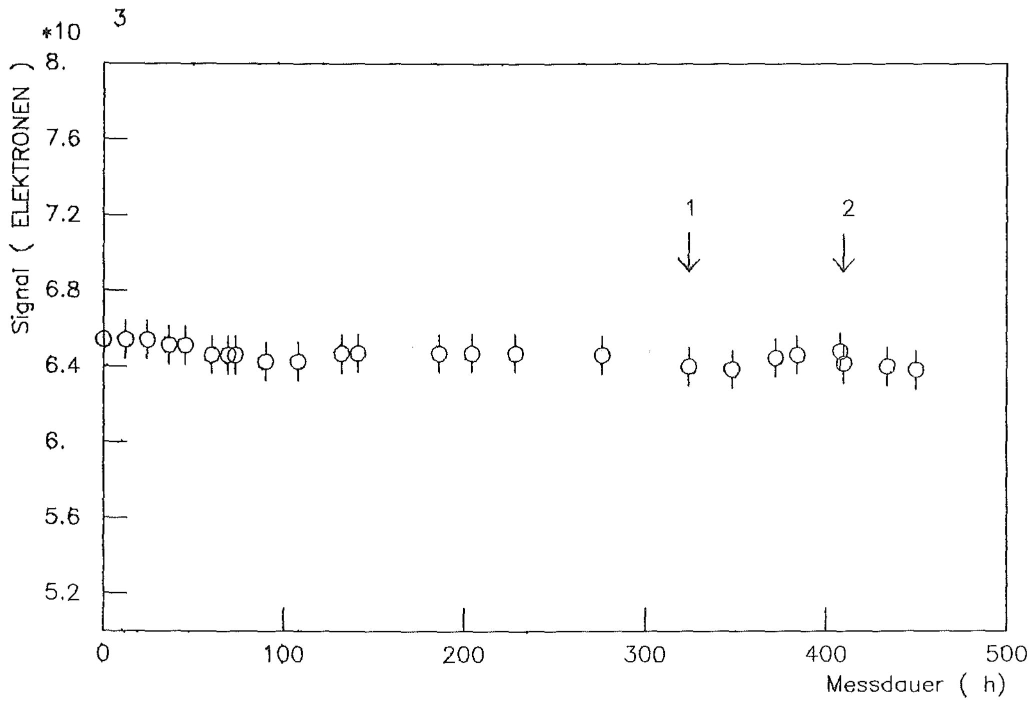

Fig.2: The pulse-height stability of a TMS ionization chamber with respect to time clapsed time moment of filling

signal decrease corresponds to an impurity rise of 0.5 ppb/d. Extrapolating this figure to a chamber in the projected central calorimeter of an air shower experiment, this implies a signal decrease of only 5% to 10% per year.

- With two modules of an uranium-TMS calorimeter the momenta of horizontal myons were measured. Advantage was taken of the bremsstrahlung and direct pair production process, which start to be important for energy loss of myons above 120 GeV in uranium. These measurements will be continued in order to obtain the horizontal myon energy spectrum.

6.1.6 AN EXTENSION FOR THE DETECTOR SYSTEM OF THE MAGNETIC SPECTROGRAPH "LITTLE JOHN"

R. Rudeloff*. S. Zagromski, W. Eyrich*, H.J. Gils, H. Jelitto,
A. Lehmann*, H. Schlösser*, H. Wirth*

Continuing our research in high angular resolution measurements using the magnetic spectrograph "Little John" (1), first results with our test version of the intermediate detector (ID) in front of the standard focal plane detector (FPD) had been obtained. Recently an improved version of the ID has been installed, which is shown in fig. 1.

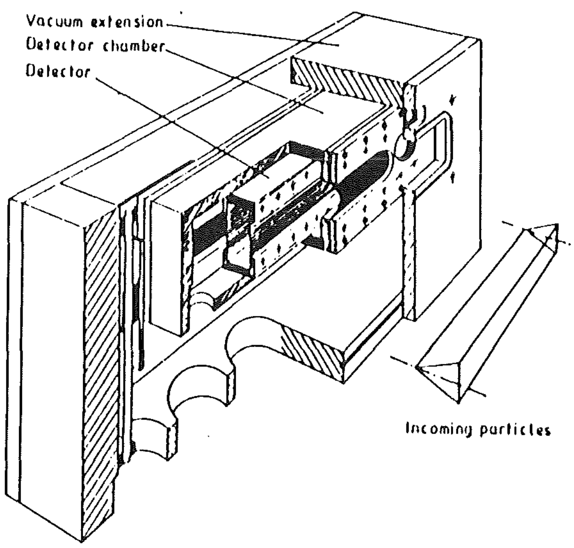

Fig. 1 Sectional drawing of the new intermediate detector (ID)

The ID is mounted between the existing vacuum tubes of the spectrograph. The detector chamber is movable motor driven in vertical direction, to allow a quick change between two different focal planes. The system is compatible to the various existing detector arrangements (2). In order to decrease angular straggling caused by the counting gas Ar/CH_4, an optional He gas filling in the detector chamber can be used.

As already discussed in the last annual report, the improved angular resolution allows an intersection of the acceptance in horizontal direction. This is provided by measuring the angles of the scattered particles in the region of the focal plane, which is obtained from the difference X1-X2 of the horizontal coordinates at the two position sensitive detectors (ID and FPD). Thus a resolution of the acceptance angle of about 0.3° can be reached.

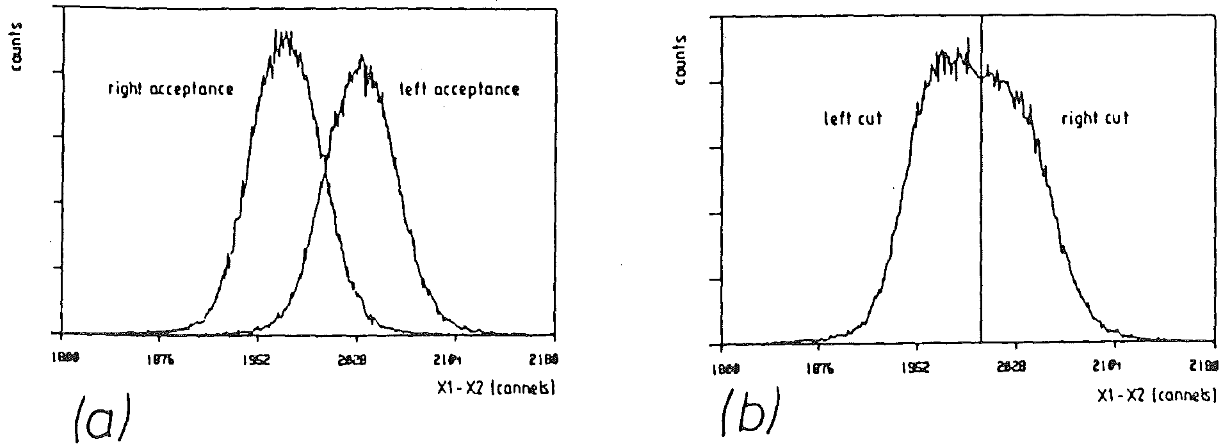

Fig. 2a X1-X2 left and right half of the acceptance
b X1-X2 full acceptance.

This procedure is demonstrated for a ^{6}Li-scattering experiment on ^{12}C. Fig. 2a shows the two X1-X2 peaks belonging to two different measurements with the left and the right part of the acceptance ($\Delta\theta$=0.5°, respectively). Fig. 2b shows the peak at fully opened acceptance ($\Delta\theta$=1.0°). One possible acceptance intersection by software cuts is indicated in Fig. 2b (dashed line). As an example the cross section of the elastic peak is shown in Fig. 3 with and without acceptance intersection. One can clearly see the improved angular resolution from $\Delta\theta$=1.0° to $\Delta\theta$=0.5°, provided by this method, without reduction of the acceptance during the measurement. Further studies to subdivide the acceptance into smaller parts are still in progress.

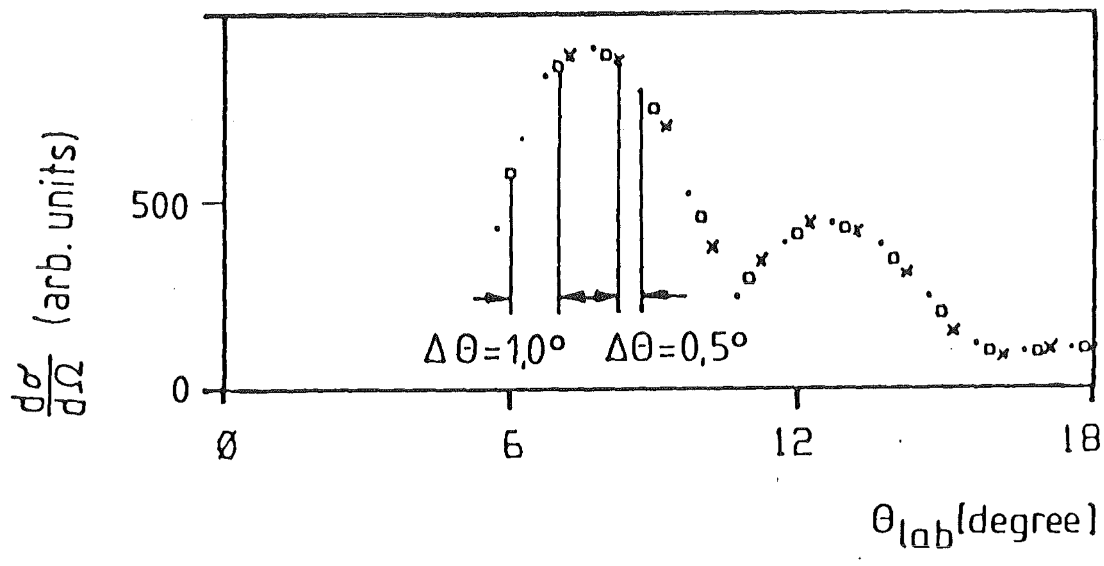

Fig. 3 Cross section of the elastic peak on ^{12}C at θ_{lab} 5° - 18°
o = without intersection, x = right cut, · = left cut.

Another important aspect to use the angular information are systematic tests of ionoptical parameters for various settings of the magnetic elements. Second order imaging effects are observable and will be studied in more detail.

(1) R. Rudeloff, S. Zagromski, A. Lehmann, H.J. Gils, W. Eyrich, H. Schlösser, J. Kiener, H. Wirth, Annual Report KfK 4405 (1988) p. 113

(2) S. Zagromski, H.J. Gils, H. Rebel, W. Eyrich, A. Hofmann, H. Schlösser, KfK-internal Report 1986 (unpublished)

* Physikalisches Institut der Universität Erlangen-Nürnberg

6.2 INSTRUMENTATION

6.2.1 EFFICIENCY AND LINE SHAPES OF A LARGE NaI DETECTOR

G.Fink, P.Doll, S.Hauber, H.O.Klages, K.T.Knöpfle*

For extracting count rates from gamma-ray spectra it is necessary to know the line-shapes and efficiencies of the detector system. We measured the absolute efficiency of a 16x16x24 cm^3 NaI-detector, with a 10x10 cm^2 collimator at the front face, surrounded by 5 cm NE 102A plastic scintillator anti-coincidence shield using γ-rays of 15.1 MeV by means of two methods.

The first method uses the inelastic proton scattering to the 15.11 MeV state in ^{12}C in the $^{12}(p,p'\gamma)^{12}C$-reaction (1) for a proton energy of 22.36 MeV. Monitoring the incoming proton flux and measuring the gamma-ray count rate in the NaI-detector at Θ_{lab} = 125° and the proton recoil spectra in coincidence, it is possible to determine absolute efficiencies.

Fig.1 shows the proton energy spectrum taken with a 2 mm silicon detector, which was set-up in a scattering chamber. The spectrum inset shows the coincidence spectrum after subtracting all the background.

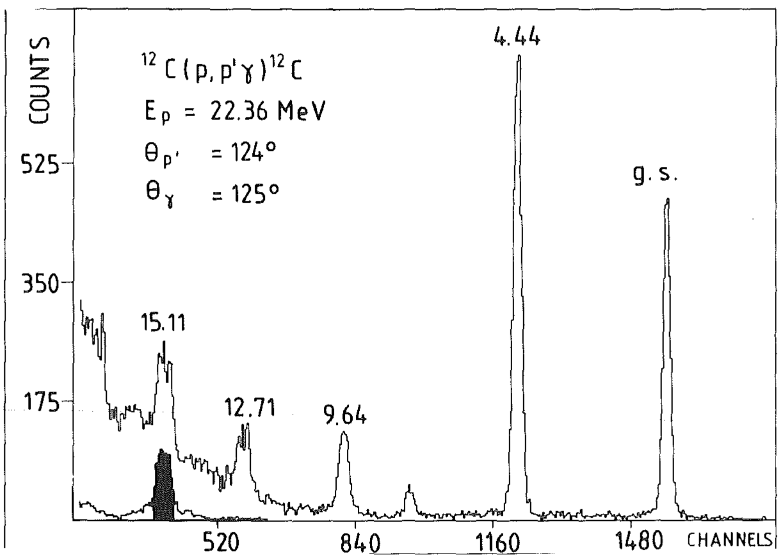

Fig.1: Proton energy spectra of the $^{12}(p,p'\gamma)^{12}C$-reaction. The spectrum inset shows the coincident (p,γ) yield.

Fig.2 shows a gamma-ray spectrum in the NaI-detector with an EGS-simulation described below. The full width at half maximum (FWHM) of the peak was taken from the high energy side of the peak. The summed region was taken from 1.75 widths below to 0.9 widths above the peak. Taking all events in the NaI-detector (no rejection in the anti coincidence shield) we optained an efficiency $\varepsilon(E_\gamma$ = 15.1 MeV) = 0.31 ± 0.10.It should be mentioned that there might be an additional systematic uncertainty in the

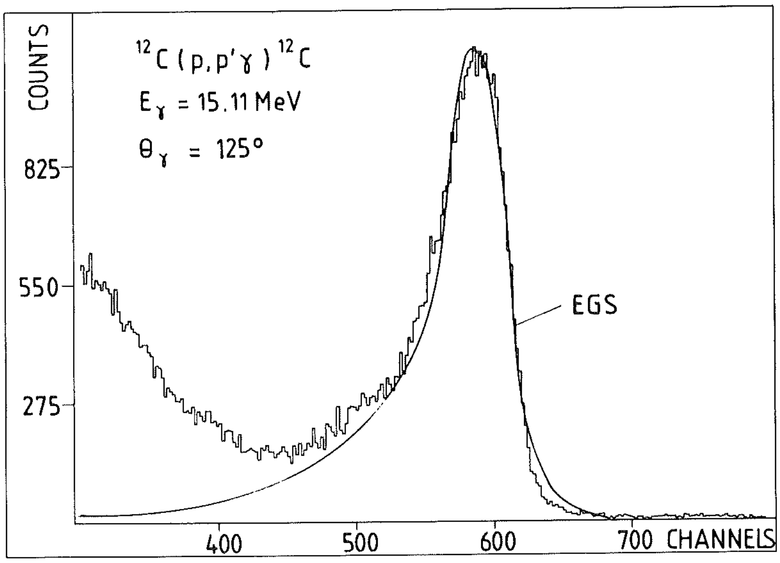

Fig.2: Gamma-ray spectrum of the $^{12}(p,p'\gamma)^{12}C$ reaction at an energy of E_γ = 15.11 MeV. The difference between the experimental curve and the EGS-simulation at lower energies is due to still existing background

$^{12}(p,p')^{12}C$ differential cross section. The second method makes use of the $^{12}(p,\gamma)^{13}N$ reaction in the vicinity of the $E_x(E_p)$ = 15.07 (14.24) MeV resonance in ^{13}N. A thick target yield curve measured with the NaI-detector at Θ_{lab} = 125° determines the absolute efficiency, since the number of gamma rays per proton is known at the resonance (2). With the same summed region we come up with E_γ = 0.46 ± 0.02.

In a third step Monte-Carlo-simulations of the electro-magnetic processes in our detector were performed using the EGS-code. We also explicitely include photoelectron statistics (effects of scintillation light intensity, light collection efficiency and phototube quantum efficiency). These effects contribute only a few % FWHM to the resolution at energies above 100 MeV (3), and are therefore neglected by other authors. At energies below 30 MeV these effects contribute more than 50% and must be included when comparing calculated line shapes and efficiencies. This is the first time that this is done and that it is possible to calculate absolute efficiencies. We determine $\varepsilon(E_\gamma$ = 15.1 MeV) = 0.71 in the same summed region. The discrepancy between the measurements and the simulations is not yet understood.

(1) H.V.Geramb, K.Amos, R.Sprickmann, K.T.Knöpfle, M.Rogge, D.Ingham and C.Mayer-Böricke, Phys.Rev. C12 (1975) 1697

(2) R.E.Marrs, E.G.Adelberger, K.A.Snover and M.D.Cooper, Phys.Rev. Lett. 35 (1975) 202

(3) J.P.Miller, E.J.Austin, E.C.Booth, K.P.Gall, E.K.McIntyre and D.A.Whitehouse, NIM A270 (1988) 431

*MPI Kernphysik, Heidelberg, FRG

6.2.2 A CAMAC CONTROLLED 16 STEP ATTENUATOR

H. Müller

The CAMAC controlled attenuator was developed for the automatic adjustment of energy and time signals from the 42 modules of the Karlsruhe BaF_2 detector. Twelve independent channels are integrated in one CAMAC module of 1/25 width. Each channel contains four fixed attenuators (Mini-Circuit Lab., AT-series, DC to 1500 MHz) that can be combined in binary steps of 1, 2, 4 and 8 dB to yield attenuation factors up to 15 dB. Various channels can be connected to obtain any desired attenuation. If all attenuators are inactive, the insertion loss is below 0.1 dB.

The fixed attenuators are addressed by coaxial relays (Teledyne 712-12). Switching the relays by capacitor discharge reduces the power consumption per relay to the DC values of 4V/10 mA. This means, that each CAMAC module requires at most 500 mA. The status of the 48 relays is shown on the front panel of the CAMAC module via LEDs. A block diagram of the module is given in Fig. 1.

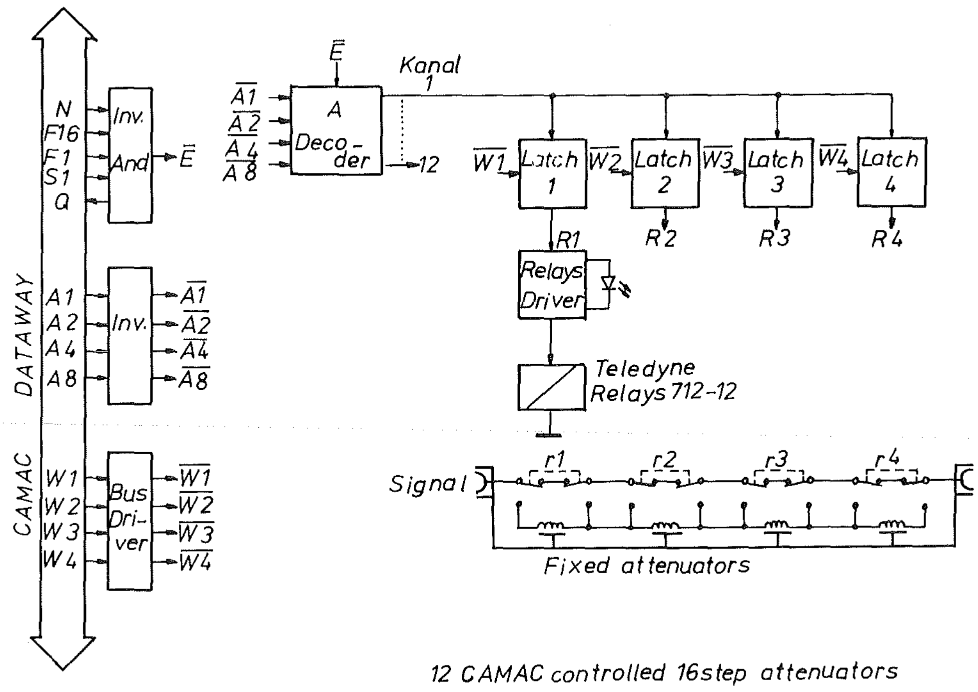

Fig. 1 Block diagram of the CAMAC controlled 16 step attenuator.

6.3. ACCELERATORS

6.3.1 OPERATION OF THE KARLSRUHE ISOCHRONOUS CYCLOTRON (KIZ)

F. Schulz, H. Schweickert

During the period of report the isochronous cyclotron KIZ was in full operation (Tables 1 and 2). The 7100 h of beam time for experiments was the largest that we have ever achieved in a single year. However, even with the almost round-the-clock operation we could not fulfill all the beam time requirements. In 1987/1988 our machine was overbooked by more than 30 %. This situation is not expected to change before the end of 1989.

The highlights concerning the performance of the machine were the extraction of up to 2.5 µA of $^{6}Li^{3+}$-ions at 156 MeV and the availability of 100 µA α-particles in the internal beam from an improved internal source.

Table 1: Beam statistics of KIZ from July 1987 to June 1988

Cyclotron Operational	With Internal Ion Source		With external Ion Sources		Total	
For Experiments	3317 h	39.8 %	3779 h	45.4 %	7096 h	85.2 %
Beam Development, Testing new Components, Developments for Isotope Production	218 h	2.6 %	181 h	2.2 %	399 h	4.8 %
Total Time of Operation with the Beam on Targets	3535 h	42.5 %	3961 h	47.6 %	7495 h	90.0 %
Scheduled shut-down for Maintenance, Repair and Installation	222 h	2.7 %	96 h	1.2 %	318 h	3.8 %
Unscheduled Shut-down	247 h	3.0 %	247 h	3.0 %	511 h	6.1 %
Total Shift Time	4003 h	48.1 %	4322 h	51.9 %	8325 h	100.0 %

*Polarized Deuterons 1922 h; $^{6}Li^{3+}$-Ions (156 MeV) 2039 h

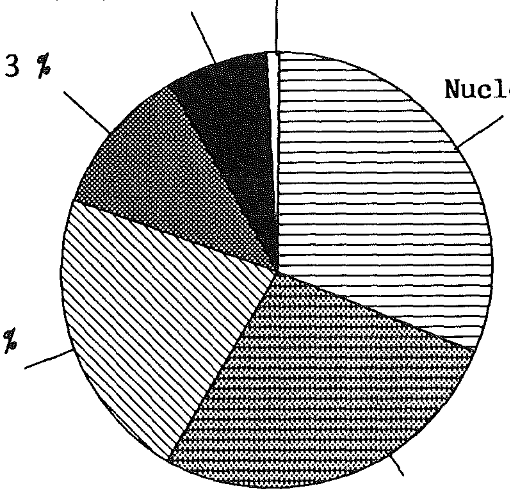

Table 2: Use and users of KIZ from July 1987 to June 1988

Internal Users		
Institut für Kernphysik I	1474.0 h	20.7 %
Institut für Kernphysik III	1099.0 h	15.6 %
Institut für Materialforsch.u. Festkörperphysik II	702.1 h	9.9 %
Institut für Radiochemie	59.4 h	0.8 %
Irradiation of Machine Parts	507.2 h	7.1 %
	3841.7 h	54.1 %
External Users		
Technische Universität München	1042.1 h	14.7 %
Universität Erlangen	754.8 h	10.6 %
Freie Universität Berlin	731.7 h	10.3 %
Universität Tübingen	582.6 h	8.2 %
Max-Planck-Institut Heidelberg	45.0 h	0.6 %
Universität Münster	43.6 h	0.6 %
Universität Bonn	19.6 h	0.3 %
Universität Münster	14.8 h	0.2 %
Universität Mainz	10.5 h	0.1 %
Universität Stuttgart	6.4 h	0.1 %
Universität Heidelberg	3.6 h	0.1 %
	3254.7 h	45.9 %
Total	7096.4 h	100.0 %

6.3.2 OPERATION OF THE COMPACT CYCLOTRON (KAZ)

J. Möllenbeck, H. Schweickert

During the period of report the cyclotron was operated successfully for isotope production and irradiation of machine parts, as well as for basic research. The 4510 h of beamtime was distributed equally among these activities. The demand for beam time compared to the previous year increased by about 700 h. Nevertheless, the machine is only booked for about 60 % of the maximum available time.

The reliability of the machine was again excellent and no major breakdowns occurred during operation.In order to reduce the activation by protons stripped by the residual gas (about 5 % of the beam current) all parts exposed to these particles are now shielded by aluminium and carbon. This way the dose to the operational staff could be further reduced to < 800 mrem/man year.

6.3.3 ON THE EXTERNAL ION SOURCES OF THE KARLSRUHE CYCLOTRON

H.P. Ehret, R. Ernst, L. Friedrich, E. Huttel, J. Kaltenbaek, F. Schulz, L. Wiss, P. Ziegler, U. Zimmermann

The status of the Karlsruhe polarized deuteron facility is now characterized by a 52 MeV beam of 0.2 - 0.3 μA with a measured vector polarization of 0.53 which can be obtained routinely. For this a 10 keV beam of 10 - 20 μA within 500 mm mrad has to be delivered by the atomic beam source PASKA. The reliability of the source could be further increased by replacing the original SENTEC/ANAC control unit by a SIMATIC controller and by replacing the cryopumps by turbopumps. Further improvement of the beam quality is underway as follows:

1. An ECR-ionizer has been tested succesfully in cooperation with P.A. Schmelzbach at the PSI. It is intended to replace the EB-ionizer of the PASKA by an advanced ECR-ionizer next year.
2. A new dissociator similar to the Jaccard-SIN design is under development. Different configurations have been tested in a separate experimental arrangement. The design is simpler than the Glavish design for the dissociator of PASKA.

LISKA III, the ECR source for Li^{+++} ions used at present, is a two-stage source and delivers so far the best results concerning stability,

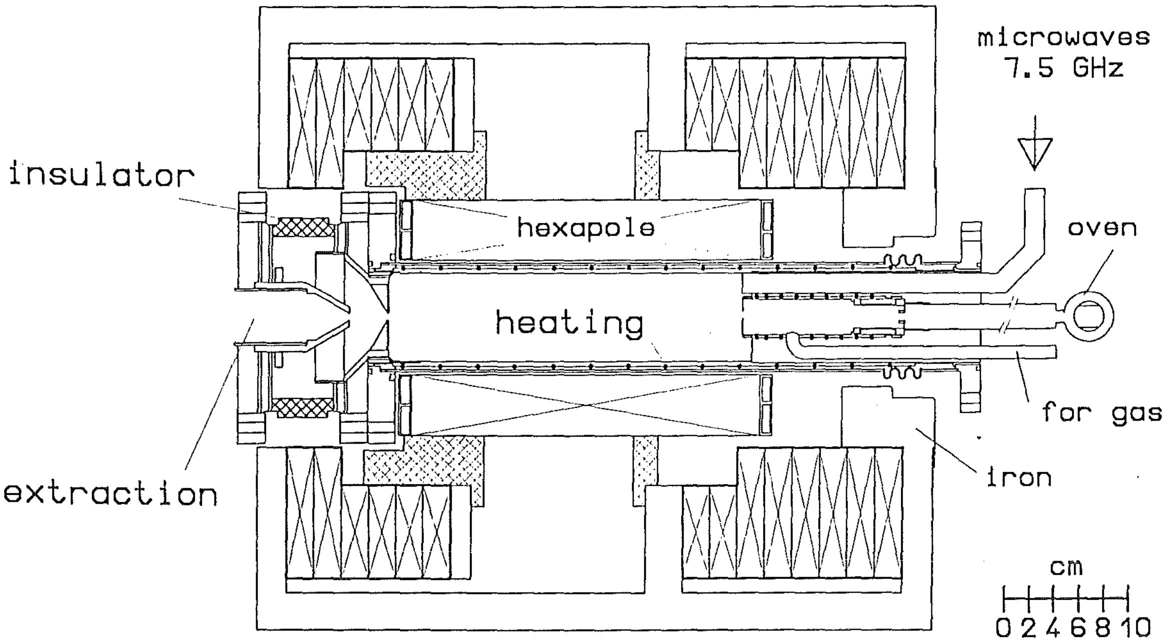

Fig. 1: LISKA III

operating time and intensity. The essential characteristics of this source (Fig. 1) are described below. Lithium vapor from an oven is guided into a small cylindrical (28 mm diameter) vacuum chamber, where it is ionized by 7.5 GHz microwaves in the 2 ω_{ce} mode [1]. One resonance zone is inside the first stage plasma chamber, the other follows immediately after the 3 mm diameter hole from which ions and neutrals escape into the second stage. The microwave power is guided off-axis into the vacuum chamber of the second stage. To couple sufficient microwave power from the second stage into the first stage, the 3 mm diameter hole in between is extended to a 0.2 mm wide slot, so that only one microwave power has to be adjusted. A very important experience gained with all preceding versions of the source was that an efficient and homogeneous heating is of fundamental importance. Hence the plasma chamber of LISKA III is a double wall construction. The inner tube of 6.5 cm diameter is heated electrically up to about 400 °C. For thermal insulation it is surrounded by vacuum, which is maintained in an outer tube. In this way the CoSm5 magmets can be placed as close as possible to the plasma. To obtain an optimum temperature distribution five heating currents have to be adjusted carefully. Separately heated are the oven, the vapor pipe, plasma chamber one, plasma chamber two and the plasma electrode. The diameter of the extraction hole is 0.8 cm and the gap between the electrodes is 3 cm.

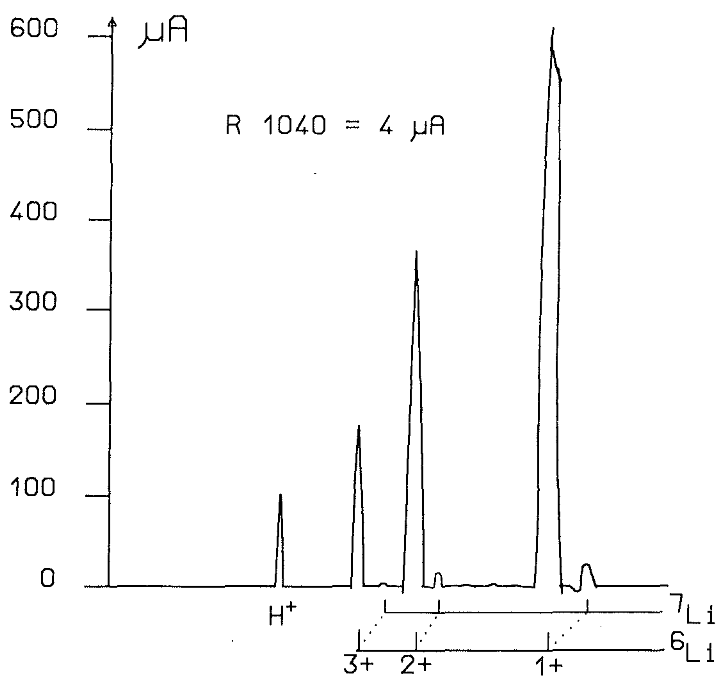

Fig. 2: Charge state distribution of the Li beam from LISKA III

The charge state distribution obtained with Li is shown in Fig. 2. The small admixture of ^{7}Li enables the discrimination between the $^{6}Li^{+++}$ ions and the hydrogen molecular ions, if one assumes that there is no difference between the relative charge state distribution of both Li isotopes. So it is concluded that 60 μA $^{6}Li^{+++}$ are delivered by the source, an improvement of a factor of ten compared with LISKA I.

LISKA III has now been operated for more than 1600 h without refilling the Li oven. The extracted 156 MeV Li^{+++} beam is typically 1.0 μA (2.5 have been extracted at maximum). About 100 W of microwave power are needed and the total power consumption is 70 kW.

References:

[1] B. Jacquot, P. Briand, F. Bourg et R. Geller
Nucl. Instr. and Meth. A 269 (1988) 1

6.3.4 IONIZATION OF A POLARIZED HYDROGEN ATOMIC BEAM IN AN ECR DISCHARGE

L. Friedrich, E. Huttel and P.A. Schmelzbach *

The question of the possible use of an electron cyclotron resonance ionizer for a polarized ion source has been raised at several workshops on polarized ion production [1]. The characteristic features of this ionization method and possible depolarization effects have been discussed by Clegg et al. [2,3].

Fig. 1 shows a schematic view of the first ECR-ionizer for an atomic beam source built in Karlsruhe.

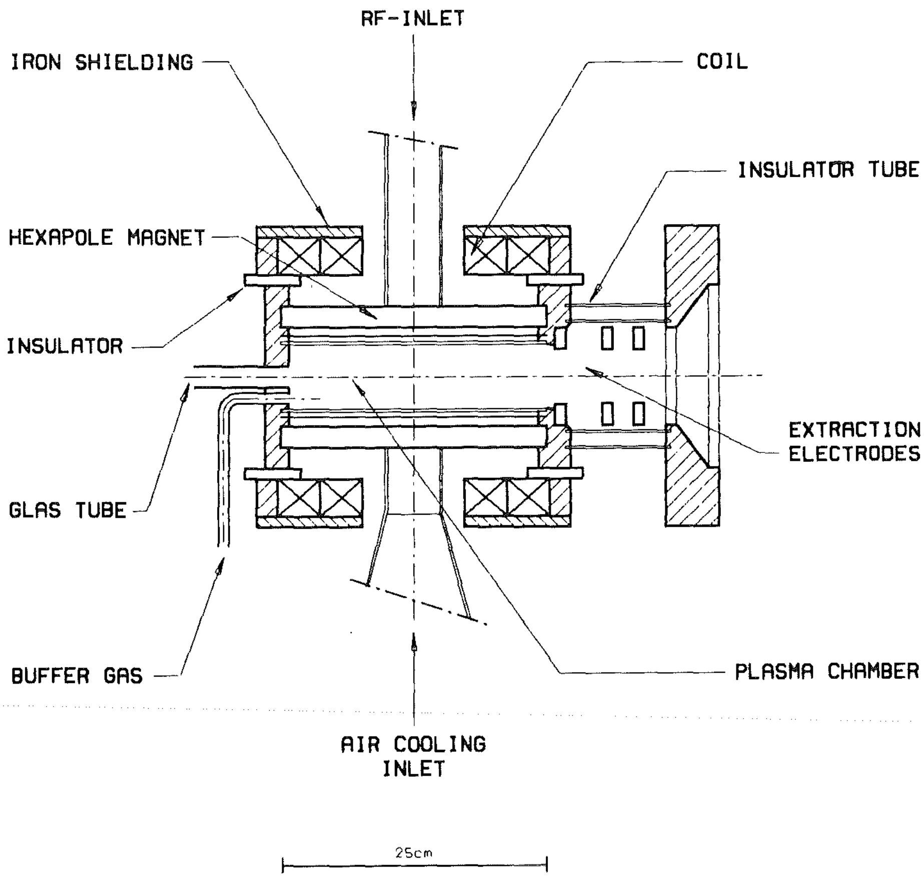

Fig. 1: Schematic view of the ECR ionizer. The plasma is confined longitudinally by the field of a pair of solenoid magnets and radially by the field of a permanent sextupole magnet. Microwaves of 2.45 GHz frequency are transmitted into the plasma chamber. The plasma chamber consists of a 300 mm long Pyrex tube of 60 mm diameter. Cooling is provided by a fan.

After some basic tests at KFK the ionizer was incorporated into a testbench at PSI. An atomic beam source similar to the one now operating at the PSI injector cyclotron delivered a 30 K cold atomic beam of about 5×10^{16} atoms/sec. By means of a strong field transition (3-5) a deuteron beam is produced with a tensor polarization of -1. The atoms enter the ECR ionizer through the Pyrex tube of 20 mm diameter. The extracted ions are focused by two electronic lenses into a 90° deflection magnet. After the deflection the tensor polarization was measured by a polarimeter using the T(d,n)α reaction at about 40 keV. Polarization did not depend on the magnetic field strength and the microwave power, indicating that no depolarizing hyperfinestructure mixing occurs in the ECR-zone. Concerning the polarization, the geometry and material of the source are much more important.

A polarization of 20 % was observed at the beginning with a classical stainless steel extraction system with 10 mm holes. Paving the plasma electrode and any other metal part, which could be seen by the atomic beam and the plasma electrode, with Pyrex result in 40 % polarization. With a large diameter extraction system, allowing an almost undisturbed passage of the atomic beam through the ionizer 85 % were finally achieved.

To obtain information about the beam quality the emittance of the polarized beam after the 90° deflection was measured (Fig. 2). The measurement device, was the same as had been used earlier to measure the emittance of the Karlsruhe polarized source PASKA.

With a three-electrode system, giving a beam with good transmission to the polarimeter, 150 µA of polarized deuterons with an emittance area of 60 mm mrad $\sqrt{\text{MeV}}$ were observed after the 90° analyzing magnet. Corresponding values for present sources equipped with an EB-superionizer are 75 µA within an estimated emittance of 80 mm mrad $\sqrt{\text{MeV}}$ at PSI and 30 µA within a measured emittance of 100 mm mrad $\sqrt{\text{MeV}}$ at Karlsruhe. The smaller intensity of the Karlsruhe source is due to the different performance of the atomic beam apparatus. These first results are very promising for the improvement of polarized ion sources based on the atomic beam method. It is intendend to equip both the sources at PSI and at KFK with an ECR-ionizer in the near future. An advanced model is assembled at present in Karlsruhe and will be tested soon.

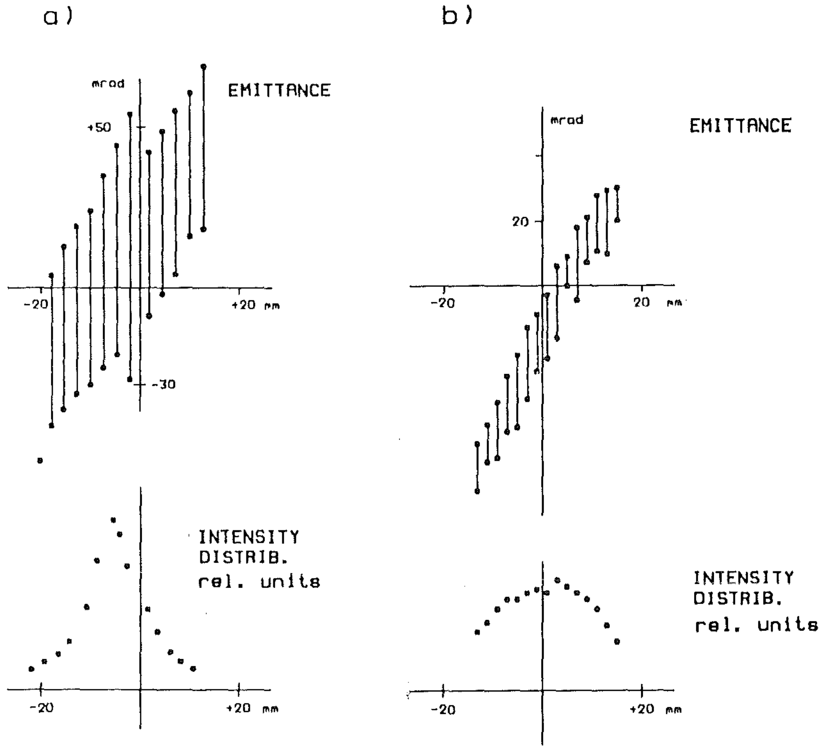

Fig. 2: Measured emittance and intensity distribution of a polarized deuteron
beam obtained with
a) an EB ionizer (PASKA, total current 30 µA)
b) the ECR ionizer (total current 150 µA)

*) Paul Scherrer Institute, CH-5234 Villigen, Schweiz

References

[1] S. Jaccard
Proceedings of the Int. Workshop on Pol. Proton Sources, Ann Arbor, AIP Conf. Proc. 80 (1982) 95

[2] T.B. Clegg, V. König, P.A. Schmelzbach and W. Grüebler
Nucl. Instr. and Meth. A238 (1985) 195

[3] T.B. Clegg and M.B. Schneider
Proceedings of the Int. Workshop on Pol. Sources and Targets, SIN, Montana, Helv. Phys. Acta 59 (1986) 553

6.3.5 DEVELOPMENT OF SIMPLE MEASURING DEVICES FOR NUCLEAR MEDICINE

M. Betz, J. Bialy, J.W. Peters, M. Schmitt

The measurement of time-dependent biological functions, e.g. renal or thyroid gland clearance and blood-pool analysis, is gaining importance in the field of nuclear medicine. At present complicated and very expensive camera systems (SPECT, Anger Cameras) are used for these function-diagnostic methods, although primarily designed for "picture-oriented" diagnostic methods and therefore less suitable for time-dependent measurements. In order to perform these kind of diagnostics in a simpler and cheaper way, a portable gamma measuring device called "Engypan" (engy=nearby) was developed. Several single-probe detector systems are connected to a "hand-held" micro-computer via a specially adapted counting interface. With these probes placed on the interesting regions of the human body, their time-dependent activity curves can be obtained and stored. After the necessary mathematical manipulation, the desired diagnostical information about the biological function can be deduced from these curves. Intensive discussions with nuclear physicians showed, that such a device is a useful tool in addition to the existing "picture-oriented" diagnostic systems. Fig. 1 shows the system in its transportation case.

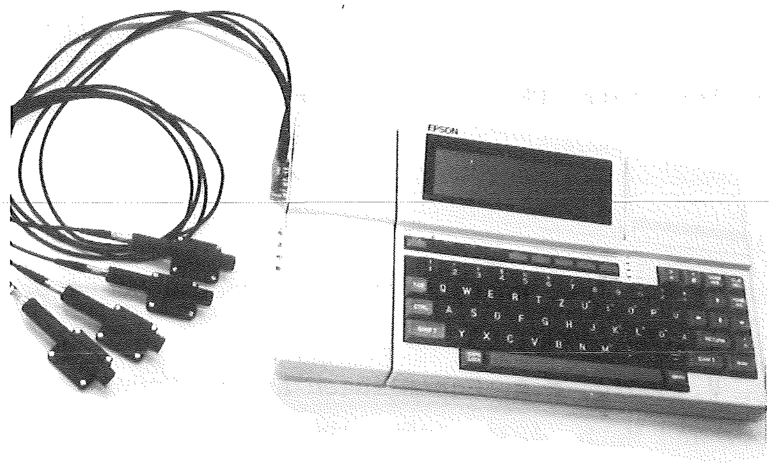

Fig. 1: ENGYPAN system

A new measuring interface was developed, which is capable of handling extremely high count rates and up to 12 detectors. Its complex design and the area limitations (7.5 cm x 8.5 cm max.) made the use of advanced multilayer, SMD and PAL techniques necessary.

First prototypes of the final design are under test now together with the required adaption of detector electronics and software. Also a new compact and portable detector concept was developed last year to avoid the disadvantages (low efficiency, no energy resolution) of the GM counters used up to now. First tests are being carried out with CsJ-scintillation material, a photodiode light collector and a super compact hybride preamplifier. The detector size is comparable to that of the GM detector, but its efficiency is at least ten times higher. However, some noise and stability problems have still to be solved.

6.3.6 PRODUCTION OF ISOTOPES FOR MEDICAL APPLICATIONS

K.H. Assmus, V. Bechtold, H.D. Dennerlein, H. Dohrmann, D. Erbe, E. Foßhag, A. Hanser, E. Heitz, S. Höllmüller, R. Hüfner, N. Kernert, J. Kraft, W. Maier, A. Martin, H. Ripp, U. Sahm, S. Uhlemann

Several radioactive isotopes for medical diagnosis are routinely produced at the Karlsruhe compact cyclotron (CP42H$^-$). The status of the various isotopes is as follows:

Ultra pure J-123

The amount of J-123 produced with the gas target system KIPROS could be increased by nearly 20 % compared to last year. KIPROS again was operating without any failures. In the autumn of 1987 the new hot cells for the processing and filling were taken into operation. The filling and distribution takes place in a nitrogen atmosphere under laminar flow. The processing is computer-supported and semiautomatic which leads to a stabilization of the chemical quality of the product.

Parallel to the routine production a "turn key" iodine production system (KIPROS, fig. 1) was built-up for a pharmaceutical company in St. Louis, USA. The acceptance tests were carried out to buyer's satisfaction in

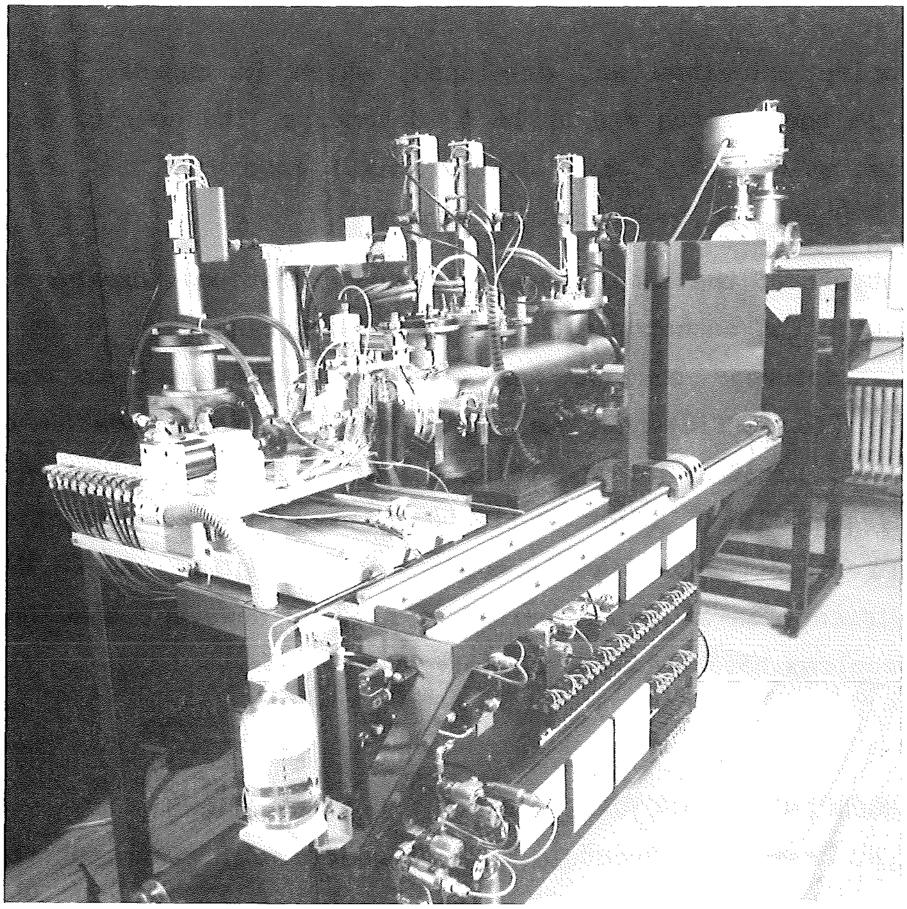

Fig. 1: The iodine production system KIPROS built for a pharmaceutical company in US. KIPROS is fully microprocessor operated

Karlsruhe early summer. The schedule forsees to install the KIPROS system end of August '88 at the customer.

Rb-81/Kr-81m generator and ultra pure Rb-81

No substantial changes have occured in the production. The number of generators is nearly unchanged compared to last year. However, the proportion of ultra pure rubidium has increased to 40 % - 50 % of the total rubidium production. The massseparated Rb-81 is produced twice a week with activities of 2-5 GBq at the time of separation for several research hospitals in Germany.

Rb-81/Kr-81m liquid generator

The prototype development of the application system and the related generator has been completed. These prototypes will be tested in a research hospital in southern Germany. In view of the expected additional investment costs and licensing fees for the Bundesgesundheitsamt (German Drug Administration) it was decided not to continue with the project until some experience with the prototype is available and the future market can be better evaluated.

6.3.7 RADIONUCLIDE TECHNIQUE FOR MECHANICAL ENGINEERING (RTM)

R. Blank, E. Bollmann, P. Fehsenfeld, B. Gegenheimer, P. Herrmann, A. Kleinrahm, H. Roth, B. Schüssler

The recent upward trend in the activation service to industry and research laboratories has continued during the period of report. The evident increase of interest in the on-line wear and corrosion measuring technique (RTM) has emanated from such diverse industries as gears and large journal bearing manufacturers, oil and lubricant industry, engine research and developing laboratories. The predominant application of RTM diagnostics is still the development in mechanical and processing engineering in industry and not so much in plant condition monitoring.

The new irradiation facility installed recently at the compact cyclotron has been intensively used for the activation service. An example of application, a cylinder liner (400 mm in diameter, 870 mm in length, 540 kp total weight) of a large marine diesel engine, is shown in fig. 1 in the irradiation position in front of the cyclotron beam tube. The RTM diagnostics have been applied successfully, improving service time and reliability of such engines.

Work in the development of RTM has been carried out mainly in thin layer activation of new materials like cermets and ceramics. This work has been performed in cooperation with the Institut für Materialforschung IMF I/KfK and with the Daimler-Benz A.G. and the Detroit Diesel Corporation.

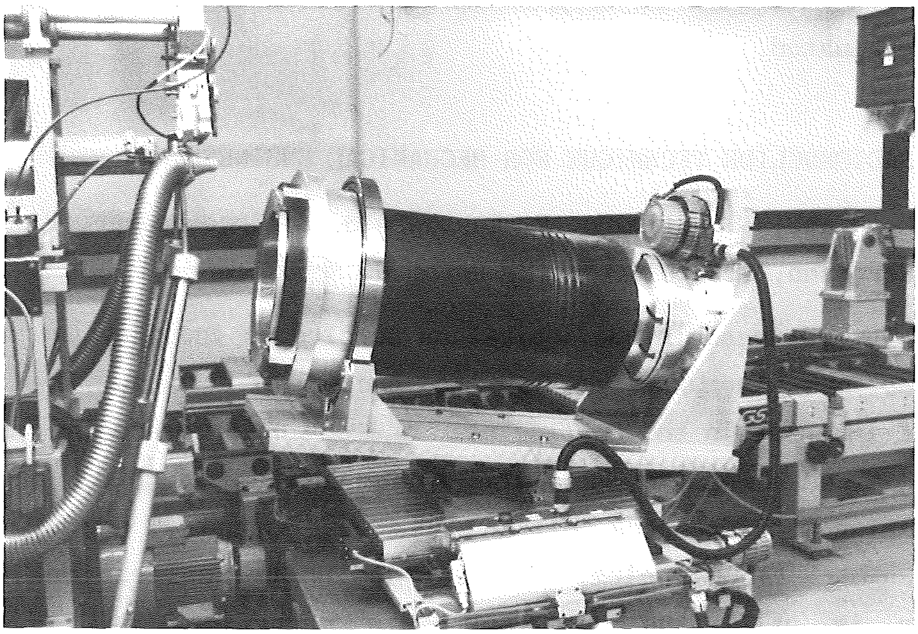

Fig. 1: A Cylinder liner (400 mm in diameter, 870 mm in length,540 kp total weight) of a marine diesel engine, positioned in front of the beam tube of the compact cyclotron for irradiation in a ring zone on the inner wall of the liner at TDC (Top Dead Center) of the first piston ring.

6.4 APPLICATIONS

6.4.1 APPLICATIONS OF X-RAY SPECTROMETRY IN NUCLEAR FUEL REPROCESSING

H. Eberle, P. Matussek, I. Michel-Piper, H. Ottmar (1)

When properly designed and adapted to the specific measurement problem, energy-dispersive X-ray techniques can handle in a straightforward manner a significant part of the routine analytics for actinides and other elements in a reprocessing plant. Due to their flexibility they offer possibilities for both off-line and in-line applications, covering the range from high-accuracy measurements on batch samples for accountancy and for verification in international safeguards up to continuous in-line operation for timely process monitoring. Some of the respective instruments have already successfully demonstrated their capability and performance in real applications. With potential improvements in sensitivity, X-ray spectrometry will be capable of determining actinides directly from radioactive process solutions at concentration levels, which may cover a range of about 6 orders of magnitude.

(1) Proc. Int. Conf. on Nuclear Fuel Reprocessing and Waste Management, "RECOD 87", Vol. 2 (1987) 890.

6.4.2 IMPLEMENTATION OF THE V MASK-TECHNIQUE AS A TOOL IN INSTRUMENT CONTROL

H. Eberle, N. Peter*

Two K-edge densitometers - one of them combined with a K-XRF system - are presently installed at the European Institute for Transuranium Elements, Karlsruhe, to perform concentration measurements of uranium and plutonium in feed and product solutions from reprocessing.

A standard procedure during the operation of these instruments includes regular measurements on suitably selected reference samples for the purpose of instrument control. The reference samples consist of uranium and plutonium metal foils and of sealed uranium solutions.

In order to make practical use of the experimental data from the control measurements, a method of data analysis is required which can detect and quantify potential systematic trends in the instrument response. For this purpose a special technique, the so-called 'V-Mask Technique', has been proposed and tested on the actual measurement data (1).

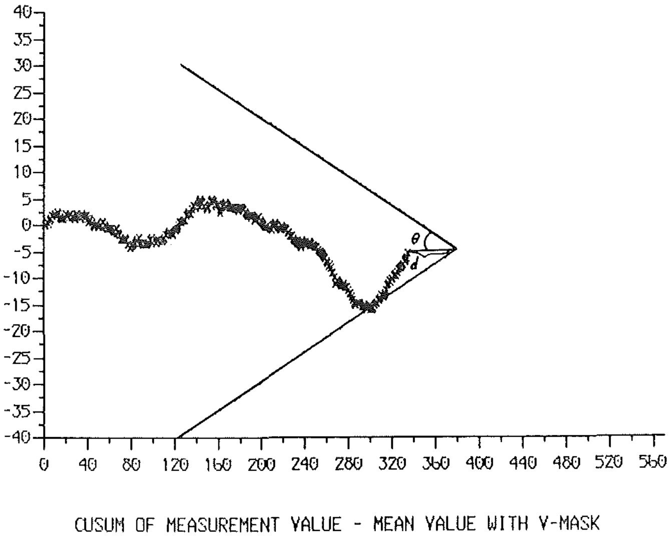

Fig. 1 V-mask superimposed on the CUSUM chart. A new trend was here detected at measurement 299.

To detect a trend in the control measurements, a V-shaped mask is superimposed on the CUSUM chart of these data. The vertex is pointed horizontally forward and set at a distance *d* ahead of the most recent point. The other parameter describing the V-shaped mask is the angle θ between the obliques and the horizontal (Fig. 1). So, the properties of the V-mask depend on the choice of *d* and θ. These two parameters can be calculated from each measurement series itself (1).

If the shape of the V-mask is known, the mask is successively applied to the CUSUM chart of the measurement series, starting from the first data point. The first value which is not enveloped from the mask (Fig. 1) indicates that a new trend begins. The V-mask technique is then again successively applied to the CUSUM-chart of the remaining data points, until the next trend is detected. In this manner the long-term response of the instrument is monitored, and the detection of small systematic trends in these control measurements indicates possible small instrument variabilities.

The technique principally seems to be capable of providing statements about the onset and magnitude of trends in control measurement series. A disadvantage of the program is that it requires a relatively large number of data points. Otherwiese the parameters *d* and θ of the V-mask cannot be determined.

(1) R. Beedgen, N. Peter, EUR 11041 EN, ESARDA 21 (1987) 285

* Institut für Datenverarbeitung in der Technik, Kernforschungszentrum Karlsruhe

6.4.3 DEVELOPMENT OF AN X-RAY SPECTROMETER FOR SAFEGUARDS VERIFICATION MEASUREMENTS

H.Ottmar

In the framework of the 'Joint Programme on the Technical Development and Further Improvement of IAEA Safeguards between the Government of the Federal Republic of Germany and the International Atomic Energy Agency (IAEA)' we are currently developing an X-ray spectrometer for the measurement of uranium and plutonium in solutions. After its completion the instrument will be installed at the Safeguards Analytical Laboratory (SAL) of the IAEA in Seibersdorf, Austria, fulfilling there two main objectives: (1) to serve as demonstration and training unit, having in view possible future in-plant installations of this type of equipment for on-site verification measurements, and (2) to take over part of the routine analytical measurements to be performed at SAL on safeguards verification samples.

The principal design of the X-ray spectrometer is based on our successfully demonstrated 'Hybrid Instrument' which combines the proven energy-dispersive X-ray techniques of K-edge densitometry and fluorescence analysis of K series X-rays (1). Both methods employ a common X-ray tube with maximum ratings of 160 kV/4 mA as photon source. The present instrument will be coupled to a glovebox, receiving samples from there by means of a linear drive for automated measurements on up to 30 samples.

In the regular operation mode, for which the Hybrid Instrument originally had been designed, the major element(s) present at higher concentrations are accurately determined by K-edge densitometry, while the X-ray fluorescence analysis is only used as a ratio measurement for the minor elements relative to the major elements. In the present application, however, a substantial fraction of the samples will have to be measured exclusively by XRF, because the available amount of sample material is not sufficient for an accurate K-edge densitometry measurement. For this purpose the XRF branch of the instrument has to be upgraded to an accurate stand-alone technique. It is foreseen to redissolve the sample material - typically a few milligram of heavy element present as dried solution in glass vials - with a suitable spike solution. Lead has been chosen as a compromise candidate for the spike element. It offers the advantage of not interfering with X-rays from the actinide elements. On the other hand, the clear separation of the X-ray energies from the spike element and the analyte makes their measured X-ray intensities more sensitive to effects of sample composition. Therefore numerical methods will have to be used to calculate for each given sample composition the relative production rate of the different X-rays from the exciting bremsstrahlung of the X-ray tube as well as their relative attenuation in the sample.

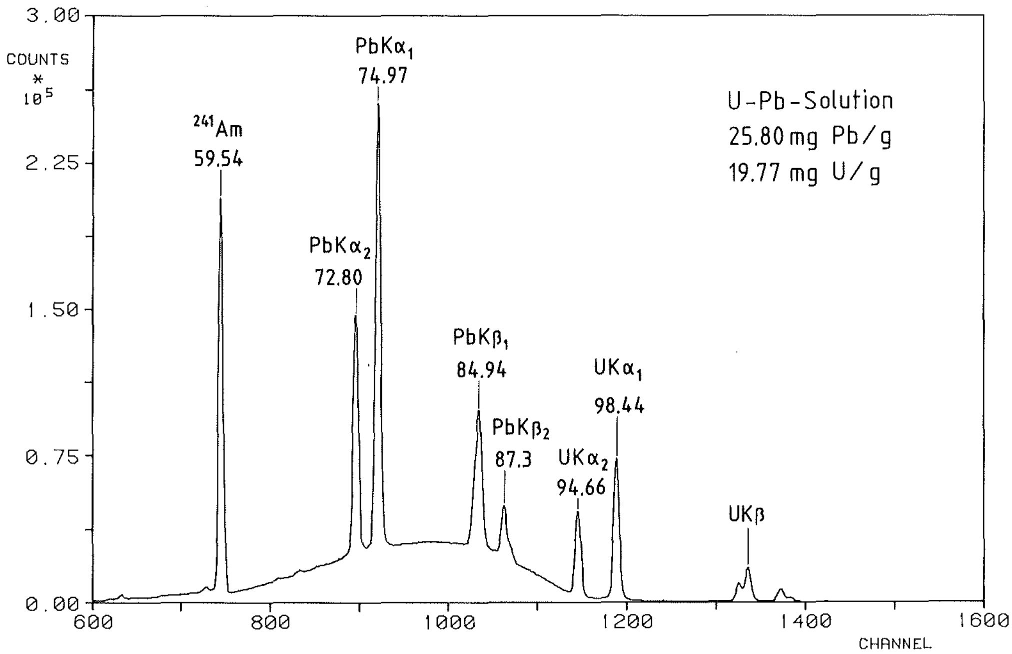

Fig. 1 XRF spectrum from a uranium solution spiked with lead. The gamma line from ^{241}Am used for the purpose of stabilization from an external gamma source.

Another problem for the correct determination and interpretation of the measured X-ray intensities arises from the fact that the X-rays are partly situated on top of the scatterd primary radiation as illustrated in the measurement example given in Fig. 1. Special procedures for calculating the overall shape of the background continuum will be incorporated in the software for data analysis in order to permit the correct determination of the net peak areas. The final goal is to achieve an overall measurement accuracy of better than 0.5%.

(1) H. Ottmar, H. Eberle, L. Koch, J. of the Inst. of Nucl. Manag. Vol. XV (1986) 632

6.4.4 TECHNICAL LAYOUT OF AN XRF IN-LINE MONITOR FOR URANIUM

I. Michel-Piper, H. Ottmar

Previously we have evaluated the performance characteristics of different variants of energy-dispersive X-ray fluorescence analysis (EDXRFA) for monitoring the uranium concentration in certain process streams of a reprocessing plant (1). The aim was to identify a suitable set-up for economic and reliable in-line operation. It turned out that this goal could principally be achieved by means of a fairly simple XRF analyzer, in which L X-rays are excited with a long-lived isotopic source (^{241}Am) and spectroscopied with a Si-detector operated at room temperature.

The technical layout of the proposed in-line monitor is shown in Fig. 1. Special attention has to be paid to the design of the flowing-through cell, and in particular to its radiation window. The latter must guarantee the safe containment of the nitric and organic radioactive process solutions, but on the other hand must also be transparent enough for the low-energy L X-rays of uranium. We have chosen sintered and finely polished boron carbide as radiation window, because this material is inert towards both acid and radiation, self-supporting and mechanically very stable. At a thickness of 1 mm the B_4C cell window still provides a transmission of 83% at 14 keV.

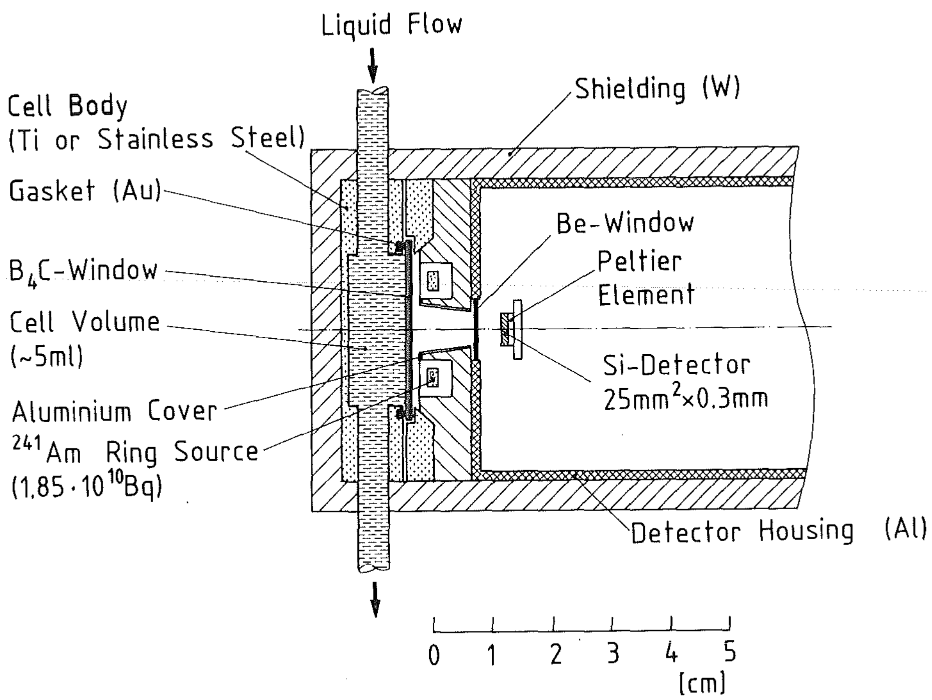

Fig. 1 Layout of the in-line XRF analyzer.

The set-up shown in Fig. 1 is designed for tightest measurement geometry in order to enhance the intensity of the fluoresced X-rays. It was found that the thickness of the solution layer can be reduced to about 5 mm without significantly deteriorating the detection limit. The sample volume then seen by the detector is about 0.7 ml. With this configuration the detection limit for uranium ranges between about 6 and 10 mg/l, depending on the level of the fission product activity in the process solution. This detection sensitivity , achieved within a counting time 10 minutes, proves to be adequate for the envisaged application.

In some of the process solutions uranium will be accompanied by significant amounts of neptunium. With the proposed XRF analyzer, in which the Si-detector is operated at about 20° C below the ambient room temperature, L X-rays from neighbouring elements cannot be discriminated because of the limited energy resolution of the detector (FWHM ≃ 1.3 keV). For an unambiguous determination of uranium an additional sensor will therefore be required which provides additional information on the concentration of neptunium in the process solutions. This information can be obtained from a passive measurement of the self-radiation using a fairly simple detector head equipped with a NaI-detector. In the presence of fission products the signal best suited for the determination of neptunium comprises the summed intensity of the 86 keV gamma ray and the K X-rays from protactinium, both emitted from the decay of ^{237}Np. With this passive measurement a detection limit of about 10 mg Np/l can be achieved within a counting time of 10 minutes from a few ml of sample volume.

(1) I. Michel-Piper, H. Ottmar, Report KfK 4405, Kernforschungszentrum Karlsruhe (1988), 145

6.4.5 IMPROVED SENSITIVITY FOR EDXRFA USING A WAVELENGTH-DISPERSIVE PREFILTER

P. Matussek, I. Michel-Piper

In usual energy-dispersive X-ray fluorescence analysis (EDXRFA) the detector views the whole spectrum of scattered and fluorescence radiation from a sample. In the special case of trace analysis of heavy elements in strongly scattering matrices (such as Uranium in aqueous or organic solutions) the lower limit of detection is determined mainly by the high intensity of the scattered primary excitation radiation. In order to improve the sensitivity of the EDXRFA in these cases a wavelength-dispersive prefilter was developed consisting of a cylindrical array of graphite monocrystals (1). The prefilter is placed between sample and detector. It serves as a band-pass for X-rays, transmitting only a limited energy region around the fluorescence lines of interest and cutting off the scattered radiation from the excitation source.

To optimize the geometry of the filter, a Monte-Carlo programme has been written, that calculates the transmission of the cylindrical prefilter. The measured and calculated transmission are given in fig. 1. The effect of the filter ist demonstrated in fig. 2 showing a spectrum obtained from a sample with 10 mg Uranium per liter.

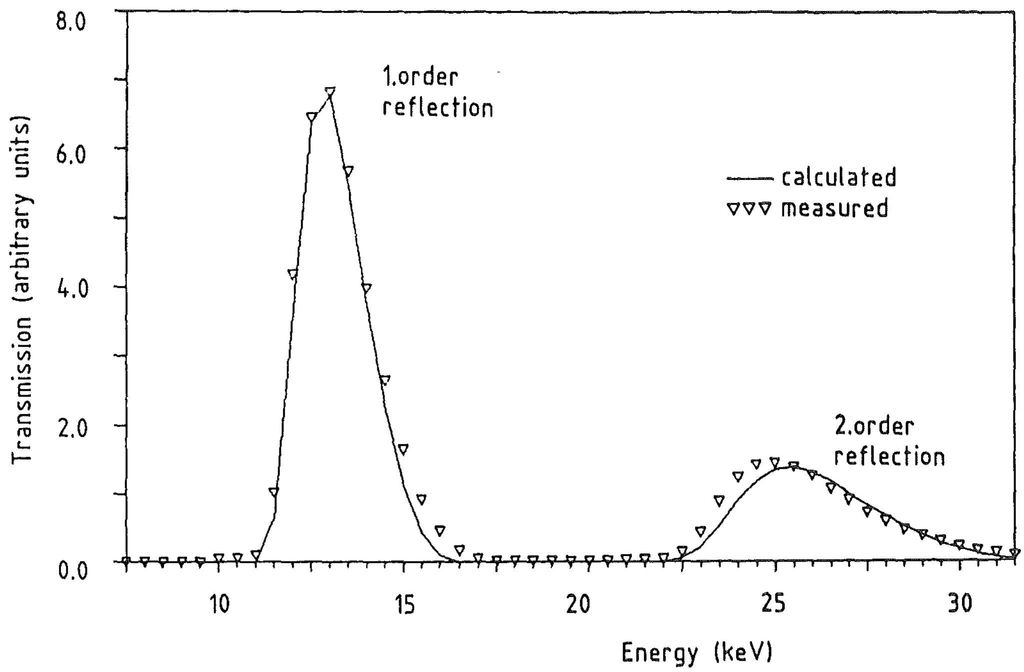

Fig. 1 Calculated and measured transmission X-rays through the cylindrical graphite filter

Relative to the amplitude of the Uranium L_{α} fluorescence line the intensity of the scattered excitation radiation from the Rh K-lines has been reduced by a factor of 500 as compared to the measurement without prefilter. The peak/background ratio for the L_{α} line has been improved by a factor of about 15. The lower limit of detection (presently achieved by using a 3 kW X-ray tube with Rhodium anode) is about 0.2 mg U/l for Uranium in solutions. The prefilter is also suited for the EDXRF analysis of highly radiative samples because only X-rays and gamma-rays within the narrow energy region of the filter transmission can enter the detector. First experiments have been performed on small Uranium samples by drying about 50 µl of Uranium solution on a capton foil or filter paper. The lower limit of detection was found to be about 300 pg Uranium in 10 minutes counting time.Really high active samples from waste streams of a reprocessing plant are presently prepared for measurements.

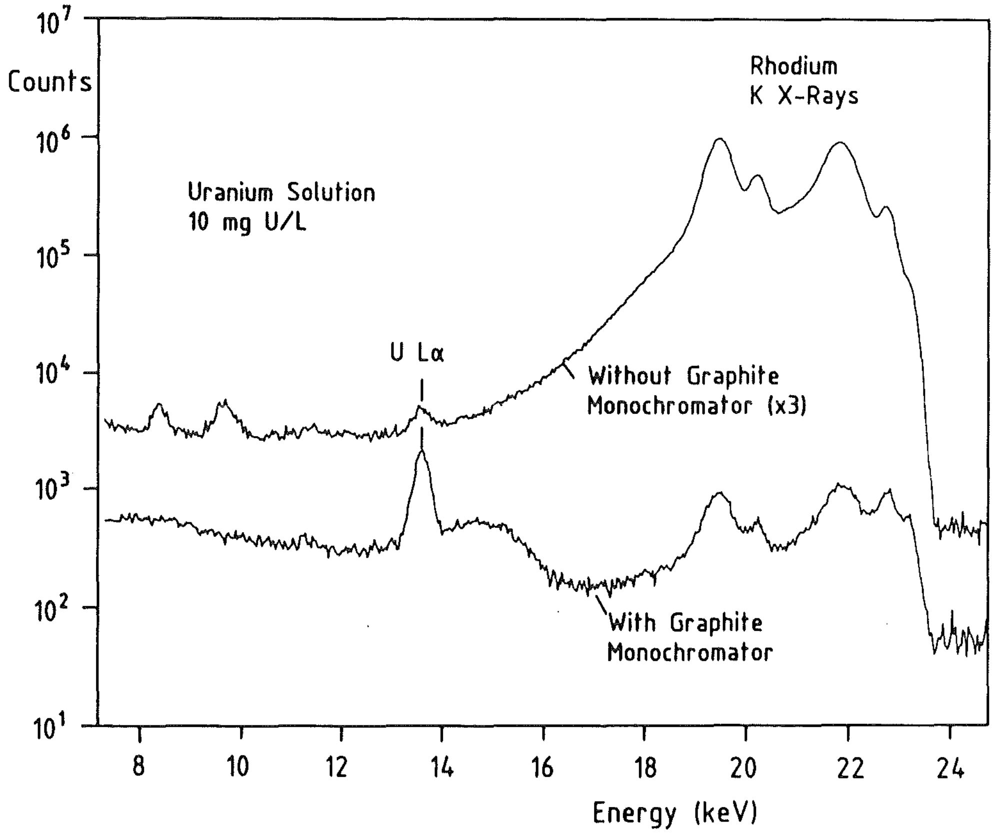

Fig 2 X-ray fluorescence spectrum from a Uranium solution with a concentration of 10 mg U/l.

(1) P. Matussek, I. Michel Piper, Report KfK 4405, Kernforschungszemtrum Karlsruhe (1988) 142

6.4.6 COPPER RESORPTION IN ISOLATED RAT HEPATOCYTES

D. Heck, A. Ochs*, H. Thom**, H.P. Buscher* (1)

Copper plays an important role both in physiology and pathology. In ionic form Cu^{++} is believed to be toxic. Our aim is to investigate the Cu-uptake by isolated rat hepatocytes in an in-vitro experiment. Hepatocytes are cultured on foils to form cellular monolayers, which are exposed to $CuSO_4$ solution. The trace elements P, S, Cl, K, Ca, Fe, Cu, Zn and Br are determined by PIXE, sweeping the proton microbeam in two dimensions across selected regions of the cell cultures. The concentration averages over positions covering the interior of hepatocytes or the intercellular gaps are formed and the behaviour of the various trace elements is studied as a function of the copper solution exposure time. In most cases cell nuclei are identified and evaluated separately.

(1) KfK Report 4428 (1988)

* Medizinische Universitätsklinik II, D-7800 Freiburg, FRG
** Institut für organische Chemie und Biochemie der Universität, D-7800 Freiburg, FRG

6.4.7 COPPER UPTAKE IN ISOLATED RAT HEPATOCYTES AND COPPER ACCUMULATION WITHIN THE RAT LIVER DURING CHOLESTASIS STUDIED BY PROTON INDUCED X-RAY EMMISSION (PIXE)

A. Ochs*, H.P. Buscher,* W. Gerok*, D. Heck, H. Thom** (1)

With proton induced X-ray emission an analytical tool for the direct trace element analysis is available, which is used for the study of copper uptake in short-time cultivated hepatocytes. The hepatocytes were exposed to a 30µM $CuSO_4$-solution. PIXE revealed uptake rates comparable to those obtained utilizing ^{64}Cu. Though the marked mean variation during the two first minutes of uptake made it more difficult to prove the linearity, these results are consistent with the present view of a facilitated transport by a special carrier protein combined with diffusional uptake.

In a second experiment the bile ducts of rats were ligated for various time periods. Within livers treated this way, a continuous increase of copper concentration was observed, preferring the acinar zone I (around the portal tracts). PIXE revealed copper concentrations up to 7000 µg/g in localized maxima (normal <50 µg/g DW) after 60 days of ligation. These data throw some doubt on the assumption that copper accumulation during extrahepatic cholestasis is non-toxic.

(1) Contribution 5th Int. Workshop on Trace Element Analytical Chemistry in Medicine and Biology, Neuherberg, April 15-18, 1988

* Medizinische Universitätsklinik II, D-7800 Freiburg, FRG
** Institut für organische Chemie und Biochemie der Universität, D-7800 Freiburg, FRG

6.4.8 EXPERIMENTAL COMPARISON OF MICRO-PIXE WITH OTHER METHODS UTILIZED FOR BIOMINERALIZATION STUDIES

T. Cichocki*, D. Heck, L. Jarczyk**, E. Rokita**,
A. Strzalkowski**, M. Sych* (1)

The present study deals with the investigation of arterial wall mineralization i.e. of inorganic compound development within artery wall under normal or pathologic conditions. Autopsy samples of human aorta as well as fragments of aorta obtained from hypercholesterolemic rabbits were used for the experiments. The samples were investigated using micro-PIXE, PIXE and PIGE techniques, infrared and Raman spectroscopy, X-ray powder diffraction and a variety of histochemical methods in order to compare the techniques based on a proton microprobe with the other methods which aimed at the investigation of inorganic deposits. Proton microprobe measurements confirm the different composition of mineral deposits found in rabbit and human aorta samples. In the case of animal aorta the apatite crystals constitute the mineral form of deposits while for human samples we deal with a mixture of different compounds. Moreover, for rabbit aorta samples the deposits were found always in the atheromas, while in human aorta sections the mineral deposits were localized in the media of the aortic wall. The proton microprobe can be considered to be a valuable addition to the experimental methods that have been applied in the study of the biomineralization process. It permits a quantitative determination of mineral deposits in situ while infrared and Raman spectroscopy as well as X-ray powder diffraction measurements may be performed only for ashed aorta samples. The possibility of in-situ measurements and high detection sensitivity seem to be the most significant advantages of a proton microprobe in the study of artery wall mineralization.

(1) Nucl. Instr. and Meth. B 31 (1988) 449

* Academy of Medicine, PL-31034 Kraków, Poland
** Institute of Physics, Jagellonian University, PL-30059 Kraków, Poland

7. LIST OF PUBLICATIONS

7.1 PUBLICATIONS AND REPORTS

ANGELOPOULOS, A.; APOSTOLAKIS, A.; ARMSTRONG, T.A.; BASSALLEK, B.; BUECHE, G.; FERO, M.; GEE, M.; GRAF, N.; KOCH, H.; LEWIS, R.A.; MANDELKERN, M.; PAPAELIAS, P.; POTH, H.; ROZAKI, H.; SAKELLIOU, L.; SCHULTZ, J.; SCHWERTEL, J.; SMITH, G.A.; USHER, T.; WOLFE, D.M.
Neutron emission from antiproton annihilation at rest in uranium.
Physics Letters B, 205(1988) S.590-94

ANSELMENT, M.; GOERING, S.; MEISEL, G.
A test of the accuracy of atomic-beam laser spectroscopy.
Zeitschrift fuer Physik D, 7(1987) S.113-18

BACHER, R.
Der Ionisierungsgrad isolierter exotischer Atome.
KfK-4347 (Januar 88)
Dissertation, Universitaet Karlsruhe 1988

BACKENSTOSS, G.; CIERJACKS, S.; FURIC, M.; HOFFART, A.; IZYCKI, M.; PETKOVIC, T.; RZEHORZ, B.; SALVISBERG, P.; SIMICEVIC, N.; STEINACHER, M.; ULLRICH, H.; WEBER, P.; WEYER, H.J.
Observation of a quasifree three-nucleon absorption mode of pions in ^{4}He.
SIN-Newsletter, 19(1987) S.NL31-NL32

BACKENSTOSS, G.; IZYCKI, M.; SALVISBERG, P.; STEINACHER, M.; WEBER, P.; WEYER, H.J.; CIERJACKS, S.; RZEHORZ, B.; ULLRICH, H.; FURIC, M.; PETKOVIC, T.; SIMICEVIC, N.
Observation of a quasifree three-nucleon-absorption mode of pions in ^{4}He.
Physical Review Letters, 59(1987) S.767-70

BEER, H.; KAEPPELER, F.; KLAY, N.; VOSS, F.; WISSHAK, K.
Die Entstehung der chemischen Elemente in Roten Riesen - Laborexperimente zur Beschreibung stellarer Prozesse.
KfK-Nachrichten, 20(1988) S.3-15

BEKK, K.; GOERING, S.; KAELBER, W.; MEISEL, G.; REBEL, H.; SAMEH, A.ALI
Determination of the supra(242m)Am nuclear moments.
Zeitschrift fuer Physik A, 330(1988) S.235-39

BORIE, E.; JOEDICKE, B.
Startup and mode competition in a 150 GHz gyrotron.
International Journal of Infrared and Millimeter Waves, 8(1987) S.207-26

BURGHARDT, B.; HOFFMANN, B. MEISEL, G.
The 3d states of ^{23}Na and ^{7}Li: determination of unresolved hyperfine splittings and radiative lifetimes.
Zeitschrift fuer Physik D, 8(1988) S.109-18

CELLO-COLLABORATION
A study of the three and four photon final states produced in e^+e^- annihilation at $35<=\sqrt{s}<=46.8$ GeV.
DESY-87-150 (November 87)
Physics Letters B, 202(1988) S.154-60

CHONGKUM, S.
Nuclear moments and isotopic variation of the mean square charge radii of strontium nuclei by atomic beam laser spectroscopy.
KfK-4318B (Oktober 87)

CICHOCKI, T.; HECK, D.; JARCZYK, L.; ROKITA, E.; STRZALKOWSKI, A.; SYCH, M.
Experimental comparison of micro-PIXE with other methods utilized for biomineralization studies.
Nuclear Instruments and Methods B, 31(1988) S.449-55

CIERJACKS, S.; HINO, Y.; RAUPP, F.; BUTH, L.; FILGES, D.; CLOTH, P.; ARMSTRONG, T.W.
Systematics of angular-dependent neutron production by 585 MeV protons on targets with 12<=A<=238: differential cross section measurements.
Physical Review C, 36(1987) S.1976-87

CRYSTAL-BARREL-COLLABORATION
Meson spectroscopy and the crystal barrel detector at LEAR.
Internat.Symp.on Medium Energy Physics, Beijing, RC, June 23-27, 1988
IEKP-MEP-87-1

CRYSTAL-BARREL-COLLABORATION
The crystal barrel project at LEAR.
4th LEAR Workshop, Villars-sur-Ollon, CH, September 6-13, 1987
IEKP-MEP-87-3

DANIEL, H.; HARTMANN, F.J.; KANERT, W.; PLENDL, H.; EGIDY, T.VON; REIDY, J.J.; KOCH, H.; KREISSL, A.; POTH, H.; ROHMANN, D.
Strong-interaction fine structure effects in antiprotonic ^{148}Nd.
Zeitschrift fuer Physik A, 326(1987) S.523-25

DOLL, P.; FINK, G.; FINLAY, R.; HAUPENTHAL, M.; KLAGES, H.O.; SCHIELER, H.; SMEND, F.; WICKE, G.
Preliminary neutron capture studies in the energy range from 18 MeV to 50 MeV.
Abrahams, K. [Hrsg.]
Capture Gamma Ray Spectroscopy : Proc.of the 6th Conf., Leuven, B, August 31 - September 4, 1987
Bristol [u.a.] : Inst.of Physics, 1988. - S.727-29
(Institute of Physics Conference Series ; 88)

DOLL, P.; BRADY, F.P.; FORD, T.D.; GARRETT, R.; KRUPP, H.; KLAGES, H.O.
Large area multiwire chamber ΔE-E telescope for (n,Z) studies in a continuous energy neutron beam.
Nuclear Instruments and Methods A, 270(1988) S.437-43

EBERLE, H.; MATUSSEK, P.; MICHEL-PIPER, I.; OTTMAR, H.
Evaluation of high-rate pulse processing in K-edge densitometry.
9th Annual Meeting of the European Safeguards Research and Development Association (ESARDA), London, GB, May 12-14, 1987
KfK-4291 (August 87)
13th Internat.Symp.on Nuclear Electronics, Varna, BG, September 12-18, 1988

FILGES, D.; CLOTH, P.; ARMSTRONG, T.W.; CIERJACKS, S.; HINO, Y.; RAUPP, F.; BUTH, L.
Systematics of angular-dependent neutron production by 585 MeV protons on targets with 12<=A<=238: validation of intranuclear cascade-evaporation model calculations.
Physical Review C, 36(1987) S.1988-94

GANTENBEIN, G.
Ein ortsempfindlicher Vieldraht-Proportionalzaehler fuer den Magnetspektrographen 'Little John'.
KfK-4427B (Mai 88)

GARCILAZO, H.
Nonexistence of Λnn or Σ⁻nn bound states.
Journal of Physics G, 13(1987) S.L63-L67

GARCILAZO, H.
Relativistic Fadeev theory of the πNN system with application to πd scattering.
Physical Review C, 35(1987) S.1804-19

GARCILAZO, H.
Polarized pion-deuteron breakup in the region of the 3,3 resonance.
Physical Review C, 35(1987) S.1820-22

GARCILAZO, H.
Relativistic Faddeev calculation of K^+d scattering.
Physical Review C, 37(1988) S.2022-31

GARCILAZO, H.; MATHELITSCH, L.
Relativistic three-body model of πN scattering.
Physics Letters B, 205(1988) S.199-203

GILS, H.J.
Density dependent effective interactions and the determination of nuclear densities in double-folding model analyses of elastic alpha-particle scattering.
KfK-4248 (Juli 87)

GILS, H.J.
Density dependent effective interactions in double-folding model analyses of elastic α-particle scattering.
Nuclear Physics A, 473(1987) S.111-28

GOEL, B.; HEERINGA, W.
Spin polarized ICF targets.
Nuclear Fusion, 28(1988) S.355-62

HABFAST, C.
Mikrowellendiagnose am LEAR Elektronenkuehler.
KfK-4188 (Juni 87)

HABFAST, C.; POTH, H.; SELIGMANN, B.; WOLF, A.; BERGER, J.; BLATT, P.; HAUCK, P.; MEYER, W.; NEUMANN, R.
Measurement of laser light Thomson-scattered from a cooling electron beam.
Applied Physics B, 44(1987) S.87-92

HECK, D.
Three-dimensional lithium microanalysis by the $^7Li(p,\alpha)$ reaction.
Proc.of the 1st Internat.Conf.on Microprobe Technology and Applications, Oxford, GB, September 1-4, 1987
Nuclear Instruments and Methods B, 30(1988) S.486-90

HECK, D.; OCHS, A.; BUSCHER, H.P.; THOM, H.
Trace element metabolism in liver cells after copper sulfate uptake.
1st Internat.Conf.on Microprobe Technology and Applications, Oxford, GB, September 1-4, 1987
Nuclear Instruments and Methods B, 30(1988) S.420-23

HECK, D.; OCHS, A.; THOM, H.; BUSCHER, H.P.
Copper resorption in isolated rat hepatocytes.
KfK-4428 (Mai 88)

HEERINGA, W.
Prospects for polarizing solid DT.
Brunelli, B. [Hrsg.]
Proc.of the Workshop on Muon Catalyzed Fusion and Fusion with Polarized Nuclei, Erice, I, April 3-9, 1987
New York [u.a.] : Plenum Publ.Co., 1987
S.235-47

HEERINGA, W.; VOSS, F.; [HRSG.]
Annual report on nuclear physics activities July 1, 1986 - June 30, 1987.
KfK-4405 (Februar 88)

JANY, P.; HEERINGA, W.; KLAGES, H.O.; ZEITNITZ, B.; GARRET, R.
Analyzing power of $n-{}^3He$ elastic scattering from 1 to 2 MeV.
Nuclear Physics A, 483(1988) S.269-81

JELITTO, H.; GILS, H.J.; REBEL, H.; ZAGROMSKI, S.
Measurements of light particle emission at very forward angles in ^6Li induced nuclear reactions at 26 MeV per nucleon.
Revue Roumain de Physique, 32(1987) S.629-35

KAEPPELER, F.
Status of the classical s-process.
Vangioni-Flam, E. [Hrsg.]
Proc.of the 2nd IAP Workshop Advances in Nuclear Astrophysics, Paris, F, July 7-11, 1987
Gif sur Yvette : Editions Frontieres 1986.
S.355-73

KAEPPELER, F.; NAQVI, A.A.; AL-OHALI, M.
Stellar cross sections at kT=52 keV: the example of ^{85}Krsupra(m).
Vangioni-Flam, E. [Hrsg.]
Proc.of the 2nd IAP Workshop Advances in Nuclear Astrophysics, Paris, F, July 7-11, 1987
Gif sur Yvette : Editions Frontieres 1986.
S.567-75

KAEPPELER, F.; WISSHAK, K.
Neuer Gamma-Detektor untersucht die stellare Elementsynthese.
Spektrum der Wissenschaft, (1988) Nr.9, S.25-34

KARMEN-COLLABORATION;
KARMEN: neutrino physics at ISIS.
Klapdor, H.V. [Hrsg.]
Neutrino Physics : Proc.of an Internat.Workshop, Heidelberg, October 20-22, 1987
Berlin [u.a.] : Springer, 1988 S.147-52

KLAGES, H.O.
Kernphysikalische Experimente mit schnellen (polarisierten) Neutronen.
KfK-Nachrichten, 20(1988) S.55-63

KLUGE, W.
Chiral symmetry breaking and the sigma-term in pion-nucleon scattering.
Peterson, R.J. [Hrsg.]
Pion-Nucleus Physics: Future Directions and New Facilities at LAMPF,
Los Alamos, N.M., August 17-21, 1987
New York, NY : American Institute of Physics, 1988. - S.247-51
(AIP Conference Proceedings; 163)

KOCH, H.
Die Suche nach Glueballs.
Der Crystal-Barrel-Detektor am Niederenergie-Antiprotonen-Ring LEAR des CERN.
Physikalische Blaetter, 43(1987) S.152-58

KOCH, H.; KUNZE, M.
Spectroscopy of light quark systems.
KfK-4298 (September 87)

KOCH, H.
Experiments in the pp-system at LEAR.
Internat.School of Nuclear Physics, Erice, I, July 16-25, 1988
IEKP-MEP-82-2

KREISSL, A.; CHARDALAS, M.; DEDOUSSIS, S.; EGIDY, T.VON; HANCOCK, A.D.; HARTMANN, J.F.; KUNERT, W.; KOCH, H.; KOEHLER, TH.; NILSSUN, A.; PENDL, H.; POTH, H.; RAICH, U.; REIDY, J.J.; ROHMANN, U.; SCHMIDT, G.; SUFFERT, M.; TAUSCHER, L.; WOLF, A.
Measurement of the antiproton magnetic moment and a determination of the spin-orbit term for the antiproton on nucleon antinucleon interactions.
Charalambous, S. [Hrsg.]
AntiProton 86 : 8th European Symp.on Nucleon-Antinucleon Interactions,
Thessaloniki, GR, September 1-5, 1987
Singapore : World Scientfic, 1987. - S.231-38

KUECHLE, M.; OTTMAR, H.; WUERZ, H.
Die Bestimmung von Plutonium in Abfallfaessern.
Atomwirtschaft-Atomtechnik, 33(1988) S.181-84

KUESTER, H.
Searches for supersymmetric particles with the Cello detector at Petra.
KfK-4294 (Februar 88)
Dissertation, Universitaet Karlsruhe 1988

LIST, W.
Messung des Wirkungsquerschnittes und der Vektoranalysierstaerke der $\pi^+d\to\pi^+pn$ Reaktion in einem kinematisch vollstaendigen Experiment.
KfK-4322 (November 87)
Dissertation, Universitaet Karlsruhe 1987

LIST, W.; BOSCHITZ, E.T.; GARCILAZO, H.; GYLES, W.; OTTERMANN, C.R.; TACIK, R.; MANGO, S.; KONTER, J.A.; VAN DEN BRANDT, B.; SMITH, G.R.
Neutron-proton final-state interaction in πd breakup: vector analyzing power.
Physical Review C, 37(1988) S.1594-99

LIST, W.; BOSCHITZ, E.T.; GARCILAZO, H.; GYLES, W.; OTTERMANN, C.R.; TACIK, R.; WESSLER, M.; WIEDNER, U.; JOHNSON, R.R.
Neutron-proton final-state interaction in πd breakup: differential cross section.
Physical Review C, 37(1988) S.1587-93

LOVAS, R.G.; KRUPPA, A.T.; BECK, R.; DICKMANN, F.
Fragmentation properties of ^{6}Li.
Nuclear Physics A, 474(1987) S.451-83

MICEK, S.; REBEL, H.; GILS, H.J.; KLEWE-NEBENIUS, H.; ZAGROMSKI, S.; SRIVASTAVA, D.K.
Single nucleon transfer reactions in ^{6}Li+^{6}Li collisions at 156 MeV.
Zeitschrift fuer Physik A, 328(1987) S.467-73

POTH, H.
Antihydrogen formation through positron-antiproton radiative combination.
Internat.Symp.on Production of Low Energy Positrons with Accelerators and Applications, Giessen, September 25-27, 1986
Applied Physics A, 43(1987) S.287-93

POTH, H.
Beam extraction with electron pick-up.
Zeitschrift fuer Physik A, 326(1987) S.483-86

POTH, H.
Von der Elektronenkuehlung zum Antiwasserstoff.
KfK-Nachrichten, 19(1987) S.74-82

POTH, H.; BARTH, H.; BUECHE, G.; HANCOCK, A.D.; KOCH, H.; KOEHLER, TH.; KREISSL, A.; RAICH, U.; ROHMANN, D.; WOLF, A.
Measurement of strong-interaction effects in light antiprotonic atoms.
Nuclear Physics A, 466(1987) S.667-84

RATYNSKI, W.; KAEPPELER, F.
Neutron capture cross section of ^{197}Au: a standard for stellar nucleosynthesis.
Physical Review C, 37(1988) S.595-604

SCHWERTEL, J.
Suche nach schmalen Linien im Spektrum der Photonen aus der Proton-Antiproton-Vernichtung in Ruhe.
KfK-4359 (Februar 88)
Diplomarbeit, Universitaet Karlsruhe 1988

SRIVASTAVA, D.K.; BASU, D.N.; REBEL, H.
Direct and sequential Coulomb break-up of ^{7}Li.
Physics Letters B, 206(1988) S.391-94

STROTH, U.; HASSE, R.W.; SCHUCK, P.
On the nuclear longitudinal charge response in the quasi-elastic peak region.
Nuclear Physics A, 462(1987) S.45-60

TAKAHASHI, K.; YOKOI, K.
Beta-decay rates of highly ionized heavy atoms in stellar interiors.
Atomic Data and Nuclear Data Tables, 36(1987) S.375-409

WIEDNER, U.; GOERING, K.; JAKI, J.; KLEIN, U.; KLUGE, W.; MATTHAEY, H.; METZLER, M.; PEDRONI, E.; FETSCHER, W.; GERBER, H.J.; KOCH, R.
Determination of the real part of the isospin-even forward-scattering amplitude of pion-nucleon scattering at 55 MeV as a test of low-energy quantum chromodynamics.
Physical Review Letters, 58(1987) S.648-50

7.2 CONFERENCE CONTRIBUTIONS

Internat.Europhysics Conf.on High Energy Physics, Uppsala, S, June 25 - July 1, 1987
Internat.Symp.on Electron and Photon Interactions at High Energies, Hamburg, July 27-31, 1987

CELLO-COLLABORATION
Single photon search with the CELLO detector.

A model independent study of the shape of the third jet in e^+e^- annihilation into multihadrons at 35 GeV.

Study of the $ee\gamma$ and $\mu\mu\gamma$ final states and search for excited leptons in e^+e^- interactions.

Tests of QED in the e^+e^- annihilation into two, three and four photons.

The K^0sub(s)K^0sub(s) final state in $\gamma\gamma$ interactions.

Search for heavy leptons.

CELLO-COLLABORATION
Model independent limits of the QCD scale parameter Λsub(ms) from e^+e^- annihilation data in the energy range from 14 to 46 GeV. (Contributed Paper)

Measurement of μ and tau pair asymmetries and determination of the topological branching ratios of the tau lepton.

Electron-Ion Collision and Laser Spectroscopy Conf., Age, S, June 22-16, 1987

BERGER, J.; BLATT, P.; HAUCK, P.; MAYER, W.; NEUMANN, R.; HABFAST, C.; POTH, H.; SELIGMANN, B.; WOLF, A.
Diagnostics of a cooling electron beam by Thomson scattering of laser light.

Internat.Symp.on Medium Energy Physics, Beijing, RC, June 23-27, 1987

HANCOCK, A.D.; KOCH, H.; KOEHLER, TH.; KREISSL, A.; POTH, H.; ROHMANN, D.; WOLF, A.; TAUSCHER, L.; NILSSON, A.; SUFFERT, M.; CHARDALAS, M.; DEDOUSSIS, S.; EGIDY, T.VON; HARTMANN, F.J.; KANERT, W.; SCHMIDT, G.; REIDY, J.J.
Study of X-rays from antiprotonic atoms.

CONTI, R.; FRIEZE, B.; GIDLEY, D.; RICH, A.; VAN HOUSE, R.; ZITZEWITZ, P.; LYNN, K.; HASEROTH, H.; HILL, C.E.; VALLET, J.L.; BERGER, J.; BLATT, P.; HAUCK, P.; MEYER, W.; NEUMANN, R.; POTH, H.; SELIGMANN, B.; SCHWAB, W.; WOERTGE, M.; WOLF, A.
A feasibility study for antihydrogen production.

MATTHAEY, H.; KLUGE, W.; GOERING, K.; GYLES, W.; JAKI, J.; METZLER, M.; TACIK, R.; WIEDNER, U.; BARNETT, B.M.; CLEMENT, H.; KRELL, S.; WAGNER, G.J.; WIEDNER, C.A.; GEORGE, D.; RENKER, D.; JOHNSON, R.R.
First measurements with the low energy pion spectrometer LEPS at SIN.

Workshop on Physics of Low Energy, Stored and Trapped Particles, Stockholm, S, June 14-18, 1987
NATO Workshop Atomic Physics with Positrons, London, GB, July 15-18, 1987

POTH, H.
Synthetization of antihydrogen.

Pion-Nucleus Physics: Future Directions and New Facilities at LAMPF, Los Alamos, N.M., August 17-21, 1987

KLUGE, W.
Chiral symmetry breaking and the sigma-term in pion-nucleon scattering.
Peterson, R.J. [Hrsg.]

2nd Internat.Oberjoch Meeting on Pion Nuclear Physics, Oberjoch, August 24-29, 1987

WIEDNER, U.
Low energy pion nuclear physics.

MATTHAEY, H.; KLUGE, W.; GOERING, K.; GYLES, W.; JAKI, J.; METZLER, M.; TACIK, R.; WIEDNER, U.; BARNETT, B.M.; CLEMENT, H.; KRELL, S.; WAGNER, G.J.; WIEDNER, C.A.; GEORGE, D.; RENKER, D.; JOHNSON, R.R.
First measurements with the low energy pion spectrometer LEPS at SIN.

194th Nat.Meeting of the American Chemical Society, New Orleans, La., August 30 - September 4, 1987

BEER, H.
s-process and solar abundances.

Internat.Symp.on Capture Gamma Ray Spectroscopy, Leuven, B, August 30 - September 4, 1987

KAEPPELER, F.
Nuclear excitation and stellar temperature.

RATYNSKI, W.; KAEPPELER, F.
The stellar capture cross section of ^{197}Au. An absolute measurement at kT=25 keV.

DOLL, P.; FINK, G.; FINLAY, R.; HAUPENTHAL, M.; KLAGES, H.O.; SCHIELER, H.; SMEND, F.; WICKE, G.
Preliminary neutron capture studies in the energy range from 18 MeV to 50 MeV.

Workshop on Radiative Capture, Sigtuna, S, August 27-30, 1987

DOLL, P.
Preliminary polarized neutron capture studies in the energy range from 18 to 50 MeV.

Proc.of the 11th European Conf.on Few Body Physics, Fontefraud, F, August 31 - Spetember 5, 1987

ULLRICH, H.; BACKENSTOSS, G.; CIERJACKS, S.; FURIC, M.; HOFFART, A.; IZYCKI, M.; POWERS, R.; PETKOVIC, T.; RZEHORZ, B.; SALVISBERG, P.; SIMICEVIC, N.; STEINACHER, M.; WEBER, P. WEYER, H.J.
Pion absorption in ^{3}He and ^{4}He nuclei.

European Nuclear Medicine Congress, Budapest, H, August 24-28, 1987

PRETSCHNER, D.P.; KOHLSTAEDT, H.; BIALY, J.; PETERS, J.
Engymetrie - a new method generation.

AntiProton 86 : 8th European Symp.on Nucleon-Antinucleon Interactions, Thessaloniki, GR, September 1-5, 1987

KREISSL, A.; CHARDALAS, M.; DEDOUSSIS, S.; EGIDY, T.VON; HANCOCK, A.D.; HARTMANN, J.F.; KUNERT, W.; KOCH, H.; KOEHLER, TH.; NILSSON, A.; PENDL, H.; POTH, H.; RAICH, U.; REIDY, J.J.; ROHMANN, U.; SCHMIDT, G.; SUFFERT, M.; TAUSCHER, L.; WOLF, A.
Measurement of the antiproton magnetic moment and a determination of the spin-orbit term for the antiproton on nucleon antinucleon interactions.
Charalambous, S. [Hrsg.]

4th LEAR Workshop, Villars-sur-Ollon, CH, September 6-13, 1987

POTH, H.
Study of antiprotonic atoms (PS 176) at LEAR.

HABFAST, C.; POTH, H.; SCHWAB, W.; SELIGMANN, B.; WOERTGE, M.; WOLF, A.; HASEROTH, H.; HILL, C.E.; VALLET, J.L.
The electron cooling device developed for LEAR.

POTH, H.; SCHWAB, W.; SELIGMANN, B.; WOERTGE, M.; WOLF, A.
MICROLEAR.

BUECHE, G.; U.A.; PS183-COLLABORATION
Strangeness content in antiproton-nucleus annihilation at rest.

BUECHE, G.; U.A.; PS183-COLLABORATION
Search for unusual behavior in neutral and charged particle emission from antiproton-nucleus annihilation at rest.

CONTI, R.; FRIEZE, B.; GIDLEY, D.; RICH, A.; SKALSEY, M.; VAN HOUSE, J.; ZITZEWITZ, P.; LYNN, K.; HASEROTH, H.; HILL, C.E.; VALLET, J.L.; BERGER, J.; BLATT, P.; HAUCK, P.; MEYER, W.; NEUMANN, R.; POTH, H.; SELIGMANN, B.; SCHWAB, W.; WOERTGE, M.; WOLF, A.
Study of antihydrogen production and experiments with atomic antimatter.

8th European Anatomical Congress, Antwerpen, B, September 6-12, 1987

CICHOCKI, T.; HECK, D.; JARCZYK, L.; ROKITA, E.; STRZALKOWSKI, A.; SYCH, M.
Investigation of inorganic deposits in selected organic matrices.

London Conf.on Positron Sensitive Detectors, London, GB, September 7-11, 1987

ENGLER, J.; KEIM, H.
Tracking chambers with room-temperature liquids.

GIORGINIS, G.; MANN, D.; WOELFLE, S.; GEMMEKE, H.; MASCHUW, R.; ZEITNITZ, B.
A liquid argon TPC.

Symp.on Giant Resonance Excitation in Heavy-Ion Collisions, Legnaro, I, September 21-25, 1987

EYRICH, W.; HOFMANN, A.; LEHMANN, A.; MOOSBURGER, M.; SCHLOESSER, H.; WIRTH, H.; GILS, H.J.; REBEL, H.; ZAGROMSKI, S.
Measurement of the (^{6}Li, ^{6}He) reaction including zero degree to study spin-isospin-transfer strength.

EYRICH, W.; HOFMANN, A.; LEHMANN, A.; MUEHLDORFER, B.; SCHLOESSER, H.; WIRTH, H.; GILS, H.J.; REBEL, H.; ZAGROMSKI, S.
Investigation of excitation and decay of isoscalar giant resonances using ^{6}Li-scattering.

IEEE Conf. 'Transactions of Nuclear Science', San Francisco, Calif., October 20-31, 1987

GEMMEKE, H.; GRANDEGGER, W.; MASCHUW, R.; PLISCHKE, P.; ZEITNITZ, B.
Detection efficiency for capture of neutrons measured with a tagged n-source.

GEMMEKE, H.; GRIMM, A.; KLEINFELLER, J.; MASCHUW, R.; ZEITNITZ, B.; EDGINGTON, J.A.
Properties of a new photomultiplier optimized to good time and energy resolution for scintillation counting.

Neutrino Physics : Proc.of an Internat.Workshop, Heidelberg, October 20-22, 1987

KARMEN-COLLABORATION; MASCHUW, R.
KARMEN: neutrino physics at ISIS.
Klapdor, H.V. [Hrsg.]

Annual Meeting of the Central Institute of Physics 'Progress in Physics', Bucuresti, R, October 22-24, 1987

JELITTO, H.; CORCALCIUC, V.; GILS, H.J.; HEIDE, N.; KIENER, J.; REBEL, H.; ZAGROMSKI, S.
Break-up reactions of supra(6,7)Li projectiles merits and restrictions of the extended Serber model.

Workshop on Van de Graaff Accelerators in Research Training and Technological Applications, Amman, JOR, November 23-27, 1987

ERNST, A.
Small Van de Graaff accelerators - automation, safety and performance.

Expertentreffen Kernphysik, Schleching, 2.-10.Maerz 1988

KAEPPELER, F.
Elementsynthese durch Neutroneneinfang - Laborexperimente und klassisches Modell.

SCHATZ, G.
Ausgedehnte Luftschauer.

Fruehjahrstagung DPG, Teilchenphysik, Freiburg, 16.-18.Maerz 1988

RANITSCH, K.H.
Grenzen fuer den QCD Skalenparameter Asub(ms).

KOPF, M.; FRIES, D.C.
Faseroptische Auslese von Triggerzaehlern fuer das elektromagnetische Kalorimeter von DELPHI.

HADINGER, U.; CELLO-COLLABORATION
Analyse von semileptonischen Ereignissen schwerer Quarks aus der e^+e^--Vernichtung.

GABRIEL, P.; CELLO-COLLABORATION
Modellunabhaengige Analyse des 3. Jets in der e^+e^--Annihilation.

HAHN, M.; CELLO-COLLABORATION
4-Jet-Ereignisse in der e^+e^--Annihilation.
Fruehjahrstagung DPG, Teilchenphysik,

HADINGER, U.; CELLO-COLLABORATION
Analyse von semileptonischen Ereignissen schwerer Quarks aus der e^+e^--Vernichtung.

Fruehjahrstagung DPG, Duenne Schichten, Dynamik und Statistische Physik, Halbleiterphysik, Magnetismus, Metallphysik, Forschungsfoerderung in Europa, Karlsruhe, 14.-18.Maerz 1988

BAYER, R.; FINKBEINER, F.; HEERINGA, W.; JANY, P.; KLAGES, H.O.; STROBELT, T.
Cryogenic particle detection.

Fruehjahrstagung DPG, Kern- und Mittelenergiephysik, Physikausstellung, Berlin, 21.-25.Maerz, 1988

DOLL, P.; FINK, G.; HAUBER, S.; HAUPENTHAL, M.; KLAGES, H.O.; SCHIELER, H.; SMEND, F.; WICKE, G.
Neutron-proton capture in the energy range from 20 to 50 MeV.

DOLL, P.; EBERHARD, V.; FINK, G.; FINLAY, R.W.; FORD, T.D.; HEERINGA, W.; KLAGES, H.O.; KRUPP, H.; WOELFL, CHR.; ZEITNITZ, B.
New polarization data and phase-shift analyses in n-p scattering.

DOLL, P.; SCHEIB, S.; KLAGES, H.O.
The charge exchange reaction $^{12}C(n,p)^{12}B$ studied with a continuous energy neutron beam.

DOLL, P.; EBERHARD, V.; FINLAY, R.W.; FORD, T.D.; HEERINGA, W.; KLAGES, H.O.; REPPENHAGEN, D.; VOLLMER, A.
Measurement of the analyzing power of neutron induced reactions on ^3He.

DOLL, P.; FINK, G.; KLAGES, H.O.; SCHEIB, S.
MWPC set-up for neutron induced reactions on ^{12}C.

FINK, G.; DOLL, P.; HAUBER, S.; HAUPENTHAL, M.; KLAGES, H.O.; SCHIELER, H.; SMEND, F.; WICKE, G.
Neutron capture studies at light nuclei in the energy range from 18 MeV to 50 MeV.

BAYER, R.; FINKBEINER, F.; HEERINGA, W.; JANY, P.; KLAGES, H.O.; STROBELT, T.
Cryogenic particle detection.

ABELE, H.; JAENTSCH, H.; NEU, R.; STAUDT, G.; STRIEBELE, CH.; EVERSHEIM, P.D.; HINTERBERGER, F.; GILS, H.J.
Elastic and inelastic α-scattering on light nuclei.

BACHER, R.; BLUEM, P.; GOTTA, D.; HEITLINGER, K.; SCHNEIDER, M.; MISSIMER, J.; SIMONS, L.M.; ELSENER, K.
Der Ionisierungsgrad isolierter exotischer Atome.

BARAN, R.; BOHNERT, U.; HELBIG, P.; HERRMANN, G.; HOFMANN, A.; KRUEGER, H.; MALZ, D.; MUELLER, R.; ORTNER, H.W.; SCHWEINZER, L.; MATTHAEY, H.; WIEDNER, U.
An efficient spectrometer with π^+ identification.

BEKK, K.; FAUBEL, W.; GOERING, S.; KAELBER, W.; MEISEL, G.; REBEL, H.; RINK, J.; SCHATZ, G.; THOMPSON, R.C.
Variation of nuclear charge radii and electromagnetic nuclear moments of thorium isotopes by stored ion laser spectroscopy.

BODMANN, B.; BURTAK, F.; FINCKH, E.; KRETSCHMER, W.; SCHILLING, F.; STAUBER, K.; STEGEN, R.; VOETISCH, D.; ZELL, E.; MASCHUW, R.
Detailed properties of the KARMEN anticounter.

CIERJACKS, S.; HOFFART, A.; RZEHORZ, B.; ULLRICH, H.; BACKENSTOSS, G.; IZYCKI, M.; SALVISBERG, B.; STEINACHER, M.; WEBER, P.; WEYER, H.J.; FURIC, M.; PETKOVIC, T.; SIMICEVIC, N.
Multinucleon pion absorption processes in the helium isotopes.

EGGER, J.; SIMONS, L.M.; ELSENER, K.; BACHER, R.; BLUEM, P.; GOTTA, D.; HEITLINGER, K.; SCHNEIDER, M.; ROHMANN, D.
Messungen von X-Rays im antiprotonischen Wasserstoff und Deuterium bei niederen Drucken (<=300 mbar).

EYRICH, W.; DIETZEL, R.; HOFMANN, A.; LEHMANN, A.; MOOSBURGER, M.; RUDELOFF, R.; SCHLOESSER, H.; WIRTH, H.; GILS, H.J.; REBEL, H.; ZAGROMSKI, S.; SCHULTE, A.; OSTERFELD, F.; UDAGAWA, T.
Investigation of isoscalar giant resonances and spin-isospin-modes using ^6Li-projectiles.

FOLGER, G.; CRYSTAL-BARREL-COLLABORATION
Das Crystal Barrel Experiment bei LEAR.

GENTNER, R.; BELLM, D.; GEMMEKE, H.; KELLER, K.; LASSEN, L.; LUECKING, W.; MARKO, W.
Neutron-neutron correlations in the compound-nucleus reaction 96 MeV $^{18}O+^{64}Ni$.

GIORGINIS, G.; WOELFLE, S.; ENGLER, J.; GEMMEKE, H.; MASCHUW, R.; ZEITNITZ, B.
A selfpurifying liquid argon time projection chamber.

GYLES, W.; JAKI, J.; JORAM, CH.; KLUGE, W.; MATTHAEY, H.; METZLER, M.; TACIK, R.; WIEDNER, U.; BARNETT, B.M.; CLEMENT, H.; KRELL, S.; WAGNER, G.J.; WIEDNER, C.A.; JOHNSON, R.R.
Low-energy pion scattering from ^{12}C.

KIENER, J.; GILS, H.J.; REBEL, H.; BAUR, G.; GANTENBEIN, G.; HEIDE, N.; JELITTO, H.; WENTZ, J.; ZAGROMSKI, S.
Looking for Coulomb break-up of 156MeV ^6Li projectiles.

KOZIK, T.; BUSCHMANN, J.; GROTOWSKI, K.; BRZYCHCRYK, J.; GILS, H.J.; HEIDE, N.; JELITTO, H.; KIENER, J.; MICEK, S.; REBEL, H.; SOSIN, Z.; ZAGROMSKI, S.; COLE, A.J.
Intermediate mass fragment emission in ^6Li induced nuclear reactions at E/A = 26 MeV.

KUNZE, M.; CRYSTAL-BARREL-COLLABORATION
Aufbau eines 4π-γ-Kalorimeters fuer LEAR.

MOOSBURGER, M.; DIETZEL, R.; EYRICH, W.; HOFMANN, A.; LEHMANN, A.; RUDELOFF, R.; SCHLOESSER, H.; WIRTH, H.; GILS, H.J.; REBEL, H.; ZAGROMSKI, S.
The (^6Li, ^6He) reaction at small angles on light nuclei.

NEUMANN-COSEL, P.VON; OBERSTEDT, A.; RICHTER, A.; ROESCH, W.; SCHRIEDER, G.; BELLM, D.; GENTNER, R.; KELLER, K.; LASSEN, L.; SEIBERT, U.; CASSING, W.; GEMMEKE, H.
Preequilibrium neutron emission in the system ^{40}Ar + ^{40}Ca at 15 MeV/amu.

RATYNSKI, W.; KAEPPELER, F.
The stellar capture cross section of ^{197}Au - an absolute measurement at KT = 25 keV.

SCHOTT, W.; CRYSTAL-BARREL-COLLABORATION
Das elektromagnetische Kalorimeter des Crystal Barrel Detektors: Ergebnisse eines Prototyptests im Bereich 100 MeV/c bis 400 MeV/c.

SELIGMANN, B.; POTH, H.; WOERTGE, M.; WOLF, A.
The Karlsruhe electron collector and its performance in a test set-up.

POTH, H.; SCHWAB, W.; SELIGMANN, B.; WOERTGE, M.; WOLF, A.; HASEROTH, H.; HILL, C.E.; VALLET, J.V.; BAIRD, S.; CHANEL, M.; LEFEVRE, P.; LEY, R.; MANGLUKI, D.; MOEHL, D.; MOLINARI, G.; TRANQUILLE, G.
Results from electron cooling experiments at LEAR.

WISSHAK, K.; KAEPPELER, F.; GUBER, K.; VOSS, F.
The Karlsruhe 4π barium fluoride detector.

ZAGROMSKI, S.; GANTENBEIN, G.; GILS, H.J.; KIENER, J.; EYRICH, W.; LEHMANN, A.; RUDELOFF, R.; SCHLOESSER, H.
The various detector systems at the Karlsruhe magnetic spectrograph 'Little John'.

Fruehjahrstagung DPG, Atomphysik, Massenspektrometrie, Molekuelphysik, Quantenoptik, Bonn, 21.-25.Maerz 1988

BEKK, K.; FAUBEL, W.; GOERING, S.; KAELBER, W.; MEISEL, G.; REBEL, H.; RINK, J.; SCHATZ, G.; THOMPSON, R.C.
Laserspektroskopische Messungen an gespeicherten radioaktiven Thorium-Ionen.

BEKK, K.; GOERING, S.; KAELBER, W.; MEISEL, G.; SAMEH, A.
Laserspektroskopische Atomstrahlmessungen am Grundzustand von supra(242m)Am.

3.Jahrestagung der Deutschen Gesellschaft fuer Nuklearmedizin, Aachen, 21.-22.Maerz 1988

BECHTOLD, V.; SCHWEICKERT, H.
Wirtschaftliche und logistische Gesichtspunkte bei Klinik PET's mit zentrale Zyklotron.

5th Internat.Workshop on Trace Element Analytical Chemistry in Medicine and Biology, Neuherberg, April 15-18, 1988

CICHOCKI, T.; HECK, D.; JARCZYK, L.; ROKITA, E.; STRZALKOWSKI, A.; SYCH, M.
Elemental composition of the human artherioslerotic arteries.

8th Internat.Workshop on Photon-Photon Collisions, Shoresh, IL, April 24-28, 1988

CELLO-COLLABORATION; APEL, W.A.
K^0sub(s)Kπ production in tagged and untagged γγ interactions.

Workshop on Low Temperature Detectors, Annecy-Le-Vieux, F, May 2-6, 1988

BAYER, R.; FINKBEINER, F.; HEERINGA, W.; JANY, P.; KLAGES, H.O.; STROBELT, T.
Cryogenic particle detectors at Karlsruhe.

Internat.Conf.on Nuclear Data for Science and Technology, Mito, J, May 30 - June 3, 1988

WISSHAK, K.; GUBER, K.; KAEPPELER, F.; KRISCH, J.; MUELLER, H.; RUPP, G.; VOSS, F.
The Karlsruhe 4π BaF_2 detector.

KAEPPELER, F.
Neutron capture rates for stellar nucleosynthesis.

CIERJACKS, S.; SMITH, A.B.
Neutron sources: present practice and future potential.

3rd Internat.Conf.on Nucleus Nucleus Collisions, St.Malo, F, June 6-11, 1988

GILS, H.J.; KIENER, J.; JELITTO, H.; REBEL, H.; ZAGROMSKI, S.; BAUR, G.
Search for non-resonant Coulomb break-up of ^{6}Li at Esub(Li) = 156 MeV.

5.Fachgespraech der KfK-Veranstaltungsreihe 'Technologietransfer durch Kooperation', 16.Juni 1988

BIALY, J.; PETERS, J.W.; PRETSCHNER, D.P.; SCHMITT, M.
Moderne Engymetrietechnik.

HECK, D.
Spurenelementbestimmung in einzelnen Zellen durch Protonen-induzierte Roentgenstrahlung mit einer Ortsaufloesung von 3 µm.

BECHTOLD, V.; SCHWEICKERT, H.
Radioisotope fuer die Medizin.

1st European Particle Accelerator Conf., Roma, I, June 7-11, 1988

SCHMELZBACH, P.A.; FRIEDRICH, L.; HUTTEL, E.
An ECR ionizer for a polarized hydrogen ion source.

POTH, H.; SCHWAB, W.; SELIGMANN, B.; WOERTGE, M.; WOLF, A.; MEDENWALDT, R.
MICROLEAR: a low energy deceleration and storage device.

POTH, H.; SCHWAB, W.; SELIGMANN, B.; WOERTGE, M.; WOLF, A.; CONTI, R.; RICH, A.
Can position sources for storage rings be built cheaper?

16th Summer School on Quantum Optics, Bachotek, PL, June 19-25, 1988

MEISEL, G.
Atomic spectroscopy with dye lasers.

MEISEL, G.
Precision laser spectroscopy of hydrogen, cobalt, sodium and lithium.

MEISEL, G.
Technology of dye lasers for spectroscopic application of high precision.

Internat.Conf.on Applications of Nuclear Techniques, Crete, GR, June 26 - July 2, 1988

BECHTOLD, V.
Industrial applications of the Karlsruhe compact cyclotron.

REBEL, H.
Astrophysical aspects of projectile break-up reactions.

5th Internat.Conf.on Nuclear Reaction Mechanisms, Varenna, I, June 13-18, 1988

7.3 SEMINARS

DOLL, P.
Experimente zum Einfang schneller polarisierter Neutronen an leichten Kernen.
Vortr.: Universitaet Tuebingen, 15.Januar 1988

DOLL, P.; FINK, G.; HAUBER, S.; HAUPENTHAL, M.; KLAGES, H.O.; SCHIELER, H.; SMEND, F.; WICKE, G.
Neutron capture studies on light nuclei at the Karlsruhe cyclotron.
Vortr.: Triangle Universities Nuclear Laboratory, Durham, N.C., 9.Juni 1988
Vortr.: Los Alamos National Laboratory, Los Alamos, N.M., 6.Juli 1988
Vortr.: Crocker Nuclear Laboratory, Davis, Calif., 12.Juli 1988

CIERJACKS, S.
Systematics of angular-dependent neutron production by high energy protons.
Vortr.: Joint Research Centre, Geel, B, 7.Juli 1987

BECHTOLD, V.
Isotopenproduktion am Karlsruher Kompakt Zyklotron (KAZ).
Vortr.: Technische Bundesanstalt, Braunschweig, 16.Dezember 1987

GOERING, K.; KLEIN, U.; KLUGE, W.; MATTHAEY, H.; METZLER, M.; WIEDNER, U.; PEDRONI, E.; FETSCHER, W.; GERBER, H.J.
Pion-nucleon-scattering and chiral symmetry breaking of low energy QCD (sigma-term).
Vortr.: Universitaet Mainz, 10.Dezember 1987

HUTTEL, E.
Erzeugung polarisierter Teilchen.
Vortr.: Universitaet Tuebingen, 20.November 1987

KAEPPELER, F.
The classical s-process - a possibility to constrain stellar models.
Vortr.: Universitaet Turin, I, 20.April 1988
Vortr.: Inst.f.Astronomie, Universitaet Bologna, I, 21.April 1988

KAEPPELER, F.
Element synthesis by neutron capture reactions.
Vortr.: Inst.of Atomic Energy, Beijing, RC, 18.Mai 1988
Vortr.: Inst.of Nuclear Sciences and Technology, Sichuan, RC, 25.Mai 1988

KAEPPELER, F.
Der Beta-Zerfall in Sternen.
Vortr.: Inst.f.Strahlenphysik, Universitaet Stuttgart, 1.Juli 1988

KLAGES, H.O.
Experimente zur Untersuchung ausgedehnter Luftschauer.
Vortr.: Universitaet Bern, CH, 19.Juni 1987
Vortr.: Universitaet Wien, A, 16.+17.Dezember 1987

KLAY, N.
Thermische Anregung von Kernniveaus in Sternen.
Vortr.: Universitaet Mainz, 8.Februar 1988

MEISEL, G.
Laser spectroscopy of small samples.
Vortr.: Politechnika Poznanska, Poznan, PL, 26.Oktober 1987

POTH, H.
Electron cooling.
CERN Accelerator School, Berlin, 26.September 1987

REBEL, H.
Break-up of light nuclear projectiles - access to nuclear cross sections of astrophysical interest.
Vortr.: CNRS, Orsay, F, 15.Maerz 1988

SCHATZ, G.
Kernphysik und die Entstehung schwerer Elemente in Sternen.
Vortr.: Universitaet Muenchen, 23.November 1987
Vortr.: Physikalisches Kolloquium, Universitaet Kiel, 7.Juni 1988

SCHATZ, G.
Synthese schwerer Elemente in Sternen.
Vortr.: Physikalisches Kolloquium, Universitaet Frankfurt, 15.Juni 1988

SRIVASTAVA, D.K.
Coulomb break-up of light projectiles.
Vortr.: Kolloquium des IKP der KFA Juelich, 8.Juni 1988

THOMPSON, R.C.
Ion traps, laser cooling and quantum jumps.
Vortr.: Universitaet Bonn, 7.September 1987

WISSHAK, K.
Der Karlsruher 4π BaF_2 Detektor: Messung von Neutroneneinfangquerschnitten fuer ein detailliertes Verstaendnis der Synthese schwerer Elemente im s-Prozess.
Vortr.: Inst.f.Kernchemie, Universitaet Mainz, 2.Mai 1988

8. PERSONNEL

HEAD OF THE INSTITUTE IKI: PROF.DR.B.ZEITNITZ

Scientific and Technical staff:

Apel, W.-D., Dr.
Bayer, R.
Bolz, J.
Daumiller, K.
Deschner, K.
Deutsch, G.
Dittmann, R.
Doll, P., Dr.
Drexlin, G., DP
Eberhard, V., DP
Engler, J., Dr.
Fink, G., DP
Finkbeiner, F.
Foltin, G.
Fries, D.C., Prof.Dr.
Gabriel, P., DP
Gettert, M.
Gemmeke, H., Dr.
Giorginis, G., Dr.
Grandegger, W., DP
Gumbsheimer, R., DI(FH)
Hahn, A.
Hahn, M.
Hauber, S.
Haupenthal, M.
Heeringa, W., Dr.
Hoss, A.
Hucker, H.
Husson, L., Ing.
Jany, P., DP
Keim, H., Ing.
Klages, H.O., Dr.
Kleinfeller, J., Dr.
Knapp, J., Dr.
Kriegleder, W., DP
Markofsky, T.
Maschuw, R., Dr.
Mayer, H.-J., Dr.
Mielke, H. H.
Müller, H., Prof.Dr.
Plischke, P., Dr.
Poth, H., Dr.
Rapp, J.
Reppenhagen, D.
Riegel, M.
Scheib, S.
Schieler, H.
Schmalz, G., DI
Schmidt, F.K., Dr.
Schneider, H., Dr.
Skacel, H.
Spohrer, G.
Strobelt, T.
Völker, G., DP
Vollmer, A.
Wochele, J., DP
Wölfle, S., DP
Wölfl, Chr., Dr.
Wolf, J.
Ziegler, P.

Head of the Section III: Prof. Dr. Gerd Schatz

Scientific and technical staff :

Antoni, I., Fr.

Beer, H., Dr.

Bekk, K., Dr.

Dorn, A. (Diplomand)

Eberle, H., Ing.

Feurer, B.

Friederich, H.-M., Fr.

Garcia-Orijuela, C. (Praktikant)

Gerstenhöfer, Th., Dipl.-Phys. (Doktorand)

Gils, H.J., Priv.-Doz., Dr.

Gsottschneider, G. (Diplomand)

Guber, K. (Diplomand)

Göring, S., Dipl.-Phys.

Hanser, A., Dr.

Heck, D., Dr.

Heide, N., Dipl.-Phys. (Doktorand)

Jelitto, H., Dr.

Kälber, W., Dipl.-Phys. (Doktorand)

Käppeler, F., Dr.

Kiener, J., Dipl.-Phys.

Klay, N., Dipl.-Phys.

Köhler, A., Fr.

Kowalewska, D., Fr., Dipl.-Phys. (Doktorandin)

Matussek, P., Dipl.-Phys.

Meisel, G., Priv.-Doz., Dr.

Michel-Piper, I., Fr., Dipl.-Ing. (FH)

Müller, H.

Oehlschläger, J., Dipl.-Math.

Ottmar, H., Dr.

Pietruk, P. (Diplomand)

Ratzel, U. (Diplomand)

Rebel, H.G., Prof. Dr.

Rink, J. (Diplomand)

Rupp, G.

Schmidt, K.A., Dipl.-Phys.

Steininger, R. (Diplomand)

Voß, F., Dr.

Wentz, J. (Diplomand)

Wisshak, K., Dr.

Zagromski, S., Dipl.-Ing. (FH)

Guest scientists :

Basu, S.K., Dr.

Brâncuş, I.M., Dr.

Corcalciuc, V., Dr.

Srivastava, D.K., Dr.

Zhao, W., Fr., Dipl.-Phys.

Head of the Cyclotron Laboratory: Dr. H. Schweickert

Scientific and Technical Staff:

Acharya, H., Fr.
Assmus, K.H
Bauer, G.*
Bechtold,V., Dr.*
Bialy,J.
Biber, J.
Blank, R.*
Bollmann,E.,Dipl.-Phys.*
Dennerlein, H.D.*
Dohrmann, H., Ing.
Dressel, M.
Dressen, R.
Ehret, H.-P.
Erbe, D.
Erdel, E.
Ernst, R.
Fehsenfeld, P., Dr.
Feuerstein, P., Frl.
Fischböck, T.*
Foßhag, E., Dr.*
Franz, J.
Friedrich, L., Dr.*
Gegenheimer, B.
Günther, O.
Heger, V.
Heidenreich, K.
Heinzmann, H., Dipl.-Inf.
Heitz, E.
Herrmann, P.
Höllmüller, S., Fr.*
Holler, H.
Hüfner, R., Dr.*
Huttel, E., Dr.*
Kaltenbaek, J.
Kappel, W.-R., Ing.
Kauther, P.
Kernert, N., Dipl.-Phys.*
Kessel, M.
Kirste, E., Fr.
Klar, T., Diplomand
Kleinrahm, J., Dr.*
Klinger, G.
Konrad, J.
Kraus, H.*
Krieg, U.
Lang, R.
Maier, W.
Mangold, D.
Mayl, R.*
Martin, A.*
Möck, W.
Möllenbeck, J., Ing.*
Peters, J., Dipl.-Phys.*
Rämer, Ch., Fr., Ing.
Ripp, H.*
Roth, H.
Sahm, U., Dr.
Schimpf, P.
Schmitt, M.*
Schönstein, E.
Schüssler, B.
Schütz, R.
Schulz, F., Ing.
Seidel, H.
Seitz, J.
Seufert, H.
Sheikh, S.*
Staub, M.
Stöbener, E., Ing.
Süpfle, M.
Thouw, T., Dr.
Uchatius, R.,Fr.
Uhlemann, S.,Fr.*
Wiss, L.
Ziegler, P.
Zimmermann, H.
Zimmermann, U.

* Specially-financed